



Universidade do Minho
Escola de Engenharia

Mariana Isabel dos Santos Rodrigues da Silva

**Computational Modelling of Human Lower Limb for
Reproduction of Walking Dynamics with Muscles:
Healthy and Pathological Cases**

Tese de Mestrado

Mestrado Integrado em Engenharia Biomédica

Trabalho efetuado sob a orientação de

Professor Doutor Óscar Samuel Novais Carvalho

Professor Doutor João Paulo Flores Fernandes

Professor Doutor João D. C. do S. Espregueira-Mendes

Outubro de 2018

DECLARAÇÃO

Nome: Mariana Isabel dos Santos Rodrigues da Silva

Endereço eletrónico: mariana.2301.santos.silva@gmail.com Telefone: +351 913 295 781

Número do Bilhete de Identidade: 13644752

Título da dissertação: Computational Modelling of Human Lower Limb for Reproduction of Walking Dynamics with Muscles: Healthy and Pathological Cases / Modelação Computacional do Membro Inferior Humano para a Reprodução da Dinâmica da Marcha com Músculos: Casos Saudável e Patológico

Orientador(es):

Professor Doutor Óscar Samuel Novais Carvalho

Professor Doutor João Paulo Flores Fernandes

Professor Doutor João D. C. do S. Espregueira-Mendes

Ano de conclusão: 2018

Designação do Mestrado: Mestrado Integrado em Engenharia Biomédica

DE ACORDO COM A LEGISLAÇÃO EM VIGOR, NÃO É PERMITIDA A REPRODUÇÃO DE QUALQUER PARTE DESTA TESE/TRABALHO

Universidade do Minho, ___/___/_____

Assinatura:

ACKNOWLEDGMENTS

After several months of working in this dissertation, I am writing this section in which I would like to express my sincere appreciation to all the people surrounding me and who made the development and conclusion of the dissertation possible. It has been a period of substantial learning for me, both in the area related to my cycle of studies, and on a personal level, and to that I am very grateful.

I would first like to thank the Erasmus Program and my supervisor at Technical University of Munich, Dr.-Ing. Daniel Renjewski. Thank you for guiding me throughout the course of my studies during the five-month duration of the Erasmus Program and by motivating me to keep diving into the approached subjects, trying to make me research and find solutions by my own.

Still in Munich, I would really like to express my sincere gratitude to the Catholic Mission of Portuguese Language. Thank you very much to Padre José Maria, Daniela M., Daniela, Daniel and all the other people of the Portuguese community helping me making me feel at home in Munich and helping me getting to know the culture of the city.

I would like to express a sincere acknowledgment to my supervisors in Portugal. To Professor Doutor Paulo Flores for introducing me into the field of biomechanics. I never knew what really motivated me in working. I knew I liked health care and mechanics, but never knew how to combine the two, and then biomechanics arose. Besides making me find my motivation, thank you very much for all the support and guidance given throughout the development of my dissertation. To Professor Doutor Óscar Carvalho for always questioning my work, helping me look more critically at my results and for always giving me new ideas and tasks to better develop my work.

To all my friends (Ana Fernandes and her family, Bruno Freitas and his family, Maria Miguel, Mariana Ferreira, Ana Luísa Carvalho and Catarina Miranda) a very special thank you for helping me and for always being there motivating me to continue.

Last but definitely not least, I want to express my utmost gratitude to all my family. I want to thank my parents, Isabel Santos and Manuel Silva, and my brother, Manuel José Silva, for always being there to encourage me to continue and to support me in every aspect. In particular, I would like to express my gratitude to my grandparents, Francisco Santos and Amélia Monteiro. Thank you for always being there throughout my entire life and for always giving me your entire all, your love and support. I hope you are proud of my achievements and continue to inspire my life.

Mariana Silva, October 2018

RESUMO

A biomecânica do movimento compreende o estudo e análise do movimento realizado por seres vivos, quer seja para melhorar o seu desempenho ou prevenir e tratar lesões. O primeiro é amplamente aplicado ao estudo do desporto e ao auxílio prestado aos atletas para desempenhar um movimento pretendido. De modo a ajudar na prevenção e tratamento de lesões, a biomecânica visa providenciar conhecimento acerca das propriedades mecânicas dos tecidos humanos, das cargas mecânicas a que eles estão sujeitos durante o movimento e de terapias relacionadas com prevenção e reabilitação. Atua no sentido de auxiliar na projeção estratégias de reabilitação e dispositivos médicos de assistência.

Este trabalho compreende o uso de um modelo biomecânico do membro inferior humano previamente desenvolvido por Geyer & Herr (2010). O modelo inclui a reprodução dos sistemas esquelético, muscular e neuronal humanos com o objetivo de produzir o movimento do modelo. Esta abordagem foi utilizada para estudar eventos que ocorrem a nível articular, considerando, por exemplo, a amplitude de movimento e os torques produzidos, durante uma marcha fisiológica e patológica com lesão do ligamento anterior cruzado (LAC). Esta patologia está associada a atividades, tais como o basquetebol, envolvendo mudanças rápidas na direção combinadas com aceleração e desaceleração do corpo. Estas ações causam lesões do LAC e por vezes levam à sua rutura, provocando a necessidade de procedimentos de reabilitação e cirúrgicos para melhorar a qualidade de vida dos pacientes.

Para o modelo biomecânico saudável, considerando os ângulos das juntas, os resultados apresentam uma concordância muito boa com a literatura. Os dados cinéticos demonstram algumas semelhanças, bem como discrepâncias. O torque da articulação do tornozelo é o que mais se aproxima da literatura, enquanto que o torque da anca e do joelho apresentam diferenças tanto em magnitude (maior do que o esperado), como em forma. Os padrões de ativação muscular também apresentam diferenças quando comparados com a literatura. Sugestões são dadas para minimizar estas ocorrências.

A implementação da patologia consistiu na diminuição do torque produzido pelos músculos (quadríceps e hamstrings) afetados pela lesão do ligamento anterior cruzado após reconstrução cirúrgica. A variável mais próxima da literatura é a força vertical de reação com o solo, enquanto que os restantes dados cinéticos diferem. Sugestões são dadas de forma a equivaler mais os resultados com a literatura.

PALAVRAS-CHAVE

Biomecânica, Modelo Biomecânico, Modelação Muscular, Patologia do Joelho, Ligamento Anterior Cruzado

ABSTRACT

Biomechanics of movement comprises the study and analysis of the movement performed by living beings, whether by improving its performance or by preventing and treating injury. The former is extensively applied to understanding sports and to help athletes performing a desired movement. In order to help preventing and treating injury, biomechanics aims at providing knowledge on the mechanical properties of human tissues, the mechanical loads they feel during movement, and on therapies related to prevention and rehabilitation. It acts to help design rehabilitation procedures and assistive medical devices.

This work comprises the use of a biomechanical model of the human lower limb previously developed by Geyer & Herr (2010). The model possesses the reproduction of the human skeletal, muscular and neural systems in order to produce the model's movement. This approach was used to study the events occurring at joint level, regarding, for instance, its range of motion and produced torques, during physiological and anterior cruciate ligament (ACL) pathological gait. This gait pathology is associated with activities, such as basketball, involving rapid changes in direction combined with acceleration and deceleration of the body. These actions cause ACL injuries and sometimes lead to its rupture, provoking the need for surgical and rehabilitation procedures to improve the patient's life quality.

For the healthy biomechanical model, regarding the joints' angles, the results present very good agreement with results found in literature. The kinetic data show some similarities, as well as discrepancies. The ankle joint torque is the closest to literature findings, whilst the hip and knee joint torque present differences both in magnitude (higher than expected) and in shape. The muscular activation patterns also present differences when compared to literature. Suggestions are made in order to minimize these occurrences.

The implementation of pathology consisted in diminishing the torque produced by the muscles (quadriceps and hamstrings) affected by an anterior cruciate ligament injury after its surgical reconstruction. The variable closer to literature findings is the vertical ground reaction force, whilst the other kinetic and kinematic data differ. Suggestions are made in order to make the results more equivalent to literature.

KEYWORDS

Biomechanics, Biomechanical Model, Muscle Modelling, Knee Pathology, Anterior Cruciate Ligament Injury

TABLE OF CONTENTS

Acknowledgments.....	iii
Resumo.....	v
Abstract.....	vii
List of Figures.....	xii
List of Tables.....	xxii
Nomenclature.....	xxv
1. Introduction	1
1.1. Motivation	2
1.2. Scope and Objectives	3
1.3. Organization of the Dissertation	4
1.4. Contribution of the Work.....	6
2. Human Lower Limb: Anatomy and Function	7
2.1. Basic Terminology of Human Movement.....	8
2.2. Skeletal System.....	13
2.3. Articular System	15
2.4. Muscular System.....	24
2.5. Summary and Discussion	28
3. Muscle-Tendon Unit	29
3.1. General Description	30
3.2. Muscle-Tendon Unit Structure.....	31
3.3. Joint Actuation	36
3.4. Factors Affecting Muscle-Tendon Unit Force Generation	40
3.5. Muscle-Tendon Unit Modelling.....	47
3.6. Summary and Discussion	52
4. Requirements for the Biomechanical Model Utilized.....	53
4.1. Methodology Adopted	54
4.2. Biomechanical Model Description	55
4.3. House of Quality Development.....	57
4.3.1. Customer Requirements	57

4.3.2.	Technical Specifications.....	59
4.3.3.	Target or Limit Value.....	61
4.3.4.	Other Considerations	63
4.4.	Critical Analysis.....	66
4.5.	Summary and Discussion	69
5.	Description of the Biomechanical Model Utilized	71
5.1.	Biomechanical Model's General Considerations	72
5.2.	Biomechanical Model's Muscle Actuation Layer	81
5.3.	Biomechanical Model's Neural Control Layer	91
5.4.	Ground Interaction Model	93
5.5.	Optimization.....	101
5.6.	Summary and Discussion	101
6.	Implementation and Validation	103
6.1.	Model Preparation.....	104
6.1.1.	Optimization Problem	104
6.1.2.	Solver Determination	108
6.2.	Healthy Model.....	112
6.2.1.	Kinetic and Kinematic Outcomes	113
6.2.2.	Sensitivity Analysis – Vertical Ground Reaction Force.....	124
6.2.3.	Vertical Ground Reaction Force – Detailed Study	126
6.2.4.	Muscular Activation Outcomes	131
6.3.	Pathological Model.....	136
6.3.1.	Anterior Cruciate Ligament: Injury and Treatment Strategies.....	137
6.3.2.	Computational Implementation of the Knee Joint Pathology.....	140
6.3.3.	Kinetic and Kinematic Outcomes	141
6.3.4.	Muscular Activation Outcomes	146
6.4.	Summary and Discussion	148
7.	Concluding Remarks	149
7.1.	Conclusions	150

7.2. Future Developments	151
Bibliographic References.....	153
Appendix I – Language Utilized in the Simulink® Environment	160

LIST OF FIGURES

Figure 2.1 – Anatomical reference position used to describe human movement. To facilitate this description, the human body is sectioned by three planes: frontal, sagittal and transverse. The directional terms are also represented: anterior-posterior, medial-lateral, superior-inferior and proximal-distal. Adapted from Palastanga & Soames (2012).....	8
Figure 2.2 - Illustration of the gait cycle with the corresponding events and phases. The events and phases correspond to the leg in analysis in the gait cycle, which in this case is the more shaded one (right leg). 1 – Loading response; 2 – Midstance; 3 – Terminal stance; 4 – Preswing; 5 – Initial swing; 6 – Midswing; 7 – Terminal swing. Adapted from Neumann (2013).....	11
Figure 2.3 – a) Anterior, b) lateral and c) posterior views of the bones comprising the right lower limb. Adapted from Schuenke, Schulte, et al. (2009).	13
Figure 2.4 - Bony structures of the right a) lateral pelvic girdle and b)/c) anterior and posterior, respectively, thigh and leg. Adapted from Schuenke, Schulte, et al. (2009).	14
Figure 2.5 – Illustration of the bones of the right human foot. This body segment is divided into tarsus, metatarsus and phalanges. a) Superior view. M, L and I the represent medial, intermediate and lateral cuneiform bones b) Medial view. Adapted from Schuenke, Schulte, et al. (2009).	15
Figure 2.6 – Right hip joint. a) Anterior, b) lateral, c) anterior with ligaments and d) posterior with ligaments views of the structures that comprise the hip joint. Adapted from Schuenke, Schulte, et al. (2009).	18
Figure 2.7 – Movements of the hip joint. a) Flexion, b) extension, c) abduction and adduction, d) external rotation and e) internal rotation. Adapted from Palastanga & Soames (2012).....	18
Figure 2.8 – The knee is a three-joint structure composed by the superior tibiofibular, the patellofemoral and the tibiofemoral joints. a) Frontal and b) lateral views. The right knee is represented. Adapted from Schuenke, Schulte, et al. (2009).....	19
Figure 2.9 - Kinematics of the patella during tibiofemoral extension. The circle represents the maximal contact point between the patella and the femur. The blue arrows represent the direction of motion. The red arrow represents the quadriceps femoris tendon. Adapted from Neumann (2013).	19
Figure 2.10 - Motion of the knee joint. In the sagittal plane, the tibiofemoral joint of the knee enables flexion (a) and extension (b). In the transverse plane, the tibiofemoral joint enables internal (a) and external (b) rotation. Adapted from Palastanga & Soames (2012).	20
Figure 2.11 - Structures comprising the knee joint. a) Transverse, b) anterior and c) posterior views of the right knee joint. Adapted from Schuenke, Schulte, et al. (2009).....	21

Figure 2.12 - Illustration of the joints comprised in the human foot. The right foot is represented. a) Anterior, b) medial with tibia, c) superior and c) medial without tibia views. Intercuneiform Joint, Cuneocuboid Joint, Naviculocuneiform Joint, Calcaneocuboid Joint, Cuboideonavicular Joint, Tarsometatarsal Joint, Talocalcaneonavicular Joint, Subtalar Joint, Intermetatarsal Joint, Metatarsophalangeal Joint, Interphalangeal Joint. Adapted from Schuenke, Schulte, et al. (2009). 23

Figure 2.13 - Foot motion. Plantar-/dorsiflexion (a), eversion/inversion (b) and (c) abduction/adduction are performed around the medial/lateral (sagittal plane), posterior/anterior (transverse plane) and superior/inferior (frontal plane) axes. Adapted from Palastanga & Soames (2012). 23

Figure 2.14 - Muscles acting around the hip joint. a) Anterior view. b) Anterior view with rectus femoris, iliopsoas and tensor fasciae latae (TFL) removed. c) Anterior view with rectus femoris, iliopsoas, TFL, gluteus medius and minimus, piriformis, obturator externus, adductor brevis and longus and gracilis removed. d) Posterior view. e) Posterior view with gluteus maximus and medius partially removed. The right lower limb is represented. Adapted from Schuenke, Schulte, et al. (2009). 25

Figure 2.15 - Muscles crossing the knee joint. a) Anterior view. b) Anterior view with sartorius and rectus femoris removed. c) Lateral view. d) Posterior view. e) Posterior view with gastrocnemius removed. The right lower limb is represented. Adapted from Schuenke, Schulte, et al. (2009). 26

Figure 2.16 - Muscles comprised in the foot. a) Anterior view. b) Posterior view. c) Posterior view with soleus and gastrocnemius removed. d) Lateral view. e) Superior view. f) Superior view with flexor digitorum brevis removed. The right lower limb is represented. Adapted from Schuenke, Schulte, et al. (2009). 28

Figure 3.1 – Representation of a muscle-tendon unit. A skeletal muscle connects the bones of the skeleton by means of tendons located at their ends. Adapted from Oatis (2009). 30

Figure 3.2 - Types of muscular contractions. a) Isometric. b) Concentric. c) Eccentric. Adapted from Openstax College (2013). 31

Figure 3.3 - Organization of the skeletal muscle with the identification of its structures. Adapted from Oatis (2009). 32

Figure 3.4 - Sarcomere structure. A sarcomere is the basic contractile unit of a muscle. It is composed by thin and thick filaments and their arrangement produces the structure of the sarcomere. Adapted from Zatsiorsky & Prilutsky (2012). 33

Figure 3.5 - Parallel fibred (fusiform and strap) and pennate (unipennate, bipennate and multipennate) muscles. Adapted from Oatis (2009). 34

Figure 3.6 - Illustration of the pennation angle, α , comprised between the force produced by the muscle fibres, F_{Fibres} , and the force exerted on the tendon, F_{Tendon} . Adapted from Hall (2012). 35

Figure 3.7 - Structural elements comprised within a tendon. Adapted from Oatis (2009). 36

Figure 3.8 - Representation of a motor unit (formed by the interaction between the motor neuron and muscle fibres) and the neuromuscular junction. Adapted from Tavares da Silva (2003). 37

Figure 3.9 - Events occurring when a muscle is stimulated. a) Twitch. b) Summation. c) Tetanus. Adapted from Openstax College (2013). 38

Figure 3.10 - Processes occurring from neural signal sending until the production of muscular force. When a neural signal arrives to the axons of a motoneuron, it is propagated to the adjacent muscle fibres, provoking muscle stimulation. This occurrence enables ACh to be release in the synaptic cleft, provoking muscle activation. When the muscle is activated, calcium ions are released into the muscle fibres, initiating muscular contraction, which in turn leads to muscular force production. 38

Figure 3.11 – Illustration of quadriceps muscle group force, F_{Quad} , moment arm, r , joint's centre of rotation (COR), application angle, γ , and distance between the muscle's attachment to bone and the joint's COR, d . Adapted from Schuenke, Schulte, et al. (2009) and Oatis (2009). 39

Figure 3.12 - Alterations occurring in a muscle's lever arm with joint position. Application to the hamstrings muscle group. The orange line represents the lever arm. Adapted from Oatis (2009). 40

Figure 3.13 - Force-length relation of the active part of a muscle. Adapted from Desai (2018). 42

Figure 3.14 - Illustration of a typical force-length relation of a muscle comprising the passive, active and combined components of this curve. Adapted from Oatis (2009). 43

Figure 3.15 - Force-velocity relation of a muscle. The point located in the transition from eccentric to concentric contraction represents the maximum isometric force a muscle is able to generate. Adapted from Oatis (2009). 44

Figure 3.16 - Relation between energy liberation, $(F+a)v$, and load, F . Adapted from Hill (1938). 45

Figure 3.17 – Changes in muscle force (F) with respect to variations in velocity (v) and length (l). Adapted from Buhrmann & Di Paolo (2014). 46

Figure 3.18 - Experiments used to determine the origin of muscle elasticity. a) Quick-release apparatus. b) Tension-time curve. c) Length-time curve. Adapted from McMahon (1984). 47

Figure 3.19 - Elements used to model an MTU. Adapted from Palastanga & Soames (2012). 49

Figure 3.20 - Simplest model to calculate force production by an MTU. The force depends only on the muscle activation and maximum isometric force. This model does not include the pennation angle, neither force-length and force-velocity relations. Adapted from Anderson (2007). 49

Figure 3.21 - Simplest model to calculate force production by an MTU with the inclusion of the influence of the pennation angle, α , and CE's properties, that is, muscle activation, A_{MTU} , and maximum isometric force, F_{max} . Adapted from Anderson (2007). 50

Figure 3.22 - Model used to calculate force generated by an MTU, which is modelled as a parallel elastic element (PE) and a contractile element (CE), in parallel with each other. The force depends on the characteristics of these two elements, including force-length and force-velocity relations. This model does not include the pennation angle. Adapted from Anderson (2007). 50

Figure 3.23 - Model used to calculate the force generated by an MTU, which is modelled as a parallel elastic element (PE) and a contractile element (CE), in parallel with each other. The force depends on the characteristics of these two elements, as well as on the pennation angle, α , verified between the tendon and the muscle fibres. Adapted from Anderson (2007). 51

Figure 3.24 – Model of an MTU, which is modelled as a series elastic element (SE) representing the tendon in series with a parallel elastic element (PE) and a contractile element (CE), in parallel with each other. Adapted from Anderson (2007). 51

Figure 4.1 - Quality Function Deployment methodology phases. 53

Figure 4.2 - House of Quality general template. 55

Figure 4.3 - Biomechanical model used. The model comprises 7 segments (one HAT, two thighs, two shanks and two feet), connected by 6 revolute joints (two hip, two knee and two ankle joints). The model comprises the soleus muscle (SOL), tibialis anterior muscle (TA), biarticular gastrocnemius muscle (GAS), vasti lumped muscle group (VAS), biarticular hamstring muscle group (HAM), hip flexor muscle group (HFL) and gluteus muscle group (GLU). Adapted from Geyer & Herr (2010). 57

Figure 4.4 - Sagittal plane joint angles used to defined Neumann (2013) range of motion. 63

Figure 4.5 - Developed house of quality. 65

Figure 5.1 – An overview of the layers or modules used in the construction of the biomechanical model. 71

Figure 5.2 - Biomechanical model used in this work. Left and right legs are coloured in red and blue, respectively. HAT is coloured in grey. a) Model's isometric view, with the indication of its segments and joints. b) Definition of the joints angles as in the work of Geyer & Herr (2010). θ_H, θ_K and θ_A represent the hip, knee and ankle joint angles, respectively. 73

Figure 5.3 - Movements of HAT segment throughout gait. The HAT rotates about the z-axis (out of the plane), situated at the hip joint. Besides, its centre of mass travels forward, in the x direction. Lastly, the

y position of the HAT alters during gait, moving up and down. The brown line below the biomechanical model represents the ground. 74

Figure 5.4 - Base (B) and follower (F) logic applied in the definition of the biomechanical model. Example given with the world frame, rigid transform and ground. The rigid transform enables the transformation of the origin of the world frame (B) into the origin of the frame in the centroid of the ground (F). It places the latter, one meter away from the origin of W. 75

Figure 5.5 - a) Rotation performed based on the Planar Joint Frame, {P}, to acquire the World Frame, {W}. A rotation about the x axis of -90 degrees is performed. b) Part of the Body Mechanics layer built. Note the base and follower ports of the rigid transform block between W and the planar joint. The mechanism configuration block is not shown here. 76

Figure 5.6 - Modelling approach used to construct the left foot segment. a) Illustration of the foot with the four points important to its construction: ball, heel, ankle and location of the centroid of the foot solid. The ball point is coloured in grey. This is the point from which the other three components are built. The location of the centroid of the foot solid, the ankle and the heel are coloured in yellow, blue and green, respectively. The red coloured lines illustrate the shank segment (see Figure 5.2), explained later. This segment was only drawn to give a better understanding of the concept described here. b) A subsystem to model the left foot segment is used, which comprises the definition of the heel and ankle points, and the foot solid, based on the frame of the ball point. This frame is the same as the frame of the planar joint since they are directly connected, and no transformation is done between them. 76

Figure 5.7 - Illustration of the biomechanical model construction using Simulink blocks. Starting from the world frame, defining the ground solid until the creation of the left foot. 77

Figure 5.8 - Sagittal plane view of the biomechanical model. a) Centre of mass distance, joint location and segment's length definition. b) Biomechanical model joint's initial conditions. Left Leg: $\theta_A=85^\circ$, $\theta_K=175^\circ$ and $\theta_H=175^\circ$. Right Leg: $\theta_A=90^\circ$, $\theta_K=175^\circ$ and $\theta_H=150^\circ$ 79

Figure 5.9 - Illustration of the block construction of the biomechanical model implemented in Simulink, including the definition of the segments (foot, shank, thigh and HAT) and joints (ankle, knee and hip). Light red and blue blocks indicate the left and right legs, respectively. 80

Figure 5.10 - MTUs comprised in the biomechanical model. This illustration comprises only the MTUs pertaining to one leg. The other leg contains the same MTU distribution. SOL - soleus muscle, TA - tibialis anterior muscle, GAS - biarticular gastrocnemius muscle, VAS - vasti lumped muscle group, HAM - biarticular hamstring muscle group, HFL - hip flexor muscle group and GLU - gluteus muscle group. Adapted from Geyer & Herr (2010). 81

Figure 5.11 - Muscle-Tendon Unit model. In normal physiological ranges of operation, CE produces force in line with SE. However, on one hand, if CE tends to stretch more than its optimum length, $l_{CE} > l_{opt}$, PE engages, preventing CE's overextension. On the other hand, if the geometry of the leg tends to make SE slack, $l_{MTU} - l_{CE} < l_{slack}$, BE prevents CE from collapsing. Adapted from Geyer & Herr (2010)..... 82

Figure 5.12 - General modelling blocks used to determine an MTU torque. Example given for the SOL muscle. SOL ATTACHMENT and SOL DYNAMICS are subsystem and mask subsystem blocks, respectively. The S_{MTU} SOL block arises from the Neural Control Layer, giving the stimulation, S_{MTU} , necessary to the MTU performance during model's motion. This part is only approached in the subsequent section..... 83

Figure 5.13 - SOL ATTACHMENT subsystem containing the implementation of the equations to calculate SOL's lever arm, r_{MTU} , variation of MTU length, Δl_{MTU} , and total MTU length, l_{MTU} . Blocks with a square and triangular shape enclose constants and blocks with rectangular shape with rounded ends are inputs and outputs of the subsystem, named Inports and Outports, respectively. θ is an input and r_{MTU} and l_{MTU} are outputs. θ is the ankle angle from Figure 5.12, from the Body Mechanics layer. 84

Figure 5.14 - Part of the MTU dynamics approached so far: calculation of CE's force-velocity relation, $f_v(v_{CE})$. S_{MTU} is the muscle's neural stimulation and is an input of the mask, calculated in the Neural Control layer (explained later). Output of the mask is the muscle's activation, A_{MTU} , which is used in the same layer as S_{MTU} , as well as in the Muscle Actuation layer. The transformation from neural stimulation, S_{MTU} , to muscular activation, A_{MTU} , is done by means of a Transfer Fnc block, named Excitation Contraction Coupling and whose expression is the one from Eq. 5.21. The inputs of SE, BE, PE and CE's force-length relations are either divided by l_{slack} or l_{opt} , since it makes it easier to resolve the equations inside the subsystems. Inside SE, BE, PE and CE subsystems, Eq. 5.12, $f_v(l_{BE})$ part of Eq. 5.16, $f_v(l_{PE})$ part of Eq. 5.15 and Eq. 5.10, respectively, are implemented by means of blocks in a similar manner as Figure 5.13. 90

Figure 5.15 - Inside the MTU DYNAMICS mask used to calculate the force produced by the MTU. The components within the mask are equally modelled to all MTUs. What differentiates the MTU and that uniquely characterizes it, is the definition of four individual muscle parameters, F_{max} , v_{max} , l_{opt} and l_{slack} . $f_{SE}(\epsilon)$, f_{BE} , f_{PE} and f_{CE} are the force-length relations of SE, BE, PE and CE, respectively. S_{MTU} and A_{MTU} are the MTU's stimulation and activation, respectively. $f_v(v_{CE})$ is the force-velocity relation of CE. 91

Figure 5.16 - Example of modelling joint mechanical soft limit for the hip joint. 93

Figure 5.17 - Detection of leg's gait phase, whether it is stance or swing, based on ball and heel contact sensors. The brown line below the biomechanical model represents the ground. Adapted from Geyer & Herr (2010)..... 94

Figure 5.18 - Occurrence of contact. Contact occurs if the CP (circles) falls below y_0 , which is the reference value. 95

Figure 5.19 - Relation between the capacity of the ground to restore its shape after impact: perfectly a) elastic and b) inelastic cases. F_y represents the vertical ground reaction force applied by the ground on the CP. 95

Figure 5.20 - Illustration of the interaction between horizontal ground reaction forces. Sliding changes to stiction if $x_{CP} < x_{lim}$. Stiction changes to sliding if $F_{x,st} \geq \mu_{st} F_y$. x_{st} is the stiction reference point, from this point on, sliding changes to stiction. 97

Figure 5.21 - General overview of the ground contact model implemented in Simulink. The model is an enabled subsystem (Contact Model), comprising two other similar subsystems to model stiction (Stiction Model) and sliding (Sliding Model), along with the vertical GRF. The contact sensor block enables the activation or not of the contact model subsystem, that is, if contact is detected (detection of contact is explained above and in Figure 5.18) this subsystem is activated to calculate its outputs, in this case, the GRF. The sliding and stiction enabled subsystems are also activated or not by means of the friction switch block. If, within this switch, stiction is detected, the stiction model is resolved, and the sliding model is disabled, and vice versa. 97

Figure 5.22 – a) Truth table and diagram of the NOR gate (Harris & Harris, 2012). b) Truth table of the SR Latch circuit. In the middle, there is the representation of this circuit with X and Y NOR gates, and on the right there is a simpler illustration of the circuit (Roth, 2004). 99

Figure 5.23 - Inside the friction switch subsystem. Stick and slide are inputs to the S-R circuit and Q and \bar{Q} are outputs. Q is connected to a terminator block and Q determines the output of S-R circuit. 99

Figure 6.1 - Types of children formation in the genetic algorithm. a) Elite child. b) Mutation child. c) Crossover child (adapted from MathWorks (2018b)). 105

Figure 6.2 - Restrictions implemented in Simulink® to perform optimization. a), b), c) d) and e) refer to the bullet points above. 108

Figure 6.3 - Illustration of the COM between two objects with different masses, m_1 and m_2 , separated by distances x_1 and x_2 111

Figure 6.4 – Position of the overall centre of mass of the biomechanical model. Three tested solvers are displayed. a) Forward position and b) vertical position of the overall COM. 111

Figure 6.5 – Vertical Ground Reaction Force normalized to percentage of body weight for walking movement. These graphs are normalized to percentage of gait cycle. The black vertical line marks the occurrence of toe off. a) Literature results obtained from Neumann (2013). Toe off occurs at 60.0% of

gait cycle. b) Biomechanical model's results (30Hz low-pass filtered). Toe off occurs at 59.6% of gait cycle. In this figure, it is displayed the mean \pm standard deviation. 114

Figure 6.6 – Hip joint angle, θ_h , for walking movement. These graphs are normalized to percentage of gait cycle. The black vertical line marks the occurrence of toe off. a) Literature results obtained from Neumann (2013). Toe off occurs at 60.0% of gait cycle. b) Biomechanical model's results. Toe off occurs at 59.6% of gait cycle. In this figure, it is displayed the mean \pm standard deviation. 117

Figure 6.7 – Knee joint angle, θ_k , for walking movement. These graphs are normalized to percentage of gait cycle. The black vertical line marks the occurrence of toe off. a) Literature results obtained from Neumann (2013). Toe off occurs at 60.0% of gait cycle. b) Biomechanical model's results. Toe off occurs at 59.6% of gait cycle. In this figure, it is displayed the mean \pm standard deviation. 118

Figure 6.8 – Ankle joint angle, θ_a , for walking movement. These graphs are normalized to percentage of gait cycle. The black vertical line marks the occurrence of toe off. a) Literature results obtained from Neumann (2013). Toe off occurs at 60.0% of gait cycle. b) Biomechanical model's results. Toe off occurs at 59.6% of gait cycle. In this figure, it is displayed the mean \pm standard deviation. 119

Figure 6.9 – Hip joint torque for walking movement. These graphs are normalized to percentage of gait cycle and to body mass. The black vertical line marks the occurrence of toe off. a) Literature results obtained from Neumann (2013). Toe off occurs at 60.0% of gait cycle. b) Biomechanical model's results. Toe off occurs at 59.6% of gait cycle. In this figure, it is displayed the mean \pm standard deviation. ... 121

Figure 6.10 - Knee joint torque for walking movement. These graphs are normalized to percentage of gait cycle and to body mass. The black vertical line marks the occurrence of toe off. a) Literature results obtained from Neumann (2013). Toe off occurs at 60.0% of gait cycle. b) Biomechanical model's results. Toe off occurs at 59.6% of gait cycle. In this figure, it is displayed the mean \pm standard deviation. ... 123

Figure 6.11 – Ankle joint torque for walking movement. These graphs are normalized to percentage of gait cycle and to body mass. The black vertical line marks the occurrence of toe off. a) Literature results obtained from Neumann (2013). Toe off occurs at 60.0% of gait cycle. b) Biomechanical model's results. Toe off occurs at 59.6% of gait cycle. In this figure, it is displayed the mean \pm standard deviation. ... 124

Figure 6.12 - Influence of the vertical contact stiffness, k_v , on the vertical ground reaction force. Results are normalized to % of body weight and to % of gait cycle..... 125

Figure 6.13 - Influence of the vertical ground relaxation speed, y_{max} , on the vertical ground reaction force. Results are normalized to % of body weight and to % of gait cycle..... 126

Figure 6.14 - Influence of 0.5 kN/m decreases of the vertical contact stiffness, k_v , on the vertical ground reaction force. Results are normalized to % of body weight (BW) and to % of gait cycle. Initial k_v value: 78.4kN/m..... 127

Figure 6.15 – Influence of 10 kN/m decreases of the vertical contact stiffness, k_v , on the vertical ground reaction force. Results are normalized to % of body weight (BW) and to % of gait cycle..... 127

Figure 6.16 - Influence of decreases of the vertical contact stiffness, k_v , from 20kN/m to 10kN/m, on the vertical ground reaction force. Results are normalized to % of body weight (BW) and to % of gait cycle. 129

Figure 6.17 - Comparison of vertical ground reaction force curves generated by different values of vertical contact stiffness. Initial value of 78.4 kN/m and tested values of 15, 13 and 12 kN/m. 130

Figure 6.18 – Graphs showing the comparison between joint angles and torques with a vertical contact stiffness of 78.4 kN/m and 15 kN/m. Results are normalized to % of gait cycle. a) Hip joint angle. b) Knee joint angle. c) Ankle joint angle. d) Hip joint torque. e) Knee joint torque. f) Ankle joint torque.. 131

Figure 6.19 – Comparison between the muscular activations of the seven muscles included in the biomechanical model. On each bullet point, the first figure that appears regards to literature, whilst the second regards to the biomechanical model’s result. Results are normalized to % of gait cycle. a) HFL - hip flexor muscle group is compared to the adductor longus muscle. b) GLU - gluteus muscle group is compared to the gluteus maximus muscle. c) HAM - biarticular hamstring muscle group is compared to the semimembranosus muscle. d) VAS - vasti lumped muscle group is compared to vastus lateralis muscle. e) GAS - biarticular gastrocnemius muscle. f) SOL - soleus muscle. g) TA - tibialis anterior muscle. See Chapter 2 for more information about the functions of these muscles. 134

Figure 6.20 – Anterior cruciate ligament (ACL) tear. 137

Figure 6.21 - Biomechanical model vertical ground reaction force normalized to % of body weight and to % of gait cycle (30Hz low-pass filtered). 142

Figure 6.22 – Healthy and pathological (ACL-reconstructed) kinematic results of the biomechanical model. These graphs are normalized to % of gait cycle. a) Hip joint angle. b) Knee joint angle. c) Ankle joint angle. 143

Figure 6.23 – Healthy and pathological (ACL-reconstructed) kinetic results of the biomechanical model. These graphs are normalized to % of gait cycle. a) Hip joint torque. b) Knee joint torque. c) Ankle joint torque. 144

Figure 6.24 – Comparison between healthy and pathological muscle activation patterns throughout one gait cycle. Results are normalized to % of gait cycle. a) HFL - hip flexor muscle group. b) GLU - gluteus

muscle group. c) HAM - biarticular hamstring muscle group. d) VAS - vasti lumped muscle group. e) GAS - biarticular gastrocnemius muscle. f) SOL - soleus muscle. g) TA - tibialis anterior muscle. See Chapter 2 for more information about the functions of these muscles. 147

Figure I.1 - Implementation of a sensor to measure the translation of Frame in the x, y and z axes in relation to the World Frame. 165

LIST OF TABLES

Table 2.1 - Description of the directional terms used in human anatomy to define the position of a body structure in relation to another. These terms are related to the cardinal planes. An X is used to determine the inclusion of the directional term when referring to a cardinal plane. Adapted from Hall (2012), Knudson (2007) and Oatis (2009)	9
Table 2.2 - Cardinal planes movements of the human body (Hall, 2012)	10
Table 2.3 - Types of synovial joints of the body. Adapted from Flores (2006), Neumann (2013), Openstax College (2013)	16
Table 2.4 - Joints comprised in the foot. Adapted from Ridola, Cappello, et al. (2007), Standring (2008)	22
Table 2.5 - Muscles that cross the hip joint and movement they produce according to their action (Neumann, 2013). TFL designates tensor faciae latae	25
Table 2.6 - Muscles that cross the knee joint and movement they produce (Neumann, 2013). Vastus group comprises the vastus intermedius, vastus lateralis and vastus medialis muscles. Quadriceps femoris muscle group comprises rectus femoris, vastus intermedius, vastus lateralis and vastus medialis muscles. Hamstrings muscle group comprises semimembranosus, semitendinosus and biceps femoris muscles	26
Table 2.7 - Muscles comprised in the foot are divided into extrinsic and intrinsic. Intrinsic muscles pertain only to the foot, while extrinsic muscles cross the ankle joint, pertaining to the foot and leg (Palastanga & Soames, 2012; Standring, 2008).....	27
Table 4.1 - Customer requirements for the biomechanical model	58
Table 4.2 - Technical specifications for the biomechanical model. In between parenthesis, there is the unit of the specification	59
Table 4.3 - Target or limit values for the technical specifications	61
Table 5.1 - Anthropometric parameters of the biomechanical model's segments (adapted from Geyer & Herr (2010)), including body geometry and physical properties. The body geometry parameters include the segments' length, width, thickness, radius and shape. The physical properties include the segments' mass and moments of inertia. Other parameters included in the table are the centre of mass distance and joint location, which are defined as the distance between the distal end of the segment being analysed and its COM or proximal joint, respectively	79
Table 5.2 - MTUs individual parameters. The MTU attachment parameters are the ones used by Geyer & Herr (2010), which were estimated from (Maganaris, 2001, 2003; Muraoka, Kawakami, et al., 2001;	

Oda, Kanehisa, et al., 2005) or from Geyer & Herr (2010) anatomical estimates. Muscle lever arm is represented by r_0 . The angle at which the muscle lever arm reaches its maximum is θ_{max} . The angle where $l_{MTU} = l_{opt} + l_{slack}$ is θ_{ref} , being the angle that corresponds to the muscle rest length. ρ is a factor that accounts for muscle's pennation angle, ensuring that the MTU's fibre length stays within physiological limits. Muscle parameters were estimated from Yamaguchi, Sawa, et al. (1990), being the ones used by Geyer & Herr (2010). The maximum isometric force, F_{max} , was estimated from individual or grouped muscle's physiological cross-sectional area. The maximum contraction speed, v_{max} , is set to 6 l_{opt}/s for slow twitch muscles and to 12 l_{opt}/s for fast twitch muscles. l_{opt} and l_{slack} correspond to CE's optimum fibre length and SE's slack length, respectively. All these parameters were taken from Geyer & Herr (2010) 87

Table 5.3 - Pre-Stimulation of each MTU	92
Table 6.1 – Solver, respective elapsed time and method used by Simulink® to resolve the model's dynamics	110
Table 6.2 - Error percentage between the assumed theoretical value, Ode15s, and the experimental values, Ode23t and Ode23tb, for forward and vertical COM position.....	112
Table 6.3 - Reference values for the parameters used in the sensitivity analysis	125
Table 6.4 - Quadriceps and Hamstrings muscle group strength (N.m/kg) deficits in the injured and uninjured leg after anterior cruciate ligament reconstruction and rehabilitation procedures (Thomas, Villwock, et al., 2013)	139
Table 6.5 - Quadriceps and hamstrings muscle groups test deficits results	141

NOMENCLATURE

2D – two dimensional	K – knee
3D – three dimensional	MTU – muscle-tendon unit
A – ankle	ODE – ordinary differential equation
ACh – acetylcholine	PCSA – physiological cross-sectional area
ACL – anterior cruciate ligament	PE – parallel elasticity element
B/F – base and follower frames	Q – quadriceps muscle group
BE – buffer elasticity element	QFD – quality function deployment
BMI – body mass index	R – reset
Ca ²⁺ - calcium ions	RAM – random access memory
CAD – computer aided design	ROM – range of motion
CE – contractile element	S – set
COM – centre of mass	SE – series elasticity element
COR – centre of rotation	SOL – Soleus muscle
CP – contact point	TA – Tibialis anterior muscle
CPG – central pattern generator	TFL – tensor fasciae latae
CSA – cross-sectional area	VAS – vasti lumped muscle group
DOF – degrees of freedom	W – world frame
EMG – electromyography	
fDOF – functional degrees of freedom	<u>Parameters</u>
FEM – finite element method	μ_{sl} – sliding friction coefficient
GA – genetic algorithm	μ_{st} – stiction friction coefficient
GAS – biarticular gastrocnemius muscle	τ_{MTU} – MTU torque
GLU – gluteus muscle group	τ – muscle torque
GRF – ground reaction forces	τ_{ecc} – time constant of the excitation-contraction coupling
H – hamstrings muscle group	τ_{cmd} – sum of the torques commanded by the neuromuscular swing control
H – hip	τ_{limit} – the sum of torques produced by the model's mechanical hard stops
HAM – biarticular hamstring muscle group	
HAT – head, arms and trunk	
HFL – hip flexor muscle group	
HoQ – house of quality	

τ_{penalty} – penalty torque	ρ – factor that accounts for muscle pennation angles
Δy_{ref} – ground penetration at which	a – pennation angle
Δy_{CP} – ground penetration	γ – application angle
Δt_{tm} – signal propagation time delay	ω – width of the bell-shaped $f(l_{\text{CE}})$
Δl_{MTU} – variation of MTU length	ϵ_{SE} – tendon strain
Δx_{CP} – variation of CP's horizontal position	ϵ_{ref} – reference strain with $f_{\text{SE}}(\epsilon)=1$
Δx_{CP} velocity– CP's velocity normalized to	ϵ_{PE} – PE reference strain
Δ – weak (3)	ϵ_{BE} – BE reference compression
\ominus – strong (9)	a – shortening heat constant
\bigcirc – medium (6)	$A_{0,\text{MTU}}$ – MTU pre-activation state
– none (0)	A_{MTU} – muscle activation
\uparrow – higher better	b – absolute rate of energy liberation constant
\downarrow – lower better	c – residual force factor
\diamond – nominal	d – distance between the muscle's attachment to bone and the joint's COR
$+$ – positive correlation	$\frac{dA_{\text{MTU}}(t)}{dt}$ – rate of change in muscle activation
$-$ – negative correlation	F – load or force
θ – joint angle	$f_0(x)$ – objective function
θ_{max} – joint angle at which r_{MTU} reaches its maximum	F_{BE} – BE's produced force
θ_{H} – biomechanical model's hip joint angle	F_{CE} – CE's produced force
θ_{K} – biomechanical model's knee joint angle	F_{Fibres} – muscle fibres force
θ_{A} – biomechanical model's ankle joint angle	$f_i(x)$ – constraints to the objective function with limits $b_i, i=1, \dots, m$
θ_{max} – joint angle at which r_{MTU} reaches its maximum	$f_i(\Delta y_{\text{CP}})$ – vertical ground reaction force force-length relation
$\theta_{\text{UpperLimit}}$ – overextension angle	$f_i(\Delta \dot{y}_{\text{CP}})$ – vertical ground reaction force force-velocity relation
$\dot{\theta}$ – angular velocity	$f(l_{\text{BE}})$ – BE's force-length relation
θ_{ref} – joint angle at which $l_{\text{MTU}} = l_{\text{opt}} + l_{\text{slack}}$	
k_{q} – soft limit stiffness	

$f(l_{CE})$ – CE's force-length relation
 $f(l_{PE})$ – PE's force-length relation
 $f(l_{SE})$ – SE's force-length relation (general models, chapter 3, section 3.5)
 F_{max} – maximum isometric force
 F_{MTU} – MTU force
 F_{Muscle} – muscle force
 F_{PE} – PE's produced force
 F_{Quad} – force produced by the quadriceps muscle group
 F_{SE} – SE's produced force
 $f_{SE}(\epsilon)$ – SE's force-length relation (biomechanical model)
 F_{Tendon} – tendon force
 $f_v(v_{CE})$ – CE's force-velocity relation
 $F_{x,sl}$ – horizontal ground reaction force (sliding)
 $F_{x,sl}$ – sliding force
 $F_{x,st}$ – horizontal ground reaction force (stiction)
 $F_{x,st}$ – stiction force
 F_y – vertical ground reaction force
 g – gravitational acceleration
 G_{MTU} – MTU's gain factor
 K – curvature constant of CE's $f_v(v_{CE})$ with $v_{CE} < 0$
 k_x – horizontal ground stiffness
 k_y – vertical ground stiffness
 l – muscle length
 l_{CE} – Contractile element length
 l_{min} – BE rest length
 l_{MTU} – Muscle Tendon Unit Length
 l_{opt} – Contractile element or sarcomere optimum length
 l_{slack} – Series Elastic Element or tendon slack length
 m – biomechanical model's mass
 N – CE's force-velocity relation eccentric force enhancement
 P_{MTU} – MTU muscle force or length reflex signal
 r – muscle moment arm
 r_0 – constant lever arm
 r_{MTU} – MTU lever arm
 $S_{0,MTU}$ – MTU's pre-stimulation
 S_{MTU} – muscle stimulation
 T – tension
 T_0 – isometric tetanus
 v – muscle's shortening velocity
 v_{CE} – CE's velocity
 v_{max} – muscle's maximum contraction velocity
 v_{x0} – biomechanical model's initial velocity
 W_m – metabolic energy consumption of the biomechanical model muscles'
 x – biomechanical model's distance travelled over the simulation time.
 x^* – optimal or a solution of the optimization problem
 x_0 – integrator initial condition
 x_{cm} – system's overall centre of mass
 x_{CP} – CP's horizontal position
 \dot{x}_{CP} – CP's horizontal velocity

x_{HAT} – forward position travelled by the HAT

x_{lim} – minimum CP's speed below which sliding switches to stiction

x_{st} – point at which stiction engages (horizontal reference point)

y_0 –ground contact model vertical reference value

y_{CP} – CP's vertical position

\dot{y}_{CP} – CP's vertical velocity

\dot{y}_{max} – maximum ground relaxation speed

1. INTRODUCTION

This chapter provides a general overview of the themes approached in the present dissertation. In the first section, the motivation to develop this work is approached, followed by the description of the scope and objectives to be achieved over its course. The organization of this dissertation, including a brief description of the content present within each chapter, is provided in the subsequent section, followed by the explanation of the contributions it aims at providing.

1.1. Motivation

According to Knudson (2007), biomechanics comprises the study and analysis of the movement performed by living beings. This study is done by means of the application of mechanics' principles and laws, which are concerned with the description of motion and its causes, namely forces acting on the bodies. Essentially, biomechanics provides the tools necessary for understanding how living beings produce their movement.

Biomechanics is applied to the study of human motion whether by improving its performance or by preventing and treating injury. The former is extensively applied to understanding sports and to help athletes perform a movement in which technique is the dominant factor, rather than anatomical structure. The improvement of human performance is also related to the design of the equipment used by the athletes, as well as their composing materials. This field of biomechanics, therefore, deals with the research associated, not only with the enhancement of the performance of a certain athletic movement, but also with all kinds of equipment used in sports, which is conducted in biomechanics labs (Knudson, 2007).

The latter field of application of biomechanics is much more widely researched than the one related with sports performance. In order to help preventing and treating injury, caused for instance by overuse of joints or other anatomical structures, biomechanics aims at providing knowledge on the mechanical properties of human tissues, on the mechanical loads they feel during human movement, and on therapies related to injury prevention and rehabilitation. To this end, biomechanics acts in order to help design rehabilitation tasks and assistive medical devices to improve patients' quality of life (Knudson, 2007).

Even though these are two distinct fields of application of biomechanics, they are intrinsically connected since understanding injury prevention and rehabilitation is a major variable influencing the ability of improving an athlete's performance. Therefore, the studies related to biomechanics and sport medicine may help prevent the occurrence of injuries by the development of prevention strategies, and, in case of injury occurrence, biomechanics aids in developing rehabilitation strategies and assistive medical devices to help restore the function of the affected anatomical structure, as previously referred (Knudson, 2007).

The field of biomechanics uses biomechanical models to study human motion during physiological and/or pathological scenarios, analysing its movements and estimating muscular and joint forces, as well

as external forces acting on the body. These biomechanical models aim at analysing athletic performance, optimizing sports equipment, studying ergonomics related with comfort, analysing gait and diagnosing pathologies and analysing vehicle safety. To this end, the simulation of human motion with the use of computational techniques requires the implementation of the previously referred biomechanical models, being essentially mathematical representations that aim at correctly describing the behaviour of the human body and its interaction with the surrounding environment by applying laws of mechanics (Tavares da Silva, 2003).

This work comprises the use of a biomechanical model of the human lower limb previously developed by Geyer & Herr (2010). The model possesses the emulation of the human skeletal, muscular and neural systems in order to produce its movement. This approach was used to study the events occurring at joint level, regarding, for instance, its range of motion and produced torques, during physiological and anterior cruciate ligament (ACL) deficient pathological gait. This gait pathology is related to activities, such as basketball, involving rapid changes in direction combined with acceleration/deceleration of the body. These actions cause ACL injuries and sometimes lead to its rupture (Hall, 2012; Neumann, 2013; Standing, 2008).

1.2. Scope and Objectives

The knee joint comprises movements necessary for healthy human locomotion. The location of this joint between the long bones of the lower extremity, combined with its weight-bearing and locomotion functions, makes this joint susceptible to injury. Knee pathologies are very common and can occur in people of all ages, interfering with activities of the daily life (Hall, 2012; Reid, Bush, et al., 2010).

The anterior cruciate ligament (ACL) tear is a traumatic knee injury and most patients suffering from it lack dynamic joint stability, which makes it difficult to perform daily life activities. The key to restoring normal movement lies with re-training and restoring strength in the muscles affected by the injury (Gardinier, Manal, et al., 2012). This knee joint injury restricts in several levels the patient's life, making the development of more effective strategies to address and improve muscle weakness around the joint very important to improve patient's rehabilitation and return to daily life activities.

As mentioned in the previous section, biomechanics may help in the development of prevention and rehabilitation strategies to improve human's life quality when the patient is affected by some kind of injury. Therefore, the purpose of this work is to use a computational biomechanical model of the lower limb equipped with the muscles of the human muscular system that produce movement in the sagittal

plane, in order to study human walking dynamics in healthy and pathological cases. This strategy aims to, in the future, aid in the development of more efficient rehabilitation strategies to be prescribed after an ACL rupture.

The approach begins with the development of a biomechanical model representing a healthy patient. From this point, pathology is modelled by adjusting the parameters that enable the mimicking of the dynamics and kinematics of patients after an ACL reconstruction.

To this end, the specific objectives of this work are the following:

- To comprehend the anatomy and biomechanics of the human lower limb;
- To comprehend the anatomy, structure and modelling approached of the muscles;
- To define requirements and specifications for the biomechanical model;
- To develop a lower limb biomechanical model;
- To validate the adopted solution.

The final developed biomechanical model must be capable of presenting muscle activations, joint motion and torques similar to the state of the human body the model is representing, whether it is healthy or pathological.

1.3. Organization of the Dissertation

The present dissertation is divided into seven chapters, namely Introduction, Human Lower Limb: Anatomy and Function, Muscle-Tendon Unit, Requirements for the Biomechanical Model Utilized, Biomechanical Model Developed, Implementation and Validation and Concluding Remarks.

The first chapter comprises the description of the motivation and scope, as well as the objectives related to the development of the dissertation. A general overview of the organization of this work is also provided, terminating with the explanation of the contributions of the work developed.

Chapter 2 is called “Human Lower Limb: Anatomy and Function” and comprises an overview of the anatomy of the lower limb, which involves all the structures going from the pelvic girdle until the foot, inclusive. Firstly, it is explained the terminology associated with human movement, since it is of utmost importance to the understanding of this dissertation. After establishing the nomenclature used throughout this work, the anatomy of the human lower limb is presented, including a description of the skeletal, the articular and the muscular systems.

“Muscle-Tendon Unit” is the name given to the third chapter and involves a detailed understanding of the structures comprised within a muscle-tendon unit (MTU), their behaviour and how to computationally model them. An MTU comprises all the structures of the muscle belly and its tendinous attachments at both of its ends. The cascade of processes involved in the production of joint motion is explained, followed by an understanding of the factors affecting the force generated by an MTU, namely its length and velocity of contraction. The chapter continues with a description of the elements used to model a muscle-tendon unit in computational mechanics, based on all the explanations given throughout the entire chapter.

Chapter 4 comprises one of the specific objectives of this dissertation, namely the definition of requirements for the biomechanical model. Considering its content, the chapter is named “Requirements for the Biomechanical Model Utilized”. It presents the methodology applied, which is called Quality Function Deployment (QFD). QFD comprises four phases, it follows that only one of them was used, the House of Quality, involving the determination of the customer requirements for the biomechanical model under development, which are then translated into technical specifications. All the parameters approached to develop this phase of QFD are explained in this chapter and a critical analysis is performed at the end.

The following chapter comprises a description of the biomechanical model utilized in this work and is called “Biomechanical Model Developed”. The model used is based on the one developed by Geyer & Herr (2010) and relates neural signals to Hill-type muscle models, which in turn produce joint torques that promote the model’s movement. The construction of the model comprises modules, involving the construction of its segments and joints, the modelling of its muscle-tendon unit dynamics, comprising the calculation of the overall joint torque produced by the MTUs around that joint, and modelling of MTU stimulations and activations. This implementation is explained throughout the chapter.

Chapter 6 is called “Implementation and Validation” and comprises a description of the strategies implemented to make the biomechanical model present healthy and pathological conditions. Firstly, an optimization problem was resolved, whose aim was to encounter a set of optimal parameters that made the model produce a natural gait with the minimum metabolic cost spent. After this, the determination of the solver to be used in the simulation of the walking model was performed. Besides these model preparation strategies, this chapter also comprises the demonstration of the obtained results, as well as their discussion. This demonstration is done either for the healthy and for the pathological cases.

Chapter 7 summarizes the main conclusions drawn out of the present dissertation and provides some recommendations for future developments.

1.4. Contribution of the Work

This dissertation contributes mainly to the area of biomechanical computer simulations aiming at improving patient's quality of life after injury. Specifically, it promotes the application of a biomechanical model to study the kinematics and dynamics of physiological walking gait, introducing then the analysis of the same variables to a model modified to mimic a knee pathology, in this case, the anterior cruciate ligament tear after surgical reconstruction.

Before providing an understanding of how physiological human walking is achieved in level ground, this dissertation also intends to find contributions in the field of customer requirements and technical specifications regarding the biomechanical model. This aims at providing the reader with a more conscious knowledge of what the user needs the biomechanical model to be incorporated with for their simulation studies. After understanding the requirements that must be implemented in the model, whether being expressly related to the customer or with the associated technical specifications, in order to satisfy the user, the biomechanical model's physiological walking kinematics and kinetics are analysed and then pathology is introduced.

By introducing pathology to the biomechanical model utilized, this dissertation aims at providing a more detailed understanding about the analysed knee pathology. With the acquisition of this knowledge, it is expected that this work might contribute to the perception of the mechanisms underlying pathological gait, providing a better insight into possible and new rehabilitation strategies to be used in restoring the patients' knee function after ACL rupture or reconstruction.

2. HUMAN LOWER LIMB: ANATOMY AND FUNCTION

In the present chapter, an overview of the anatomy of the lower limb is presented. The human lower limb comprises all the structures that run from the pelvic girdle until the foot, inclusive. The chapter begins with a section whose aim is to explain the terminology associated with human movement, being the one used throughout the entire dissertation.

After establishing the nomenclature, the anatomy of the lower limb is explained, being divided into three sections. The first one explains the bony structures that comprise this part of the human body, as well as the ligaments that connect those bones. To this set of structures it is given the name of skeletal system. After this section, the articular system is approached in which the three major articulations of the lower limb, namely hip, knee and ankle, are described in detail, including the movements they enable the human body to perform. The ending part of the chapter is associated with the exposure of the musculature of the lower limb, divided into four main parts, being gluteal and iliac regions, thigh, leg and foot. Finally, a summary and discussion of the themes approached is carried out.

The main aim of this chapter is to provide the reader with a set of anatomical terms that allow him/her to become acquainted with the nomenclature used in the field of investigation in which this dissertation is included. Besides this aim, it is also desirable that the reader interiorizes the anatomical structures that compose the human lower limb in order to understand the work developed in this dissertation.

2.1. Basic Terminology of Human Movement

To understand the basic terminology of human movement, it is essential to possess knowledge of human anatomy. This field comprises the study of the human body's structure, providing designations for structures and joint motions relevant to human movement (Knudson, 2007; Standring, 2008).

According to Standring (2008), the anatomical descriptions are performed assuming that the human body is in the anatomical reference position. As seen in Figure 2.1, this reference position is characterized by the body standing erect and facing forwards, with the feet slightly separated, with the toes facing forward, and the arms hanging relaxed at the sides of the body, with the palms facing forward. This is not a natural standing position, however, it is the orientation of the human body conventionally used to describe human movement (Hall, 2012; Standring, 2008).

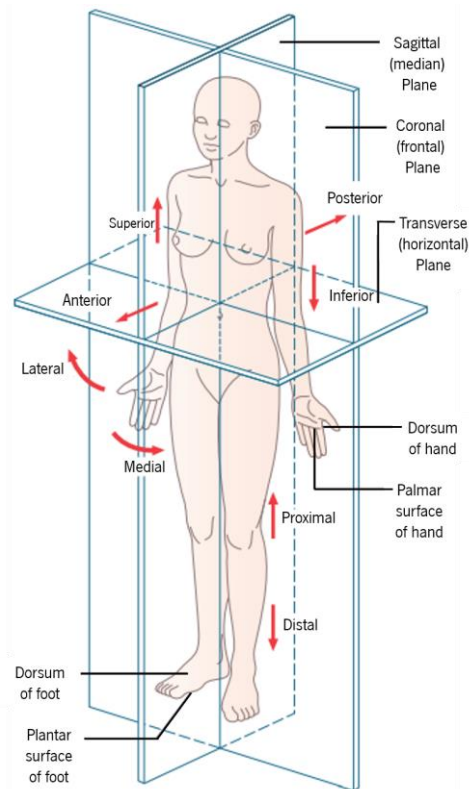


Figure 2.1 – Anatomical reference position used to describe human movement. To facilitate this description, the human body is sectioned by three planes: frontal, sagittal and transverse. The directional terms are also represented: anterior-posterior, medial-lateral, superior-inferior and proximal-distal. Adapted from Palastanga & Soames (2012).

Figure 2.1 also comprises the three imaginary anatomical planes utilized to perform a three-dimensional analysis of human motion. These are also referred to as cardinal planes, namely frontal or coronal, sagittal or median and transverse or horizontal planes. They are composed by anatomically aligned axes, being superior/inferior and medial/lateral, superior/inferior and posterior/anterior, and

posterior/anterior and medial/lateral, used for the frontal, sagittal and transverse planes, respectively. Regarding the anatomical reference position, the three anatomical cardinal planes all intersect at a single point, which is known as the human body's centre of mass (Hall, 2012; Standring, 2008).

In addition to this description of using planes and axes, anatomy also uses several directional terms when describing the position of a body structure in respect to another (Hall, 2012; Oatis, 2009). Some of these terms are related to the anatomical axes. Table 2.1 comprises the description of these directional terms, as well as which of them are used when referring to the cardinal planes.

Table 2.1 - Description of the directional terms used in human anatomy to define the position of a body structure in relation to another. These terms are related to the cardinal planes. An X is used to determine the inclusion of the directional term when referring to a cardinal plane. Adapted from Hall (2012), Knudson (2007) and Oatis (2009)

Directional Terms		Cardinal Planes		
Name	Description	Frontal	Sagittal	Transverse
Superior	Structures closer to the head.	X	X	
Inferior	Structures away from the head and closer to the feet.	X	X	
Anterior	Structures towards the front of the body.		X	X
Posterior	Structures towards the back of the body.		X	X
Medial	Structures towards the midline of the body.	X		X
Lateral	Structures away from the midline of the body.	X		X
Proximal	Structures closer to the proximity of the trunk.	X	X	X
Distal	Structures at a distance from the trunk.	X	X	X

The human body is composed by many anatomical segments. Considering their location, they may be referred to as pertaining to the upper or lower extremity. These designations are related to the above-mentioned medial plane. If this plane is located at the pelvic girdle, the part of the human body above and below this plane is considered upper and lower extremity, respectively. Both legs are considered lower limbs and the arms are referred to as upper limbs.

When the human body is positioned as in Figure 2.1, all body segments are considered to be arranged in a position corresponding to zero degrees. Rotation of any segment in relation to that reference anatomical position is referred to according to the direction of motion and is measured as the angle formed between the body's actual position and the reference one (Hall, 2012). Table 2.2 contains a description of the human body's movements performed in each of the three cardinal planes.

Table 2.2 - Cardinal planes movements of the human body (Hall, 2012)

Sagittal Plane	Flexion	Decrease in joint angle. E.g. posterior rotation of the leg.
	Extension	Increase in joint angle. E.g. anterior rotation of the leg.
	Plantarflexion	Motion bringing the top of the foot away from the leg.
	Dorsiflexion	Motion bringing the top of the foot towards the leg.
Frontal Plane	Adduction	Motion bringing a segment closer to the midline of the body.
	Abduction	Motion bringing a segment away from the midline of the body.
	Lateral Flexion	Sideway rotation of the trunk.
	Elevation	Motion of the shoulder girdle in the superior direction.
	Depression	Motion of the shoulder girdle in the inferior direction.
	Radial Deviation	Rotation of the hand at the wrist in the frontal plane toward the radius.
	Ulnar Deviation	Rotation of the hand at the wrist in the frontal plane toward the ulna.
	Eversion	Outward rotation of the foot.
	Inversion	Inward rotation of the foot.
	Transverse Plane	Left/Right Rotation
Medial Rotation		Movement of a limb as a unit. Rotation towards the midline of the body.
Lateral Rotation		Movement of a limb as a unit. Rotation away from the midline of the body.
Supination		Outward rotations of the forearm.
Pronation		Inward rotations of the forearm.
Horizontal abduction		When the arm or the thigh is flexed, the movement from an anterior position to a lateral position.
Horizontal adduction		When the arm or the thigh is flexed, the movement from a lateral position to an anterior position.

In order to be able to perform these movements, the human body is provided with a set of joints or articulations that enable the relative motion between segments. These joints connect the bones that comprise the human skeleton (Gray, 1918). The human body has the capacity of executing a wide variety of movements, each of which involve several joints that all together enable the production of a particular motion (Flores, 2006).

The number of degrees of freedom (DOFs) is a very important property of a system when analysing its movement and is defined as the minimum number of independent coordinates required to describe a

system's position and configuration (Flores, 2006; Li, 2006). These DOFs describe all the movements performed by the human body or any of its structures. For instance, on one hand, a two-dimensional (2D) point mass model has two DOFs, since its motion is completely described by a horizontal and a vertical translation/coordinate. On the other hand, the three dimensional (3D) motion of a body has six DOFs, including three linear (translations) and three angular (rotations) coordinates (Knudson, 2007). In the human body, these three translations and rotations can be referred to as the movement along the three cardinal planes and rotation about the three axes, respectively. Considering this explanation, a segment in the human body has a maximum of six DOFs. However, most segments cannot achieve all these six, since the number of DOFs a joint possesses is related to its structure, which introduces constraints, and corresponds to the total number of movements it can perform (Spaulding, 2005).

The interrelated movement of the joints in the human body produce its motion during everyday tasks, such as walking or writing. Since this work is related to the computational modelling of the lower limb, the gait cycle is approached next. The lower limb comprises two main functions, namely to provide a stable base of support in standing and to propel the human body throughout gait (Dutton, 2016; Standing, 2008). Gait is a cyclical movement and normal locomotion is composed by a set of repeated gait cycles. One gait cycle is defined as the movement beginning and ending with ground contact of the same foot (Oatis, 2009). Figure 2.2 illustrates the gait cycle with the corresponding events and phases.

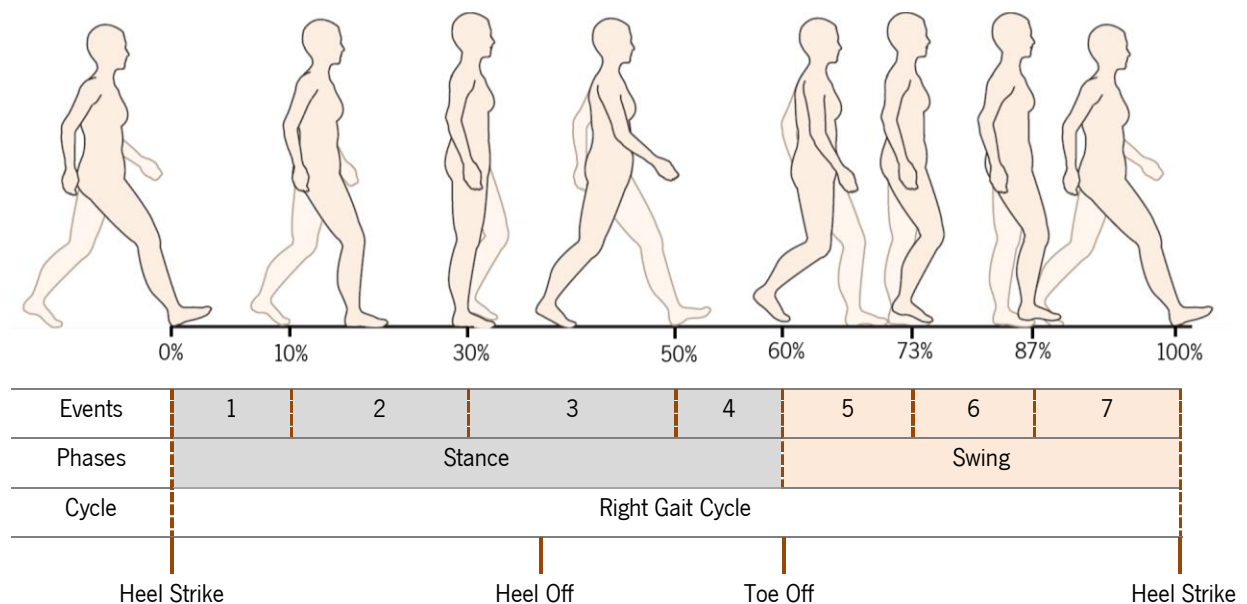


Figure 2.2 - Illustration of the gait cycle with the corresponding events and phases. The events and phases correspond to the leg in analysis in the gait cycle, which in this case is the more shaded one (right leg). 1 – Loading response; 2 – Midstance; 3 – Terminal stance; 4 – Preswing; 5 – Initial swing; 6 – Midswing; 7 – Terminal swing. Adapted from Neumann (2013).

Overall, the gait cycle is divided in two phases: stance and swing. In between these two phases of gait, seven events occur: loading response, midstance, terminal stance, preswing, initial swing, midswing and terminal swing. This cycle initializes with the stance phase, which extends to 60% of gait cycle, when it transitions to the swing phase, occurring until the end. The gait cycle of the right limb is slightly out of phase when compared to the left limb. When the right initial contact between the foot and the ground occurs in the beginning of the stance phase, the left limb is just ending its stance phase. Due to this offset between limbs, there are two periods in which the limbs are in contact with the ground. The single support task is characterized by only one foot being in contact with the ground and the double support task occurs when both limbs are in contact with the ground at the same time (Dutton, 2016; Oatis, 2009).

The stance phase of gait is characterized by the foot being in contact with the ground and the corresponding limb bearing weight. This phase begins with the initial contact between the foot and the ground, which occurs at the heel, corresponding to the heel strike. Immediately after initial contact, the first gait event occurs, namely the loading response. During this event the foot flattens on the ground and the body weight is transferred to the limb in stance. This event terminates at 10% of gait cycle, initializing the midstance, characterized by the beginning of the single support in which the contralateral leg leaves the ground. During this event, the trunk tends to glide over the foot, which is fixed on the ground. The terminal stance initiates when there is the occurrence of heel off, meaning that the heel lifts off the ground, and ends when the contralateral leg becomes in contact with the ground, supporting the body weight. The final event of stance is preswing, occurring between 50%-60% gait cycle and ends with toe off, that is, the toes of the stance limb lift off the ground (Dutton, 2016; Neumann, 2013; Oatis, 2009).

During the stance phase of gait, the foot is always in contact with the ground and therefore there is the development of forces between these two bodies in contact. The forces applied to the ground by the foot are called foot forces and, on the contrary, forces with the same magnitude but opposite direction are the ones applied to the foot by the ground, which are called ground reaction forces (GRF). There are three components of these forces: vertical, anterior-posterior and medial-lateral (Neumann, 2013).

The swing phase of gait cycle begins with the initial swing event, being characterized by the quick withdrawal of the limb from the ground. Midswing is the period in which the swing limb passes the stance limb. Terminal swing is the final phase of the gait cycle and consists on the period in which the swing limb goes towards the ground, preparing for ground contact that occurs when a new heel strike occurs. During the swing phase, no ground reaction forces exist since the foot is off the ground and no contact exists between the two bodies (Dutton, 2016; Neumann, 2013; Oatis, 2009).

2.2. Skeletal System

The human body comprises an internal framework named skeleton, which is composed by a series of bones. This internal framework can be divided into the appendicular skeleton and the axial skeleton. The latter comprises the vertebral column, the skull, the rib cage and other associated bones, and the appendicular skeleton is attached to the axial one, comprising the upper and lower limbs (Gray, 1918).

The adult skeleton is mostly constituted by a hard, connective tissue named bone or osseous tissue. In areas of the human skeleton where bones move in relation to each other, a semi-rigid form of connective tissue, named cartilage, exists to provide flexibility and an easier and smoother surface for movement. The skeletal system comprises these two types of connective tissues, and its main functions are to provide support of the body, facilitate the body's movement, store and release minerals and fat, endocrine regulation, produce blood cells and protect the internal organs (Openstax College, 2013).

The pelvic girdle enables the connection of the vertebral column to the lower limb, which comprises the thigh, the leg, the foot and the pelvic girdle. The part of the skeletal system that involves the lower limb is formed by the three fused bones of the pelvic girdle (ischium, ilium and pubis), the bones of the thigh (femur and patella), leg (tibia and fibula) and foot (tarsus, metatarsus and phalanges) (Standring, 2008). Figure 2.3 shows the anterior, lateral and posterior views of the right lower limb.

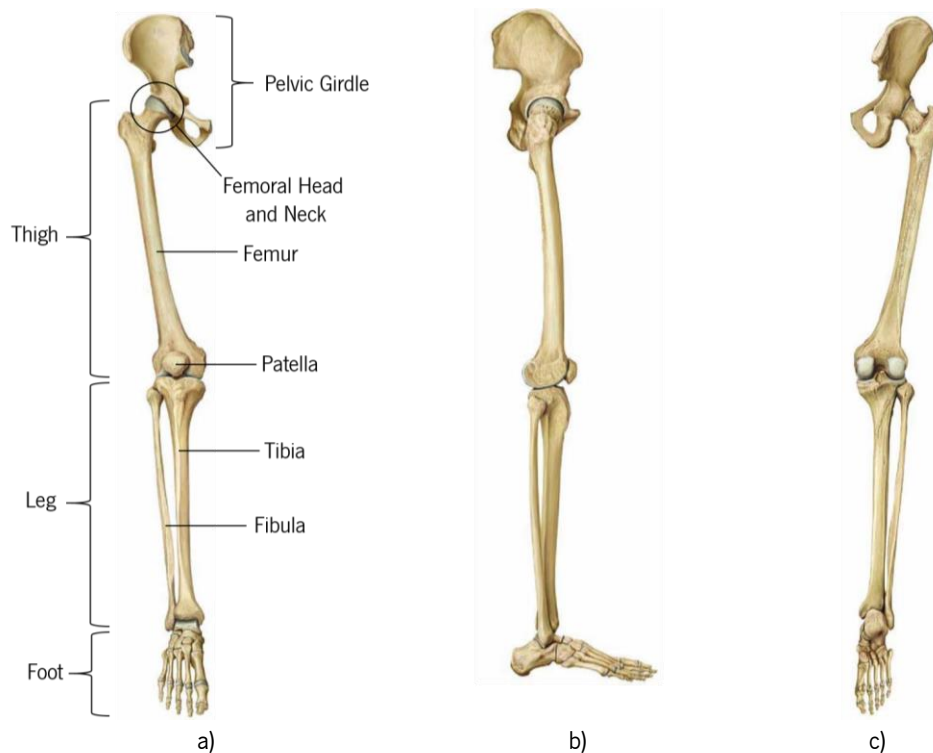


Figure 2.3 – a) Anterior, b) lateral and c) posterior views of the bones comprising the right lower limb. Adapted from Schuenke, Schulte, et al. (2009).

As previously explained, the pelvic girdle is formed by the fusion of three bones, namely ilium, ischium and pubis. The region in which these three bones fuse is called the acetabulum, which articulates with the head of the femur (Standring, 2008). Figure 2.4a shows an illustration of the bones that form the pelvic girdle, as well as the location of the acetabulum.

The femur is the longest bone in the human body, being associated with the body weight and muscular forces it is required to withstand. The femoral neck, a medial extension of the proximal femoral shaft, is connected to a rounded, articular structure, named femoral head (Figure 2.3a). The distal extremity of the femoral shaft is wider, presenting an asymmetric double condyle (condylus lateralis femoris and condylus medialis femoris) that articulates with the tibia, enabling the transmission of weight to this bone. Anteriorly, the condyles are confluent and continue into the shaft, and posteriorly they are separated by the intercondylar fossa (fossa intercondylaris) (Callaghan, Rosenberg, et al., 2003; Rodriguez-Merchan & Oussedik, 2015; Schuenke, Schulte, et al., 2009; Standring, 2008).

The proximal surface of the tibia is composed by condyles (condylus lateralis tibiae and condylus medialis tibiae), enabling the articulation with the distal femur, as referred previously. The tibia lies medial to the fibula. This bone is slenderer than the tibia and is not directly involved in transmission of weight, as the femur and tibia are. The patella is a sesamoid bone, which means that it is embedded within a tendon, named tendon of quadriceps femoris, anterior to the distal femur. It articulates with the femoral intercondylar fossa, forming the patellofemoral compartment. Its function is to protect the front of the knee and increase leverage for the quadriceps femoris tendon (Margo, Radnay, et al., 2010; Rodriguez-Merchan & Oussedik, 2015; Schuenke, Schulte, et al., 2009; Standring, 2008). Figure 2.4b and c illustrate the analysed bones and structures, pertaining both to the thigh and leg.

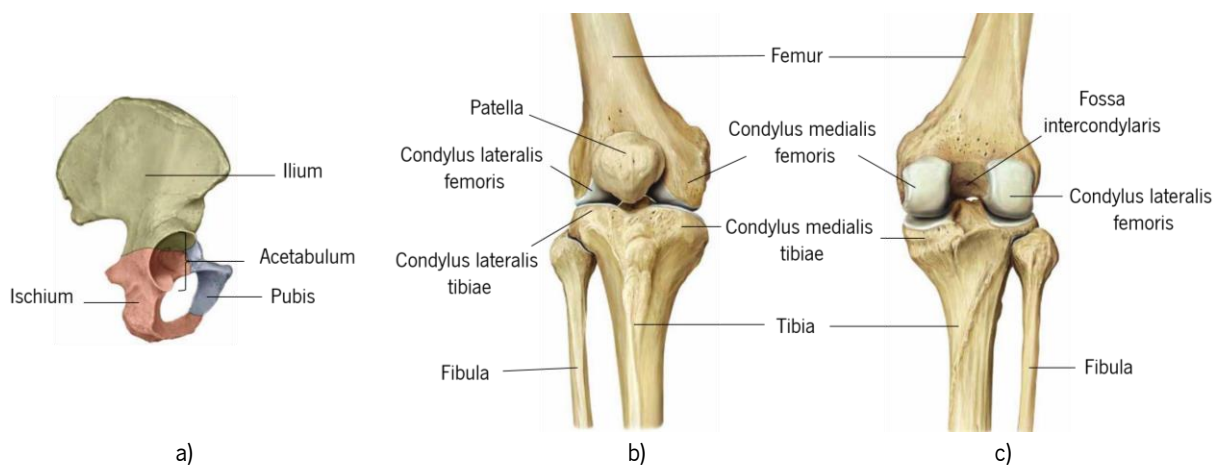


Figure 2.4 - Bony structures of the right a) lateral pelvic girdle and b)/c) anterior and posterior, respectively, thigh and leg. Adapted from Schuenke, Schulte, et al. (2009).

On the distal end of the tibia and fibula, there is the foot. It is a complex structure of the human body, being the only one that is in regular contact with the ground. It comprises three major bone groups, namely, the tarsus, metatarsus and phalanges, as seen in Figure 2.5. The first one is the more posteriorly located on the foot, while the others are located progressively more anteriorly. The tarsus and metatarsus effectively comprise the foot, whereas the toes are formed by the phalanges (Palastanga & Soames, 2012; Standing, 2008).

The tarsus bone group comprise seven irregular bones. One of the bones is the calcaneus, that projects posteriorly on the foot, forming the prominence of the heel. The other six bones are the talus, which transmits the body weight from the tibia to the calcaneus, the navicular, the cuboid and three cuneiform bones, namely medial, intermediate and lateral cuneiform. There are five different metatarsal bones. They do not have specific names, being numbered from one to five with roman numerals, from the medial side of the foot (side of the great toe). The phalanges are the constituents of the toes. There are two of them in the great toe (proximal and distal), while the remaining toes comprise three phalanges each (proximal, middle and distal) (Palastanga & Soames, 2012).

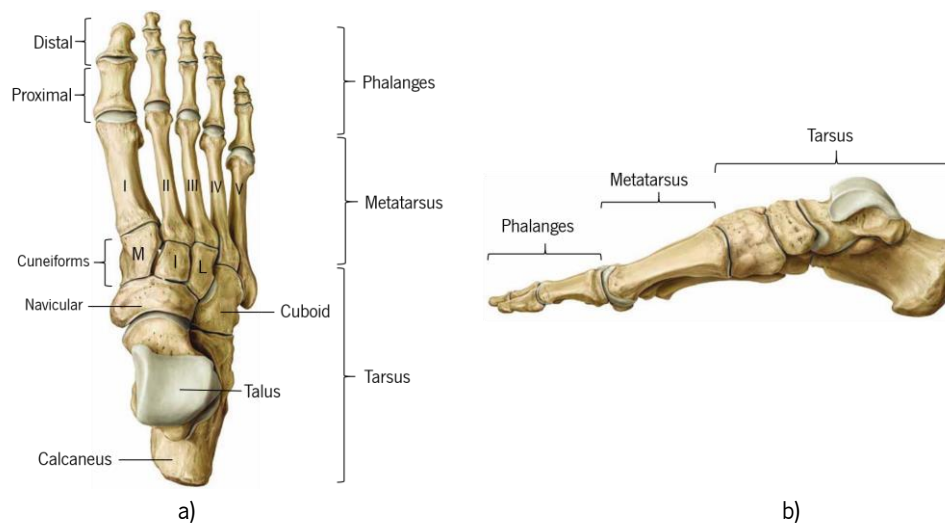


Figure 2.5 – Illustration of the bones of the right human foot. This body segment is divided into tarsus, metatarsus and phalanges. a) Superior view. M, L and I the represent medial, intermediate and lateral cuneiform bones b) Medial view. Adapted from Schuenke, Schulte, et al. (2009).

2.3. Articular System

The articular system comprises all the joints or articulations pertaining to the human body. A joint is formed when the bones of the skeleton are joined to one another, and it is through these structures that movement of the human body occurs. However, as previously explained, the type and range of motion allowed by each joint is determined by its structure and function (Openstax College, 2013).

In terms of function, the human joints can be classified as synarthroses, amphiarthroses and diarthroses, with increasing mobility from the former to the latter. The first include all the articulations in which the surfaces of the bones are in almost direct contact. These are immobile or nearly immobile joints, providing a solid union between the articulating the bones. These joints are found in between the bones of the skull. Amphiarthroses include joints in which the surfaces of the bones are connected to each other by hyaline cartilage or fibrocartilage, such as in the vertebrae. These joints possess limited motion. Finally, in diarthroses joints, the contiguous surfaces of the bones are covered with articular cartilage and a synovial membrane, being the most common joint in the human body. They are freely movable joints and there is no direct connection between the articular surfaces of the bones forming the joint. This type of joint is found on the knee. This functional classification of joints is based on the amount of mobility it enables (Gray, 1918; Openstax College, 2013; Standring, 2008).

The joints present in the human body can also be classified based on their structure as fibrous, where the bones are connected by fibrous connective tissue, cartilaginous, where the bones are joined by hyaline cartilage, or synovial joints, where the articulating surfaces of the bones are not directly connected. A synovial joint is characterized by being a low-friction, low-wear load bearing system in which it is verified the presence of a cavity within which the bones articulate with each other. The presence of articular cartilage at a synovial joint prevents the occurrence of friction between the bones once it covers the entire articulating surface of each bone. Delimiting the inner surface of the articular capsule is a thin synovial membrane, whose cells secrete synovial fluid that provides lubrication to further reduce the friction between the bones. Outside of the articulating surface, the bones are connected by ligaments (fibrous bands that span two or more bones, being critical to the static stability of articulations), tendons and muscles providing strength, support and allowing normal movements (Blewis, 2008; Callaghan, Rosenberg, et al., 2003; Openstax College, 2013).

Synovial joints can be further classified based on the shape of the articulating surfaces. There are six types of synovial joints, which are presented and described in Table 2.3.

Table 2.3 - Types of synovial joints of the body. Adapted from Flores (2006), Neumann (2013), Openstax College (2013)

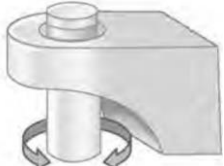
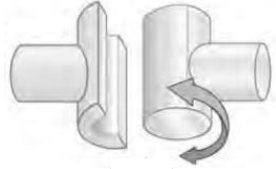
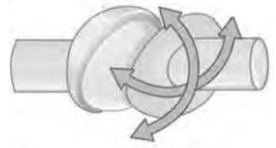
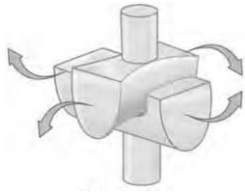
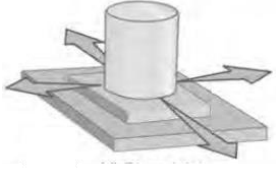
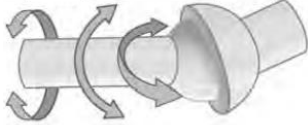
Name	Description	Example	Illustration
Pivot	Occurs when a bone has a projection that fits in an opening of another enabling rotation.	Humeroradial joint	

Table 2.3 (continued) - Types of synovial joints of the human body. Adapted from Flores (2006), Neumann (2013), Openstax College (2013)

Name	Description	Example	Illustration
Hinge	Occurs when the convex end of one bone articulates with the concave end of the other bone, enabling flexion and extension along a unique axis.	Interphalangeal joint	
Condyloid	Occurs when the thin depression at the end of one bone articulates with a rounded end from the adjacent bone.	Metacarpophalangeal joint	
Saddle	Occurs when the articulating surfaces of the bones have a saddle shape, being concave in one bone and convex in the other.	Sternoclavicular joint	
Plane	Occurs when the articulating surfaces of the bones are flat, allowing them to slide against each other.	Intertarsal joints	
Ball-and-Socket	Occurs when the rounded head of one bone (ball) fits into the concave articulation (socket) of the other bone.	Coxofemoral (hip) joint	

The human lower limb comprises three major joints, namely hip, knee and ankle. According to Oatis (2009), the motion of each joint of the lower limbs is more commonly analysed in the sagittal plane, since the motion in this plane is the largest and easier to measure.

The hip joint is a synovial ball-and-socket joint (see Table 2.3). The head of the femur (ball) articulates with the acetabulum of the hip bone or pelvic girdle (socket). This joint supports the weight of the human body and therefore necessitates to provide strength and stability during locomotion (Affatato, 2012; Openstax College, 2013; Standing, 2008). The acetabulum includes a deep and large articulation area in which the femoral head settles, comprising a structure that further deepens it, the acetabular labrum. This is a fibrocartilage layer attached to the outer boundary of the acetabulum. The neighbouring articular capsule includes numerous thickened areas forming the intrinsic ligaments, namely iliofemoral,

pubofemoral and ischiofemoral ligament. They arise from the hip bone at the margins of the acetabulum, attaching in a spiral manner to the femur at its neck's base. Besides these ligaments, another one inside the articular capsule exists, the ligament of the head of the femur or ligamentum teres, spanning from the acetabulum to the femoral head (Openstax College, 2013; Standring, 2008). Figure 2.6 comprises the analysed components of the hip joint.

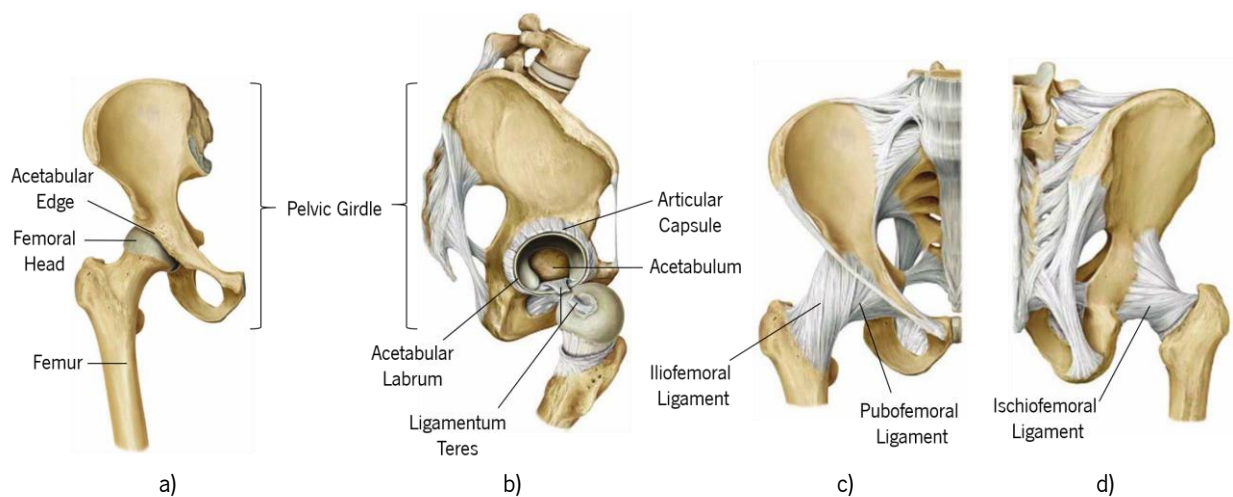


Figure 2.6 – Right hip joint. a) Anterior, b) lateral, c) anterior with ligaments and d) posterior with ligaments views of the structures that comprise the hip joint. Adapted from Schuenke, Schulte, et al. (2009).

Considering that the hip joint enables motion in three cardinal planes, it presents three degrees of freedom, namely flexion-extension (sagittal plane), abduction-adduction (frontal plane) and internal-external rotation (transverse plane). Figure 2.7 illustrates the hip joint motion. Femoral-on-pelvic and pelvic-on-femoral terms describe the rotation of the femur about a relatively fixed pelvis and vice-versa.

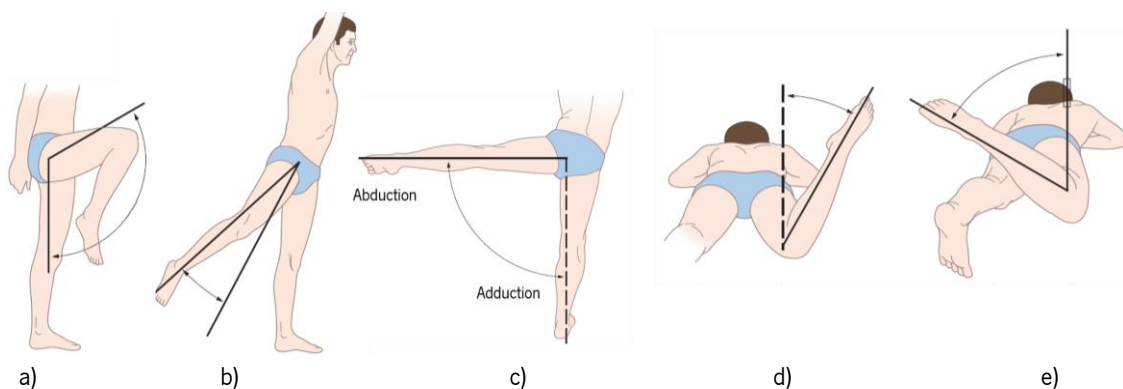


Figure 2.7 – Movements of the hip joint. a) Flexion, b) extension, c) abduction and adduction, d) external rotation and e) internal rotation. Adapted from Palastanga & Soames (2012).

Distally to the hip joint, there is the knee joint, which is the largest synovial joint in the human body, being located between the femur, tibia and fibula. Due to the relatively unequal nature of the joint surface,

the knee joint is inherently unstable (Affatato, 2012; Standing, 2008). The knee is a three-joint structure that is composed by the superior tibiofibular, the patellofemoral and the tibiofemoral joints (Figure 2.8).

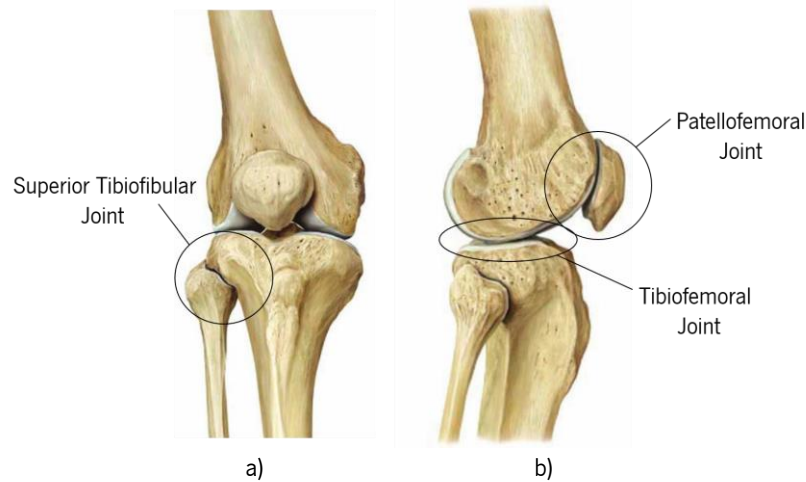


Figure 2.8 – The knee is a three-joint structure composed by the superior tibiofibular, the patellofemoral and the tibiofemoral joints. a) Frontal and b) lateral views. The right knee is represented. Adapted from Schuenke, Schulte, et al. (2009).

The superior tibiofibular joint is an almost plane synovial joint located between the lateral tibial condyle and the fibular head. Within this joint, very limited movement occurs, being essentially gliding. The patellofemoral joint is a complex synovial joint. The articular surface of this joint involves the adaptation of the articular surface of the patella to that of the femur. The posterior surface of the patella is covered with articular cartilage, which reduces the friction between these two bones. During normal gait, as the knee joint extends or flexes, there is the occurrence of gliding between the articular surfaces of the patella and the femur. With the knee joint flexed, the patella is located in the inferior part of the femur, gliding to a more superior part of the femur as the knee extends. This motion of the patella relative to the femur is illustrated in Figure 2.9 (Fulkerson & Shea, 2004; Hall, 2012; Neumann, 2013; Standing, 2008; Walter Shelton, 2010).

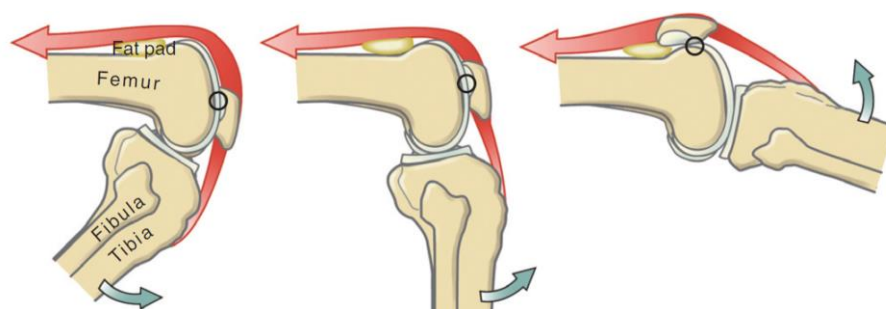


Figure 2.9 - Kinematics of the patella during tibiofemoral extension. The circle represents the maximal contact point between the patella and the femur. The blue arrows represent the direction of motion. The red arrow represents the quadriceps femoris tendon. Adapted from Neumann (2013).

The tibiofemoral joint is a modified synovial hinge joint that lies between the small, nearly flat tibial condyles and the larger, convex femoral condyles. The articular surfaces enable extensive knee motion in the sagittal plane, which is translated into one degree of freedom, that is, flexion-extension. This is the primary motion of the knee joint. Besides this movement, in the transverse plane the knee joint has a relatively minor degree of freedom translated into internal-external rotation. These two movements combined enable the performance of daily activities, such as, walking, squatting and running. Figure 2.10 represents the movements enabled by the tibiofemoral joint (Neumann, 2013; Openstax College, 2013; Standring, 2008).

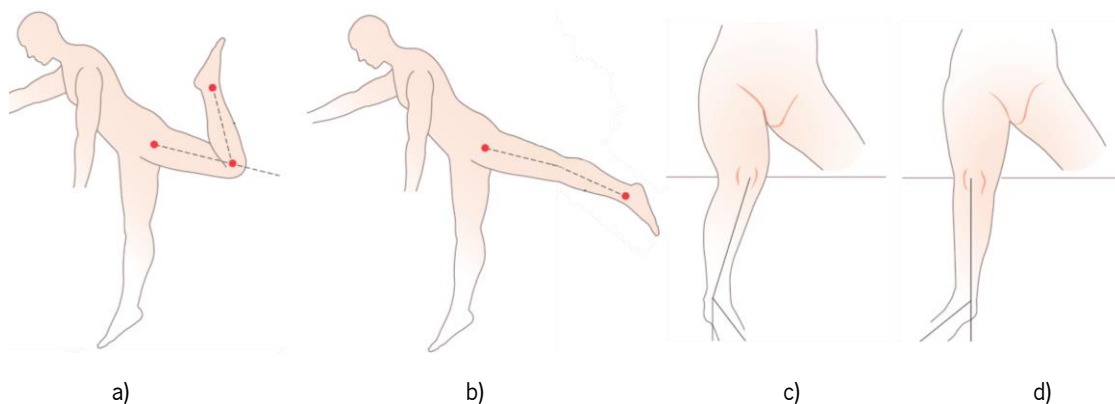


Figure 2.10 - Motion of the knee joint. In the sagittal plane, the tibiofemoral joint of the knee enables flexion (a) and extension (b). In the transverse plane, the tibiofemoral joint enables internal (a) and external (b) rotation. Adapted from Palastanga & Soames (2012).

In between the femur and the tibia, there is the presence of menisci (Figure 2.11a). The menisci are intracapsular, fibrocartilaginous laminae. Their function is to widen and deepen the tibial articular surfaces that accommodates the femoral condyles. They also stabilize the tibiofemoral articulation, assist lubrication, and may cushion the underlying bone from forces generated during extreme flexion and extension. Their proximal surfaces are smooth and concave and in contact with the articular cartilage on the femoral condyles. Their distal surfaces are smooth and flat, resting on the tibial articular cartilage. The knee comprises two types of menisci: the medial meniscus (meniscus medialis) and the lateral meniscus (meniscus lateralis) (Standring, 2008).

Besides the menisci, the knee joint possesses some other structures, the ligaments, which provide stability to the articulation. The cruciate ligaments, so called because they cross each other, are very strong structures. There are two of these ligaments, named anterior and posterior with reference to their tibial attachments, ACL and PCL, respectively (Standring, 2008). In addition to these ligaments, there are many others, namely, anterior menisiofemoral ligament (ligament of Humphrey), the posterior

menisfemoral ligament (ligament of Wrisberg), the fibular collateral ligament (ligamentum collaterale fibulare), the tibial collateral ligament (ligamentum collaterale tibiale), the patellar ligament (ligamentum patellae) and the transverse genual ligament (ligamentum transversum genus) (Openstax College, 2013; Standring, 2008).

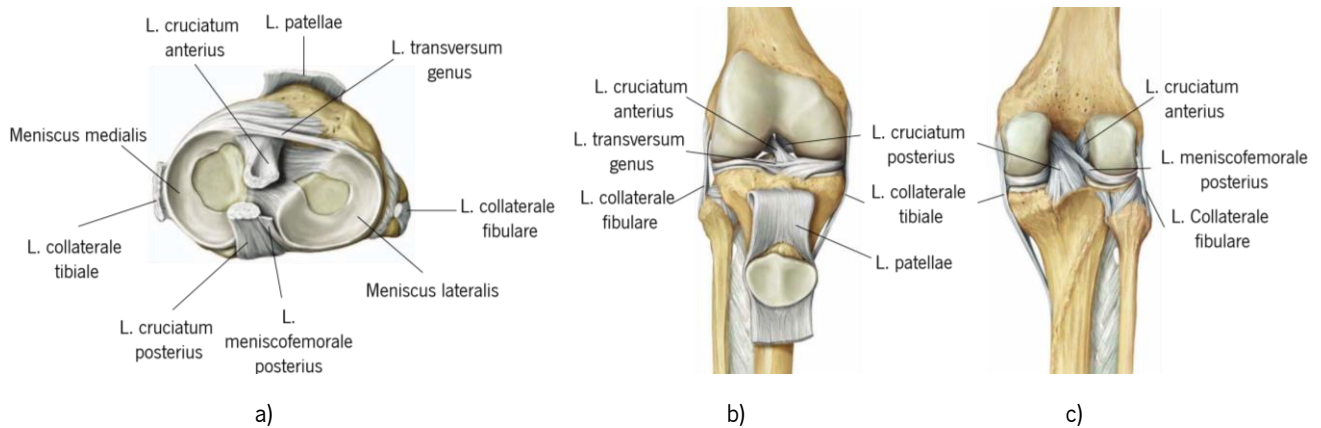


Figure 2.11 - Structures comprising the knee joint. a) Transverse, b) anterior and c) posterior views of the right knee joint. Adapted from Schuenke, Schulte, et al. (2009).

The more distal joints of the lower limb are included in the foot. The human foot comprises 28 bones, establishing a total of 31 joints. The ankle or talocrural joint is a hinge joint, allowing only plantar- and dorsiflexion of the foot in the sagittal plane. It is the articulation located between the talus bone of the foot and the distal ends of the tibia and fibula bones. The talus bone contains three areas of articulation. In the superior part, it articulates with the inferior part of the tibia, being the portion of the ankle joint that carries the body weight between the leg and the foot. The medial and lateral parts of the talus articulate with the medial part of the tibia and the lateral part of the fibula, respectively. This configuration prevents side-to-side movements of the talus (Openstax College, 2013; Standring, 2008).

The human foot is also able to produce movement in the frontal plane, namely inversion and eversion. This motion is provided by a joint located between the tarsal bones of the posterior part of the foot, more specifically between the talus and the calcaneus bones, called subtalar joint. Besides this joint, the one located between the navicular and the talus and the calcaneus and the cuboid bones also contribute to this motion. These are all classified as plane (see Table 2.3) (Openstax College, 2013).

To provide support and prevent abnormal side-to-side and twisting motion of the talus and calcaneus bones during frontal plane movements of the foot, there are several ligaments involving the talocrural joint. These ligaments arise from the medial and lateral parts of the tibia and fibula, respectively, and secure themselves to the talus and calcaneus bones. They are the deltoid ligament, the anterior and

posterior talofibular ligaments and the calcaneofibular ligament (Openstax College, 2013; Standring, 2008). According to Standring (2008), the joints existent in the foot are the ones presented in Table 2.4 and illustrated in Figure 2.12.

Table 2.4 - Joints comprised in the foot. Adapted from Ridola, Cappello, et al. (2007), Standring (2008)

Joint Name and Type	Articulating Surfaces	Involved Ligaments
Ankle or Talocrural (Hinge)	Located between the talus and the tibia and fibula's distal ends.	Deltoid, anterior and posterior talofibular and calcaneofibular collateral ligaments.
Inferior Tibiofibular (Fibrous)	Located between the distal end of the fibula and the tibia.	Anterior and posterior tibiofibular ligaments and the interosseous ligament.
Talocalcaneal or Subtalar (Saddle)	Posteriorly located between the calcaneus and talus.	Lateral, medial and interosseous talocalcaneal and cervical ligament.
Talocalcaneonavicular (Plane and Ball-and-Socket)	Formed between talus and calcaneus/navicular bones.	Talonavicular and plantar calcaneonavicular ligaments.
Calcaneocuboid (Saddle)	Distal surface of the calcaneus and the proximal part of cuboid.	Calcaneocuboid ligaments.
Naviculocuneiform (Plane)	Distal surface of the navicular and cuneiform bones.	Dorsal and plantar ligaments.
Cuboideonavicular (Fibrous)	Located between the cuboid and navicular bones.	Dorsal, plantar and interosseous ligaments.
Intercuneiform (Plane)	Located between the cuneiform bones.	Dorsal, plantar and interosseous ligaments.
Cuneocuboid (Plane)	Located between the lateral surface of the cuneiform and the medial surface of the cuboid.	Dorsal, plantar and interosseous ligaments.
Tarsometatarsal (Approximately Plane)	Between the tarsal bones and the bases of the metatarsal bones	Dorsal and plantar tarsometatarsal and interosseous cuneometatarsal I.
Intermetatarsal (Plane)	Formed between the bases of the metatarsal bones.	Dorsal and plantar intermetatarsal ligaments.

Table 2.4 (continued) - Joints comprised in the foot. Adapted from Ridola, Cappello, et al. (2007), Standing (2008)

Joint Name and Type	Articulating Surfaces	Involved Ligaments
Metatarsophalangeal (Condyloid)	Located between the metatarsal heads and the phalangeal bases.	Plantar, deep transverse and collateral ligaments.
Interphalangeal (Hinge)	Located between the phalangeal heads and the adjacent phalangeal bases	Collateral and plantar ligaments

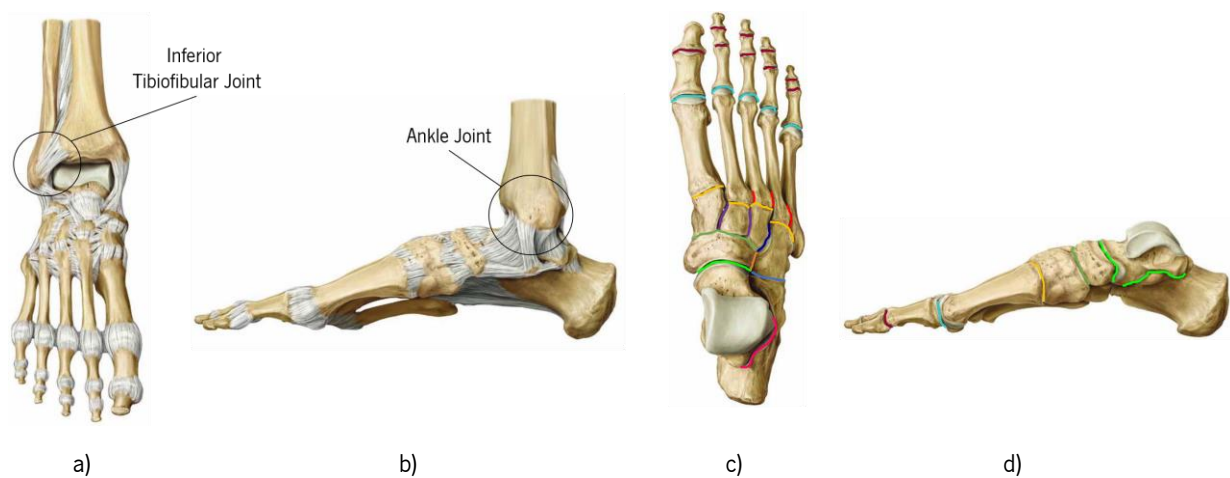


Figure 2.12 - Illustration of the joints comprised in the human foot. The right foot is represented. a) Anterior, b) medial with tibia, c) superior and c) medial without tibia views. Intercuneiform Joint, Cuneocuboid Joint, Naviculocuneiform Joint, Calcaneocuboid Joint, Cuboideonavicular Joint, Tarsometatarsal Joint, Talocalcaneonavicular Joint, Subtalar Joint, Intermetatarsal Joint, Metatarsophalangeal Joint, Interphalangeal Joint. Adapted from Schuenke, Schulte, et al. (2009).

The joints comprised in the human foot enable the movements it can produce. In the sagittal plane, the foot can perform plantar- and dorsiflexion. Eversion and inversion are performed in the frontal plane and adduction and abduction in the transverse plane (Palastanga & Soames, 2012).

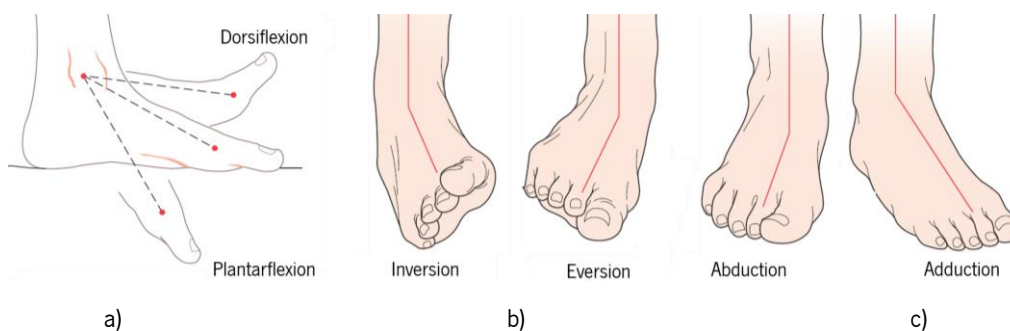


Figure 2.13 - Foot motion. Plantar-/dorsiflexion (a), eversion/inversion (b) and (c) abduction/adduction are performed around the medial/lateral (sagittal plane), posterior/anterior (transverse plane) and superior/inferior (frontal plane) axes. Adapted from Palastanga & Soames (2012).

2.4. Muscular System

The muscles present in the human body are tissues of the body and there are four types of them, namely skeletal, cardiac and smooth muscles. The skeletal muscle depends completely on signals from the nervous systems, while cardiac and smooth muscles are influenced by them at some degree, but can also respond to other stimuli, such as hormones. Muscles are connected to bones, cartilage, ligaments and skin. This connection is made either directly or by means of fibrous structures, called tendons or aponeuroses, located at the ends of the muscle (Gray, 1918; Openstax College, 2013).

Cardiac muscle is found in the heart and is associated with pumping the blood through the body by the circulatory system. Smooth muscle is found coating internal organs, enabling, for instance, the food to move through the digestive system. The skeletal muscle has the function contracting and producing movement of the skeleton. It prevents excessive or abnormal movements of the joints present in the body, promoting skeletal stability and preventing structures' damage. For instance, by pulling the bones associated with a determined joint, it can become misaligned and produce abnormal movement. Muscles' role is to prevent these occurrences and maintain the joint in a stable configuration. Skeletal muscles are the ones approached in this section (Openstax College, 2013).

Standring (2008) states that the anterior part of the lower limb possesses the majority of the extensor activity, while the posterior part is dominated by the flexors' muscles. However, the opposite is true at the hip joint. Essentially the muscles present in the lower limb are designed to maintain the body's equilibrium during locomotion. They usually act around more than one joint, being unusual for any of its joints to move in isolation. According to Standring (2008), the muscles of the lower limb can be divided into muscles of the iliac and gluteal regions, thigh, leg and foot.

The hip joint is located in the gluteal region, being, as previously explained, a ball-and-socket synovial joint with three degrees of freedom. To be able to produce this motion, not only its configuration intervenes, but the muscles that act around the joint are also very important. Muscles that lie anteriorly to the hip joint tend to act to flex it, and those located posteriorly tend to extend it. Muscles on the medial and lateral parts of the hip joint produce its adduction and abduction (Palastanga & Soames, 2012).

The muscles around a joint can be classified as having primary or secondary actions. Muscles that have a primary action are the ones that effectively produce the movement the body is performing. A muscle is said to have a secondary action if it assists the primary muscle to achieve the motion it is performing (Neumann, 2013). Table 2.5 comprises the muscles that act around the hip joint.

Table 2.5 - Muscles that cross the hip joint and movement they produce according to their action (Neumann, 2013). TFL designates tensor fasciae latae

Action	Flexion	Extension	Adduction	Abduction	Internal Rotation	External Rotation
Primary	Iliopsoas	Gluteus Maximus	Pectineus			Gluteus Maximus
	Sartorius	Biceps Femoris	Adductor Longus	Gluteus Medius		Piriformis
	TFL	Semitendinosus	Gracilis	Gluteus Minimius	-	Obturator Internus
	Rectus Femoris	Semimembranosus	Adductor Brevis	TFL		Gemellus Superior
	Adductor Longus	Adductor Magnus	Adductor Magnus			Gemellus Inferior
	Pectineus					Quadratus Femoris
Secondary	Adductor Brevis	Gluteus Medius	Biceps Femoris	Piriformis	Gluteus Minimius	Gluteus Medius
	Gracilis	Adductor Magnus	Gluteus Maximus	Sartorius	TFL	Gluteus Minimius
	Gluteus Minimius		Quadratus Femoris		Adductor Longus	Obturator Externus
					Adductor Brevis	Sartorius
				Pectineus	Biceps Femoris	

Figure 2.14 comprises the muscles of Table 2.5 that act around the hip joint to perform the movements it is characterized with.

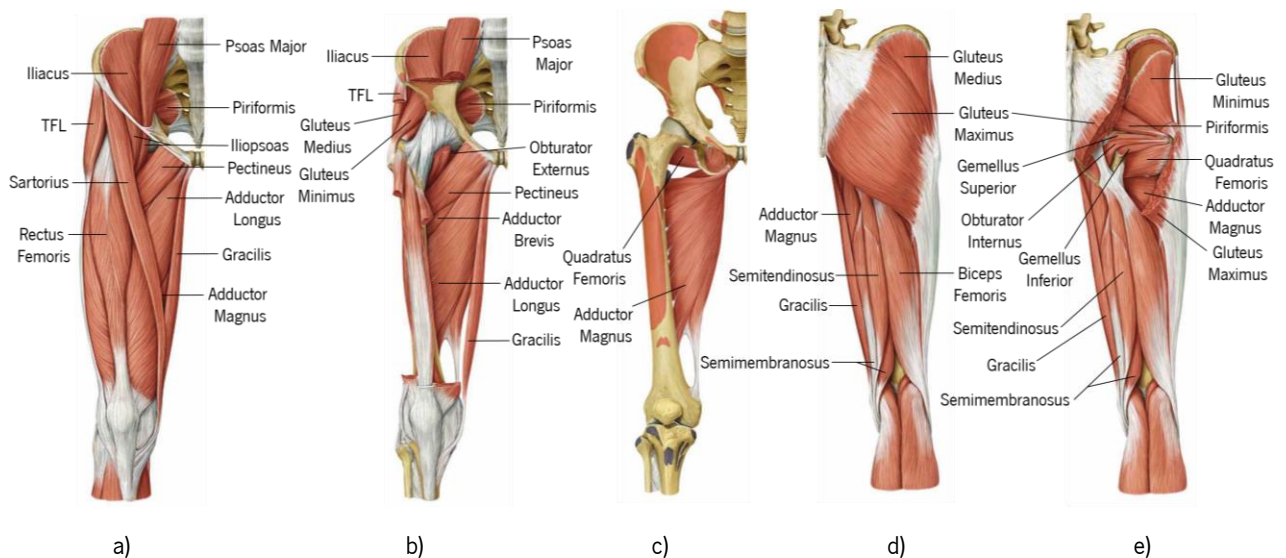


Figure 2.14 - Muscles acting around the hip joint. a) Anterior view. b) Anterior view with rectus femoris, iliopsoas and tensor fasciae latae (TFL) removed. c) Anterior view with rectus femoris, iliopsoas, TFL, gluteus medius and minimus, piriformis, obturator externus, adductor brevis and longus and gracilis removed. d) Posterior view. e) Posterior view with gluteus maximus and medius partially removed. The right lower limb is represented. Adapted from Schuenke, Schulte, et al. (2009).

The knee joint is located in between the thigh and leg regions. There are several muscles that play important roles in the knee articulation, enabling the range of movements it comprises. Table 2.6 comprises the muscles that act around the knee joint. All knee flexor muscles, except for the short head of the biceps femoris and the popliteus, are two-joint muscles, crossing the hip and knee joints. Their

ability to produce effective force can be influenced by the relative position of the two joints over which they pass (Callaghan, Rosenberg, et al., 2003; Margo, Radnay, et al., 2010).

Table 2.6 - Muscles that cross the knee joint and movement they produce (Neumann, 2013). Vastus group comprises the vastus intermedius, vastus lateralis and vastus medialis muscles. Quadriceps femoris muscle group comprises rectus femoris, vastus intermedius, vastus lateralis and vastus medialis muscles. Hamstrings muscle group comprises semimembranosus, semitendinosus and biceps femoris muscles

Muscle Name	Extension	Flexion	Internal Rotation	External Rotation
Quadriceps Femoris	X			
Rectus Femoris	X			
Vastus Group	X			
Sartorius		X	X	
Gracilis		X	X	
Popliteus		X	X	
Semimembranosus		X	X	
Semitendinosus		X	X	
Biceps Femoris		X		X
Hamstrings		X		
Gastrocnemius		X		
Plantaris		X		

Besides producing movement around the knee joint, some of these muscles produce hip movements. Sartorius enables hip flexion, external rotation and abduction. Gracilis performs hip flexion and adduction. Rectus femoris flexes the hip. Semimembranosus, semitendinosus and biceps femoris extend the hip. Besides hip movements, some of these muscles also influence the ankle: gastrocnemius and plantaris enable ankle plantarflexion. Figure 2.15 illustrates the muscles comprised in Table 2.6.

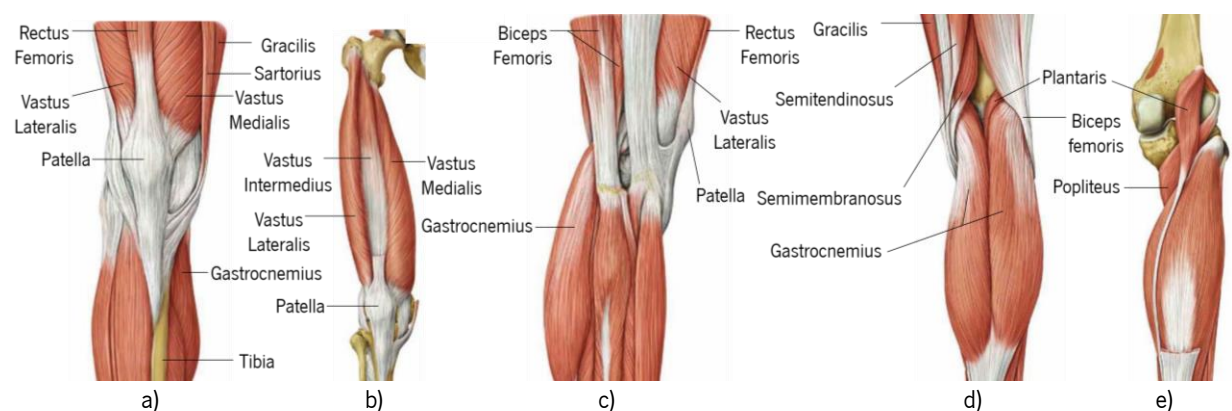


Figure 2.15 - Muscles crossing the knee joint. a) Anterior view. b) Anterior view with sartorius and rectus femoris removed. c) Lateral view. d) Posterior view. e) Posterior view with gastrocnemius removed. The right lower limb is represented. Adapted from Schuenke, Schulte, et al. (2009).

According to Standring (2008), the foot comprises intrinsic and extrinsic muscles. The former are the ones contained entirely within the foot, enabling flexion, extension, adduction and abduction of the toes. The extrinsic muscles are the ones in which their tendons cross the ankle, moving and stabilizing this joint. Besides the ankle, distally, these muscles also help stabilize the other joints comprising the foot. The extrinsic muscles are divided in three groups, regarding their position of the lower limb. Tibialis anterior, extensor hallucis longus, extensor digitorum longus and fibularis tertius pertain to the anterior group. The lateral group contains the fibularis longus and fibularis brevis muscles. Gastrocnemius, soleus, plantaris, tibialis posterior, flexor digitorum longus and flexor hallucis longus pertain to the posterior group (Standring, 2008). Table 2.7 contains the muscles of the foot.

Table 2.7 - Muscles comprised in the foot are divided into extrinsic and intrinsic. Intrinsic muscles pertain only to the foot, while extrinsic muscles cross the ankle joint, pertaining to the foot and leg (Palastanga & Soames, 2012; Standring, 2008)

Extrinsic Muscles			
Foot Plantarflexion	Foot Dorsiflexion	Foot Inversion	Foot Eversion
Gastrocnemius			
Soleus			
Plantaris	Tibialis anterior	Tibialis posterior	Fibularis longus, brevis
Fibularis longus	Fibularis tertius	Tibialis anterior	and tertius
Fibularis brevis			
Tibialis posterior			
Intrinsic Muscles			
Toes Extension	Toes Flexion	Toes Adduction	Toes Abduction
	Flexor digitorum longus		
	Flexor digitorum brevis		
Extensor hallucis longus	Flexor hallucis longus		Abductor hallucis
Extensor digitorum longus	Flexor hallucis brevis	Adductor hallucis	Abductor digiti minimi
Extensor digitorum brevis	Flexor accessorius	Plantar interossei	Dorsal interossei
Lumbricals	Flexor digiti minimi brevis		
	Interossei		
	Lumbricals		

Besides the movements present in the above table, flexor digitorum longus and flexor hallucis longus provide also foot plantarflexion. Extensor digitorum longus and extensor hallucis longus promote foot dorsiflexion as well (Palastanga & Soames, 2012). Figure 2.16 comprises the muscles that pertain to the foot.

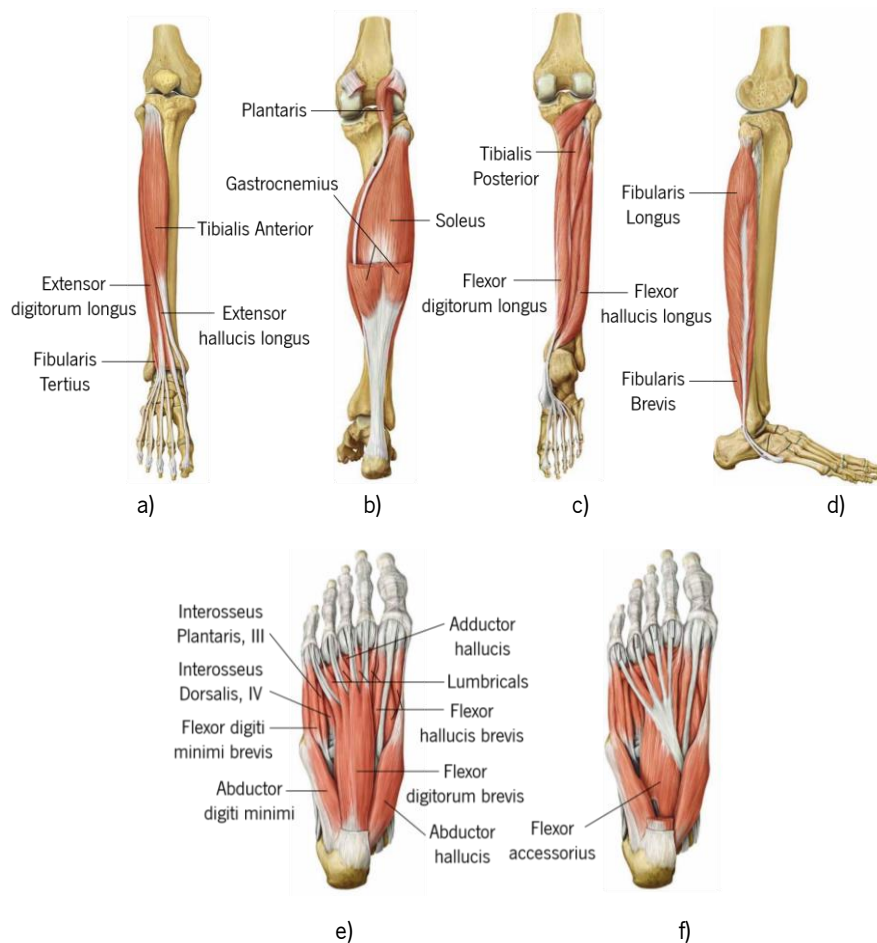


Figure 2.16 - Muscles comprised in the foot. a) Anterior view. b) Posterior view. c) Posterior view with soleus and gastrocnemius removed. d) Lateral view. e) Superior view. f) Superior view with flexor digitorum brevis removed. The right lower limb is represented. Adapted from Schuenke, Schulte, et al. (2009).

Tendons, like ligaments, are dense connective tissues, but instead of connecting bone to bone, these structures' function is to attach muscles to bones. They are located at the ends of each muscle (Oatis, 2009). In the above figures of this section, tendons are the white structures at the ends of the muscles. Tendons of the lower limb include the Achilles, patellar and quadriceps tendons, for instance.

2.5. Summary and Discussion

In this chapter, the anatomy of the human lower limb is presented. The knowledge of the nomenclature used in this anatomical field, namely the directional terms, cardinal planes as well as movements' designations, is important to use a unified and precise language when describing the human lower limb throughout the dissertation. Besides this knowledge, the familiarity with anatomical terms related to this part of the human body is important to understand the developed work. To this end, the skeletal, articular and muscular systems of the human lower limb were described.

3. MUSCLE-TENDON UNIT

In the present chapter, a description of the muscle-tendon unit (MTU) is given. The aim of this chapter is to provide the reader with a detailed understanding of the structures comprised within a muscle-tendon unit, their behaviour and how to computationally model an MTU.

The chapter begins with the definition of the components involving a muscle-tendon unit. Essentially, an MTU comprises all the structures of the muscle belly and its tendinous attachments at both of its ends. After this clarification, it is explained the structure of these components and their arrangement in the human body.

The following section involves the description of how joint motion is produced. Essentially, the central nervous system sends a neural signal, which arrives to the muscle fibres by means of a motoneuron. This muscular stimulation provokes muscular activation, which in turn produces muscular contraction. Contraction of the skeletal musculature enables the bony structures attached to it to move and produce joint motion.

After understanding how joint motion is produced, the factors affecting the force generated by an MTU are explored. Essentially, force generation is dependent on the muscle's length and shortening or lengthening velocity and, therefore, force-length, force-velocity and force-length-velocity relations are established. To understand this, a description of a muscle's mechanical behaviour to produce joint motion is given. The chapter continues with a description of the elements or components used to model an MTU in computational mechanics, based on all the explanations given throughout this chapter. Finally, the chapter ends with a summary and discussion of the themes was approached.

3.1. General Description

As approached in section 2.4, skeletal muscles produce movement of the human skeleton by receiving stimuli or signals from the nervous system and contracting. Besides allowing physiological movements, these muscles also prevent abnormal joint motion, providing joint stability. Due to the regular organization of their constituting protein filaments, actin and myosin, skeletal muscles are capable of powerful contractions. They are attached to the bones of the skeletal system by means of tendons at their ends. Essentially, tendons are dense, regular connective tissues, whose fibres are arranged in a parallel manner regarding one another, being composed by collagen. This arrangement provides tendons with a good capacity of resisting tensile loads (Oatis, 2009; Tavares da Silva, 2003).

The human movement is achieved by contractions performed by the muscle fibres, whose entire muscle is connected to tendons. The primary action of a muscle is to contract and thus produce joint motion. Overall, the muscle receives a signal from the nervous system indicating it needs to contract. The contraction is expanded to all muscle belly's tissue, which, in turn, extends to both proximal and distal tendinous attachments. The proximal and distal attachments of a muscle to a tendon are known as its origin and insertion, respectively. The muscular contraction produced by the muscle fibres is transmitted to tendons during movement. Since tendons are attached to the bones of the skeleton, this transmission produces joint motion (Fukunaga, Kawakami, et al., 2002; Zatsiorsky & Prilutsky, 2012).

A muscle without its tendinous attachments is referred to as muscle belly. The functional unit that produces joint motion consists of the muscle belly and its respective tendon, that is, the muscle-tendon unit (Zatsiorsky & Prilutsky, 2012). Figure 3.1 illustrates the arrangement of a skeletal muscle and its respective tendons around the bones of the skeletal system.

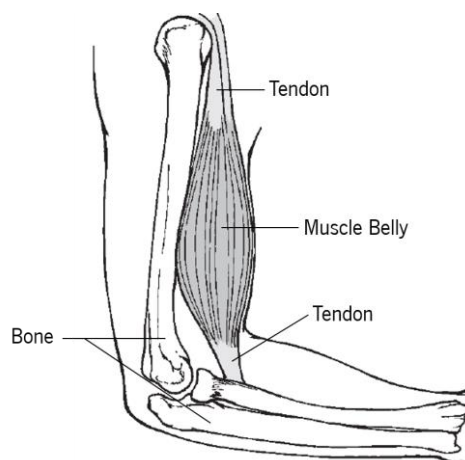


Figure 3.1 – Representation of a muscle-tendon unit. A skeletal muscle connects the bones of the skeleton by means of tendons located at their ends. Adapted from Oatis (2009).

The force generated by a muscular contraction is called muscle tension or force. There are three types of muscular contractions according to macroscopic muscle length alterations. If a contraction does not alter the muscle's length, it is called an isometric contraction. In this type of contraction, no movement is performed by the joint. For instance, if a person is trying to lift a load with their hand but the muscle tension applied is equal to the load, no movement is performed. This way, the muscle is contracting without macroscopic shortening or lengthening (Figure 3.2a). However, if a contraction causes muscle shortening or lengthening, it is referred to as concentric (Figure 3.2b) or eccentric (Figure 3.2c) contraction, respectively. For example, a concentric contraction occurs when a person is lifting a load with their hand, promoting flexion of the elbow joint. On the contrary, if the load is too heavy to be lifted, even though the person is contracting the muscle, its tension cannot overcome the load, and therefore the elbow joint extends. It is important to recognize that this classification is done according to the muscle's macroscopic change in length. Note that, on the microscopic level, the muscle's length changes in all these cases, even in an isometric contraction (Oatis, 2009; Standring, 2008).

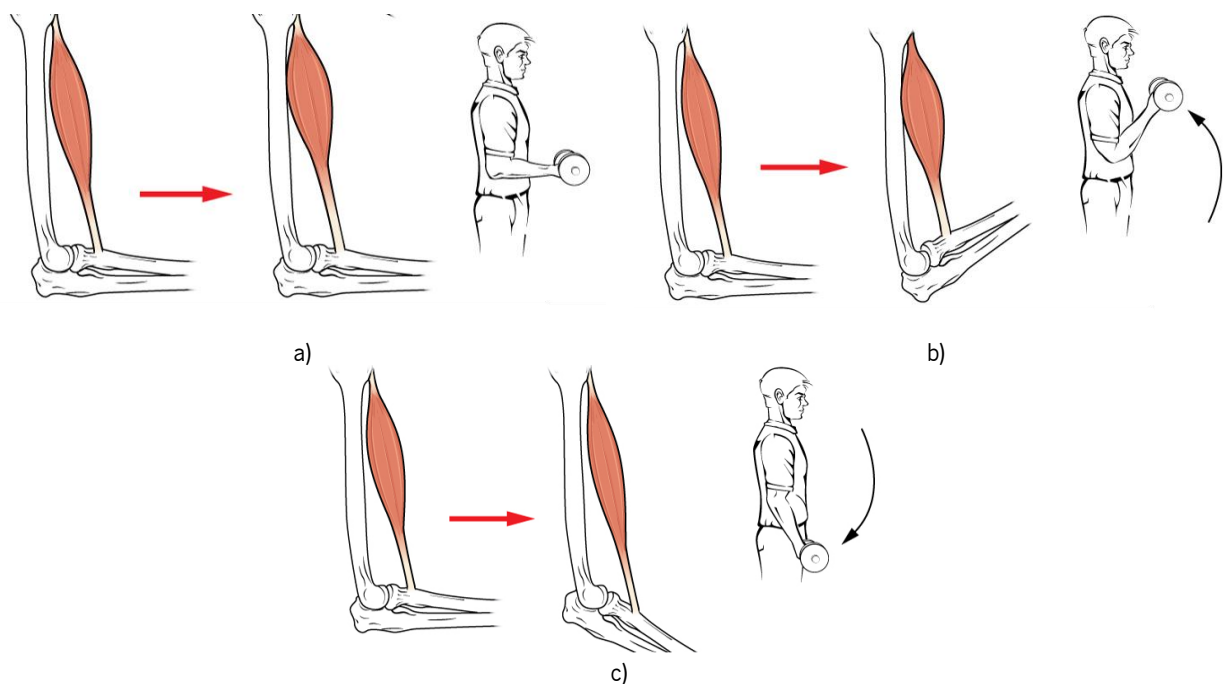


Figure 3.2 - Types of muscular contractions. a) Isometric. b) Concentric. c) Eccentric. Adapted from Openstax College (2013).

3.2. Muscle-Tendon Unit Structure

In section 3.1 it was approached the constituents of a muscle-tendon unit, namely the muscle belly and its tendinous attachments to the bones of the skeletal system. In the present section, the structure of these two tissues is addressed.

The skeletal muscle is composed by a set of muscle fascicles, divided into smaller structures called muscle fibres. A muscle fibre is a long cell that is composed by smaller units, the myofibrils. These are composed by subunits called sarcomeres, arranged end to end in a parallel manner along the length of the muscle fibre. Each sarcomere contains two myofilaments, the thin filaments comprise actin proteins and the thick filaments comprise myosin proteins. The set of muscle fibres are embedded in a tubular membrane, called sarcolemma, being surrounded by a layer of collagenous tissue, known as endomysium. The perimysium encloses the muscle fascicles, binding adjacent fascicles. Finally, the entire muscle is enclosed by other layer of connective tissue called epimysium (Oatis, 2009). Figure 3.3 presents an illustration of the components that make up the structure of the entire skeletal muscle.

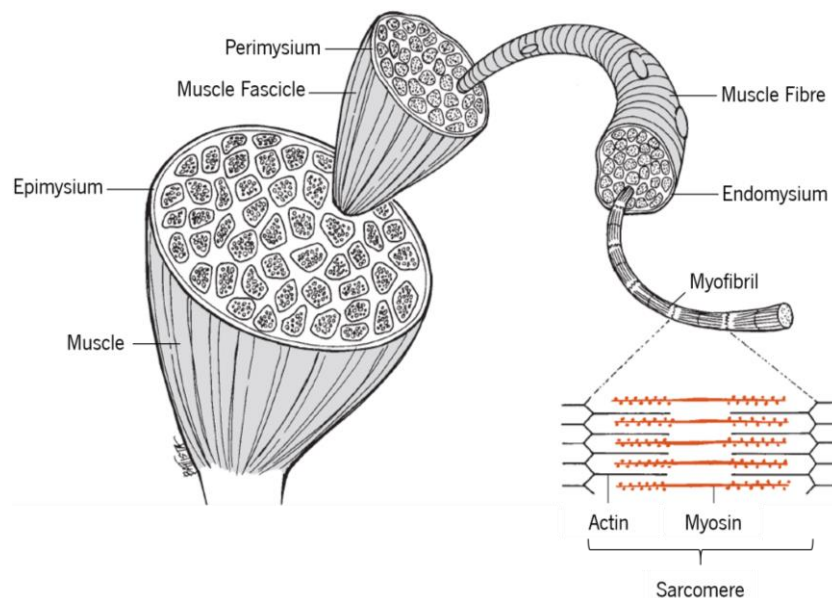


Figure 3.3 - Organization of the skeletal muscle with the identification of its structures. Adapted from Oatis (2009).

As already explained, the main function of the skeletal muscle is to contract. The basic unit of muscular contraction is the sarcomere and the contraction of the whole muscle is the sum of the contraction occurring at each sarcomere. By observing Figure 3.4, several important regions of the sarcomere can be identified. The thin actin filaments are more abundantly encountered than the thick myosin filaments within the sarcomere, being anchored at both ends of the sarcomere at the Z-line and projected to the interior of the sarcomere, where they surround the myosin filaments. This particular arrangement is repeated in all sarcomeres that compose the muscle, providing it with its characteristic striated aspect. The quantity of the two contractile proteins is strongly related with the amount of contraction force a muscle can produce. The Z-line is a protein sheet and the distance between two adjacent Z-lines corresponds to the sarcomere length (Oatis, 2009; Tavares da Silva, 2003).

The darker region of the sarcomere is the one which extends to the length of the myosin filaments and is given the name of A band. The region of the sarcomere containing only actin filaments is called I-band, being also referred to as light region. The H zone of the sarcomere is the one in which there is no superimposition of the two myofilaments, actin and myosin, containing only myosin filaments. In the middle of this zone there is the M-line, containing the proteins strands that hold together the myosin filaments. Titin is a protein that connects of the thick myosin filaments to the Z-line (Tavares da Silva, 2003; Zatsiorsky & Prilutsky, 2012).

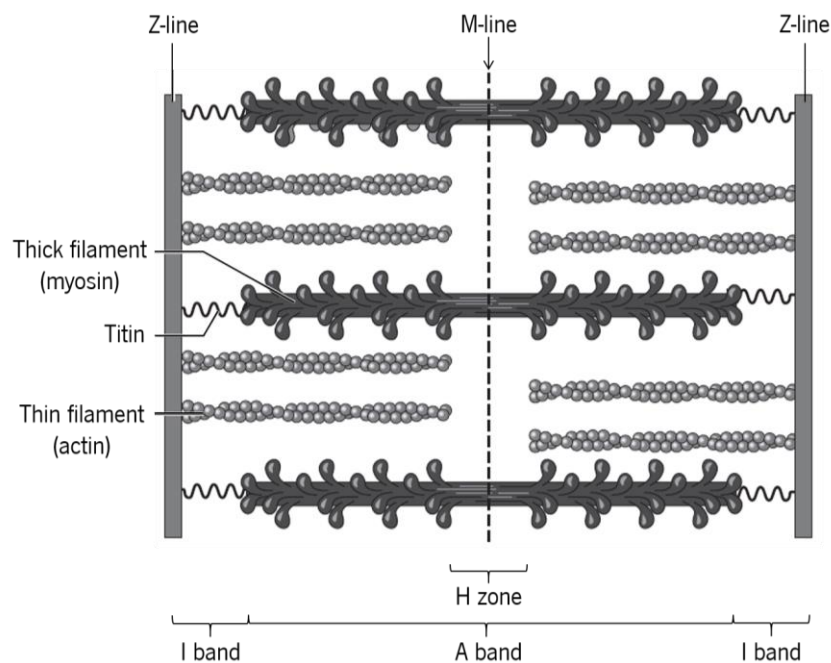


Figure 3.4 - Sarcomere structure. A sarcomere is the basic contractile unit of a muscle. It is composed by thin and thick filaments and their arrangement produces the structure of the sarcomere. Adapted from Zatsiorsky & Prilutsky (2012).

As previously explained, muscles are composed by sets of muscle fibres, whose arrangement can vary significantly amongst different muscles. The differences in fibre arrangements influence the ability of a muscle to produce force. Muscle fibres exert forces along their longitudinal axes, while muscles do this along tendons. In some muscles, their fascicles are connected to tendons at difference angles, and due to this arrangement, the direction of an individual muscle fibre force and the tendon force direction can be different. Considering the angle at which muscle fascicles insert into tendons, muscles can be classified into two major categories as parallel or pennate (Oatis, 2009; Zatsiorsky & Prilutsky, 2012).

Parallel fibred muscles contain muscle fibres approximately parallel to each other along the entire length of the muscle and roughly parallel to the longitudinal axis of the muscle. In these muscles, fascicles are arranged along the line of force action of the MTU. Parallel fibred muscles can be divided into either

fusiform or strap. The former possess prominent tendons at both ends of the muscle, whose muscle fibres taper to insert into tendons. Strap muscles have less prominent tendons at their ends, and therefore their fibres taper less into them (Figure 3.5) (Oatis, 2009; Zatsiorsky & Prilutsky, 2012).

Pennate muscles possess one or more tendons that extend to most of the length of the entire muscle. In this case, muscle fibres run obliquely to insert into these tendons, meaning that muscle fascicles attach to the tendon at an angle, named pennation angle. The pennation angle corresponds to the angle formed between the tendon and the muscle fibres. In pennate muscles, since muscle fibres do not run parallel to the line of action of the entire muscle, but rather run at an angle, the direction of muscle fibre shortening, and therefore fibre force, and tendon force are different. According to the number of tendons causing pennation, muscles are classified as unipennate, bipennate and multipennate. Unipennate and bipennate muscle possess one and two pennation angles, respectively. Multipennate muscles contain multiple pennation angles (Figure 3.5) (Oatis, 2009; Zatsiorsky & Prilutsky, 2012).

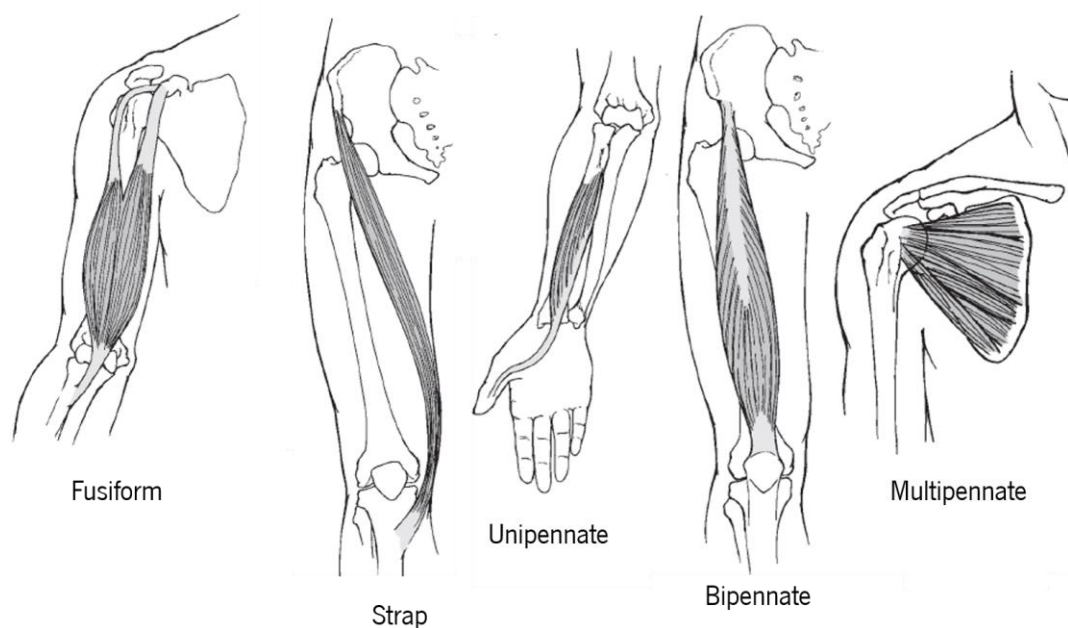


Figure 3.5 - Parallel fibred (fusiform and strap) and pennate (unipennate, bipennate and multipennate) muscles. Adapted from Oatis (2009).

When a parallel fibred muscle contracts, the shortening that it suffers is primarily the result of the shortening of the fibres it comprises. On the contrary, on pennate muscles, the shortening of their fibres provokes their rotation about their tendon insertion, progressively increasing the pennation angle. The greater the pennation angle, the smaller the amount of effective force transmitted to the tendon to produce joint motion by moving the attached bones (Hall, 2012). Figure 3.6 comprises an illustration of

the angle formed by the muscle fibres force, F_{Fibres} , and the tendon force, F_{Tendon} , called the pennation angle, α . Tendon force is calculated as:

$$F_{\text{Tendon}} = F_{\text{Fibres}} \cos(\alpha) \quad (3.1)$$

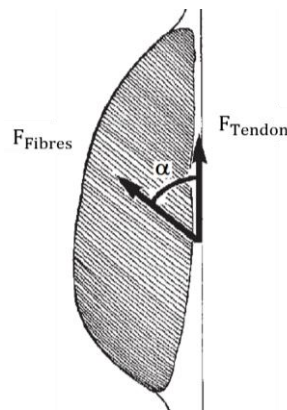


Figure 3.6 - Illustration of the pennation angle, α , comprised between the force produced by the muscle fibres, F_{Fibres} , and the force exerted on the tendon, F_{Tendon} . Adapted from Hall (2012).

As previously referred, pennation reduces the effective force a muscle can produce with the increase in pennation angle. As inferred from the Figure 3.5, parallel fibred muscles possess longer fibres than pennate muscles, and therefore the former permit greater muscle shortening than the latter. Considering this, parallel fibred muscles are able to move body segments through larger ranges of motion than pennate muscles. However, pennate muscles can be packed with more fibres than parallel fibred muscles and therefore the total force produced by the pennate muscle can be greater than the force generated by a parallel muscle with the same volume. A disadvantage of pennate muscles is that, since the muscle fibres are positioned at an angle regarding the muscle line of action, only one component of the fibre force contributes to the force transmitted to the tendon. Additionally, fibres in pennate muscles are shorter than parallel fibred muscles and possess fewer sarcomeres, so their maximum contraction displacement is smaller (Hall, 2012; Oatis, 2009; Zatsiorsky & Prilutsky, 2012).

As previously explained, tendons are composed by connective tissue and their main function is to transmit muscle forces to bones. These structures are made up of longitudinally arranged collagen fibres oriented mainly along the tendon length. Fibres are composed by several fibrils, which in turn comprise subfibrils. These subfibrils are divided into microfibrils, being composed by a molecule called tropocollagen. Tendons and their fibres are surrounded by three matrices of connective tissues. Paratenon is the connective tissues that lays in between the tendon and its sheath, allowing the tendon to move freely. The epitenon lays below the paratenon. Finally, the endotenon covers each fibre bundle

(Oatis, 2009; Zatsiorsky & Prilutsky, 2012). Figure 3.7 presents an illustration of the structure of a tendon, with the identification of its constitutive elements.

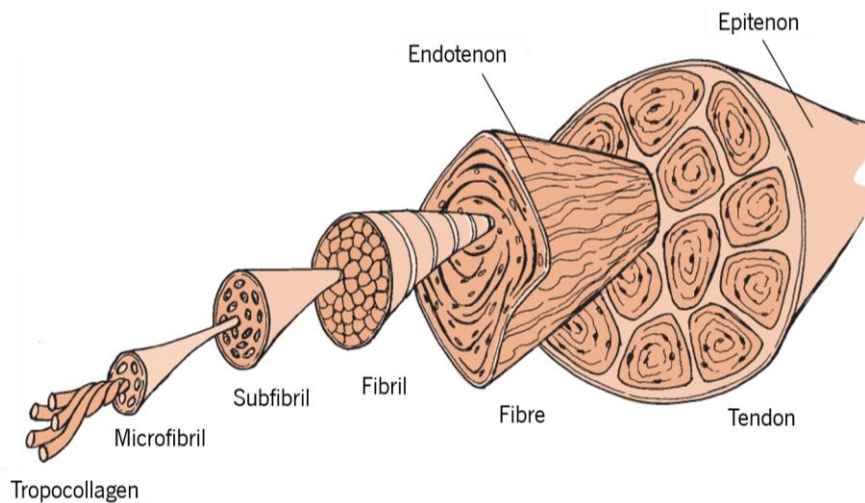


Figure 3.7 - Structural elements comprised within a tendon. Adapted from Oatis (2009).

3.3. Joint Actuation

According to Sandow (1952), the excitation-contraction coupling is used to describe the sequence of occurrences that begin with the propagation of the neural signal from the nervous system on the muscle's surface membrane and leads to the contraction of muscle fibres (Caillé, Ildefonse, et al., 1985). To produce muscular contraction, the nervous system sends a neural signal or action potential, which is propagated through specialized cells, the motoneurons. The set formed by a motoneuron and the individual muscle fibres it innervates is called a motor unit. The neural signal sent by the nervous system stimulates the muscle fibres, activating them, which are then capable of contracting and producing a muscle force. The activation of a muscle fibre describes the time lag that occurs between the sending of a neural signal and the effective muscle fibre contraction (Tavares da Silva, 2003).

Motoneurons possess at their ends structures called axon terminals, which connect the motoneuron to the muscle fibre. To this connection is given the name of neuromuscular junction. A muscle is stimulated when a neural signal from a motoneuron arrives at the neuromuscular junction. This muscular stimulation causes a neurotransmitter, named acetylcholine or ACh, which is contained within vesicles, to be released into postsynaptic clefts, which are small gaps located in between the axon terminals and the muscle fibre, provoking muscular activation. ACh is responsible for muscle fibre activation, disseminating across the cleft and binding to specialized receptors located on the muscle fibre membrane. This provokes a local depolarization of the muscle fibre membrane, which rapidly propagates to the entire muscle. This

alteration in membrane polarization originates the release the calcium ions (Ca^{2+}) that will take part in muscular contraction occurring at sarcomere level. The calcium ions bind to a protein called troponin. This occurrence acts as a trigger, causing the actin filaments to bind to myosin filaments (crossbridges), beginning the contraction of the muscle. Contraction occurs by the sliding of the two filaments relative to each other, according to the sliding filament theory. When the neural signal ends, the concentration of calcium ions within the muscle fibres is reduced, inhibiting the crossbridges between the two myofilaments and the muscle relaxes (Oatis, 2009; Sperelakis, 2012; Tavares da Silva, 2003). Figure 3.8 presents a representation of a motor unit, as well as the structures comprising the neuromuscular junction.

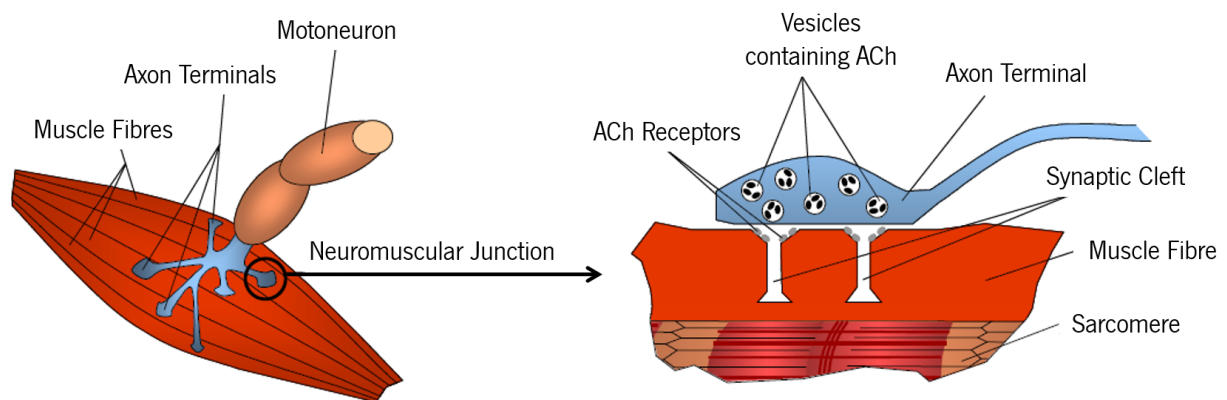


Figure 3.8 - Representation of a motor unit (formed by the interaction between the motor neuron and muscle fibres) and the neuromuscular junction. Adapted from Tavares da Silva (2003).

After activation, the muscle contracts and produces force, which depends on two physiological processes. The muscular force production may be influenced by the frequency of neural signals or stimuli that arrive at muscle fibres or on the recruitment of additional motor units, of larger size (Tavares da Silva, 2003).

Regarding the first process, if only a single neural signal or stimulus of low intensity reaches the motoneuron, a twitch contraction occurs (Figure 3.9a). If the frequency of the signal increases, the twitch repeats and, if this repetition occurs before the muscle has time to relax, it tends to add up. To this process is given the name of summation (Figure 3.9b). According to Tavares da Silva (2003), the increase in stimulation frequencies tends to reduce the time gap occurring between two consecutive twitches. Since the muscle has no time to fully relax before the following twitch arises, they add up. If the frequency of stimuli increases so much that the muscle contraction reaches its peak force and plateaus at that level, it produces a tetanic contraction (Figure 3.9c) (Hall, 2012; Openstax College, 2013).

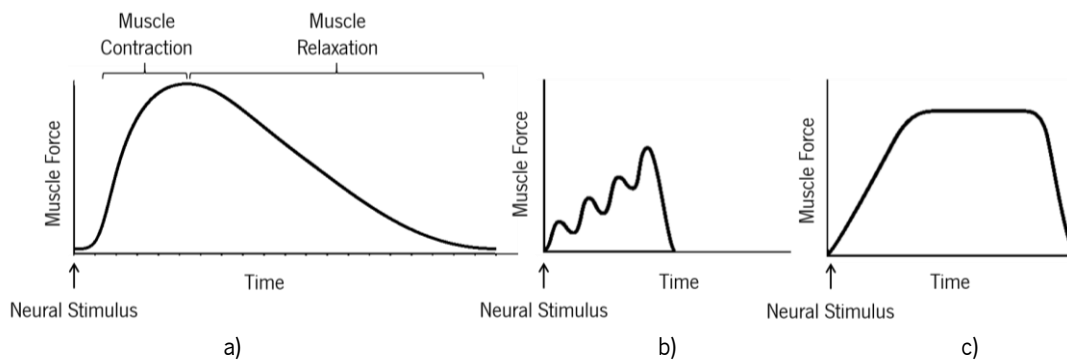


Figure 3.9 - Events occurring when a muscle is stimulated. a) Twitch. b) Summation. c) Tetanus. Adapted from Openstax College (2013).

It is important to consider that in Figure 3.9a, there is a time delay between the occurrence of the neural stimulus and the initiation of muscular contraction. This time delay is called latent period and is the time that the neural stimulus takes to be propagated along the muscle fibre. In Figure 3.9b and c this latent period also occurs (Openstax College, 2013).

Some muscle fibres may contract quicker than others after the time they are stimulated. Based on this response to neural signals, muscle fibres are classified as fast twitch and slow twitch. Essentially, fast twitch fibres contract at about one-seventh the time required by the slow twitch fibres to contract. A motor unit comprises the same type of fibres (fast or slow twitch). However, most skeletal muscles possess both slow and fast twitch fibres, with the relative amounts varying considering the muscle and the individual. In events requiring fast, powerful muscular contractions, for instance, sprinting or jumping, fast twitch fibres are very important. In events related to endurance testing, such as distance running, slow twitch muscles are required (Hall, 2012).

Figure 3.10 shows a schematic of the sequence of events occurring from neural signal sending until muscular force production.

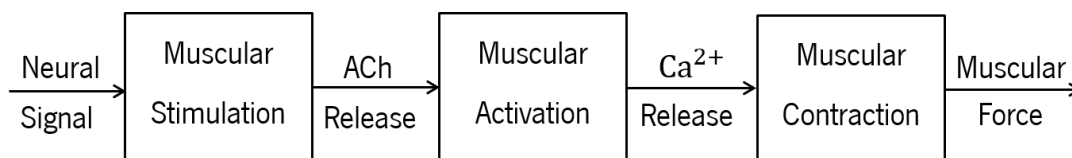


Figure 3.10 - Processes occurring from neural signal sending until the production of muscular force. When a neural signal arrives to the axons of a motoneuron, it is propagated to the adjacent muscle fibres, provoking muscle stimulation. This occurrence enables ACh to be release in the synaptic cleft, provoking muscle activation. When the muscle is activated, calcium ions are released into the muscle fibres, initiating muscular contraction, which in turn leads to muscular force production.

The force produced by the muscle is then transmitted to its adjacent tendon mainly through shear stresses exerted on neighbouring fibres. This occurs where the muscle fibres meet the collagen ones

pertaining to the tendon. This force is then transmitted to the bone, producing joint motion. To the connection between a tendon and a bone is called enthesis (Zatsiorsky & Prilutsky, 2012).

Since the primary activity of a muscle is to shorten, it produces a tensile force. However, a force generates a torque if it is exerted at some distance from the point of rotation. This tensile force pulls the attached bones and generates a torque at the joint(s) crossed by the muscle. The ability of a muscle to produce a torque is regarded as muscle strength, which is the unit used to perform experimental measurements. There are some variables influencing a muscle's ability to generate a torque, such as muscle's size, moment arm, stretch, contraction velocity, level of muscle fibre recruitment and types of fibres composing the muscle (Oatis, 2009). These are approached over the course of this chapter.

A muscle's moment arm or lever arm, r , is the perpendicular distance from the muscle force line of action, F , to the point of rotation, which is the joint's centre of rotation (COR) location. As seen in Figure 3.11, it depends on the distance between the muscle's attachment to bone and the joint's COR, d , and on the angle, named application angle, γ , formed between the line of muscle force production and d (Oatis, 2009). The lever arm is calculated as:

$$r = d \cdot \sin(\gamma) \quad (3.2)$$

The muscle torque, τ , created by muscular contraction, is directly related to the moment arm:

$$\tau = F \cdot r \quad (3.3)$$

Figure 3.11 illustrates the force produced by the quadriceps muscle group, F_{Quad} , the centre of rotation of the knee joint, COR, and the muscle's moment arm, r .

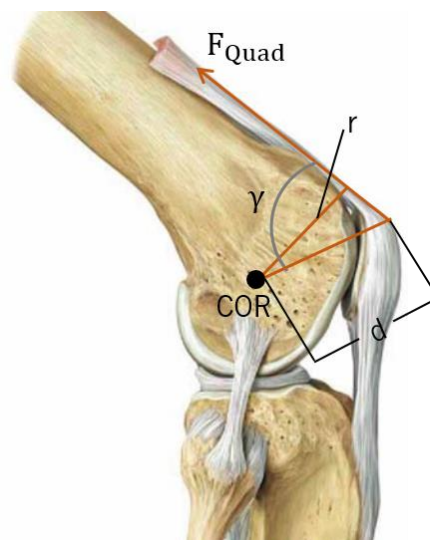


Figure 3.11 – Illustration of quadriceps muscle group force, F_{Quad} , moment arm, r , joint's centre of rotation (COR), application angle, γ , and distance between the muscle's attachment to bone and the joint's COR, d . Adapted from Schuenke, Schulte, et al. (2009) and Oatis (2009).

There is a relation between a muscle's lever arm and the position of the joint it spans, considering its flexed or extended position, shortening or extending the muscle. For instance, the hamstrings muscle group possesses a bigger lever arm when the knee joint is in a flexed position, rather than when it is in an extended position (Figure 3.12).

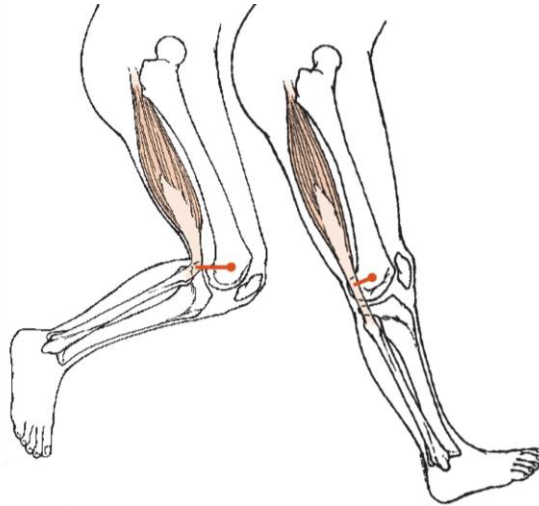


Figure 3.12 - Alterations occurring in a muscle's lever arm with joint position. Application to the hamstrings muscle group. The orange line represents the lever arm. Adapted from Oatis (2009).

3.4. Factors Affecting Muscle-Tendon Unit Force Generation

In the present section, the relation existing between an MTU force production and its length or velocity of contraction is approached, substantiated with an explanation of the mechanical behaviour of this unit. This is approached since the magnitude of the force generated by a muscle is influenced by its contraction velocity and the length of the muscle when the neural signal arises (Hall, 2012).

The distance from the muscle origin to insertion, that is, the length of the MTU, is not always constant during the entire range of motion of the joint (see Figure 3.2). When a joint angle changes, that distance also changes. This alteration in muscle's length profoundly influences the muscle's force generation ability and therefore studies of muscle's force-length relations began (Zatsiorsky & Prilutsky, 2012).

As previously explained, when a neural signal stimulates a motor unit, the muscle fibres pertaining to it are activated to contract and to produce a muscle force. Muscular contractions occur at sarcomere level and result from the formation of cross-bridges between the thick myosin and the thin actin filaments, that is, actin from either side of the sarcomere tends to slide over myosin towards each other, provoking the shortening of the I-band and maintaining the length of the A-band constant. The Z-lines move towards each other and the H zone disappears. Due to this sliding of thin filaments over thick filaments, their

individual total lengths are believed to remain constant during the course of muscular contraction. The number of cross-links formed is proportional to the force production (Hall, 2012; Oatis, 2009; Tavares da Silva, 2003). The four main researchers who introduced this sliding filament theory of muscular contraction were Jean Hanson, Hugh Huxley, Andrew Huxley and Rolf Niedergerke (Squire, 2016).

The active part of the force-length relation is a result of the degree of overlap between the actin and myosin filaments occurring within the sarcomere. Let us think that there are five situations of sarcomere length (Figure 3.13). The first is the one representing a situation in which there is maximum superimposition of actin (orange in Figure 3.13) and myosin (purple in Figure 3.13) filaments and in which titin (green in Figure 3.13) does not allow any space. The Z-lines are maximally closer to each other and the myosin filaments cannot pull the Z-lines any closer. So, considering this, there is no work these filaments can do and therefore the force of contraction is zero. Besides this, actin has some polarity, which means that it only binds to a specific myosin molecule. In the first situation, this is not occurring, that is, actin does not have affinity with the adjacent myosin filament and therefore they do not bind, not producing any contraction force. Therefore, there are 0 out of 20, for instance, myosin filaments working (Desai, 2018).

On situation two, since there is space in between the Z-line and the myosin filament, titin is more stretched and there is a small amount of work these filaments can do. This work is not maximal since there are still some overlapping issues (yellow circles in Figure 3.13) and the muscle is not able to produce its maximum force of contraction because not all myosin filaments are connected to the ones they have affinity with. There are 16/20, for instance, myosin filaments working (Desai, 2018).

On the third situation there is a much more spread out state and it is observable that the two actin filaments are not superimposed. This enables the connection between filaments with affinity to each other and this time all the myosin can work. As one can observe, the sarcomere is progressively getting longer, and the force of contraction is progressively increasing. Since all the myosin filaments are attached to their corresponding actin filaments, they can work and produce force, which is the maximum force of contraction. In this stage, there are 20 out of 20, for instance, myosin filaments working (Desai, 2018).

Note the slopes of the curves formed between point 1 and 2 and point 2 and 3. The first slope is bigger than the second since initially there was no space at all between the Z-lines of the sarcomere and no work was able to be performed. After some stretching of the sarcomere, work was possible, and the force of contraction increased a lot. On the second slope, since work was already being performed, the increase in muscle force was not that high as in the first case (Desai, 2018).

In the fourth case, the sarcomere length increases more than in the third case, but the force of contraction remains constant. This occurs since all the myosin filaments are working and no more can be put to work since there are no more available. As in the previous stage, there are 20 out of 20 myosin filaments working (Desai, 2018). The length at which there is maximal force production is called optimum length (Zatsiorsky & Prilutsky, 2012).

In the fifth situation, the sarcomere length is maximal, and titin is completely stretched. Since the myosin filaments are no longer touching the actin ones, there is not force of contraction and therefore there are again 0 out of 20 myosin filaments working (Desai, 2018).

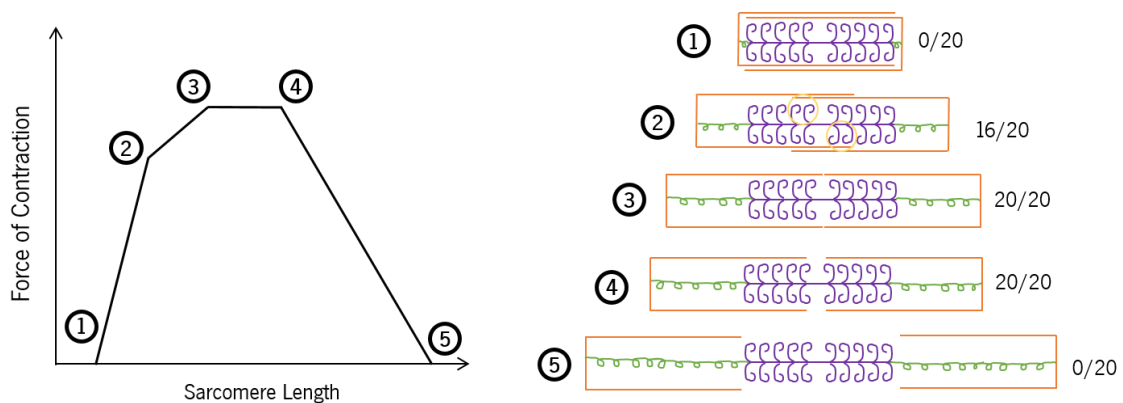


Figure 3.13 - Force-length relation of the active part of a muscle. Adapted from Desai (2018).

The length, inferior to the optimum length, at which no active force can be generated by a muscle is defined as sarcomere active slack length (Zatsiorsky & Prilutsky, 2012).

Besides comprising active components, muscles also pertain passive ones. These passive structures are the noncontractile components of the muscle belly, namely epimysium, perimysium and endomysium, and their adjacent tendons. There are some studies performed on the entire muscle (comprising the muscle belly and its tendons), that demonstrate that as a muscle is progressively stretched, when no contraction is performed, there is a length at which it begins to resist the imposed stretch. As the stretch increases, the pull the muscle exerts against that stretch also increases. This is attributed to the elastic behaviour of the passive structures comprised within the muscle (Figure 3.14).

The response of a muscle's contractile and elastic structures together is examined by measuring the resistance to increasing stretch while simultaneously inducing a muscular contraction. Experiments performed on this basis determine that when the muscle length is very small, allowing no passive recoil, neural stimulation produces a contractile force. With continuous stimulation and increase in stretch, the muscular force increases until it reaches a peak, at resting length. This is the length of the muscle in the

body during anatomic position. With increasing stretch, the force felt by the entire muscle continues to increase. Subtracting the results of the passive test from the results of the combined action of active and passive structures, the active component is determined. This active component in the whole muscle is similar to the one determined at sarcomere level (Oatis, 2009; Zatsiorsky & Prilutsky, 2012). The passive, active and total force-length relation is illustrated in Figure 3.14.

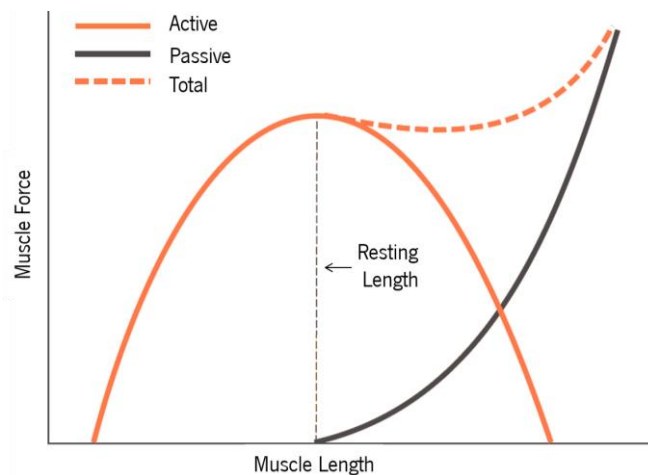


Figure 3.14 - Illustration of a typical force-length relation of a muscle comprising the passive, active and combined components of this curve. Adapted from Oatis (2009).

In summary, if a muscle is stretched beyond its equilibrium length with no neural stimulation, it opposes the stretch force, resisting it, and, therefore, the force of resistance is the passive force. If the muscle possesses a length smaller than its equilibrium length but this time neural stimulation is acting, the force recorded at the muscle's ends arises due to active force. At lengths longer than the equilibrium length with the muscle under stimulation, the recorded force values are due to the summation of both active and passive force components (Zatsiorsky & Prilutsky, 2012).

The response of a muscle to stretching is dependent of the ratio of active and passive elements comprising the entire muscle and on the architecture of the individual muscle (Oatis, 2009). Considering this statement, the force-length relation may be slightly different from the one present on Figure 3.14.

The velocity with which the muscle shortens or lengthens is also an important variable influencing the muscle's ability to produce a force. The force-velocity relation curve of a muscle possesses two regions, the eccentric and concentric ones. The point located in between them represents the maximum isometric force a muscle can produce, which is defined as the maximum amount of force it can generate at maximal activation, A_{max} and optimum sarcomere length, l_{opt} . A greater maximum isometric force is attributed to stronger muscles. However, regardless of the magnitude of this force, the general shape of

the force-velocity curve remains the same (Hall, 2012) and is illustrated in Figure 3.15. Contraction velocity is dependent on the size and type of muscle.

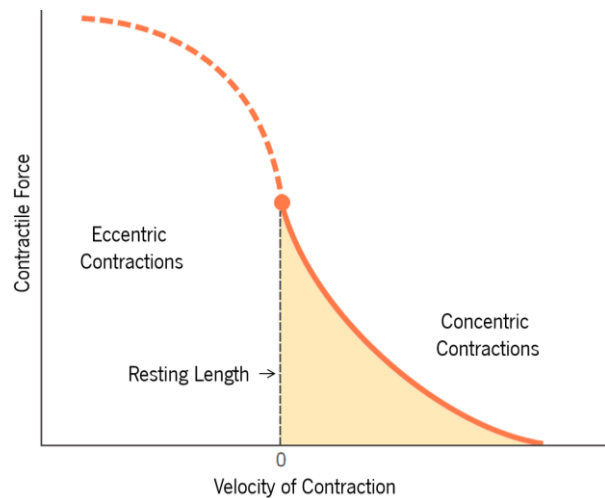


Figure 3.15 - Force-velocity relation of a muscle. The point located in the transition from eccentric to concentric contraction represents the maximum isometric force a muscle is able to generate. Adapted from Oatis (2009).

Hill in 1938 was the first author describing the force-velocity relation for concentric muscular contractions. Since his mathematical relation is only related to maximally activated muscles, it is not applicable to muscle actions performed during most daily activities. The shape of the concentric part of the force-velocity curve is related to the rate of energy production in a muscle (Hall, 2012).

Hill (1938) states that during muscle shortening, there is a release of energy in two independent forms, being heat proportional to the shortening distance, x ,

$$\text{Shortening Heat} = a \cdot x \quad (3.4)$$

and mechanical work also proportional to the shortening distance, x ,

$$\text{Mechanical Work} = F \cdot x \quad (3.5)$$

a is the shortening heat constant expressed in force units as g. weight. Since the quantity a is related to a muscle's weight it is dependent on its size, and, in particular, on its cross-sectional area (CSA) (Hill, 1938). This area can be calculated in two manners: anatomical and physiological. The former corresponds to the area at the muscle's widest point, being perpendicular to the length of the entire muscle. The physiological CSA is calculated as the area in which all the muscle fibres are contained (Oatis, 2009). F is the load lifted by the muscle (Hill, 1938).

According to Hill (1938), the total energy liberation is

$$\text{Total Energy Liberation} = F \cdot x + a \cdot x = (F + a) x \quad (3.6)$$

and, therefore, the rate of total energy liberation is:

$$\text{Rate of Total Energy Liberation} = (F + a) \frac{dx}{dt} = (F + a)v \quad (3.7)$$

in which v is the muscle's shortening velocity.

In one of his papers, Hill found in his experiments that the rate of energy liberation, $(F+a)v$, is also a rather linear function of the load a muscle lifts, F (Figure 3.16):

$$\text{Rate of Total Energy Liberation} = b(F_{\max} - F) \quad (3.8)$$

Therefore:

$$\begin{aligned} (F + a)v &= b(F_{\max} - F) \\ \Leftrightarrow (F + a)(v + b) &= (F_{\max} + a)b \end{aligned} \quad (3.9)$$

in which b is a constant defining the absolute rate of energy liberation, having velocity's dimensions (cm/s), and F_{\max} is a muscle's maximum isometric force.

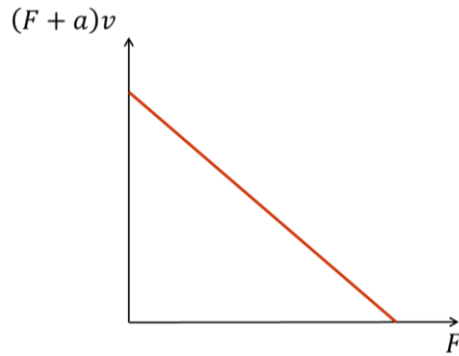


Figure 3.16 - Relation between energy liberation, $(F+a)v$, and load, F . Adapted from Hill (1938).

The first part of Eq. 3.9 is known as the characteristic Hill equation, relating muscle force and velocity during concentric contractions (force-velocity relation), representing a hyperbola (concentric part of Figure 3.15). This equation is not valid for eccentric contractions. Solving for F , Eq. 3.9 stays:

$$F = \frac{F_{\max}b - av}{v + b} \quad (3.10)$$

Setting $F=0$, it means that the muscle is unloaded and therefore its velocity is maximum, v_{\max} :

$$F_{\max} b = a v_{\max} \Leftrightarrow v_{\max} = \frac{F_{\max} b}{a} \quad (3.11)$$

In Eq. 3.9, the maximum isometric muscle force, F_{\max} , is determined for the sarcomere optimum length, l_{opt} , and therefore, in order to use it for all muscle lengths, l , the equation is modified as:

$$F = \left(\frac{F_{\max}b - av}{v + b} \right) f(l) \quad (3.12)$$

$f(l)$ is the dependence of the isometric muscle force on the muscle length (Zatsiorsky & Prilutsky, 2012).

When both force-length and force-velocity relations (Figure 3.17) are known, they are frequently combined in one expression:

$$F = F_{\max} f(v)f(l)A_{MTU} \quad (3.13)$$

where F_{\max} is the maximum isometric force, A_{MTU} is the muscle activation, $f(l)$ and $f(v)$ are the force-length and force-velocity relations, respectively. $f(l)$ can be expressed as:

$$f(l) = \exp\left(-\left|\frac{\left(\frac{l}{L_0}\right)^\beta - 1}{\omega}\right|^\rho\right) \quad (3.14)$$

in which β , ρ , and ω are constants that describe the shape and breadth of the $f(l)$ relation (Zatsiorsky & Prilutsky, 2012).

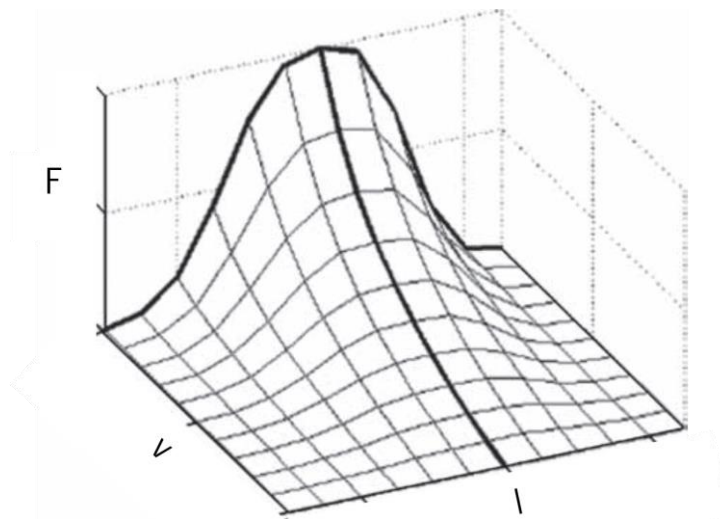


Figure 3.17 – Changes in muscle force (F) with respect to variations in velocity (v) and length (l). Adapted from Buhmann & Di Paolo (2014).

A muscle's capacity of generating force and perform mechanical work depends on the muscle's previous state, that is, whether the muscle was lengthening or shortening immediately prior to force generation. Therefore, it is very important to note that these expressions of force-length and force-velocity behaviour do not account for the preceding history of muscle action (Zatsiorsky & Prilutsky, 2012).

A muscle's activation can be characterized as a first order differential equation, relating the rate of change of muscle activation (as previously explained, that is release of ACh and the increase in concentration of calcium ions within the muscle fibres) to the muscle stimulation (as previously explained, the firing of motor units provoked by neural stimulation) (Geyer, Seyfarth, et al., 2003):

$$\frac{dA_{MTU}(t)}{dt} = \frac{S_{MTU}(t) - A_{MTU}(t)}{\tau_{ecc}(a, u)} \Leftrightarrow \tau_{ecc}(a, u) \frac{dA_{MTU}(t)}{dt} = S_{MTU}(t) - A_{MTU}(t) \quad (3.15)$$

in which $S_{MTU}(t)$ is the stimulation signal, ranging from 0 (no stimulation) to 1 (full stimulation), $A_{MTU}(t)$ is the activation signal, ranging from 0 (no contraction) to 1 (full contraction), and $\tau_{ecc}(a, u)$ is the time constant, which varies from author to author (Geyer, Seyfarth, et al., 2003).

It is also important to note that the equations approached in this section are examples of mathematical formulations used to mimic the muscle behaviour approached throughout this chapter. However, depending on the authors and their experimental results, these expressions may vary.

3.5. Muscle-Tendon Unit Modelling

The modelling of the MTU aims to attribute elements with mathematical characteristics similar to the ones found on the muscle, regarding its behaviour, which was approached in the previous section.

As previously explained, the muscle has elastic properties. Considering this knowledge, quick-release experiments were performed to determine what type of structures were responsible for this elasticity. The quick-release apparatus is shown in Figure 3.18a. Essentially this experiment holds the muscle in isometric tetanus, T_0 , until the moment when the catch mechanism is no longer supported by the electromagnet and no longer holds the muscle at constant length, but rather at constant tension, T . This tension is determined by the weight positioned in the pan. The time dependence of the tension applied to the muscle and its variation of length throughout the whole experiment is presented in Figure 3.18b and Figure 3.18c, respectively.

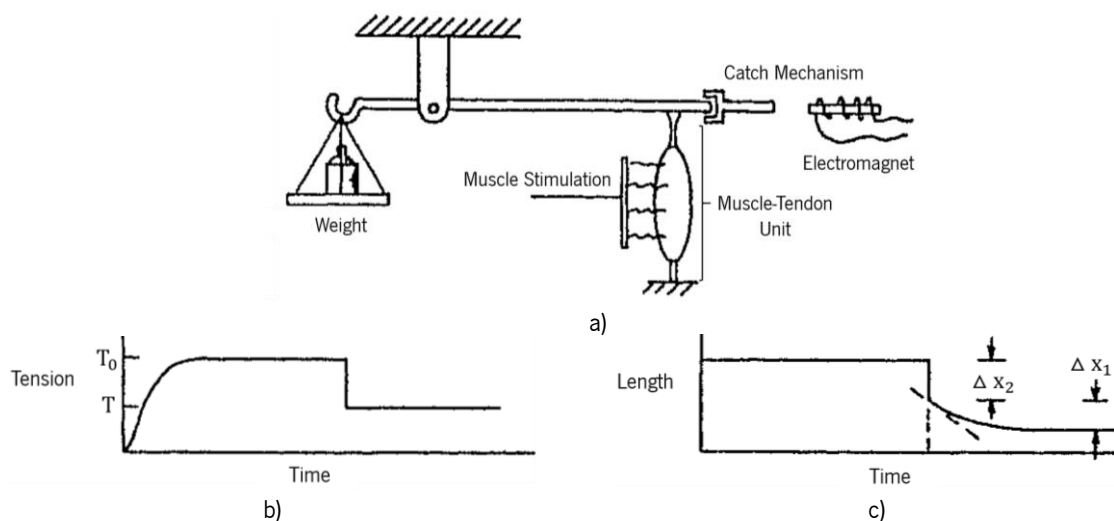


Figure 3.18 - Experiments used to determine the origin of muscle elasticity. a) Quick-release apparatus. b) Tension-time curve. c) Length-time curve. Adapted from McMahon (1984).

Observing Figure 3.18b and Figure 3.18c, one can see that the rapid change in tension is initially accompanied by a rapid change in length (Δx_2). This is consistent with the mechanical definition of a spring, comprising a unique length for every force applied, but it is not affected by the velocity the length is changing.

Supposing that the contractile part of the muscle is not capable of changing its length instantaneously, then all this rapid shortening (Δx_2) seen in Figure 3.18c is attributed to the tendon part of the muscle tendon unit, being characterized as series elastic component or element (SE) in muscle-tendon unit modelling.

From the point where this rapid change in length occurs on, any further changes in length are attributed to the contractile part of the muscle-tendon unit. These length changes (Δx_1) are dependent on time and are characterized as a contractile component or element (CE) in modelling. These considerations assume that the contractile component is damped and is not able to change its length instantaneously (McMahon, 1984).

When a muscle is being passively stretched, meaning that there is absence in muscular stimulation, it acts as a spring, comprising elastic behaviour. The muscle's behaviour in these conditions is attributed to the existence of a parallel elastic component (PE), which aims at modelling the muscular structures previously explained, named epimysium, perimysium and endomysium, which are located around the muscle belly.

However, as explained in the preceding paragraph, when a muscle is stretched and is simultaneously being stimulated, the spring-like elastic behaviour it presents is attributed to a series elastic component (SE), arising from the tendon's behaviour. These two components are termed series and parallel since the tendon and the muscular structures are in series and parallel with the muscle fibres, respectively. The muscle fibres represent CE, since their behaviour is related to muscular contraction (Hall, 2012; Zatsiorsky & Prilutsky, 2012).

Generally, the combined behaviour of muscle contraction and stretch are mechanically modelled as a contractile component (CE), representing the muscle's active properties, in parallel and in series with elastic components, representing the muscle belly tissues and the tendon at the end of the muscle, respectively (Figure 3.19) (Oatis, 2009).

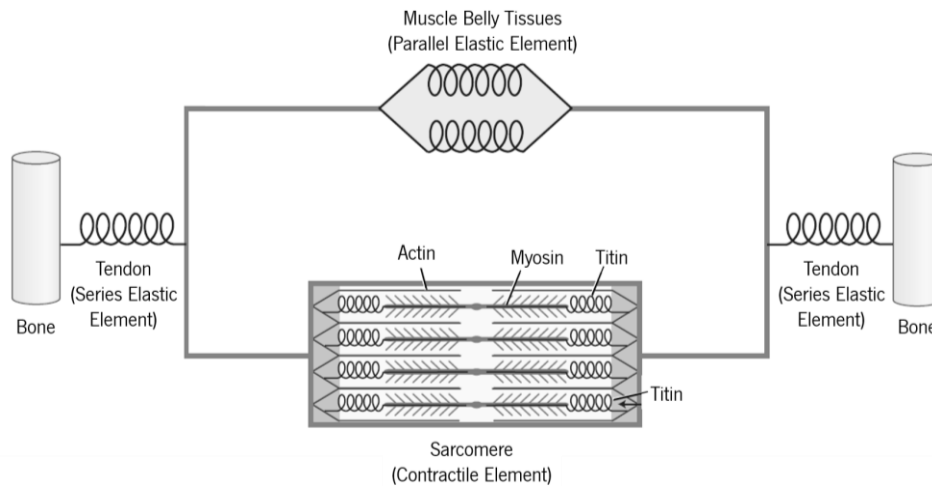


Figure 3.19 - Elements used to model an MTU. Adapted from Palastanga & Soames (2012).

There are several models used to calculate the ability of a muscle and tendon, and therefore, a muscle-tendon unit, to generate force. Over the course of the following paragraphs, five models with increasing complexity are approached, according to Anderson (2007). Note that other models can pertain different properties, attributing diverse modelling approaches to the elements of the MTU, depending on the authors and performed studies. In this section, only a general idea of the presented models is given.

The simplest model for calculating the force produced by an MTU is illustrated in Figure 3.20, including only a contractile element (CE). It does not comprise any formulation regarding the pennation angle and therefore the muscle fibres' force has the same direction as the tendon's force. The generated force is not dependent on the MTU's force-length or force-velocity relations (see section 3.4), being only related to the maximum isometric force, F_{max} , and muscle's activation, A_{MTU} , of CE (Anderson, 2007), through the following expression:

$$F_{MTU} = F_{Tendon} = F_{CE} = A_{MTU} F_{max} \quad (3.16)$$

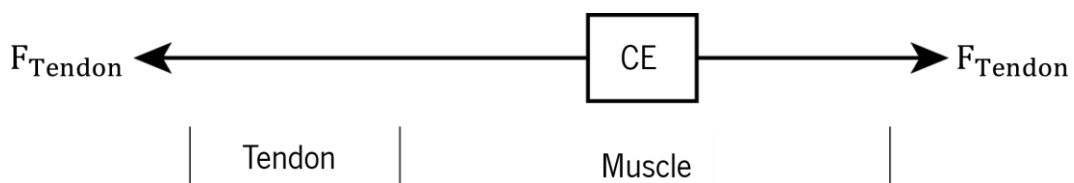


Figure 3.20 - Simplest model to calculate force production by an MTU. The force depends only on the muscle activation and maximum isometric force. This model does not include the pennation angle, neither force-length and force-velocity relations. Adapted from Anderson (2007).

The following model is similar to the one presented in Figure 3.20, however this one includes the influence of the pennation angle, α , on the force generated by the MTU and is illustrated in Figure 3.21.

In these two models, the tendon is assumed to be in series with the muscle, comprising infinitely stiff properties, that is, no elastic behaviour (Anderson, 2007).

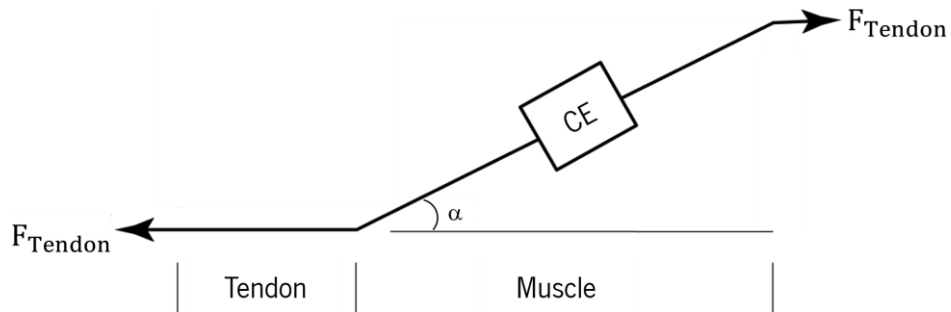


Figure 3.21 - Simplest model to calculate force production by an MTU with the inclusion of the influence of the pennation angle, α , and CE's properties, that is, muscle activation, A_{MTU} , and maximum isometric force, F_{max} . Adapted from Anderson (2007).

In similarity to the previous model (Figure 3.20), the model from Figure 3.21 does not include the influence of both the length and velocity of contraction of the structures comprised within the MTU on its force calculation. Therefore, using this model, the force produced by the MTU is similar to Eq. 3.16 but is also includes the pennation angle's influence, being calculated as (Anderson, 2007):

$$F_{MTU} = F_{Tendon} = F_{CE} \cos(\alpha) = A_{MTU} F_{max} \cos(\alpha) \quad (3.17)$$

The third model is more complex, including the MTU's force-length, $f(l)$, and force-velocity, $f(v)$ relations, however the tendon still comprises infinitely stiff properties. The force produced by the muscle-tendon unit is also dependent not only on the force produced by the contractile element, F_{CE} , but also on the one produced by the parallel elastic element, F_{PE} . As seen from Figure 3.22, this model does not account for the pennation angle, being, in this matter, similar to the one of Figure 3.20 (Anderson, 2007).

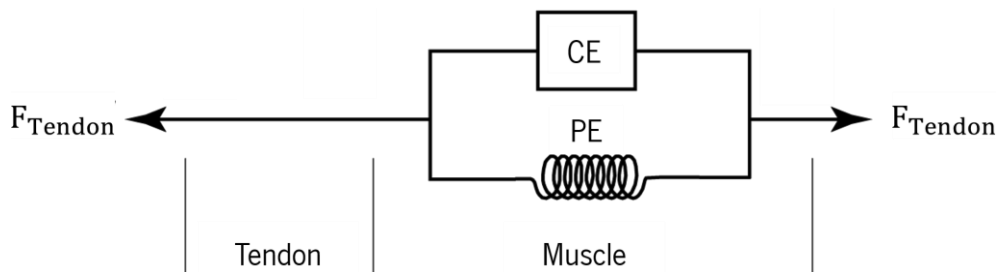


Figure 3.22 - Model used to calculate force generated by an MTU, which is modelled as a parallel elastic element (PE) and a contractile element (CE), in parallel with each other. The force depends on the characteristics of these two elements, including force-length and force-velocity relations. This model does not include the pennation angle. Adapted from Anderson (2007).

The force of the muscle-tendon unit presented in Figure 3.22 is given by:

$$F_{MTU} = F_{Tendon} = F_{CE} + F_{PE} = A_{MTU} F_{max} f_l(l_{CE}) f_v(v_{CE}) + F_{max} f_l(l_{PE}) \quad (3.18)$$

The following model is more complete than the others since, besides including PE and CE and their force-length, $f_l(l_{CE})$ and $f_l(l_{PE})$, and force-velocity, $f_v(v_{CE})$, relations, it also considers the inclusion of the muscle fibres' pennation angle, α . Therefore, the force generated by the MTU is similar to the one found on Eq. 3.18, but with the inclusion of the pennation angle. The expression, therefore, is (Anderson, 2007):

$$\begin{aligned} F_{MTU} = F_{Tendon} &= (F_{CE} + F_{PE}) \cos(\alpha) \\ &= (A_{MTU} F_{max} f_l(l_{CE}) f_v(v_{CE}) + F_{max} f_l(l_{PE})) \cos(\alpha) \end{aligned} \quad (3.19)$$

The tendon is, as in the other models, infinitely stiff. Figure 3.23 represents the referred model.

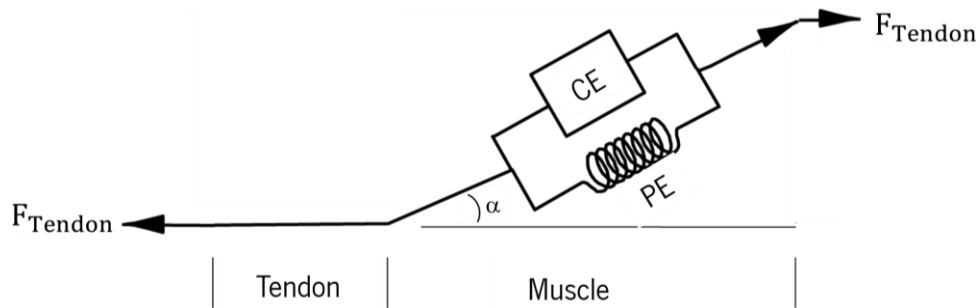


Figure 3.23 - Model used to calculate the force generated by an MTU, which is modelled as a parallel elastic element (PE) and a contractile element (CE), in parallel with each other. The force depends on the characteristics of these two elements, as well as on the pennation angle, α , verified between the tendon and the muscle fibres. Adapted from Anderson (2007).

The last model included in this work is the one presented in Figure 3.24. This model comprises a tendon modelled with an elastic behaviour (SE, series elastic element) in series with the muscle, comprising a contractile element (CE) and a parallel elastic element (PE). Considering these elements, the MTU's force is dependent on their length, $f_l(l_{CE})$, $f_l(l_{PE})$ and $f_l(l_{SE})$, and velocity of contraction, $f_v(v_{CE})$. This model does not consider the influence of the pennation angle and therefore assumes that the muscle fibres act in the same direction as the tendon (Anderson, 2007).

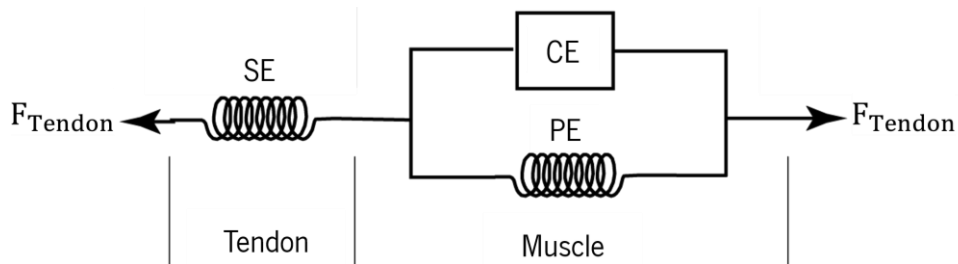


Figure 3.24 – Model of an MTU, which is modelled as a series elastic element (SE) representing the tendon in series with a parallel elastic element (PE) and a contractile element (CE), in parallel with each other. Adapted from Anderson (2007).

The expression for the MTU force for the model presented in Figure 3.24 is similar to the one of Eq. 3.18, however in the model pertaining to that equation (Figure 3.22) the tendon comprises no elastic properties, which is different from the tendon of this model, presenting those characteristics. Therefore, in these two models (Figure 3.22 and Figure 3.24), the expressions for the tendon force, which in this model is $F_{Tendon}=F_{SE}$ and in the one from Figure 3.22 is F_{Tendon} , are different. Therefore, the MTU force is as follows:

$$F_{Tendon} = F_{SE} = F_{max} f_l(l_{SE}) \quad (3.20)$$

$$F_{MTU} = F_{SE} f_l(l_{SE}) = F_{CE} + F_{PE} = A_{MTU} F_{max} f_l(l_{CE}) f_v(v_{CE}) + F_{max} f_l(l_{PE})$$

In this section, the expressions for $f(l)$ of F_{CE} , F_{SE} and F_{PE} , and $f(v)$ of F_{CE} are not detailly described since they can vary according to the author and different studies. The expressions used in the lower limb biomechanical model used in this work are explained in detail in chapter 5.

3.6. Summary and Discussion

In this chapter, the anatomy and physiology of the human skeletal muscle-tendon unit was described. An MTU is composed by the muscle belly and its tendinous attachments to bones. This structure enables the production of joint motion by contracting and moving the bones of the skeletal system attached to it. In order to do this, a muscle requires a signal from the nervous system to be sent to its muscle fibres, stimulating and activating them to contract. Depending on the muscle's structure, the magnitude of the produced muscle force of contraction varies. Essentially a muscle force of contraction, if exerted at a distance from the joint's COR, produces a joint torque, which is greater the bigger the lever arm.

A muscle force is dependent on both its length and velocity of contraction. These and other experimental result's enable us to infer that some active and passive components within the MTU are present. In computational modelling these components are modelled as a contractile, series elastic and parallel elastic components within the MTU, which are used to represent its behaviour. The ending part of the chapter presents five different biomechanical models used to calculate the force generated by an MTU, considering its components (CE, PE and SE) and their characteristics, as well as the pennation angle.

The understanding of the matter related to these fields is very important in order to understand the computational modelling of these structures throughout this dissertation.

4. REQUIREMENTS FOR THE BIOMECHANICAL MODEL UTILIZED

This chapter presents part of a methodology, which was applied to the biomechanical model utilized. The methodology is called Quality Function Deployment (QFD) and is related to the production of a product, comprising four phases (Figure 4.1). The first phase is called House of Quality and comprises the determination of the customer requirements for the product under development, which are then translated into technical specifications. The second phase involves the transformation of those key technical specifications into parts characteristics, which are then used in phase three of QFD, being translated into manufacturing specifications. These are then translated into performance indicators to monitor the production process of the product, in phase four. This structure assures that a more customer-driven product reaches the market faster and at a lower cost (Halbleib, Wormington, et al., 1993; Roberts, 2007).

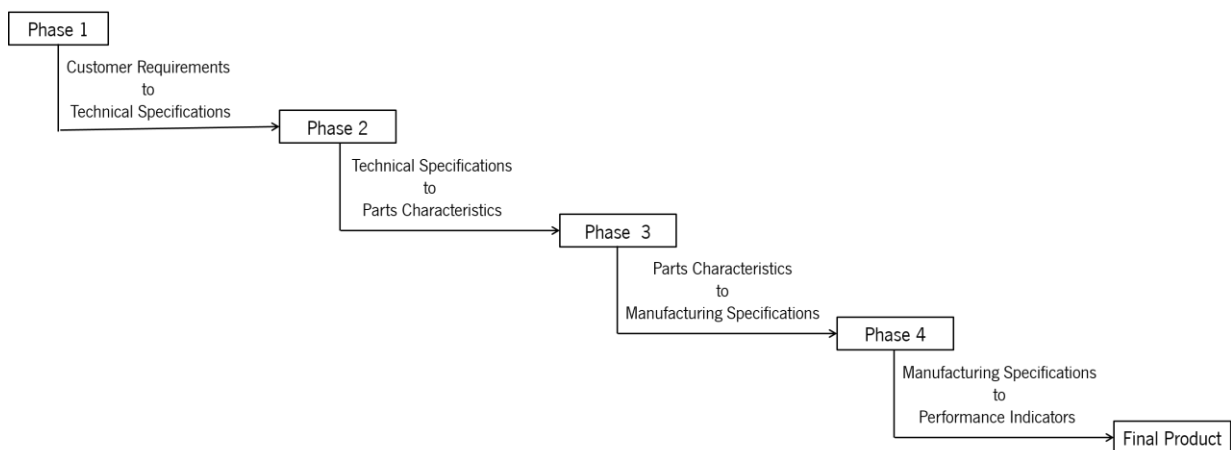


Figure 4.1 - Quality Function Deployment methodology phases.

Even though QFD comprises four phases, in this work only the House of Quality, HoQ, was included. This methodology was utilized in order to determine which customer requirements exist relative to the biomechanical model and what technical specifications are necessary to be taken into account to satisfy the first requirements. To this end, after explaining the methodology, the product, which is the biomechanical model, is described. Likewise, the customer requirements and technical specifications, as well as the target values used for the latter specifications are analysed and explained. The developed HoQ is displayed. Lastly, after explaining all the parameters involved in the construction of the phase one of QFD, a critical analysis of the developed HoQ is performed, determining which requirements are viable of including in the final biomechanical model.

4.1. Methodology Adopted

Quality Function Deployment (QFD) is a structured planning process that aims for the design of a product or service, systematically incorporating the qualitative customer needs or requirements into process or product design, by translating them into quantitative technical specifications, design targets and quality assurance points for that particular product or service. This process was developed in 1966 by Yoji Akao in Japan (Akao, 2004; Cohen, 1995; Roberts, 2007).

The methodology allows the production of higher quality and customer-driven products, getting them to reach the market faster and at a lower cost, providing a tracking system for future design or process improvements. After applying QFD to a product or process, it is expected a better understanding of the customer needs for that particular product or process, an improved organisation on the developed projects, fewer design changes later in the development process, fewer manufacturing problems and a documented product definition based on acquired customer requirements (Roberts, 2007).

The traditional Quality Function Deployment process comprises four phases, beginning with a conceptual design of the product and terminating with the planning of the production processes used to manufacture the product. The first phase is led by a cross-functional team of the marketing department, whose function is to translate customer requirements into product specifications, that, if satisfied, will assure customer satisfaction. To this phase is commonly given the name of House of Quality (HoQ). Phase two of QFD is led by the engineering department and aims to translate the key product specifications into parts characteristics. The team determines which of the assemblies, systems, subsystems or components of the product have a greater impact on meeting the product specifications. In phase three, the parts characteristics identified on the previous phase are translated into process manufacturing specifications. This part is led by the manufacturing engineering team. Manufacturing processes involved in producing the parts analysed in phase two are, at this stage, investigated. Lastly, the fourth phase involves the translation of the characteristics of the manufacturing process arising from phase three into performance indicators to monitor and control the production process.

These structured phases of QFD assure that the development of the product is targeted to the customer using it, ensuring that the development team focus on its requirements (Halbleib, Wormington, et al., 1993). In the present work, only the first phase of QFD was approached, since it was desirable to understand what requirements should be incorporated in the biomechanical model to satisfy its users.

The house of quality is the first of four stages that comprise the QFD. It enables the companies to identify and classify customer needs, determining the importance of those needs, identifying the technical specifications which may be relevant to achieve those customer desires, correlate the two and then assign objectives and priorities for the entire system's requirements. The result of the HoQ is generally a matrix (Figure 4.2) combining the referred and other parameters, including direction of improvement, correlation matrix, target or limit value, difficulty of execution and importance of customer requirements and technical specifications (Stoll, 1999). Each of these parameters are approached in the following sections.

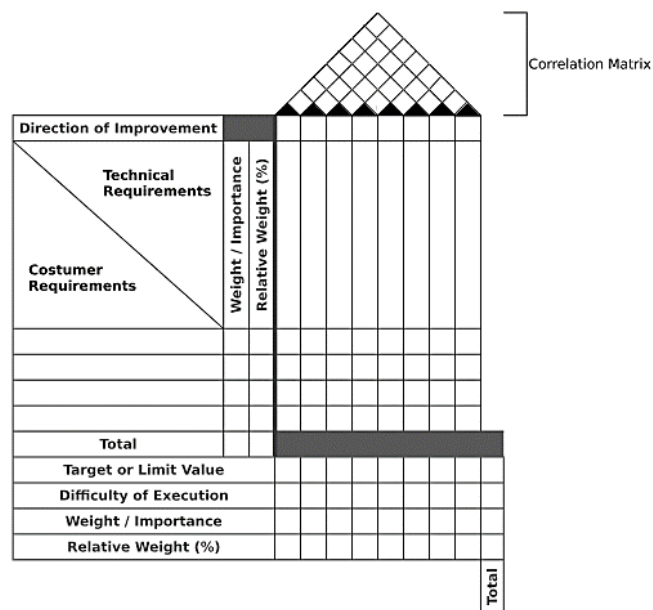


Figure 4.2 - House of Quality general template.

4.2. Biomechanical Model Description

With the developments in computer technology, the use of computer models in the field of biomechanics became widespread. Biomechanical computer models can be divided into two main groups, the multibody and the numerical models.

The first can be used in two different ways: as forward or as inverse dynamics models. In the forward dynamics models, the physical forces and moments are the given quantities, which together with geometric body data (e.g. length of a body segment) and mechanical parameters (e.g. moments of inertia) enable the calculation of the resulting body movement. The inverse models use the body's movements to compute the system's forces and moments (Engel, Herpers, et al., 2011).

The numerical models use the Finite Element Method (FEM), which is a numerical technique that searches for approximate solutions to differential equations that are difficult to obtain analytically or that

no analytical solution exists. This method divides one continuum physical problem into one discrete problem through its division into finite elements. All elements are assembled together, and it is possible to analyse the approximate system's response (Liu & Quek, 2014; Zienkiewicz, Taylor, et al., 2013).

To obtain experimental kinematic and dynamic human data to be used in study and development of these models, one must use measurement technology. For instance, force platforms dynamically quantify reaction forces when a person is walking or running across the sensor, electromyography (EMG) monitors measure action potentials of contracting muscles with electrodes attached to the human skin. This information is either used as an input for the model or is used to validate the developed model (Engel, Herpers, et al., 2011).

The biomechanical model utilized in this work is a forward dynamics model and is based on the one developed by Geyer & Herr (2010), using neural reflexes (force and length feedback) in conjunction with Hill-type muscle models to produce joint torques. In order to detect and to interchange between these neural reflexes associated with stance and swing phases of gait and to produce a natural gait, ground sensors are placed under the model's feet. Essentially, if contact is detected, stance phase reflexes (mainly extensor muscular activity) are used. However, if there is no contact between the foot and the ground, swing phase reflexes (mainly flexor muscular activity) arise. The gait cycle is generated by using such reflexes by a sequence of time-delayed reactions, that is, each muscle has associated a time delay (see section 3.3), meaning that only after that delay it influences the dynamics of the model (Dzeladini, van den Kieboom, et al., 2014).

The model is implemented in Simulink® from MATLAB® R2017b (MathWorks), comprising layers or modules that define its general characteristics (for instance, number of body segments and muscles) and that all together enable the normal functioning of the model. The Body Mechanics layer encompasses all the geometric and physical properties important to the definition of the anatomy of the model, such as the characteristics of the segments and joints. The Muscle Actuation layer contains the characterisation of the lower limb's Hill-type muscles used to perform movement. The feedback schemes and the part of the model that represents the muscles' stimulation and delays, as well as other parameters commanded by the central nervous system, are modelled in the Neural Reflex layer. These layers are approached in detail in chapter 5.

Essentially the biomechanical model comprises seven segments connected by six revolute joints. The segments are one HAT (head, arms and trunk), two thighs, two shanks and two feet. The joints comprised are two hip, two knee and two ankle joints. Considering this, the biomechanical model

represents mainly and in more detail the lower limb of the human body, being the upper limb represented only by the HAT. The characteristic language used in Simulink® is explained in Appendix I.

Besides the definition of its segments and connecting joints, the model presents a total of 14 muscle-tendon units, seven in each leg, namely, soleus muscle (SOL), tibialis anterior muscle (TA), biarticular gastrocnemius muscle (GAS), vasti lumped muscle group (VAS), biarticular hamstring muscle group (HAM), hip flexor muscle group (HFL) and gluteus muscle group (GLU). MTU modelling, as well as activation and stimulation modelling are based on the explanations given in chapter 3 and are clarified in more detail in chapter 5. Figure 4.3 presents an illustration of the biomechanical model utilized.

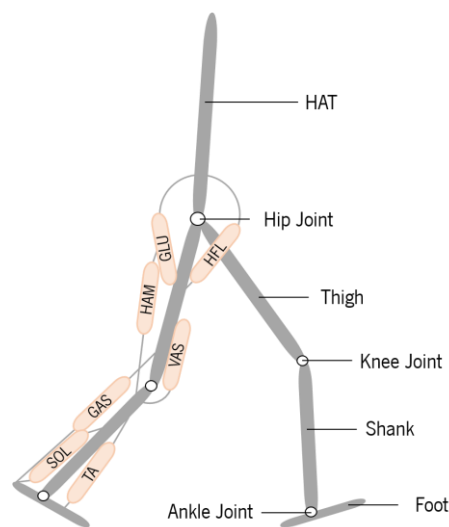


Figure 4.3 - Biomechanical model used. The model comprises 7 segments (one HAT, two thighs, two shanks and two feet), connected by 6 revolute joints (two hip, two knee and two ankle joints). The model comprises the soleus muscle (SOL), tibialis anterior muscle (TA), biarticular gastrocnemius muscle (GAS), vasti lumped muscle group (VAS), biarticular hamstring muscle group (HAM), hip flexor muscle group (HFL) and gluteus muscle group (GLU). Adapted from Geyer & Herr (2010).

4.3. House of Quality Development

In the present section of this chapter, a detailed description of the customer requirements and technical specifications, as well as every consideration taken while developing the HoQ, is presented. In the final part of the section, the developed house of quality for the biomechanical model is presented.

4.3.1. Customer Requirements

The customer requirements and the importance of getting them into the final product are typically obtained by performing market surveys of the people who consume the product being analysed. These essentially involve the function and performance requirements the consumers want to be incorporated in the product (Jacques, Ryan, et al., 1994; Logan & Radcliffe, 1997).

In this work, the customers of the biomechanical model are the people who are going to use it for biomechanical studies involving the lower limb. In order to determine their needs for the biomechanical model being studied, a small survey was performed, and the obtained results are listed and described in Table 4.1 without any particular order.

Table 4.1 - Customer requirements for the biomechanical model

Requirement	Description
Computationally Efficient	The model is required to achieve maximum productivity (to perform a required task in the minimum amount of time). This requirement is related to the hard disk space and Random Access Memory (RAM) of the computer used in the simulation of the biomechanical model and affects its execution regarding the computation time.
Self-adaptive	The model must be self-adaptive, which means that it preserves its working capability under conditions of unexpected changes. Considering that the model is walking on level ground, when it faces a terrain with irregularities (e.g. slopes or stairs), it must be capable to adapt to those changes without failing.
Realistic Output	The model must provide realistic results, meaning that its global kinematics (joint accelerations, velocities and positions) and dynamics (joint torques and forces) must resemble those of experimental human gait results.
Emulate Musculoskeletal System	The model must mimic the human musculoskeletal system, meaning that it should estimate musculoskeletal joint torques, not overcome the joints' range of motion, produce biological walking mechanics and muscle activation patterns.
Recreate Pathological Condition	The model must be able to recreate the desired pathological condition, meaning that it must have mechanisms to enable alterations in joints' range of motion (ROM) and muscle force, amongst others, in such a way that its kinematics and dynamics resemble that of a patient with a desired pathological condition.
Adjustable/Scalable	The model must be able to be modified according to each individual's musculoskeletal characteristics (for example, weight and limb's dimensions).
Perform different activities	The model must be able to perform different human daily activities such as: walking, running, sit down, stand up, stairs up and stairs down.

Table 4.1 (continued) - Customer requirements for the biomechanical model

Requirement	Description
Provide data exchange	To meet this customer requirement, the biomechanical model's outputs need to be determined and must be able to be used as inputs to other studies. For instance, determine the outputs of the model's knee joint torque and use it as input to a control strategy from another study.
Able to include an exoskeleton	The biomechanical model needs to be flexible enough so that a Computer Aided Design (CAD) model can be added to it in order to simulate the addition of an exoskeleton (e.g. its mass) in real life and to determine which alterations this additional object provokes on the model's healthy or pathological gait.

4.3.2. Technical Specifications

Technical specifications possess direct relation in meeting the previously mentioned customer requirements. These comprise the manners how to achieve to the customer needs in the final product (Logan & Radcliffe, 1997). While customer requirements are qualitative, technical specifications are quantitative parameters, being objectively quantified whenever possible (Jacques, Ryan, et al., 1994). To meet the requirements described, the following technical specifications were defined (Table 4.2):

Table 4.2 - Technical specifications for the biomechanical model. In between parenthesis, there is the unit of the specification

Specification	Description
Hard Disk Space (GB)	The computer's hard drive stores all the data belonging to the biomechanical model.
Random Access Memory or RAM (GB)	RAM plays a great role in the computer's speed and stability, particularly when performing different tasks at the same time and using resource-intensive applications. The higher the RAM, the better the computer performs while simulating the biomechanical model.
Number of Variables	Represented as inputs, such as joint angles limits and muscle parameters, and as outputs, such as forces and moments. These variables must be considered to create a biomechanical model as similar to the human body as possible. The number of variables is related to the number of data exchange variables.

Table 4.2 (continued) - Technical specifications for the biomechanical model. In between parenthesis, there is the unit of the specification

Specification	Description
Number of Dynamic Equations	Related to the dynamic equations of muscles. Must be considered in order to create a biomechanical model as similar to the human system as possible.
Slope (%)	The percentage of terrain inclination must be considered accordingly to slopes people would encounter in real life.
Error (%)	The results of the model and the experimental data from human walking present in literature must be evaluated and the error must be minimized in order to acquire better similarities between both systems.
Data Exchange (Number Of Signals)	The model must provide easy access to data so that the user can utilize it (as input) in a fast and accurate way.
Joint Power (W/kg)	The model must be able to mimic joint power according to the patient's condition it is required to simulate (healthy or pathological).
Joint Torque (Nm/kg)	The model must be able to mimic joint torque according to the patient's condition required to simulate (healthy or pathological).
Vertical Ground Reaction Force (%BW)	The model must be able to mimic vertical ground reaction forces according to the patient's condition required to simulate (healthy or pathological).
MTU Strength Reduction (%)	The model must be able to mimic MTU strength according to the patient's condition required to simulate (healthy or pathological).
Range of motion (degrees)	The model must be able to mimic the joint range of motion according to the patient's condition required to simulate (healthy or pathological).
Number of MTUs	The model must have a number of MTUs that meet the customer requirements in an optimized way, meaning that it incorporates a minimal number of muscles that mimics in the best way possible the human body (kinematics and dynamics), not increasing the computational complexity.
No. Scale Equations	Included to enable the model to be adjusted to a variety of patients.
Computation Time (s)	This variable is important to consider in order to perform simulations in the shortest period of time, however, without losing accuracy of the model's results.

4.3.3. Target or Limit Value

Establishing target values for each technical specification is necessary. This way, concrete goals are established. These target values must be measurable, being defined based on experimental results, analysis of what the competition is doing, or analysis of literature data, for example. The target values for the technical specifications demonstrated above are presented in Table 4.3.

Table 4.3 - Target or limit values for the technical specifications

Technical Specification	Target Value	Technical Specification	Target Value
Hard Disk Space (GB)	1 GB	Joint Torque (Nm/kg)	H: [-1.5, 1.5] K: [-0.75, 0.75] A: [-0.5, 2]
RAM (GB)	4 GB	Vertical Ground Reaction Force (%BW)	[0, 120]
Number of Variables	112	MTU Strength Reduction (%)	Q: [5%, 40%] H: [9% 27%]
Number of Dynamic Equations	84	Joint Range of Motion (degrees)	H: [-10, 40] K: [0, 60] A: [-20, 10]
Slope (%)	5%	Number of MTUs	14
Error (%)	5%	Number of Scale Equations	21
Data Exchange (No. Of Signals)	48	Computation Time (s)	60
Joint Power (W/kg)	H: [-2,2] K: [-1.5, 1.2] A: [-1.5, 5]		

In the above table there are some target values for the technical specifications that need to be more explained in detail. This explanation is given in the following paragraphs.

The number of variables to be considered in the model are described subsequently. On one hand, the outputs comprise the sagittal plane hip, knee and ankle joint motion (degrees), power (W/kg) and torque (Nm/kg), vertical ground reaction forces (GRF) (% of body weight) and muscle force (N) and

activation. On the other hand, the inputs include six anthropometric parameters (see Table 5.1), eight individual and seven common muscle parameters (see Table 5.2 and section 5.2), seven muscular pre-stimulations (see Table 5.3) and eight ground interaction model parameters (see Table 6.3). Eq. 4.1 comprises the calculation of this technical specification, named number of variables.

$$\begin{aligned} \text{No. of Variables} = & 2_{\text{legs}} \times (3_{\text{joint motion}} + 3_{\text{joint power}} + 3_{\text{joint torque}} + 1_{\text{GRF}} + \\ & 7_{\text{muscle force}} + 7_{\text{muscle activ.}} + 6_{\text{anthropometric param.}} + 8_{\text{individual MTU parameters}} + \\ & 7_{\text{common MTU parameters}} + 7_{\text{MTU stimulations}}) + 8_{\text{ground model}} = 112 \end{aligned} \quad (4.1)$$

The dynamic equations involve the muscle tendon unit (MTU) modelling equations (see section 5.2). These are several equations which define the muscle tendon unit, composed by an active contractile element (CE), a series elasticity element (SE), a parallel elasticity element (PE) and a buffer elasticity element (BE), behaviour of the biomechanical model. Regarding Eq. 4.2, PE only intervenes with one equation even though Eq. 5.15 presents a force-length and a force-velocity equation. However, PE's force-velocity equation is the same used to model CE's force-velocity relation (see Eq. 5.8) and therefore is accounted for in that element.

$$\text{No. Dynamic Equations} = 2_{\text{legs}} \times 7_{\text{MTU}} \times (3_{\text{CE}} + 1_{\text{SE}} + 1_{\text{PE}} + 1_{\text{BE}}) = 84 \quad (4.2)$$

The data exchange or number of signals specification includes all the parameters that act as the biomechanical model's outputs. These outputs include sagittal plane hip, knee and ankle motion, powers and torques, vertical ground reaction force and muscle forces and activations. The number of signals is therefore 48, as seen in Eq. 4.3.

$$\begin{aligned} \text{No. Signals} = & 2_{\text{legs}} \times (3_{\text{joint motion}} + 3_{\text{joint power}} + 3_{\text{joint torque}} + 1_{\text{GRF}} + \\ & 7_{\text{muscle force}} + 7_{\text{muscle activ.}}) = 48 \end{aligned} \quad (4.3)$$

The target values for the sagittal plane joint power (W/kg), joint internal torque (Nm/kg) and range joint motion (degrees) were taken from literature results of Neumann (2013). The letters H, K and A represent the designations hip, knee and ankle, respectively. The sagittal plane range of motion provided by Neumann (2013) is in accordance to the lower limb joint angles observed in Figure 4.4.

The range of vertical ground reaction force (%BW) was taken from Winter (2009) and the MTU strength reduction (%) was taken from Thomas, Villwock, et al. (2013). The letters Q and H represent quadriceps and hamstrings muscle groups, respectively.

Regarding the number of muscle-tendon units (MTUs) included in the target values, since there are seven MTU's per leg, in total the biomechanical model has 14 MTUs.

The scale equations include the equations involved in the scaling of the model for it to be adapted to different patients with different characteristics, for instance, limb length. As seen in Eq. 4.4, this specification includes all the segments comprised within the model (HAT, thigh, shank and foot) and the equation involved in the modelling of all the 14 MTU, which differ from patient to patient.

$$\text{No. Scale Equations} = 1_{\text{HAT}} + 2_{\text{legs}} \times 3_{\text{foot,shank,thigh}} + 14_{\text{MTU}} = 21 \quad (4.4)$$

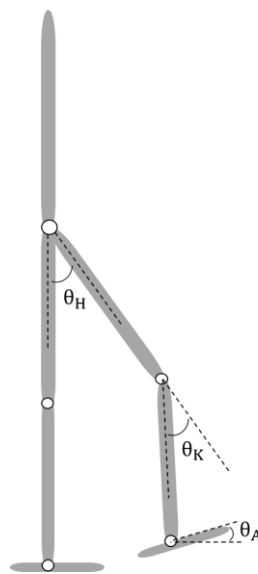


Figure 4.4 - Sagittal plane joint angles used to defined Neumann (2013) range of motion.

4.3.4. Other Considerations

There are other important parameters to include in the House of Quality, previously termed direction of improvement, correlation matrix, difficulty of execution and importance of the customer requirements and technical specifications.

At the time of asking the customers what requirements they had relative to the biomechanical model, they were also asked to rate them based on their importance relative to each other. This importance was established to vary between 1 and 5 in the following way: 1 – lower; 2 – low; 3 – medium; 4 – high; 5 – higher. For instance, a requirement with an importance of 5 has more priority to be included in the final biomechanical model than a requirement rated with 1. The determination of customer's importance is done in order to make a final decision about which requirements may be satisfied and which may not, if not all requirements are able to be met due to, for instance, economic reasons.

The direction of improvement is related to the technical specifications and determines if it is better if a specification has a higher or a lower value, or whether it does not matter. For instance, the lower the number of variables included in the biomechanical model, the better, indicating less computational costs. However, the higher the number of data signals exchange, the better. In this work, the direction of improvement was defined as: \uparrow - higher better, \downarrow - lower better and \diamond - nominal. A nominal direction of improvement means that it does not matter if the technical specification is better to be higher or lower. This is attributed to variables whose value is standardized, for instance, range of motion.

The triangle above the technical specifications represents the roof of the House of Quality and is termed correlation matrix. This section of the HoQ provides an understanding of the inter-dependencies between technical specifications. It enables the team to determine which of them have a positive relation between each other and which don't, meaning that the latter specifications are contra-indicated to coexist (Logan & Radcliffe, 1997). The correlation matrix was filled, in which "+" describes a positive correlation and "-" describes a negative one. On one hand, if the correlation is positive, then the increase/decrease of one specification leads to the increase/decrease of the other correlated with it. On the other hand, if the correlation is negative, a positive alteration of a specification leads to a negative alteration of the other. In this case, it is not possible to obtain an optimal solution for both specifications, having a necessity of compromising between the two, that is, or one specification obtains the optimal value or none of them do, never the two simultaneously.

The difficulty of execution expresses the relative difficulty of achieving a determined technical specification when compared to the others. This parameter was attributed to each technical specification, varying from 0, which means "easy to execute", to 10, which means "difficult to execute".

To establish a relation between the customer requirements and the technical specifications, four relations were defined: Θ - Strong (9), \bigcirc - Medium (6), Δ - Weak (3) and - None (0). This means that if two of them are attributed with Θ , it means that they are strongly related to each other. For instance, the computation time required to simulate the model is strongly related to its computational efficiency. If the computation time is too great, the model is not computationally efficient. The importance attributed to each technical specification is related to these relations so that the total importance of a technical specification is the sum of the values of the relations established. For instance, if a technical specification has 2 Θ , 1 \bigcirc and 3 Δ , its importance is $2 \times 9 + 1 \times 6 + 3 \times 3 = 33$. This importance is then used to determine which technical specifications are more important to be incorporated in the final model.

Considering the customer requirements and technical specifications, as well as the target values and all the other examined parameters, the House of Quality for the biomechanical human model is assembled. Figure 4.5 illustrates the developed house of quality.

Direction of Improvement																		
		↓	↑	↓	↓	◇	↓	↑	◇	◇	◇	◇	↓	↓	↓			
Technical Requirements	Weight / Importance	Relative Weight (%)	Hard Disk Space (GB)	Random Access Memory (GB)	No. Of Variables	No. Of Dynamic Equations	Slope (%)	Error (%)	Data Exchange (No. Of Signals)	Joint Power (W/Kg)	Joint Torque (Nm/Kg)	Vertical Ground Reaction Force (%BW)	MTU Strength Reduction (%)	Joint Range of Motion (degrees)	No. Of MTU	No. Of Scale Equations	Computation Time (ms)	
			Customer Requirements															
Computationally Efficient	3	9	0	0	Δ	Δ	Δ		Δ	Δ	Δ	Δ	Δ	Δ	Δ	Δ	0	
Self-adaptive	3	9			0	0	0		Δ	Δ	Δ	Δ	0	Δ	0		Δ	
Realistic Output	5	15			0	0	Δ	0	0	0	0	0	0	0	0	0	Δ	
Emulate Musculoskeletal System	4	12			0	0	Δ	0	0	0	0	0	0	Δ	0	0	0	
Recreate Pathological Condition	5	15			0	0	Δ	0	0	0	0	0	0	0	0	Δ	Δ	
Adjustable/Scalable	2	6			0	0		0	0	0	0	0		0	0	0	Δ	
Perform different activities	1	3			Δ	0	0		0	0	0	0	Δ	0	0	Δ	Δ	
Provide data exchange	5	15			0	0		0	0	0	0	0	Δ	0	Δ			
Able to include an exoskeleton	5	15			0	0			0	0	0	0	Δ	0		0	0	
Total	33	100																
Target or Limit Value			1 GB	4 GB	112	84	5%	5%	48	H: [-2,2]; K: [-1.5, 1.2]; A: [-1.5, 5]	H: [-1.5, 1.5]; K: [-0.75, 0.75]; A: [-0.5, 2]	[0, 120]	Q: [5%, 40%]; H: [9% 27%]	H: [-10, 40]; K: 10, 60; A: [-20, 10]	14	21	60	
Difficulty of Execution (0 = Easy; 10 = Difficult)			2	2	9	9	7	6	6	6	8	8	7	8	6	9	6	
Weight / Importance			6	9	57	63	30	36	63	60	60	51	45	54	48	36	39	
Relative Weight (%)			0.9	1.4	8.7	9.6	4.6	5.5	9.6	9.1	9.1	7.8	6.8	8.2	7.3	5.5	5.9	
				Total														
				657														
				100														

Figure 4.5 - Developed house of quality.

4.4. Critical Analysis

In this section, a critical analysis of the developed House of Quality is given. The results obtained regarding the customer requirement's importance, the technical specifications' importance, target value, difficulty of execution and correlation dependencies are analysed. Similarly, the relations existing between these parameters are investigated and conclusions are drawn.

Observing the importance attributed by the customer to their requirements in percentage, it is concluded that it is attributed a higher importance (15%) to the providence of realistic output by the model, to the recreation of the pathological condition, to the providence of data exchange and to the inclusion of an exoskeleton. This means that these are the requirements that mostly need to be satisfied and included in the final product, in this case, the final biomechanical model.

Importances below 15%, in decreasing order, are to be considered but with progressively less preoccupation of including them in the final product. For instance, if there are two requirements and if they cannot coexist together, the one that possess more importance attributed by the client is the one included in the final product. Even though it is not attributed with the highest importance, the emulation of the musculoskeletal system is also a very important requirement with an importance of 12% and should be taken into account in the final model.

The least important requirement is the one involving the performance of different activities. This means that the customer prefers the model to provide the characteristics enclosed in the most important requirements rather than to perform different activities. Customer requirements including the computational efficiency, self-adaptation and the adjustability of the model are intermediate in terms of importance for the client.

Regarding the relations existing between the customer and the technical specifications, only a general idea is given with examples since the results of the entire matrix are very similar regarding interpretation. The computational efficiency was chosen to be strongly related to RAM since it enables the computer to perform different activities at the same time. A higher RAM allows a higher efficiency when simulating the model since multiple programs are needed to be open, such as MATLAB®, Simulink® and MATLAB® Mechanics Explorer. The computational efficiency is also strongly related to the computation time a computer requires to perform a simulation. The lower the computational efficiency of the computer, the higher the computation time.

The number of muscle-tendon units pertaining to the biomechanical model is mediumly related to the specification of the model to be scalable. This means that, generally, the more/less MTUs, the more/less scale equations are needed when adjusting the model to other anatomic characteristics. Lastly, a weak relation is encountered between the slope and the ability to recreate a pathological condition. This was defined since the recreation of a pathology is not determined by the slope of the ground in which the model is walking in, but it might influence it, so that the slope might alter the model's gait in some way.

Moving now to the parameter above the technical specifications, named direction of improvement. It is observable that hard disk space, number of variables, number of dynamic equations, error, number of MTU, number of scale equations and computation time are all desired that the lower their value the better, since a ↓ is attributed to them. In terms of meaning, the lower the hard disk space, the better since, generally, a higher disk space indicates higher economical costs when buying a computer. The lower the number of variables, dynamics equations, MTU and scale equations included in the model, the better, since it might influence in the decrease of the computational time needed to simulate the biomechanical model.

The error between the model's results and the ones present in literature taken from human experiments is a parameter desirable to be low since it is required maximum closeness between both results (realistic output). The computation time is preferred to be low to achieve maximum productivity, meaning that a lower computation time permits a decrease in computation costs when simulating the model. A lower value is preferable but without compromising the reality of the results.

The symbol ↑ is attributed to the RAM and the number of signals for the data exchange. The higher the computer's RAM, the better since it means that the computer is able to perform various different activities at the same time. This might be an asset when simulating the model, since multiple programs are required to work at the same time. The more signals the model is capable of outputting, the better since they can be included in other studies or feedback to the model to perform further analysis.

A ◇ symbol is attributed to the slope, joint power, torque and range of motion, vertical ground reaction force and MTU strength reduction, indicating a nominal value pertaining to these specifications. These parameters all have fixed values encountered in literature and therefore they do not change, maintaining their reference value despite changes in anatomical characteristics. For instance, the normal physiological range of motion for walking gait is the one displayed in Table 4.3, independently of each human being's characteristics without any pathological condition. The same is applicable to the other specifications to which a nominal value was attributed to.

The correlation matrix was then filled. Once again, since the analysis of this block of the HoQ is very similar regarding the interpretation of the interdependencies between all the technical specifications, only some examples will be analysed. On one hand, the total number of variables is strongly correlated with the total number of MTUs and of dynamic equations. This was decided since the higher the number of MTUs present in the model, the higher the number of dynamic equations to be established, and therefore the higher the total number of variables present in the model. On the other hand, the hard disk space is negatively correlated with the computation time since a higher hard disk space might be attributed to a lower computation time required to simulate the biomechanical model.

The target values defined for each technical specification are present in Table 4.3 and were already explained in section 4.3.3, and therefore no further analysis is performed. These values were attributed based on previously approached calculations and based on literature results.

The difficulty of execution was attributed to each technical specification and it is observable that the most difficult are the number of variables, dynamics equations and scale equations, with a difficulty of 9 in a scale of 0 to 10. The value was set to 9 since these technical specifications are desired that the lower their value, the better. But this is not straight forward, due to the complexity of the model considering the recreation of the skeletal, muscular and neural systems, which includes a considerable number of variables intervening and dependent on each other.

The joint torque, vertical GRF and joint's range of motion were attributed with an 8, since they depend upon the formulation of the muscle-tendon units dynamics, the number of MTUs included in the model and on the formulation regarding the interaction between the biomechanical model and the ground. The least difficult specifications to be executed are the hard disk space and the RAM, with a difficulty of 2, since they depend on the computer used in the simulations.

Lastly, the importance of each technical specifications is calculated, as previously explained, by summing the values of each relation attributed to it. Observing the row of the importance it is observable that the two most important technical specifications are the number of dynamics equations and the number of signals provided for the data exchange, followed by the joint power and torque. This means that these four specifications are very important to be included in the final biomechanical model. The hard disk space and RAM are the least important specifications to be taken into consideration, regarding the entire set of technical specifications the biomechanical model involves. As in the customer requirements, the rest of the technical specifications are important to be met in a decreasing order of

importance. The more importance attributed to a technical specification, the more critical it is for it to be included in the model.

Overall, in conclusion, the most important customer requirements needed to be encompassed in the final model are the providence of realistic output by the model, the recreation of the pathological condition, the providence of data exchange and the inclusion of an exoskeleton. Since the one involving the performance of different activities is the least quoted in terms of customer importance, it was not included in the final model. Also, conditions for its achievement were not met.

Regarding the technical specifications, priority must be given to the number of dynamic equations and of signals provided for the data exchange, as well as to the joint's power and torque, since they have the most importance percentages. The least important features, such as the performance of different activities, the capacity of the model to be scalable and its self-adaptability, were not included in the final biomechanical model since, considering their low importance and the other included parameters (for instance, the providence of realistic output), they were not achievable in the time course of this dissertation. Based on these conclusions, the biomechanical model is approached and a detailed description of it is given in the following chapter.

4.5. Summary and Discussion

All the requirements pertaining to the biomechanical model, which were encountered during the development of phase one of Quality Function Deployment, are a valuable help in developing a model oriented towards the customer needs. This was possible since a precise analysis of the customer's requirements was achieved, attributing to the final biomechanical model the corresponding technical specifications that satisfy them. To this end, the QFD methodology enabled the guidance of the development of the biomechanical model of this work.

This chapter includes primarily a description of the methodology utilized, followed by a detailed analysis of every part of phase one of Quality Function Deployment used to construct the House of Quality. Since, in the final part of the chapter, a detailed critical analysis was performed, no discussion is included in this section.

The main conclusions taken from the application of the first phase of the Quality Function Deployment methodology is that the most important requirements to be included in the final biomechanical model are the providence of realistic output by the model, the recreation of the pathological condition, the providence of data exchange and the inclusion of an exoskeleton, regarding the customer's

requirements. Priority must also be given to number of dynamic equations and of signals provided for the data exchange, as well as to the joint's power and torque, when considering the technical specifications. This means that in order to satisfy the needs of the customers, the above-mentioned technical specifications must be taken into account in the final model.

5. DESCRIPTION OF THE BIOMECHANICAL MODEL UTILIZED

The biomechanical model utilized in this work is based on the one developed by Geyer & Herr (2010) and relates neural reflexes (force and length feedback) to Hill-type muscle models, which in turn produce joint torques. In order to interchange between these feedback schemes and to produce a natural gait, ground sensors placed under the feet are used to detect ground contact and to determine which reflexes are used. On one hand, if contact is detected, stance phase reflexes (mainly extensor muscular activity) are used. On the other hand, if contact is not detected, swing phase reflexes (mainly flexor muscular activity) arise. The gait cycle is generated by using such reflexes by a sequence of time-delayed reactions, that is, each muscle has associated a time delay, meaning that only after that delay it influences the dynamics of the model (Dzeladini, van den Kieboom, et al., 2014).

In the present chapter, a detailed description of the biomechanical model utilized is given. The Simulink construction of the model comprises four layers or modules, namely Body Mechanics, Muscle Actuation, Neural Control and Optimization, as seen in Figure 5.1. The construction of the segments and joints of the model is implemented in the Body Mechanics layer. The Muscle Actuation layer encompasses the modelling of the muscle-tendon unit (MTU) dynamics, comprising the calculation of the overall joint torque produced by the MTUs around that joint. MTU stimulations and neural reflexes (force and length feedbacks) are modelled in the Neural Control layer. Finally, the Optimization layer enables the calculation of the parameters used in the optimization problem.

This chapter provides a detailed description of the overall construction of the biomechanical model utilized in this work, by approaching each of the referred layers.

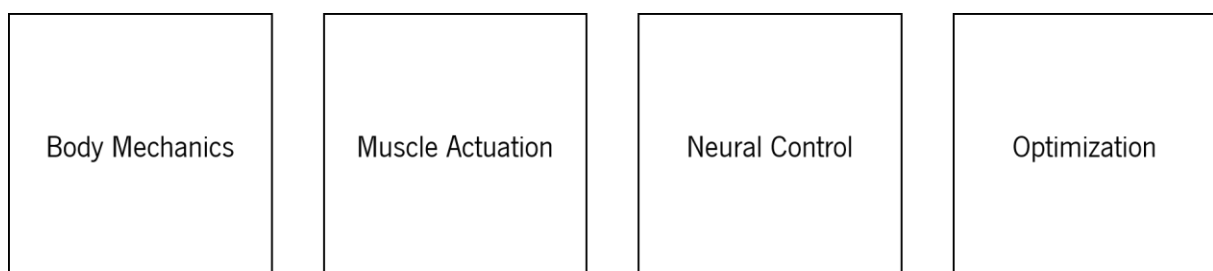


Figure 5.1 – An overview of the layers or modules used in the construction of the biomechanical model.

5.1. Biomechanical Model's General Considerations

In the present work, the biomechanical model used is based on the one presented by Geyer & Herr (2010) and was obtained from Hartmut Geyer's personal website (<https://www.cs.cmu.edu/~hgeyer/>). As referred by these authors, the model of human locomotion is driven by muscle reflex behaviours based on principles of legged mechanics, such as the reliance on compliant leg behaviour during the stance phase of gait. This arrangement is based on two theories: one defended by neuroscientists and the other by the biomechanics community. The former states that animal and human gait are controlled by neural networks of increasing complexity, and the latter defends that little motor control is needed for the development of this motion if the above-mentioned principles of legged locomotion are considered. To ensure effectiveness in the implementation of such gait characteristics, Hill-type muscles combined with neural reflexes were used, including positive force and length feedback schemes (Geyer & Herr, 2010). Since the model comprises the interaction between the skeletal (constituted by segments connected by joints), the muscular (Hill-type muscles) and the nervous (neural reflexes) systems, it can be referred to as neuromuscular biomechanical model.

As seen in Figure 5.2a, the neuromuscular model is a three-dimensional (3D) representation of the human body, being divided in seven anatomical rigid segments: two feet, two shanks, two thighs and one Head, Arms and Trunk (HAT). The segments possess local reference frames that are used to define the whole anatomy of the biomechanical model. These local frames can either be attached to their centre of mass (COM), to their centroid or to any other location that is convenient to define the anatomically correct position of the attached segments.

Each segment is connected to the immediately adjacent by a revolute joint, having its range of motion (ROM) constrained in order to ensure physiological gait and to prevent pathological movements, such as joint hyperextension or hyperflexion. Considering the previously stated and observing Figure 5.2a, the model comprises a total of six revolute joints, namely two hip, two knee and two ankle joints, whose only allowed motion is flexion/extension, in the sagittal plane, of the segments they are connected to. For instance, the knee joint allows only flexion/extension in the sagittal plane of the shank in relation to the thigh, since the other degrees of freedom in the 3D space are constrained by the revolute joint. The ROM of these joints in the biomechanical model is: $70^\circ < \theta_a < 130^\circ$, $\theta_k < 175^\circ$ and $\theta_h < 230^\circ$. The definition of the joint angles, θ , can be seen in Figure 5.2b.

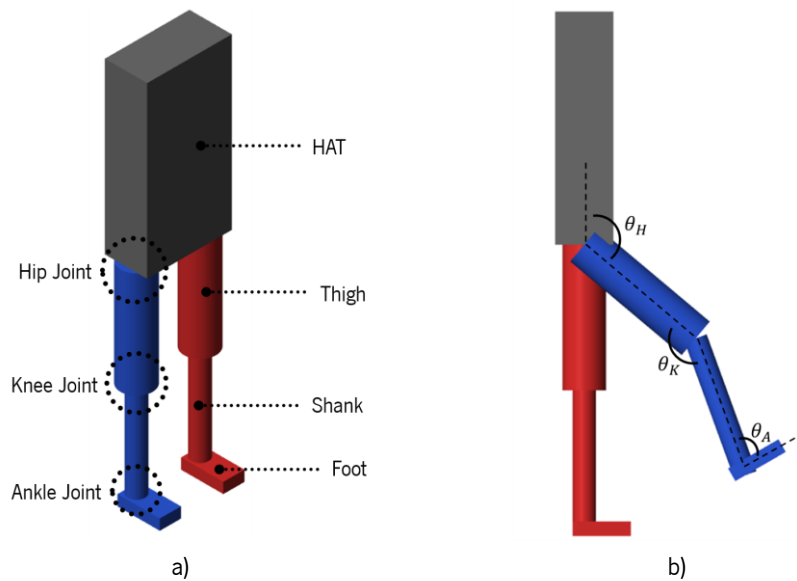


Figure 5.2 - Biomechanical model used in this work. Left and right legs are coloured in red and blue, respectively. HAT is coloured in grey. a) Model's isometric view, with the indication of its segments and joints. b) Definition of the joints angles as in the work of Geyer & Herr (2010). θ_H , θ_K and θ_A represent the hip, knee and ankle joint angles, respectively.

Considering the existence of seven segments connected by six revolute joints, as seen in Figure 5.2a, the biomechanical model comprises a total of 12 mechanical degrees of freedom (DOFs). Since each of the seven segments are constructed in the 3D space, they have a total of six DOFs individually if unconstrained, namely three rotations and three translations in the three axes, xyz. However, since they are connected by revolute joints, each segment is only allowed one DOF (rotation) in 3D space, removing the remaining five. The 12 DOFs represent the dorsiflexion and plantarflexion of both ankles, flexion and extension of both knees and hips and six DOF of HAT.

Besides possessing six degrees of freedom in the 3D space, the HAT does not perform all of them. This occurs due to the constraints imposed by the six joints, which enable movement only in the sagittal plane. Considering this, the HAT is only allowed forward translation to accompany the forward movement of the other segments, vertical movement and rotation in turn of the axis that comes out of the sagittal plane. Figure 5.3 illustrates the movements of the HAT segment throughout gait.

The above-mentioned concept of DOFs requires the distinction between mechanical degrees of freedom (DOFs) and functional degrees of freedom (fDOFs). Li (2006) distinguishes these two concepts stating that DOFs represent the minimum number of independent coordinates required to describe a system's position, while fDOFs represent the DOFs that effectively produce a determined movement. For instance, while the human body may comprise many DOFs, its number of fDOFs in a specific task may be lower, since the coordination of human joints establishes functional relations among joint variables,

and so not all the DOFs are used by an individual when performing a particular motion (Li, 2006; Li & Tang, 2007). Considering this explanation, the biomechanical model comprises 12 DOFs and 9 fDOFs.

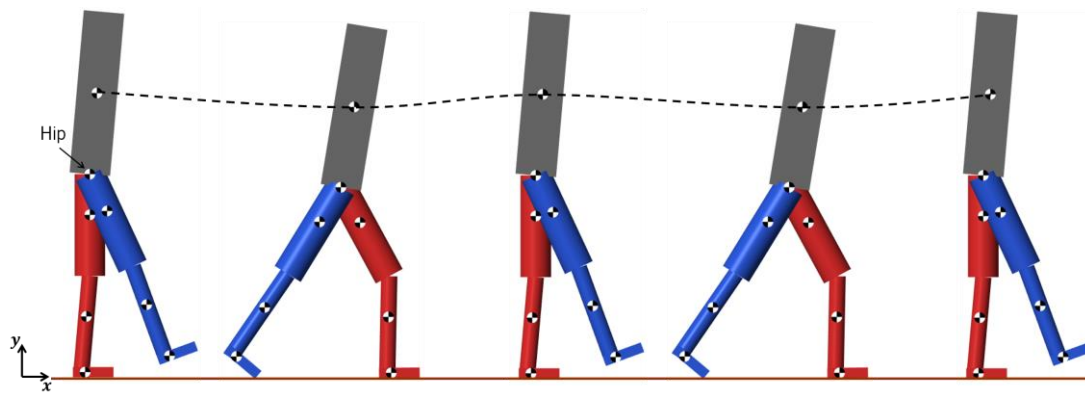


Figure 5.3 - Movements of HAT segment throughout gait. The HAT rotates about the z-axis (out of the plane), situated at the hip joint. Besides, its centre of mass travels forward, in the x direction. Lastly, the y position of the HAT alters during gait, moving up and down. The brown line below the biomechanical model represents the ground.

The biomechanical model is implemented in Simulink from MATLAB R2017b (MathWorks). Generally, it comprises four interrelated layers or modules that all together enable the functioning of the biomechanical model. These four layers are named as Body Mechanics, Muscle Actuation, Neural Control and Optimization, which are briefly described in the following paragraph.

The Body Mechanics layer encompasses all the geometric and physical properties important to the definition of the anatomy of the model, such as the characteristics of the segments and joints. The Muscle Actuation layer contains the characterisation of the lower limb's Hill-type muscles used to perform movement. The feedback schemes and the part of the model that represents the muscles' stimulations and delays, as well as other parameters commanded by the central nervous system, are modelled in the Neural Reflex layer. Finally, the Optimization layer enables the calculation of the parameters needed for optimising the model's gait. In this section, only the Body Mechanics layer is approached. The others are explained in the subsequent sections.

In the Body Mechanics layer, the geometric construction of the system initiates with the definition of the global frame, named world frame (W). W is an orthogonal, motionless, right-handed coordinate frame, being the base of all frames comprised in the system (MathWorks, 2018c).

In this layer, the definition of the components of the model in relation to each other is always made in a logic of base (B) and follower (F) frames (B/F). This means that, starting from the base frame and applying to it, for instance, certain translations and/or rotations, the follower frame will be created based on those alterations made to B. If no alterations are performed to B, F is equal to B.

After establishing of the world frame, the ground is constructed using a solid block. The ground is considered a parallelepiped with length, width and thickness of 100, 1 and 0.01 meters, respectively. By means of a rigid transform block, the frame representing the centroid of the ground is translated, in the positive x axis of W, by 1 meter in relation to the origin of the World Frame. The rigid transform block has two ports, one representing B and the other F. In this case, B is W and F is the frame in the centroid of the ground solid. Figure 5.4 shows a schematic of the modelling type described.

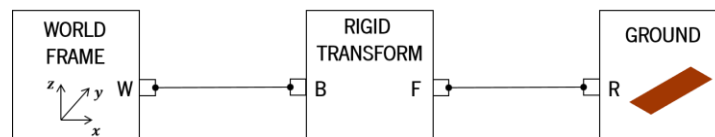


Figure 5.4 - Base (B) and follower (F) logic applied in the definition of the biomechanical model. Example given with the world frame, rigid transform and ground. The rigid transform enables the transformation of the origin of the world frame (B) into the origin of the frame in the centroid of the ground (F). It places the latter, one meter away from the origin of W.

After defining the ground and before initiating the construction of the model geometry itself, a mechanism configurations block specifies the gravity vector for the entire system. In this case, the constant gravity vector is set to be negative in the z direction in relation to W.

Before defining the left foot segment, a planar joint is implemented. This joint has two translational and one rotational degrees of freedom represented by two prismatic and one revolute joints, respectively (MathWorks, 2018d). Following the same logic described above and illustrated in Figure 5.4, in between the planar joint and the world frame, a rigid transform block is defined. In this case B is the planar joint and F is the world frame. The block performs a clockwise rotation about the x axis of the planar joint, transforming it into W. Figure 5.5a illustrates this rotation. Besides this, a translation in the z direction of the planar joint frame is performed to transfer its origin to the origin of W.

There is the possibility of defining the initial conditions of this joint, which was done. Regarding the planar joint frame illustrated in Figure 5.5a, the x-axis prismatic primitive was addressed with an initial velocity, v_{x0} , of 1.3 m/s and initial position of 0 meters. This is done in order to model the forward propulsion of the biomechanical model (v_{x0}) and to locate it at the x origin of the frame of the planar joint. The y-axis prismatic and z-axis revolute primitives were both addressed with initial velocity and position of 0 m/s and 0 meters, respectively. Considering these restrictions, the biomechanical model is located at the origin of the planar joint frame, being only prepared to perform movement in the x-axis of this frame. This is another reason why the biomechanical model is only allowed motion in the sagittal plane. Figure 5.5b shows the blocks modelled until this point of the explanation.

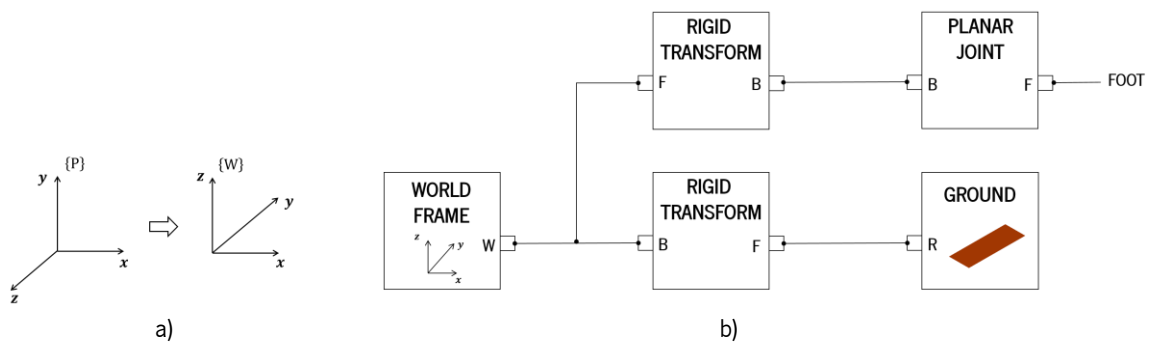


Figure 5.5 - a) Rotation performed based on the Planar Joint Frame, {P}, to acquire the World Frame, {W}. A rotation about the x axis of -90 degrees is performed. b) Part of the Body Mechanics layer built. Note the base and follower ports of the rigid transform block between W and the planar joint. The mechanism configuration block is not shown here.

The construction of the geometric part of the biomechanical model itself begins by defining the left foot. To create this body part, a subsystem is built, inside which the foot solid is defined as a parallelepiped, with dimensions as stated in Table 5.1. The foot segment comprises two contact points (CPs) also defined within the subsystem, named heel and ball, to determine whether the leg is in stance or swing phases and to determine the ground reaction forces (GRF) by means of position sensors and the ground contact model (approached later), respectively. These two points represent the heel and toes of the human body. Besides the foot solid, the heel and the ball CPs, another point is defined, named ankle. It permits the connection between the foot subsystem and the next block, a revolute joint. The ball point is directly connected to the planar joint frame, serving as a base frame from which the other three components are created (follower frames) by means of translations performed by rigid transform blocks.

Figure 5.6a shows the location of the mentioned points in the foot segment and Figure 5.6b contains the blocks modelled inside the foot segment.

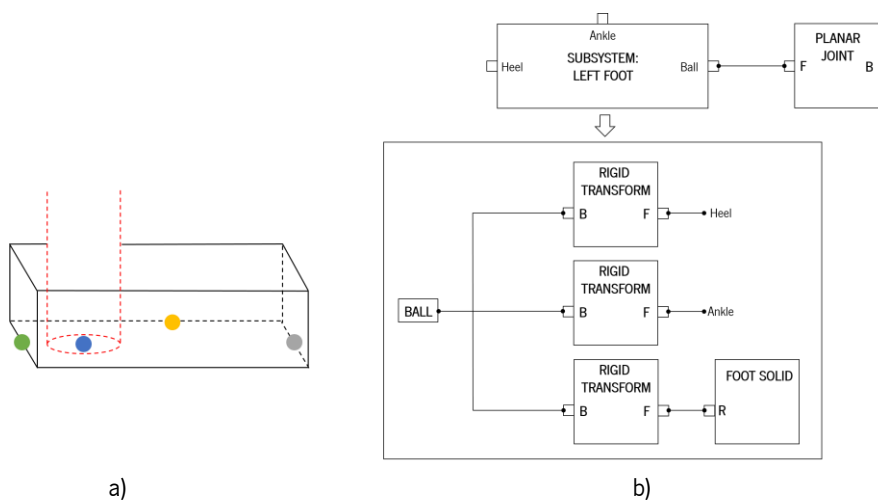


Figure 5.6 - Modelling approach used to construct the left foot segment. a) Illustration of the foot with the four points important to its construction: ball, heel, ankle and location of the centroid of the foot solid. The ball point is coloured in grey. This is the point from which the other three components are built. The location of the centroid of the foot solid, the ankle and the heel are coloured in yellow, blue and green, respectively. The red coloured lines illustrate the shank segment (see Figure 5.2),

explained later. This segment was only drawn to give a better understanding of the concept described here. b) A subsystem to model the left foot segment is used, which comprises the definition of the heel and ankle points, and the foot solid, based on the frame of the ball point. This frame is the same as the frame of the planar joint since they are directly connected, and no transformation is done between them.

Until this point, the biomechanical model is modelled as presented in Figure 5.7.

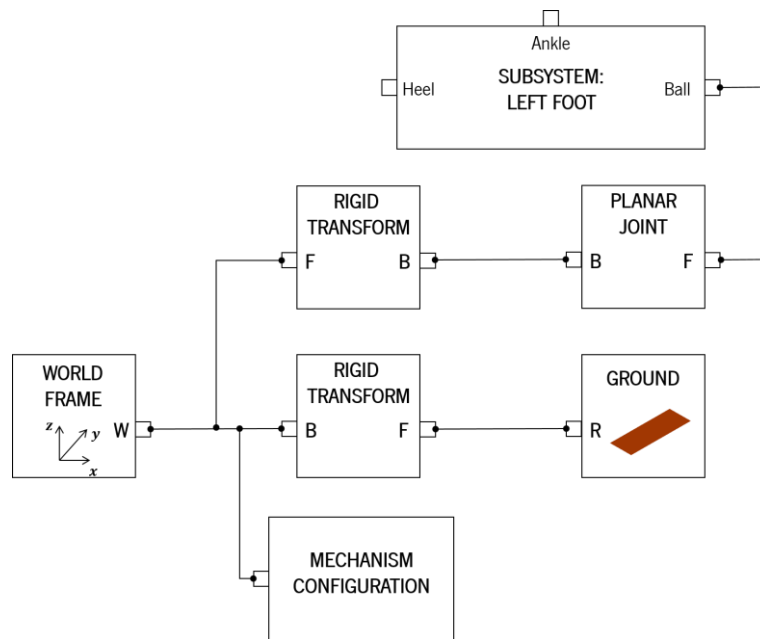


Figure 5.7 - Illustration of the biomechanical model construction using Simulink blocks. Starting from the world frame, defining the ground solid until the creation of the left foot.

The left foot subsystem is connected to the left shank by means of a revolute joint, which, in terms of human anatomy, represents the ankle joint. The connection between the foot segment and the ankle joint is made by means of the ankle point created previously in the foot (see Figure 5.6). In this case, the ankle point is the base frame from which the ankle joint frame (follower frame) will be defined. The ankle joint is a revolute joint, enabling one degree of freedom in the sagittal plane, which is the rotation in turn of the z-axis. Since no other rotations were performed, the orientation of this z-axis is the same as the one defined for the planar joint frame (see Figure 5.5a). Similarly to the planar joint, it is possible to set initial conditions for the revolute joint, such as its position and velocity. The initial position and velocity of the ankle joint are 85° and 0 rad/s , respectively. The joint is actuated by muscular moments produced by the muscles that act around it, providing the joint's angular position and velocity throughout gait as output. All joints of the model are actuated by the muscular moments produced around them. These moments arise from the Muscle Actuation layer, explained later in this chapter. For this reason, the biomechanical model is considered a forward dynamics model.

The shank segment is modelled as the foot, using a subsystem (see Figure 5.6b). It comprises rigid transform blocks that enable the creation of anatomically important points, which in this case are the knee, the centre of gravity and centroid of the shank solid.

Both the shank and the thigh segments are defined as cylinders with different radius and same lengths, being listed in Table 5.1. These segments are connected to each other by a revolute joint, anatomically representing the knee, whose base frame is the knee point created in the shank segment. The knee joint is similar to the ankle joint. The only difference is its initial position, being 175°.

The thigh is modelled as the other previously analysed segments, with the definition of important points, such as its centre of gravity, centroid and the location of a pressure sheet, based on the knee joint. This inner thigh pressure sheet block is modelled as a prismatic joint and is used in the Neural Control layer. However, this block was not further analysed. Since between this block and the next, which is the hip joint, no transformation (translation or rotation) is performed, their frames are equal.

The HAT is connected to the left thigh by means of the left hip joint, modelled as a revolute joint similar to the knee, with the same initial conditions. The HAT is modelled, once again, as a subsystem, comprising the definition of its COM and the left and right thighs points, which will determine the location of the left and right hip joints, respectively. The right leg is built in accordance to the left leg. Its joint's initial conditions are $\theta_A=90^\circ$, $\theta_K=175^\circ$ and $\theta_H=150^\circ$.

The anthropometric characteristics of the model are the ones that represent the static body geometry, e.g. segment's lengths, and physical properties, e.g. masses, as in the work of Tavares da Silva (2003). Each segment is specified by these characteristics, as stated in Table 5.1, based on the work of Geyer & Herr (2010).

The model has a total mass of 80 kg, with a total height of 185 cm. The lengths presented in the below table are considered to be a straight-line distance between adjacent joint centres of rotation (COR). The COM distance and the joint location parameters (Table 5.1) are defined as the distance between the distal end of the segment being analysed and its COM and the distal end of the segment and its proximal joint, respectively. An illustration of the definition of these two quantities can be found in Figure 5.8a. Figure 5.8b illustrates the biomechanical model with the joint's initial conditions.

Figure 5.9 presents the structure of the entire biomechanical model implemented in Simulink.

Table 5.1 - Anthropometric parameters of the biomechanical model's segments (adapted from Geyer & Herr (2010)), including body geometry and physical properties. The body geometry parameters include the segments' length, width, thickness, radius and shape. The physical properties include the segments' mass and moments of inertia. Other parameters included in the table are the centre of mass distance and joint location, which are defined as the distance between the distal end of the segment being analysed and its COM or proximal joint, respectively

			Foot	Shank	Thigh	HAT
Body Geometry	Length (mm)		200	500	500	800
	Width (mm)		10	-	-	400
	Thickness (mm)		5	-	-	200
	Radius (mm)		-	40	75	-
	Shape		parallelepiped	cylinder	cylinder	parallelepiped
Physical Properties	Mass (kg)		1.25	3.5	8.5	53.5
	Moments of Inertia (kg.m ²)	I_x	0	0.05	0.15	0
		I_y	0	0	0	0
		I_z	0.005	0	0	3
Centre of Mass (COM) Distance (mm)			140	300	300	350
Joint Location (mm)			160	500	500	-

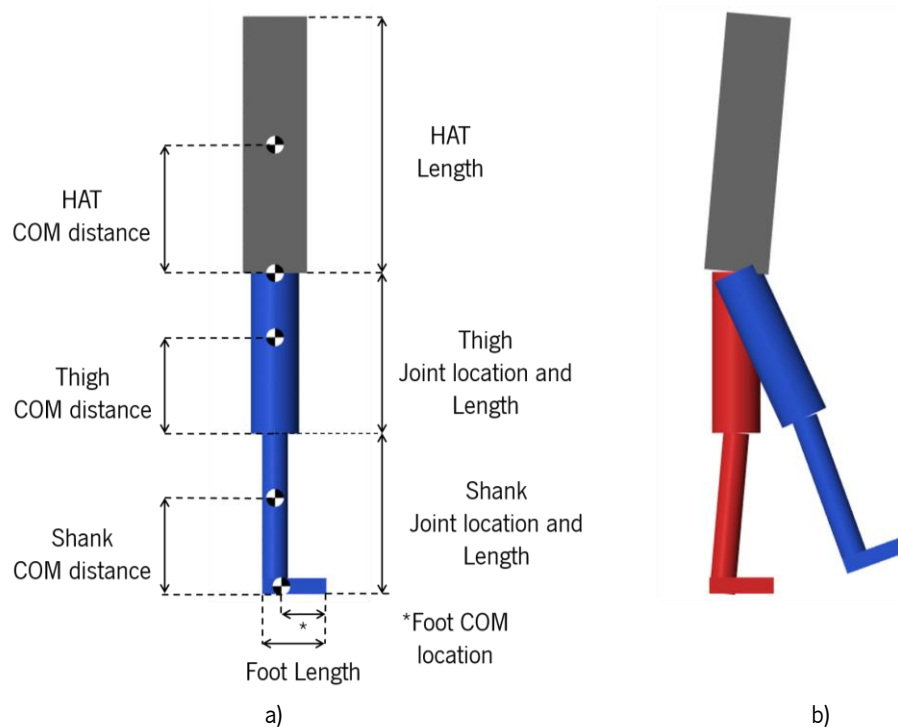


Figure 5.8 - Sagittal plane view of the biomechanical model. a) Centre of mass distance, joint location and segment's length definition. b) Biomechanical model joint's initial conditions. Left Leg: $\theta_a = 85^\circ$, $\theta_k = 175^\circ$ and $\theta_h = 175^\circ$. Right Leg: $\theta_a = 90^\circ$, $\theta_k = 175^\circ$ and $\theta_h = 150^\circ$.

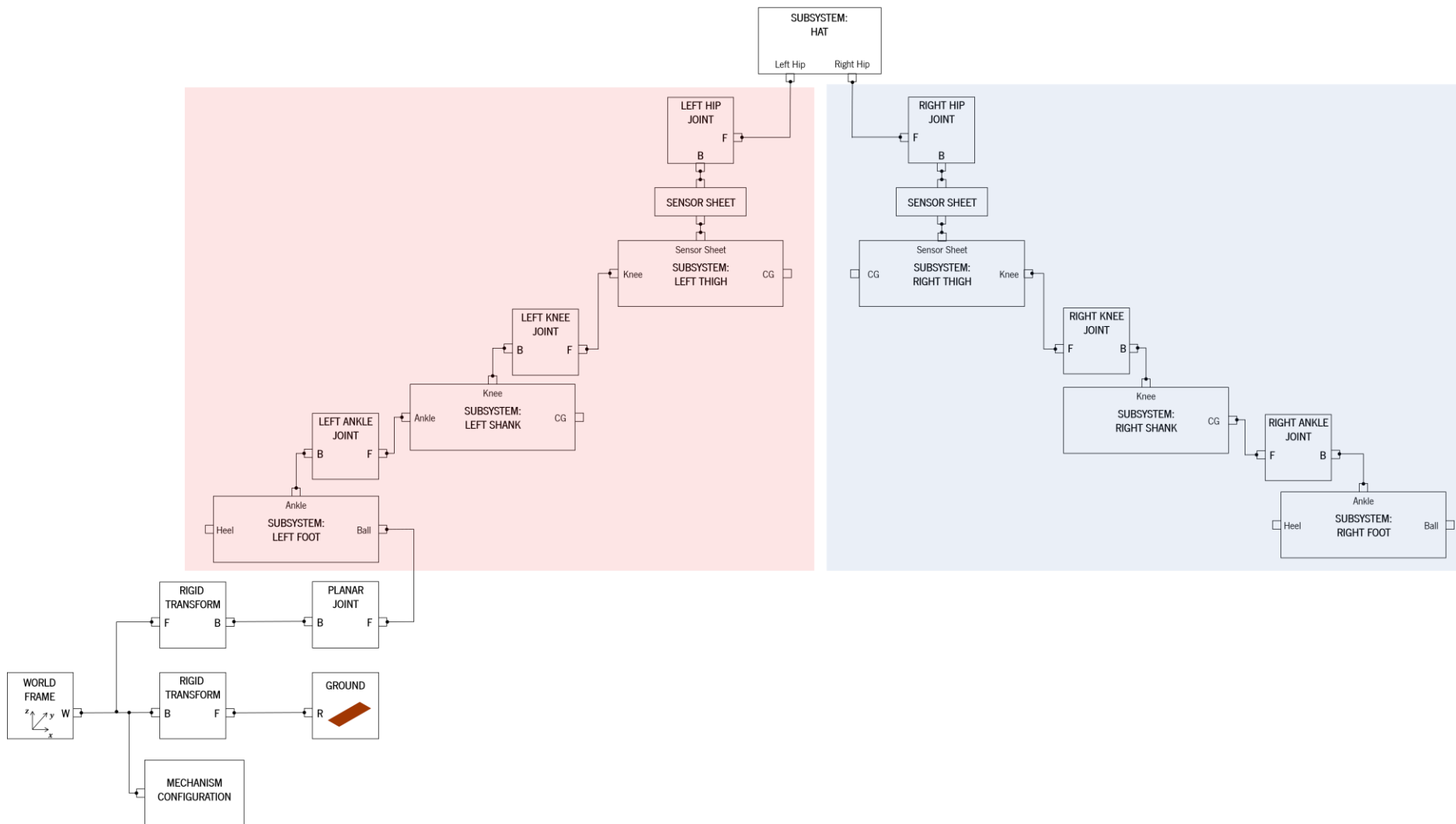


Figure 5.9 - Illustration of the block construction of the biomechanical model implemented in Simulink, including the definition of the segments (foot, shank, thigh and HAT) and joints (ankle, knee and hip). Light red and blue blocks indicate the left and right legs, respectively.

5.2. Biomechanical Model's Muscle Actuation Layer

The muscle-tendon unit model used in this work is the same as the one implemented by Geyer & Herr (2010), in which muscles are modelled together with their corresponding tendons. The biomechanical model comprises a total of fourteen muscle-tendon units (MTU), seven in each leg. The MTUs included are the soleus muscle (SOL), tibialis anterior muscle (TA), biarticular gastrocnemius muscle (GAS), vasti lumped muscle group (VAS), biarticular hamstring muscle group (HAM), hip flexor muscle group (HFL) and gluteus muscle group (GLU). Figure 5.10 shows the MTU distribution for one leg of the biomechanical model.

In chapter 2, section 2.4 it is observable that these muscles enable joint motion performance only in the sagittal plane, that is, flexion or extension of the joint(s) they act around. Since these are the only included muscles and considering the other previously implemented constraints (inclusion of revolute joints that enable joint movement in one plane only and the definition of the planar joint), the biomechanical model performs movement only in one plane, which in this case is the sagittal plane.

SOL and TA act only around the ankle joint, promoting ankle plantar- and dorsiflexion, respectively. GAS spans two joints, enabling ankle plantarflexion and knee flexion. VAS acts only around the knee joint, acting as its extensor. HAM acts around the knee and hip joints, promoting its flexion and extension, respectively. HFL and GLU span only the hip joint, promoting its flexion and extension, respectively (Dzeladini, van den Kieboom, et al., 2014).

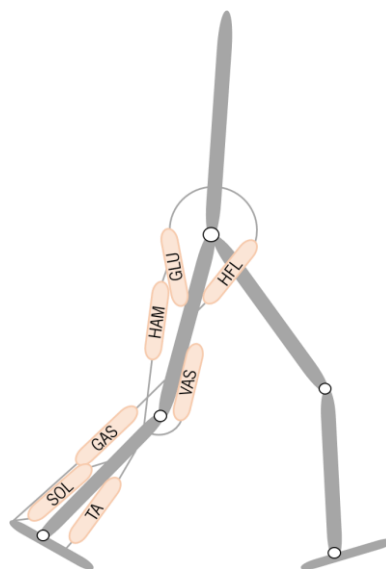


Figure 5.10 - MTUs comprised in the biomechanical model. This illustration comprises only the MTUs pertaining to one leg. The other leg contains the same MTU distribution. SOL - soleus muscle, TA - tibialis anterior muscle, GAS - biarticular gastrocnemius muscle, VAS - vasti lumped muscle group, HAM - biarticular hamstring muscle group, HFL - hip flexor muscle group and GLU - gluteus muscle group. Adapted from Geyer & Herr (2010).

All fourteen MTUs have the same structure, as seen in Figure 5.11: a Hill-type contractile element (CE), a series elasticity element (SE), a parallel elasticity element (PE) and a buffer elasticity element (BE), arranged in a similar manner as in the representation present in Figure 3.19. The active CE together with the passive elements (PE and BE) form the muscle belly. CE represents the muscle's active contractile properties, while PE and BE represent the passive behaviour of muscle fibres. The tendon is modelled as a passive element, SE, in series with the muscle belly (see chapter 3, section 3.4 and 3.5) (Dzeladini, van den Kieboom, et al., 2014).

CE produces force in line with SE. PE engages if CE stretches beyond its optimum length (l_{opt}), $l_{CE} > l_{opt}$, preventing MTU overextension. For instance, if the ankle overly plantarflexes, TA may tend to extend past its CE's l_{opt} . BE is used to prevent CE's collapse when the geometry of the leg shortens the MTU in such a way that it tends to become slack, $l_{MTU} - l_{CE} < l_{slack}$. l_{MTU} represents the length of the MTU, l_{CE} is CE's length and l_{slack} is the tendon or SE's slack length. For example, a slack SOL if the ankle performs excessive plantarflexion. Considering this, it is important to note that PE and BE are required to operate outside the normal range of operation of the whole MTU, thus playing minor roles in the muscle-tendon unit dynamics during physiological model locomotion (Geyer & Herr, 2010).

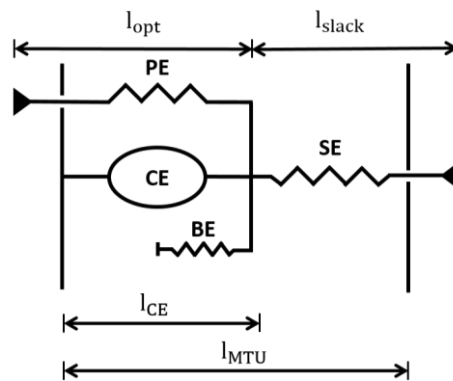


Figure 5.11 - Muscle-Tendon Unit model. In normal physiological ranges of operation, CE produces force in line with SE. However, on one hand, if CE tends to stretch more than its optimum length, $l_{CE} > l_{opt}$, PE engages, preventing CE's overextension. On the other hand, if the geometry of the leg tends to make SE slack, $l_{MTU} - l_{CE} < l_{slack}$, BE prevents CE from collapsing. Adapted from Geyer & Herr (2010).

In order to explain how these components are modelled in the Simulink environment, an example with one muscle-tendon unit is given. The other MTUs are modelled using the same principles. The muscle used to explain the modelling concept is SOL, which acts only around the ankle joint, promoting its plantarflexion. Muscles spanning two joints, for instance GAS, which spans the ankle and the knee joints, are modelled in similar manner, however, contain the influence of the two joints.

In the utilized model, muscles act on the skeleton by producing muscle torques around the joint or joints they span. The transformation from forces produced by the MTUs, F_{MTU} , to muscle torques, τ_{MTU} , is done by using constant or variable lever arms (see Figure 3.11 and section 3.3), r_{MTU} , for the hip, and ankle and knee joints, respectively. For the hip,

$$r_{MTU} = r_0 \quad (5.1)$$

and for the knee and ankle joints,

$$r_{MTU} = r_0 \cos(\theta - \theta_{max}) \quad (5.2)$$

in which r_0 is the constant lever arm, θ , is the joint angle throughout the model's movement and θ_{max} is the angle at which r_{MTU} reaches its maximum. The MTU torque is calculated as in Geyer & Herr (2010):

$$\tau_{MTU} = F_{MTU} r_{MTU}(\theta) \quad (5.3)$$

The implementation of these constant and variable lever arms in Simulink is done by means of a subsystem, which, in the case of the soleus muscle, is called SOL Attachment. Inside this subsystem Eq. 5.2 is implemented since this muscle acts around the ankle joint. In order to obtain the angle, θ , to be used on that equation, a From block, named ankle angle, arises from the Body Mechanics layer. On that layer, the ankle joint possesses a sensor to measure its angle throughout the biomechanical model's simulation. The output of that sensor is sent to the Muscle Actuation layer, by means of a Go To block which is connected to the previously mentioned From block, to be used in the calculation of the MTU lever arm. This modelling strategy is implemented to all joints of the model. If the MTU spanned two joints, in the Attachment block, instead of only inputting one joint angle, the two joint angles that the MTU spanned would act as input of the subsystem. The output of the SOL Attachment subsystem, r_{MTU} , is multiplied by the MTU's force, F_{MTU} , calculated using a mask subsystem (SOL Dynamics), which is explained latter in this section, in order to obtain the MTU torque, τ_{MTU} . Figure 5.12 shows the blocks used in Simulink to generate the torque produced by an MTU.

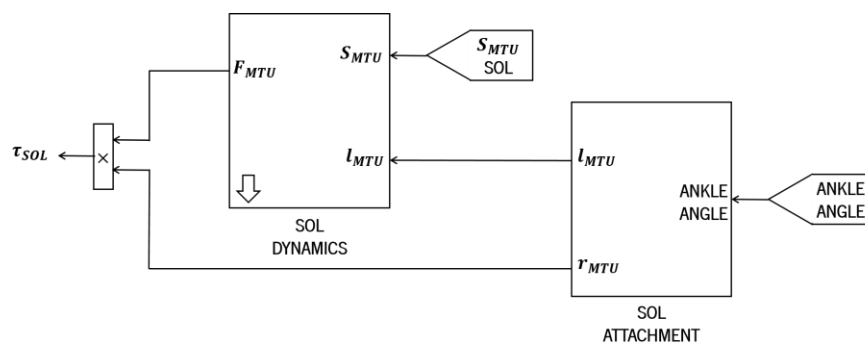


Figure 5.12 - General modelling blocks used to determine an MTU torque. Example given for the SOL muscle. SOL ATTACHMENT and SOL DYNAMICS are subsystem and mask subsystem blocks, respectively. The S_{MTU} SOL block arises from the Neural Control Layer, giving the stimulation, S_{MTU} , necessary to the MTU performance during model's motion. This part is only approached in the subsequent section.

During the model's movement, MTUs change their length. For instance, during gait the ankle joint flexes and extends, causing alterations to the length of the soleus muscle. These alterations are modelled in two different ways:

$$\Delta l_{MTU} = \rho r_0 [\sin(\theta - \theta_{max}) - \sin(\theta_{ref} - \theta_{max})] \quad (5.4)$$

for the knee and ankle joints and

$$\Delta l_{MTU} = \rho r_0 (\theta_{ref} - \theta_{max}) \quad (5.5)$$

for the hip joint, where ρ is a factor that accounts for the muscle pennation angle, ensuring that MTUs stay within physiological ROM throughout the joint's working space, and θ_{ref} is the joint angle at which $l_{MTU} = l_{opt} + l_{slack}$. The parameters for each muscle, and respective joint, regarding their attachment, are listed in Table 5.2. The values of these parameters are the ones used by Geyer & Herr (2010), which were either results from their anatomical estimates or supported by experimental evidence of the following authors (Maganaris, 2001, 2003; Muraoka, Kawakami, et al., 2001; Oda, Kanehisa, et al., 2005).

Since SOL acts only around the ankle joint, its lever arm and variation of length are calculated by the equations pertaining to the ankle joint (Eq. 5.2 and 5.4). As previously explained, in Simulink, these equations are implemented using the SOL ATTACHMENT subsystem observed in Figure 5.12, inside which Simulink blocks are used to build them, as seen in Figure 5.13. MTUs using the equations pertaining to the hip joint would be implemented in a similar manner, regarding the blocks used.

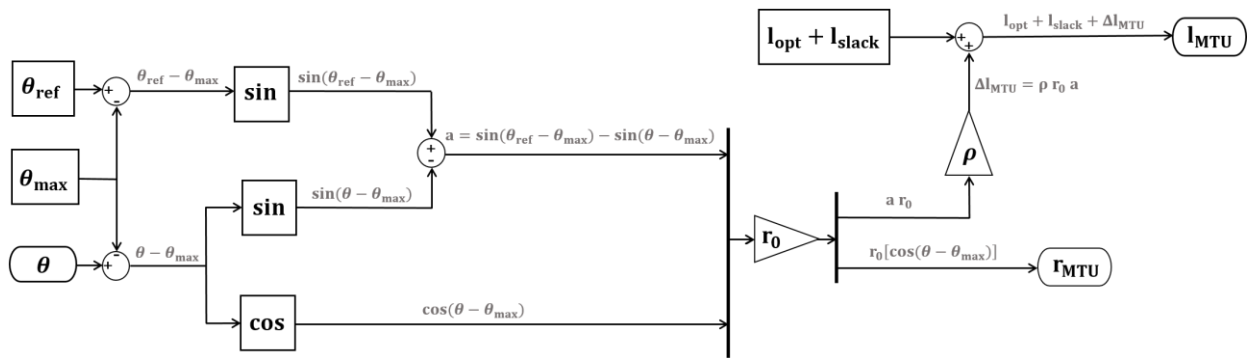


Figure 5.13 - SOL ATTACHMENT subsystem containing the implementation of the equations to calculate SOL's lever arm, r_{MTU} , variation of MTU length, Δl_{MTU} , and total MTU length, l_{MTU} . Blocks with a square and triangular shape enclose constants and blocks with rectangular shape with rounded ends are inputs and outputs of the subsystem, named Inports and Outports, respectively. θ is an input and r_{MTU} and l_{MTU} are outputs. θ is the ankle angle from Figure 5.12, from the Body Mechanics layer.

The lever arm, r_{MTU} , which is an output of the above presented subsystem, is used to calculate the torque produced by the MTU, in this case, SOL, using Eq. 5.3. However, before calculating this parameter, MTU force, F_{MTU} , must be evaluated.

A muscle's fibre arrangement affects greatly its ability to generate force (Oatis, 2009), as previously explained in Chapter 3, section 3.2. The muscle model used in this work and illustrated in Figure 5.11, does not account for the muscle's pennation angle¹, α , and therefore, the force produced by the muscle, F_{Muscle} , is all transmitted to the tendon, F_{Tendon} (Biewener, 2016):

$$F_{\text{Tendon}} = F_{\text{Muscle}} \cos(\alpha) \Leftrightarrow F_{\text{Tendon}} = F_{\text{Muscle}} \cos(0^\circ) \Leftrightarrow F_{\text{Tendon}} = F_{\text{Muscle}} \quad (5.6)$$

Within the muscle, in physiological ranges of operation (no joint overextension nor overflexion), PE and BE do not engage and therefore do not contribute to MTU's force. In these circumstances, only CE and SE influence the MTU dynamics, and Eq. 5.6 turns into $F_{\text{SE}} = F_{\text{CE}}$. Outside physiological ranges of operation, PE and BE engage and therefore influence the MTU's dynamics. Since PE engages to prevent CE's overextension, its force acts in order to shorten the CE's length and, therefore, F_{CE} and F_{PE} have the same direction. However, BE prevents CE from collapsing when the MTU shortens so much that it becomes slack. BE counteracts this action by tending to lengthen the MTU. This way, BE's force has opposite direction to CE and PE forces.

Applying the above explained logic to Eq. 5.6, F_{MTU} is directly related to the muscle model, previously shown in Figure 5.11, being calculated as in the work of Geyer & Herr (2010):

$$F_{\text{MTU}} = F_{\text{SE}} = F_{\text{CE}} + F_{\text{PE}} - F_{\text{BE}} \quad (5.7)$$

in which F_{SE} , F_{CE} , F_{PE} and F_{BE} are the forces produced by SE, CE, PE and BE, respectively.

Based on Geyer, Seyfarth, et al. (2003), the force of each contractile element of the MTU model is a product of the muscle activation, A_{MTU} , muscle's maximum isometric force, F_{max} , a force-length and a force-velocity relations, $f_l(l_{\text{CE}})$ and $f_v(v_{\text{CE}})$, respectively (see chapter 3, section 3.5):

$$F_{\text{CE}} = A_{\text{MTU}} F_{\text{max}} f_l(l_{\text{CE}}) f_v(v_{\text{CE}}) \quad (5.8)$$

with

$$\tau_{\text{ecc}} \frac{dA_{\text{MTU}}(t)}{dt} = S_{\text{MTU}}(t) - A_{\text{MTU}}(t) \quad (5.9)$$

and

$$f_l(l_{\text{CE}}) = \exp \left[c \left| \frac{l_{\text{CE}} - l_{\text{opt}}}{l_{\text{opt}} \omega} \right|^3 \right] \quad (5.10)$$

and

¹Note that the muscle model of Figure 5.11 does not account for muscle pennation angles, since the angle between the tendon (SE) and the muscle (CE, PE and BE) is 0° . However, this parameter is included in the calculation of the MTU's lever arm, as the factor ρ .

$$f_v(v_{CE}) = \begin{cases} \frac{v_{max} - v_{CE}}{v_{max} + Kv_{CE}} & v_{CE} < 0 \text{ (muscle shorteing)} \\ N + (N - 1) \frac{v_{max} + v_{CE}}{7.56Kv_{CE} - v_{max}} & v_{CE} \geq 0 \text{ (muscle lengthning)} \end{cases} \quad (5.11)$$

Equation 5.9 reflects the calculation of a muscle's activation state, A_{MTU} , which is related with a neural input stimulation, S_{MTU} , by a first-order differential equation describing the excitation-contraction coupling. τ_{ecc} is the time constant of the excitation-contraction coupling, $\tau_{ecc}=0.01$, being common to all 14 MTUs. The neural input stimulation is part of the Neural Control layer, and therefore will be discussed within that section. $\frac{dA_{MTU}(t)}{dt}$ is the rate of change in MTU activation.

In $f_i(l_{CE})$'s expression, l_{opt} is CE's optimum fibre length for maximum force production, ω describes the width of the bell-shaped $f_i(l_{CE})$ curve and c is the residual force factor. l_{CE} represents CE's length. The force-length relation, $f_i(l_{CE})$, is based on the work of Aubert (1956) (Geyer, Seyfarth, et al., 2003).

On one hand, for the muscle shortening branch, the force-velocity relation has its roots on the Hill equation (Hill, 1938), where $v_{max} < 0$ is the maximum contraction velocity, K is a curvature constant and v_{CE} is the velocity of CE. On the other hand, the equation characterizing muscle lengthening is based on Aubert (1956), where N is the eccentric force enhancement represented by the dimensionless amount of force F_{MTU}/F_{max} (Geyer, Seyfarth, et al., 2003).

The series elastic element is characterized by a nonlinear elastic force-length relation, $f_{SE}(\epsilon)$, based on the work of van Ingen Schenau (1984), (Geyer, Seyfarth, et al., 2003):

$$f_{SE}(\epsilon) = \begin{cases} \left(\frac{\epsilon_{SE}}{\epsilon_{ref}}\right)^2 & \epsilon > 0 \\ 0 & \epsilon \leq 0 \end{cases} \quad (5.12)$$

where

$$\epsilon_{SE} = \frac{l_{SE} - l_{slack}}{l_{slack}} \quad (5.13)$$

is the tendon strain. ϵ_{ref} is the reference strain with $f_{SE}(\epsilon) = 1$, l_{SE} is the SE's length and l_{slack} is the tendon's slack length. From the Simulink model implemented by Geyer & Herr (2010), SE's force, F_{SE} , is modelled as:

$$F_{SE} = F_{max} f_{SE}(\epsilon) \quad (5.14)$$

Geyer & Herr (2010) state that PE and BE are only used outside the normal range of operation of the MTU, thus playing a minor role in its dynamics during locomotion of the model, as already explained. The authors modelled these two elements as follows:

$$F_{PE} = F_{\max} \left[\frac{\left(\frac{l_{CE} - 1}{l_{opt}} \right)^2}{\varepsilon_{PE}^2} \right] f_v(v_{CE}) = F_{\max} \left(\frac{l_{CE} - l_{opt}}{l_{opt} \varepsilon_{PE}} \right)^2 f_v(v_{CE}) = F_{\max} f_l(l_{PE}) f_v(v_{CE}) \quad (5.15)$$

with F_{PE} being the force produced by PE, $\varepsilon_{PE} = \omega$ is PE's reference strain and $f_l(l_{PE})$ is PE's force-length relation and

$$F_{BE} = F_{\max} \left(\frac{\left[\frac{l_{\min} - l_{CE}}{l_{opt}} \right]^2}{\varepsilon_{BE}^2} \right) = F_{\max} \left(\frac{l_{\min} - l_{CE}}{l_{opt} \varepsilon_{BE}} \right)^2 = F_{\max} f_l(l_{BE}) \quad (5.16)$$

with F_{BE} being BE's produced force, $l_{\min} = l_{opt} - \omega$ is BE's rest length, $\varepsilon_{BE} = \omega/2$ is BE's reference compression and $f_l(l_{BE})$ is BE's force-length relation.

The MTUs are characterized by individual and common parameters, which are used to implement the MTU model in Simulink. Common parameters include the time constant of the excitation-contraction coupling, $\tau_{ecc}=0.01$, pre-activation state, $A_{0,MTU}=0.01$; CE's force-length relation width, $\omega=0.56l_{opt}$ and residual force factor, $c=0.05$; CE's force-velocity relation eccentric force enhancement, $N=1.5$ and curvature constant of CE's $f_v(v_{CE})$, $K=5$; and SE's reference strain, $\varepsilon_{ref}=0.04$. These parameters were taken from Geyer & Herr (2010), based on the work Geyer, Seyfarth, et al. (2003).

The individual parameters are the ones that pertain to each muscle and characterize it univocally. The values for these parameters used in this work are the ones used by Geyer & Herr (2010), which were estimated from other literature, (Maganaris, 2001, 2003; Muraoka, Kawakami, et al., 2001; Oda, Kanehisa, et al., 2005; Yamaguchi, Sawa, et al., 1990) or from their anatomical estimates. Table 5.2 presents these parameters.

Table 5.2 - MTUs individual parameters. The MTU attachment parameters are the ones used by Geyer & Herr (2010), which were estimated from (Maganaris, 2001, 2003; Muraoka, Kawakami, et al., 2001; Oda, Kanehisa, et al., 2005) or from Geyer & Herr (2010) anatomical estimates. Muscle lever arm is represented by r_0 . The angle at which the muscle lever arm reaches its maximum is θ_{\max} . The angle where $l_{MTU} = l_{opt} + l_{slack}$ is θ_{ref} , being the angle that corresponds to the muscle rest length. ρ is a factor that accounts for muscle's pennation angle, ensuring that the MTU's fibre length stays within physiological limits. Muscle parameters were estimated from Yamaguchi, Sawa, et al. (1990), being the ones used by Geyer & Herr (2010). The maximum isometric force, F_{\max} , was estimated from individual or grouped muscle's physiological cross-sectional area. The maximum

contraction speed, v_{max} , is set to 6 l_{opt}/s for slow twitch muscles and to 12 l_{opt}/s for fast twitch muscles. l_{opt} and l_{slack} correspond to CE's optimum fibre length and SE's slack length, respectively. All these parameters were taken from Geyer & Herr (2010)

		Ankle Joint			Knee Joint			Hip Joint		
ATTACHMENT PARAMETERS	r_0 (mm)	SOL	TA	GAS	GAS	VAS	HAM	HAM	GLU	HFL
	θ_{max} (deg)	50	40	50	50	60	50	80	100	100
	θ_{ref} (deg)	110	80	110	140	165	180	-	-	-
	ρ	80	110	80	165	125	180	155	150	180
MUSCLE PARAMETERS	F_{max} (N)	0.5	0.7	0.7	0.7	0.7	0.7	0.7	0.5	0.5
	v_{max} (l_{opt}/s)	4000	800	1500	6000	3000	1500	2000		
	l_{opt} (mm)	6	12	12	12	12	12	12	12	12
	l_{slack} (mm)	40	60	50	80	100	110	110		
		260	240	400	230	310	130	100		

From Eq. 5.8 to Eq. 5.16, it is noticeable that the only unknowns are l_{CE} and v_{CE} , from which all the other muscular variables can be derived. Considering this statement, in Simulink, Geyer & Herr (2010) computed the MTU dynamics by resolving for l_{CE} :

$$l_{CE} = \int v_{CE} dt = \int [f_v(v_{CE})]^{-1} dt \quad (5.17)$$

From Eqs. 5.7 and 5.8,

$$\begin{aligned} F_{MTU} &= F_{SE} = F_{CE} + F_{PE} - F_{BE} \\ \Leftrightarrow F_{CE} &= F_{SE} - F_{PE} + F_{BE} \end{aligned} \quad (5.18)$$

and

$$\begin{aligned} F_{CE} &= A_{MTU} F_{max} f_l(l_{CE}) f_v(v_{CE}) \\ \downarrow \\ F_{SE} - F_{PE} + F_{BE} &= A_{MTU} F_{max} f_l(l_{CE}) f_v(v_{CE}) \\ \Leftrightarrow f_v(v_{CE}) &= \frac{F_{SE} - F_{PE} + F_{BE}}{A_{MTU} F_{max} f_l(l_{CE})} \end{aligned} \quad (5.19)$$

Equation 5.19 can be further manipulated to reach the expression the author's used to model the MTU dynamics in Simulink:

$$f_v(v_{CE}) = \frac{F_{SE} - F_{PE} + F_{BE}}{A_{MTU} F_{max} f_l(l_{CE})} \quad (5.20)$$

$$\begin{aligned}
\Leftrightarrow f_v(v_{CE}) &= \frac{F_{\max} f_1(l_{SE}) - F_{\max} f_1(l_{PE}) f_v(v_{CE}) + F_{\max} f_1(l_{BE})}{A_{MTU} F_{\max} f_1(l_{CE})} \\
\Leftrightarrow f_v(v_{CE}) &= \frac{F_{\max} (f_1(l_{SE}) - f_1(l_{PE}) f_v(v_{CE}) + f_1(l_{BE}))}{A_{MTU} F_{\max} f_1(l_{CE})} \\
\Leftrightarrow f_v(v_{CE}) &= \frac{(f_1(l_{SE}) - f_1(l_{PE}) f_v(v_{CE}) + f_1(l_{BE}))}{A_{MTU} f_1(l_{CE})} \\
\Leftrightarrow A_{MTU} f_1(l_{CE}) f_v(v_{CE}) &= f_1(l_{SE}) - f_1(l_{PE}) f_v(v_{CE}) + f_1(l_{BE}) \\
\Leftrightarrow A_{MTU} f_1(l_{CE}) f_v(v_{CE}) + f_1(l_{PE}) f_v(v_{CE}) &= f_1(l_{SE}) + f_1(l_{BE}) \\
\Leftrightarrow f_v(v_{CE})(A_{MTU} f_1(l_{CE}) + f_1(l_{PE})) &= f_1(l_{SE}) + f_1(l_{BE}) \\
\Leftrightarrow f_v(v_{CE}) &= \frac{f_1(l_{SE}) + f_1(l_{BE})}{A_{MTU} f_1(l_{CE}) + f_1(l_{PE})}
\end{aligned}$$

To implement this expression and to resolve the MTUs' dynamics, a Simulink mask was created. In SOL's example, the mask is the SOL DYNAMICS block, as seen in Figure 5.12. Each of the 14 MTUs have a similar mask block. However, the difference lies within the definition of four parameters that characterize each muscle uniquely, as seen in Table 5.2: F_{\max} , v_{\max} , l_{opt} and l_{slack} . These parameters are used in Eq. 5.7 to Eq. 5.20. Besides these parameters, what distinguishes the MTU force is its stimulation and, consequently, its activation. In addition to these parameters, others are required, previously termed the common parameters.

Inside the Simulink mask, the force-length relations for each of the four elements of the MTU (CE, SE, PE and BE) are calculated using subsystems based on the equations provided above. The implementation of these equations within the subsystems is similar to the one presented in Figure 5.13.

The activation state is also calculated, and, since this is a first-order differential equation (ODE), it cannot be directly resolved. Considering this, the La Place Transform is used:

$$\begin{aligned}
\tau_{ecc} \frac{dA_{MTU}(t)}{dt} &= S_{MTU}(t) - A_{MTU}(t) \\
\hline
&\quad \text{La Place Transform} \\
\tau_{ecc} A_{MTU}(s)s &= S_{MTU}(s) - A_{MTU}(s) \\
\Leftrightarrow \tau_{ecc} A_{MTU}(s)s + A_{MTU}(s) &= S_{MTU}(s) \\
\Leftrightarrow A_{MTU}(s) (\tau_{ecc}s + 1) &= S_{MTU}(s) \\
\Leftrightarrow \frac{A_{MTU}(s)}{S_{MTU}(s)} &= \frac{1}{(\tau_{ecc}s + 1)} \\
\Leftrightarrow \frac{1}{(0.01s + 1)} &= H(s)
\end{aligned} \tag{5.21}$$

After implementing PE, BE, CE and SE's force-length relations, CE's force-velocity relation, $f_v(v_{CE})$, is resolved using Eq. 5.20. Figure 5.14 demonstrates the modelling of the MTU dynamics until this point.

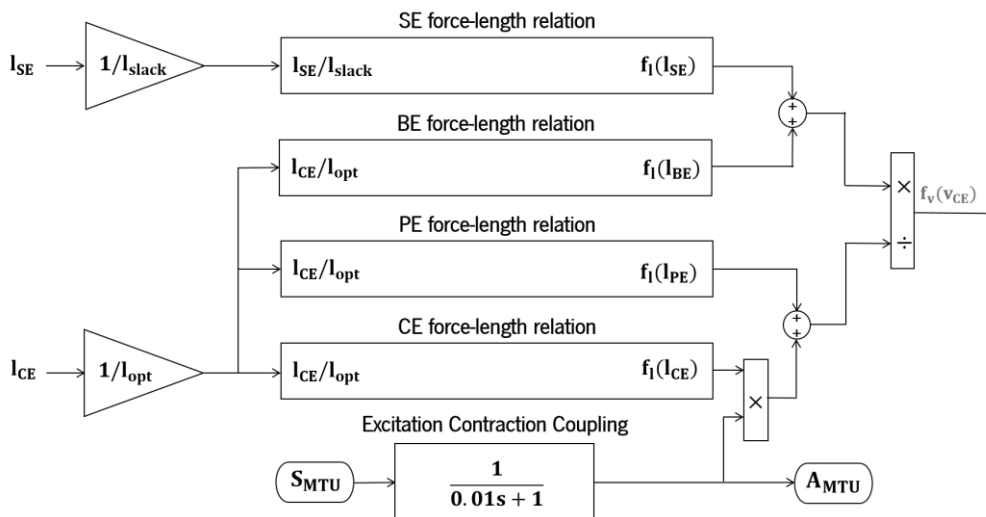


Figure 5.14 - Part of the MTU dynamics approached so far: calculation of CE's force-velocity relation, $f_v(v_{CE})$. S_{MTU} is the muscle's neural stimulation and is an input of the mask, calculated in the Neural Control layer (explained later). Output of the mask is the muscle's activation, A_{MTU} , which is used in the same layer as S_{MTU} , as well as in the Muscle Actuation layer. The transformation from neural stimulation, S_{MTU} , to muscular activation, A_{MTU} , is done by means of a Transfer Fnc block, named Excitation Contraction Coupling and whose expression is the one from Eq. 5.21. The inputs of SE, BE, PE and CE's force-length relations are either divided by I_{slack} or I_{opt} , since it makes it easier to resolve the equations inside the subsystems. Inside SE, BE, PE and CE subsystems, Eq. 5.12, $f_l(I_{BE})$ part of Eq. 5.16, $f_l(I_{PE})$ part of Eq. 5.15 and Eq. 5.10, respectively, are implemented by means of blocks in a similar manner as Figure 5.13.

After obtaining $f_v(v_{CE})$, v_{CE} is computed using the inverse of Eq. 5.11 and multiplying the result for $v_{max} I_{opt}$, characteristic of the MTU being analysed. Using an integrator block, Eq. 5.17 is solved for I_{CE} , with an initial condition, x_0 , equal to $x_0 = I_{MTU} - I_{slack}$. I_{MTU} is an output of the block that models the MTU attachment, previously approached (see Figure 5.12 and Figure 5.13).

I_{CE} is used in the force-length relations of BE, PE and CE, as seen in Figure 5.14. Besides, it is also used to calculate I_{SE} as $I_{SE} = I_{MTU} - I_{CE}$ (see Figure 5.11). Considering Eq. 5.7, an MTU force is equal to the force exerted in its series elastic element. Since BE and SE engage only outside the physiological range of operation of the MTU, is it expected that, within physiological ranges, they do not produce any force. During model's walking simulation, this is observed. This way, $F_{SE} = F_{CE}$, and therefore the force of the MTU is totally defined by the force in SE. Considering this, in Simulink, the MTU force is the force of SE, calculated by multiplying the SE's force-length relation, $f_{SE}(\epsilon)$, by the maximum isometric force, F_{max} ,

characteristic of the MTU being analysed, in this case, SOL (see Eq. 5.14). Figure 5.15 shows the modelling of the whole MTU dynamics using Simulink blocks.

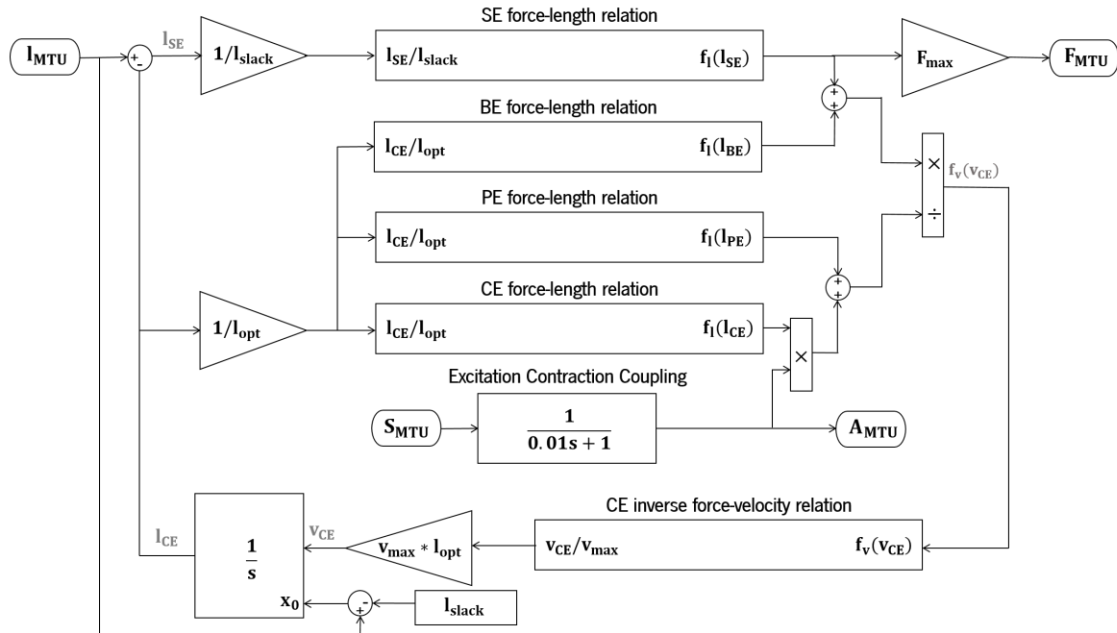


Figure 5.15 - Inside the MTU DYNAMICS mask used to calculate the force produced by the MTU. The components within the mask are equally modelled to all MTUs. What differentiates the MTU and that uniquely characterizes it, is the definition of four individual muscle parameters, F_{max} , v_{max} , I_{opt} and I_{slack} . $f_{SE}(\epsilon)$, $f_{l(BE)}$, $f_{l(PE)}$ and $f_{l(CE)}$ are the force-length relations of SE, BE, PE and CE, respectively. S_{MTU} and A_{MTU} are the MTU's stimulation and activation, respectively. $f_v(v_{CE})$ is the force-velocity relation of CE.

5.3. Biomechanical Model's Neural Control Layer

According to Geyer & Herr (2010), unlikely humans, that have a central pattern generator (CPG) that provide rhythmic activity to the leg extensor and flexor muscles, the model's muscular reflexes generate MTU stimulation sufficient to generate walking movements. The left and right legs have separate stance and swing reflexes, which are selected based on contact sensors located at the toes and heel (ball and heel CP, respectively) of each foot to detect ground (the ground contact is explained in the following section). Generally, if contact is detected, the leg is in stance and stance reflexes are used. Conversely, if contact is not detected, the leg is in the swing phase and reflexes pertaining to this phase of gait are applied. As a result, the model's dynamic interaction with its surrounding environment becomes a vital part of generating muscular activities (Geyer & Herr, 2010).

Since the study of the Neural Control layer was not the focus of this dissertation, only superficial understanding of it was achieved. It is known that within this layer, the swing and stance muscular reflexes (muscle length and force feedbacks) used to model the biomechanical model's motion are implemented.

For instance, muscular stimulation's equations arising from Geyer & Herr (2010) and Geyer, Seyfarth, et al. (2003) are implemented, and the results are posteriorly used in the Muscle Actuation Layer, more precisely in Eqs. 5.9 and 5.21 to calculate the MTU activation.

A general expression for the muscular stimulation, S_{MTU} , is (Geyer & Herr, 2010; Geyer, Seyfarth, et al., 2003):

$$S_{MTU}(t) = \begin{cases} S_{0,MTU} & t < \Delta t_m \\ S_{MTU_0} \pm G_{MTU} F_{MTU}(t - \Delta t_m) & t \geq \Delta t_m \end{cases} \quad (5.22)$$

where $S_{0,MTU}$ is the constant MTU's pre-stimulation, G_{MTU} is the gain factor, F_{MTU} is the MTU force (see Figure 5.12 and Figure 5.15) or length reflex signal and Δt_m is the signal propagation time delay. $S_{0,MTU}$ is characteristic of each muscle, as seen in Table 5.3.

Table 5.3 - Pre-Stimulation of each MTU

	SOL	TA	GAS	VAS	HAM	GLU	HFL
$S_{0,MTU}$	0.01	0.01	$1.1/F_{max}$	$1.1/ F_{max}$	0.01	0.01	0.05

For more understanding about neuromuscular control of the biomechanical model, it is recommended the analysis of the following papers (Geyer & Herr, 2010; Geyer, Seyfarth, et al., 2003; Thatte & Geyer, 2016).

Besides muscular stimulations, joints' soft limits are also modelled within the Neural Control layer. As previously stated, all joints pertaining to the model have constrained range of motion in order to enable physiological gait. Outside the ROM, joints' soft limits engage, preventing abnormal movement of the joint. These limits are modelled in order to produce a torque that acts to counteract the one produced by the joint, preventing it to go further than the physiological ROM, that is its overextension or overflexion.

This strategy is similar to the one used by Tavares da Silva (2003), named penalty approach. It is based on the definition of a circumduction cone, with its tip in the joint's centre of rotation. Inside this cone, any joint position is considered to be within the joint's range of motion, that is, it is a feasible position. If the joint position is outside this cone, then a penalty torque arises. In order to determine whether the joint position is outside the circumduction cone, the spherical coordinates of the actual joint position are calculated (Tavares da Silva, 2003).

The strategy implemented in the biomechanical model is similar. The physiological range of motion of each joint is defined ($70^\circ < \theta_A < 130^\circ$, $\theta_K < 175^\circ$ and $\theta_H < 230^\circ$, as previously explained in section 5.1) and

if the current joint position, θ , is outside that ROM, then the penalty torque arises, counteracting the torque produced by the joint and preventing any unfeasible joint position. The formulation of the soft limits is as follows:

$$\tau_{\text{penalty}} = -k_{\theta} \Delta\theta \left(1 - \frac{\dot{\theta}}{\dot{\theta}_{\text{max}}}\right), \text{ with } \Delta\theta > 0 \quad (5.23)$$

in which the values for soft limit stiffness, k_{θ} , and maximum relaxation speed, $\dot{\theta}_{\text{max}}$, are 0.3 Nm/deg and 1 deg/s, respectively. The implementation of this formulation in Simulink is illustrated for the hip joint in Figure 5.16.

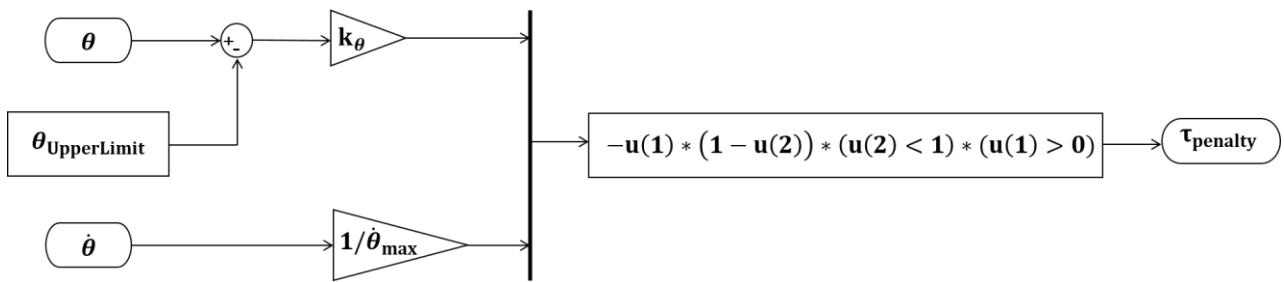


Figure 5.16 - Example of modelling joint mechanical soft limit for the hip joint.

The result of the upper and lower branches of Figure 5.16, is $k_{\theta} (\theta - \theta_{\text{UpperLimit}}) = k_{\theta} \Delta\theta$ and $\dot{\theta} \frac{1}{\dot{\theta}_{\text{max}}} = \frac{\dot{\theta}}{\dot{\theta}_{\text{max}}}$, respectively. θ , $\dot{\theta}$ and $\theta_{\text{UpperLimit}}$ are the measured joint angle and angular velocity throughout the course of simulation and the overextension angle, respectively. Since the hip joint's range of motion is $\theta_H < 230^\circ$, this joint only has an upper limit from which the hip joint angle cannot overcome. The rectangular block interrelates these two expressions to form Eq. 5.23 of the mechanical joint soft limit:

$$-u(1) * (1 - u(2)) = -k_{\theta} \Delta\theta * \left(1 - \frac{\dot{\theta}}{\dot{\theta}_{\text{max}}}\right) \quad (5.24)$$

in which $u(1)$ is the result of the upper branch and $u(2)$ is the result of the lower branch. $u(1)$ has to be greater than 0, as in Eq. 5.23. $u(2)$ is lower than one since in Eq. 5.23: $1 - \frac{\dot{\theta}}{\dot{\theta}_{\text{max}}} > 0 \Leftrightarrow \frac{\dot{\theta}}{\dot{\theta}_{\text{max}}} < 1$.

Since both the hip and knee joint only have an upper angle limit in their range of motion, they are similarly modelled, as seen in Figure 5.16. However, since the ankle joint possesses upper and lower limits, the Simulink modelling is slightly different. Besides having the blocks observed in the above figure, it has as well the implementation of the joint's lower limit, representing the overflexion angle.

5.4. Ground Interaction Model

In section 5.1, it was introduced the concept that each foot segment had two contact points (CP): namely the heel and the ball, anatomically representing the heel and toes of the human body, respectively. It was also referred that these CPs were used to detect ground interaction and, if contact was sensed between the CP and the ground, the ground contact model would be resolved, calculating the generated ground reaction forces (GRF).

The detection of ground interaction is done by means of contact sensors (see Appendix I) connected to the contact points, to measure their position during gait. The determination of whether there is contact or not between a CP and the ground, enables the determination of which phase of gait, stance or swing phase, the model is at. If contact is detected, it means that the leg corresponding to that CP in contact with the ground is in the stance phase. On the contrary, if contact is not detected, it means that the corresponding leg is in swing phase and no GRF are measured. Figure 5.17 illustrates this concept. This complex does not function only as a contact detector. The determination of whether the leg is in swing or stance phases, besides determining the ground reaction forces, also enables the formation of muscle stimulations specific for that phase of gait. If the leg is in stance, stimulations only pertaining to stance will be calculated, moving the leg accordingly to that phase of the gait, and vice-versa. However, this concept regards to the Neural Control Layer, previously approached.

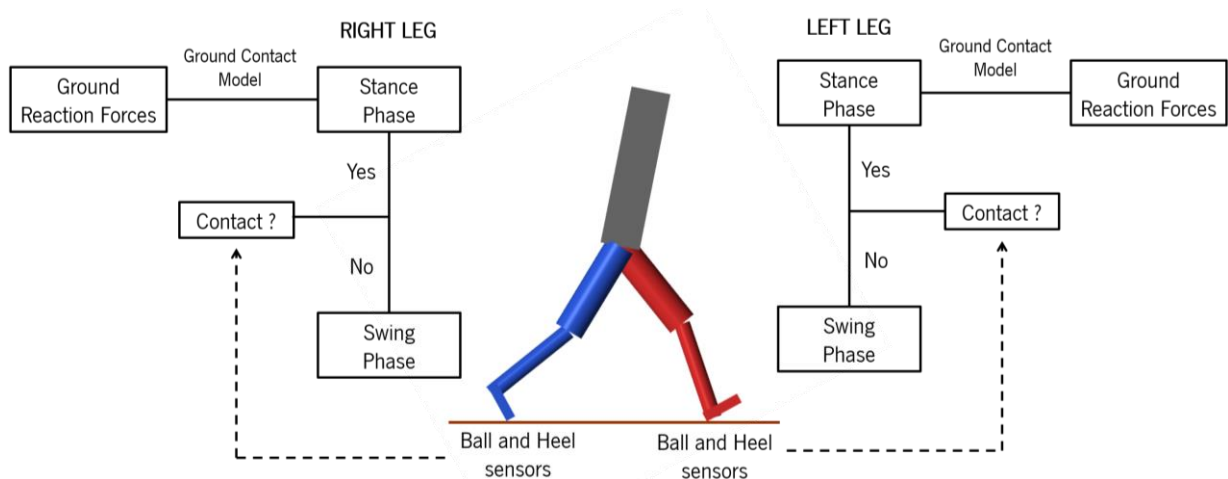


Figure 5.17 - Detection of leg's gait phase, whether it is stance or swing, based on ball and heel contact sensors. The brown line below the biomechanical model represents the ground. Adapted from Geyer & Herr (2010).

As referred by Geyer & Herr (2010), contact occurs if the at least one of the CPs' position falls below a determined reference value, y_0 . Figure 5.18 illustrates this concept. When the foot impacts the ground, meaning that there is contact between at least one of the CPs and the ground, two contact forces arise:

the vertical and horizontal ground reaction forces. Even though the model is built in the 3D space, the GRF has only two components since the simulation of the model is only performed in a 2D plane (sagittal).

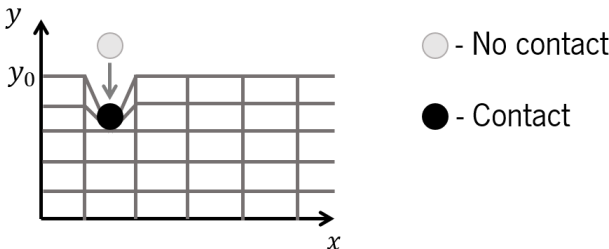


Figure 5.18 - Occurrence of contact. Contact occurs if the CP (circles) falls below y_0 , which is the reference value.

Geyer & Herr (2010), defined the vertical GRF as a spring-damper model motivated by other literature (Günther & Ruder, 2003; Scott & Winter, 1993). By treating the vertical GRF as the sum of a spring and a damper, the authors state that the parameters of the contact model can be interpreted as two basic material properties: ground stiffness, k_v , arising from the spring element, and maximum ground relaxation speed, \dot{y}_{max} , arising from the damper term. This latter parameter determines how quickly the ground can restore its original shape after being deformed, due to the impact with the CP. As explained by the authors, on one hand if, after the impact, the ground always pushes the CP upwards, restoring its initial shape, $\dot{y}_{max} = \infty$ (perfectly elastic impact) (Figure 5.19a). On the other hand, if, after the impact, the ground pushes the CP downwards but cannot push it upwards, the ground cannot restore its original shape after the impact, $\dot{y}_{max} = 0$ (perfectly inelastic impact) (Figure 5.19b).

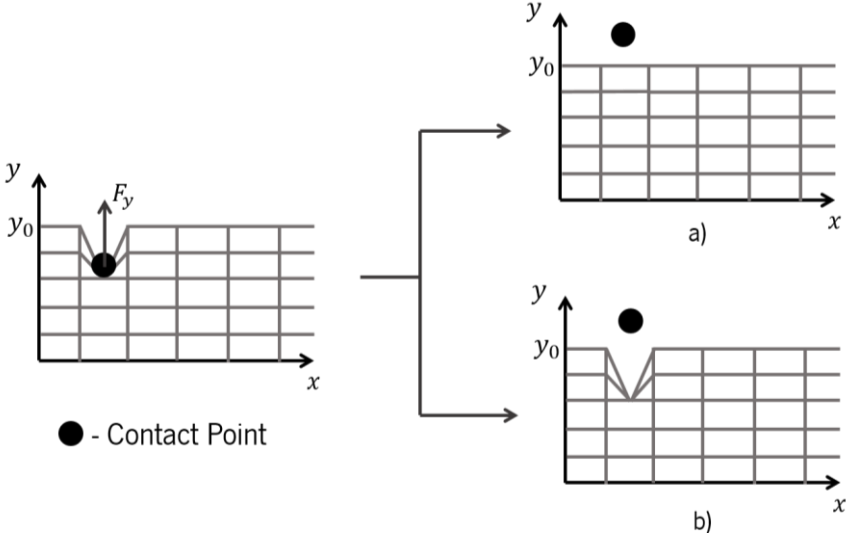


Figure 5.19 - Relation between the capacity of the ground to restore its shape after impact: perfectly a) elastic and b) inelastic cases. F_y represents the vertical ground reaction force applied by the ground on the CP.

Considering the description above, the vertical ground reaction force, F_y , is a product of a force-length relation, $f_l(\Delta y_{CP})$, and a force-velocity relation, $f_v(\Delta \dot{y}_{CP})$, calculated according to the following expressions (Geyer & Herr, 2010):

$$k_y = \frac{F_{ref}}{\Delta y_{ref}} \quad (5.25)$$

$$f_l(\Delta y_{CP}) = \frac{\Delta y_{CP}}{\Delta y_{ref}} \quad (5.26)$$

$$f_v(\Delta \dot{y}_{CP}) = 1 - \frac{\dot{y}_{CP}}{\dot{y}_{max}} \quad (5.27)$$

$$F_y = -F_{ref} f_l(\Delta y_{CP}) f_v(\Delta \dot{y}_{CP}) \quad (5.28)$$

$$\Leftrightarrow F_y = -F_{ref} \frac{\Delta y_{CP}}{\Delta y_{ref}} \left(1 - \frac{\dot{y}_{CP}}{\dot{y}_{max}}\right), \text{ with } \Delta y_{CP} > 0 \text{ and } \frac{\dot{y}_{CP}}{\dot{y}_{max}} < 1$$

where k_y is the vertical contact stiffness, Δy_{CP} is the ground penetration ($\Delta y_{CP} = y_0 - y_{CP}$), Δy_{ref} is the ground penetration at which $F_y = F_{ref}$ when $\dot{y}_{CP} = 0$, \dot{y}_{CP} is the CP's vertical velocity and \dot{y}_{max} is the maximum ground relaxation speed. Geyer & Herr (2010) used the following values for the parameters above described: $k_y = 78.4$ kN/m and $\dot{y}_{max} = 3$ cm/s.

Geyer & Herr (2010) have also used this formulation to model the joints' mechanical soft limits. This part is implemented in the Neural Control layer and is discussed in more detail in that section (Eq. 5.23).

Besides the vertical ground reaction force, the ground also applies a horizontal force to the CP. This is modelled in two different ways: as a sliding (kinetic friction) and as a stiction (static friction) force. After initial ground contact, the horizontal GRF is modelled as kinetic friction, opposing the CP's movement:

$$F_{x,sl} = -\text{sgn}(\dot{x}_{CP}) \mu_{sl} F_y \quad (5.29)$$

where \dot{x}_{CP} is the CP's horizontal velocity, $\mu_{sl} = 0.8$ is the sliding friction coefficient and F_y is the vertical ground reaction force, previously explained. When the CP slows down to below a minimum speed, $\dot{x}_{lim} = 1$ cm/s, the horizontal model switches to a stiction force, which is modelled in a similar manner as F_y :

$$F_{x,st} = -k_x \Delta x_{CP} (1 + \text{sgn}(\Delta x_{CP}) \Delta \dot{x}_{CP}^*) \quad (5.30)$$

where $k_x = 7.84$ kN/m is the horizontal contact stiffness, $\Delta x_{CP} = x_{CP} - x_{st}$, where x_{CP} is the CP's position, is the shift from the point x_{st} at which stiction engages and $\Delta \dot{x}_{CP}^*$ is the CP's velocity normalized to $\dot{x}_{max} = 3$ cm/s.

A CP's horizontal GRF changes from sliding to stiction if $|\dot{x}_{CP}| < \dot{x}_{lim}$ and returns to sliding if $F_{x,st} \geq \mu_{st} F_y$, with a stiction coefficient of $\mu_{st} = 0.9$. Figure 5.20 illustrates this interchange between GRF.

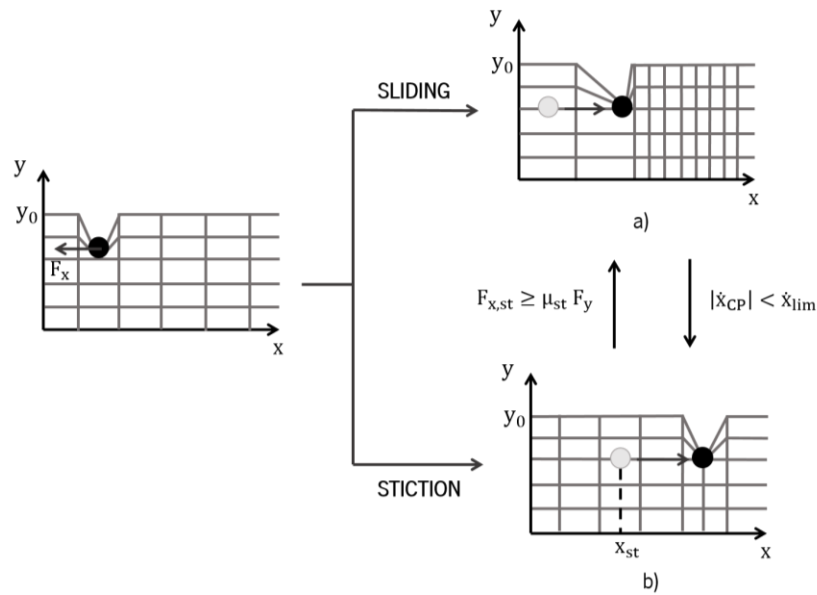


Figure 5.20 - Illustration of the interaction between horizontal ground reaction forces. Sliding changes to stiction if $|\dot{x}_{CP}| < \dot{x}_{lim}$. Stiction changes to sliding if $F_{x,st} \geq \mu_{st} F_y$. x_{st} is the stiction reference point, from this point on, sliding changes to stiction.

During ground contact, there is always two force components acting on the CP, the vertical and the horizontal one, as previously explained. Besides the interchange that occurs in the horizontal GRF (sliding and stiction), the vertical GRF is always acting on the CP, that is, independently of what type of horizontal GRF that is acting, the vertical GRF always exists. As seen in Figure 5.21, the contact model is implemented in Simulink by means of an enabled subsystem, inside which two others, sliding and stiction models, are implemented, each calculating the vertical and their respective horizontal GRF.

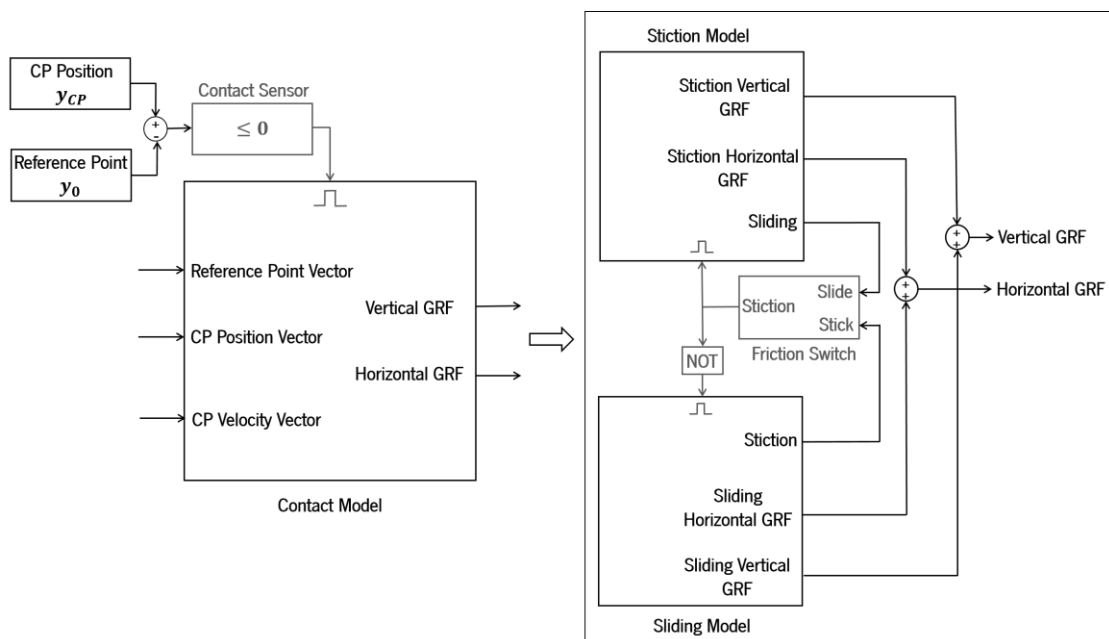


Figure 5.21 - General overview of the ground contact model implemented in Simulink. The model is an enabled subsystem (Contact Model), comprising two other similar subsystems to model stiction (Stiction Model) and sliding (Sliding Model), along with the vertical GRF. The contact sensor block enables the activation or not of the contact model subsystem, that is, if contact

is detected (detection of contact is explained above and in Figure 5.18) this subsystem is activated to calculate its outputs, in this case, the GRF. The sliding and stiction enabled subsystems are also activated or not by means of the friction switch block. If, within this switch, stiction is detected, the stiction model is resolved, and the sliding model is disabled, and vice versa.

To determine whether there is contact or not between a CP and the ground, the contact sensor block is implemented in Simulink, essentially being a compare to zero block. This block is directly connected to the enable port of the contact model enabled subsystem, in order to enable or disable it. What this block does is compare the result of the difference between the current CP position, y_{CP} , and the reference point, y_0 , and zero. If that difference is lower than zero, contact is detected (see Figure 5.18), and the contact model subsystem is enabled, beginning to resolve its dynamics. Essentially, what this block does to detect contact is:

$$\begin{array}{c}
 \overbrace{y_{CP} - y_0 < 0 ? \Leftrightarrow y_{CP} < y_0 ?} \\
 \hline
 \left[\begin{array}{cc}
 y_{CP} < y_0 \Rightarrow \text{Contact exists} & y_{CP} > y_0 \Rightarrow \text{There is no contact}
 \end{array} \right.
 \end{array} \tag{5.31}$$

The output of the contact sensor block is a logic value, either a 0 or a 1. If 0 is the output, it means there is no contact and the contact model is not resolved. If the output is 1, then the contact model subsystem is enabled, resolving its dynamics.

In the contact model subsystem, the inputs are the reference point vector and the CP position and velocity vectors. The first vector comprises the vertical and horizontal reference points, y_0 and x_{st} , respectively. And the CP position and velocity vectors contain the current position and velocity of the CP, respectively, measured through a sensor.

Considering that contact is detected, meaning that the contact model subsystem is enabled, the friction switch block decides which horizontal ground reaction force is acting, whether it is sliding or stiction, since it is connected to the enable port of both subsystems. This switch is a subsystem comprising a Set-Reset (R-S) Flip Flop. In fact, even though the block is named Flip-Flop, it represents a Latch, since it does not present any clock input.

There are several ways to construct the S-R Latch, however all of them share the same simple diagram and truth table. The truth table is a representation of the sequence of logic inputs that produce a determined logic output. In this thesis, this circuit is explained using two NOR gates, that is, their output is 1 only when both inputs are 0. Figure 5.22a represents the truth table and diagram of a NOR gate.

The inputs of the S-R Latch system are S (set) and R (reset), and its outputs are Q and \bar{Q} , being complementary, that is when $Q=1$, $\bar{Q} = 0$, and vice versa. From electronics, circuits that present the property that its output depends not only on its current input but also on the past sequence of inputs are called sequential switching circuits (Roth, 2004). The S-R Latch is one of these circuits, since the output of each NOR gate, Q and \bar{Q} , is connected to one of the inputs of the other (Nair, 2002). Figure 5.22b illustrates the S-R Latch truth table and diagrams. In Simulink the “Set” or true state occurs when $Q=1$, and the “Reset” or false state occurs when $Q=0$.

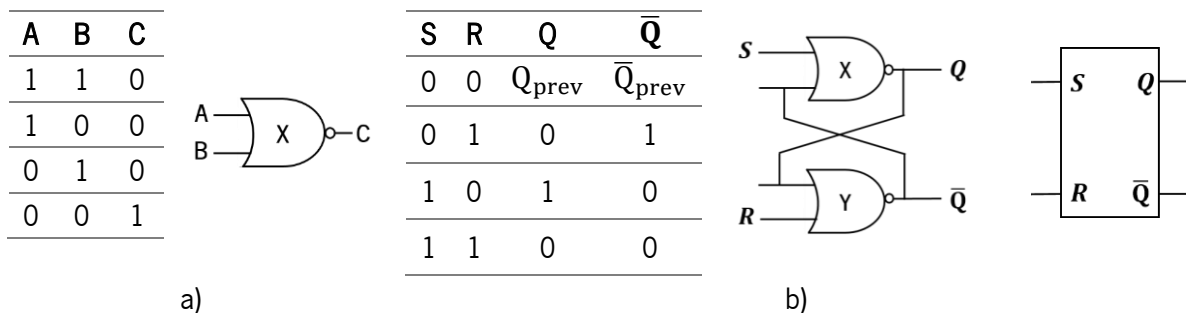


Figure 5.22 – a) Truth table and diagram of the NOR gate (Harris & Harris, 2012). b) Truth table of the SR Latch circuit. In the middle, there is the representation of this circuit with X and Y NOR gates, and on the right there is a simpler illustration of the circuit (Roth, 2004).

In Simulink, the Q output of the S-R circuit is the output of the friction switch subsystem, called Stiction, since \bar{Q} is connected to a Terminator block and performs no function in the contact model (Figure 5.23). Considering this, the value of Q is the one which is going to enable or disable the sliding and stiction model subsystems.

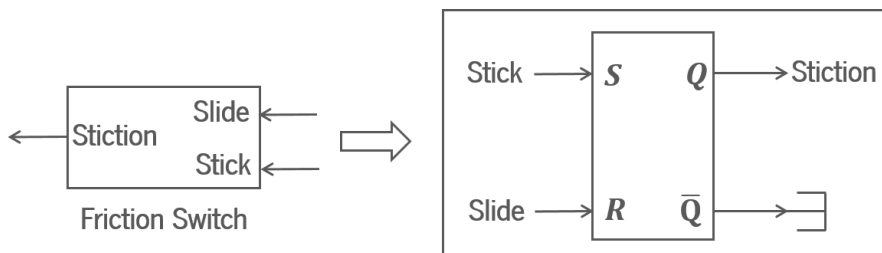


Figure 5.23 - Inside the friction switch subsystem. Stick and slide are inputs to the S-R circuit and Q and \bar{Q} are outputs. \bar{Q} is connected to a terminator block and Q determines the output of S-R circuit.

As previously explained, when a CP impacts the ground, besides the vertical GRF, a horizontal GRF arises, being firstly defined as sliding. In Simulink, it is possible to determine Q's initial condition, which was set to 0. With this initial condition, the stiction model is disabled, and the sliding model is enabled. This occurs because in between the friction switch and the sliding model there is a NOT logical operator, which turns $Q=1$, enabling the sliding model.

If the conditions that favour the occurrence of stiction ($|\dot{x}_{CP}| < 1 \text{ cm/s}$) are met, the Q logic turns to 1 and the sliding model is disabled, enabling the stiction model. Once in stiction, if $F_{x,st} \geq \mu_{st} F_y$, the model changes back to sliding. These two equations are implemented inside the sliding and stiction model subsystems, respectively, in a similar manner as the one presented in Figure 5.13. The outputs of these equations, sliding and stiction (Figure 5.21 and Figure 5.23), are logical values (0 or 1), which will take part in the friction switch subsystem as inputs, slide and stick, respectively, enabling the interchange between horizontal GRF.

The above-presented S-R Latch truth table represents four cases to model this interchange between sliding and stiction, including the conditions stated above. When sliding occurs, the slide input is 1 and the stick is 0, that is $R=1$ and $S=0$, Q is reset to 0 and $\bar{Q} = 1$, meaning that the stiction and the sliding models are disabled and enabled, respectively. This occurs since a logic 0 and 1 enter the enable port of the stiction and sliding subsystems, respectively. Even though $Q=0$ when it exits the friction switch, in between the sliding model and the friction switch there is a NOT gate that makes its output a complementary logic value of the input, and this way $Q=1$, enabling the sliding model. However, when stiction occurs, the stick is set to 1 and slide is 0, that is $S=1$ and $R=0$, Q is set to 1 and $\bar{Q} = 0$, that is the stiction model is enabled, and the sliding model is disabled. When neither of the inputs are 1, Q and \bar{Q} remember their previous value, Q_{prev} and \bar{Q}_{prev} , respectively. Asserting both inputs means that the latch should be set and reset at the same time, which is impossible. The circuit responds by making both outputs 0 (Harris & Harris, 2012).

Considering the above explanation, inside the sliding and stiction model subsystems, there is the modelling of the vertical GRF (Eq. 5.28), stiction or sliding vertical GRF from Figure 5.21, as well as, the respective horizontal GRF, sliding (Eq. 5.29) or stiction (Eq. 5.30) horizontal GRF from the same figure. Besides, the conditions that enable the interchange between the two horizontal GRF, are also modelled. On one hand, the output of the stiction model named sliding, encodes the modelling of $F_{x,st} \geq \mu_{st} F_y$ and if this condition is met, a logic 1 is the output, which enters the friction switch and sliding changes to stiction. On the other hand, the output of the sliding model named stiction, encodes the following expression: $|\dot{x}_{CP}| < v_{lim}$, that is, if this condition is met, the output is a logic 1 and stiction changes to sliding.

This modelling type is similar to the one from Figure 5.13, in which the equations mentioned above are implemented by means of constant, sum and other blocks.

5.5. Optimization

An optimization problem has the form of (Boyd & Vandenberghe, 2004):

$$\begin{aligned} & \text{minimize } f_0(x) \\ & \text{subject to } f_i(x) \leq b_i, i = 1, \dots, m \end{aligned} \tag{5.32}$$

In Eq. 5.32, x is the optimization variable of the problem and $f_0(x)$ is the objective function, that is, the function desired to be optimized. The functions $f_i(x)$ set constraints to the objective function with limits b_i , $i=1, \dots, m$. A vector x^* is called optimal or a solution of the optimization problem 5.32, if it exhibits the minimum objective value amongst all the other vectors that satisfy the constraints of the optimization problem. Equation 5.32 represents the problem of making the best possible choice of a vector, with a minimum cost, from a set of candidate choices, all of them fulfilling the constraints employed (Boyd & Vandenberghe, 2004).

Mathematical optimization is used in many applications, such as civil, chemical, mechanical and aerospace engineering. In most of them, this tool is used as an aid to decision making (Boyd & Vandenberghe, 2004), in a sense that, since there are too many variables that make the system work, it is desirable to look for the best set of those variables that fulfil Eq. 5.32 in order to obtain the best performance of the system.

Essentially, it was determined that, to produce a natural walking gait (kinetics and kinematics), the biomechanical model would be required to travel the maximum distance possible without falling, while spending the minimum amount of energy. Since the variables needed for the optimization problem are acquired through the calculation of equations, their Simulink implementation is similar to the one in Figure 5.13.

The Optimization layer or module includes the calculation of all the variables that take part in the optimization problem. Since this part was developed within the aim of this dissertation, it will be further explained in the following chapter (section 6.1).

5.6. Summary and Discussion

This chapter encloses a detailed description of the biomechanical model used throughout this work. Accompanying the explanation of its implementation in Simulink from MATLAB R2017b (MathWorks), a description the physical laws that support its construction, is given.

The biomechanical model used in this dissertation has its roots on the one developed by Geyer & Herr (2010). The model is implemented in Simulink, comprising four layers or modules that, interrelating, describe its overall motion and behaviour. The first layer being described is the Body Mechanics, which comprises the implementation of the general form of the model, regarding the definition of its segments and joints. Within this layer, segments' lengths, masses and moments of inertia are defined. Besides this definition, the assembly of all the segments and joints enable the construction of the general geometric form of the biomechanical model.

Following the Body Mechanics, the Muscle Actuation layer is approached. Its description comprises the explanation of the fundamental laws used to model the muscle-tendon unit's dynamics. The muscle model used is based on the Hill muscle model and includes four elements, namely a contractile element (CE), a series elasticity element (SE), a buffer elasticity element (BE) and a parallel elasticity element (PE). These elements are arranged and modelled in such a manner that their interaction mimics the constitution and behaviour of the skeletal muscle throughout human movement.

The Neural Control layer must calculate the muscular stimulations needed to make the biomechanical model produce a natural walking gait. By giving the stimulations necessary to the muscle, the muscle activations are calculated, and the dynamics of the muscle model can be resolved. Besides this function, this layer also enables the implementation of the joint's soft limits, preventing abnormal movement during gait or during the any other movement performed by the biomechanical model.

Finally, the optimization layer is briefly described since the main core of that part is presented in the following chapter. Essentially, this layer comprises the calculation of all the variables needed for the optimization problem implemented.

If no optimization is needed, meaning that the model is performing a natural walking gait or other desired movement, this layer does not intervene in the model's behaviour. In this case, the interaction between the other three layers enable the production of the desired movement.

Besides the layers that comprise the neuromuscular model, the model of the interaction with the ground is explained. Essentially this model describes the ground as two basic material properties: stiffness and relaxation speed. The definition of the vertical and horizontal ground reaction forces depends on those properties.

6. IMPLEMENTATION AND VALIDATION

In the present chapter, the processes involved in the implementation and validation of the biomechanical model utilized throughout the development of this dissertation are described in detail. Firstly, the model had to undergo two strategies in order to prepare it for simulation regarding healthy and pathological gait. These strategies consisted in the development and resolution of an optimization problem using MATLAB's genetic algorithm, as well as the determination of which Simulink solver to use.

After the preparation of the biomechanical model, the study of the kinetic (joint torques and vertical ground reaction force), kinematic (joint angles) and muscular activation data for both the healthy and pathological (anterior cruciate ligament injury after surgical repair and rehabilitation procedures) biomechanical models are analysed and commented. A brief summary and discussion is provided in the last section of this chapter.

6.1. Model Preparation

In this section, the preparation of the biomechanical model is described. The optimization problem implemented is defined in detail, including all the restrictions made to the model in order to make the optimization converge into a natural gait (with physiological kinetics and kinematics) solution. After obtaining a model with walking characteristics as desired, the determination of which solver to be used in the following simulations is done.

6.1.1. Optimization Problem

The main core of this section deals with the optimization problem implemented so that the biomechanical model would present a physiological walking gait, considering its kinematics and kinetics.

Using the model for the first time, it was discovered that, with the conditions it was set with, it would not perform more than two steps without falling. Investigation was done in order to understand why this was occurring and, from analysing Thatte & Geyer (2016), and the model from Geyer's website, it was determined that a set of 23 input parameters, called "Gains", as they were established, might not be the optimal set to produce a natural walking gait. Considering this conclusion, there is the need for optimization in order to look for a set of these parameters that enable the biomechanical model to produce a gait that appear natural, which means that it produces physiological human kinematics and kinetics.

Regarding the explanation provided in section 5.5, and following the same logic as Thatte & Geyer (2016), 23 parameters were subject to optimization, including reflex feedback gains and swing leg control parameters. Some of these parameters were the MTU gains (see Eq. 5.22). In Geyer's folder containing the biomechanical model, the gains subject to optimization were calculated as:

$$G = \text{InitialGuess}^{\text{OptmExp}} \quad (6.1)$$

InitialGuess is a 23x1 matrix containing previously defined values (obtained from the model downloaded from Geyer's website), probably obtained from literature or his experiments. The optimization variable is OptmExp, that is, the exponents of the initial guess. A possible explanation to the fact that what is being optimized are the exponents of the gains and not the gains themselves, is that optimizing the exponents might make the optimization procedure converge quicker.

Thatte & Geyer (2016), relied on the Covariance Matrix Adaptation Evolution Strategy (CMAES) as their optimization function. However, in this dissertation the Genetic Algorithm was used instead of CMAES, since it was better understood. A genetic algorithm (GA) is a method for solving both constrained and unconstrained optimization problems based on a natural selection process that mimics biological

evolution. A GA optimization problem is composed by individuals, which compose a population. An individual is any point to which the objective function is applied to. In this case, an individual of this optimization problem is one biomechanical model. To further define GA, the number of generations is required to be set. After GA goes through the current set of individuals that compose the population and applying to it the objective function, it produces a new population with different characteristics from the previous one. Each consecutive new set of individuals, or each new population, is called a new generation (MathWorks, 2017b, 2018a).

The algorithm initiates the simulation by creating a random set of individuals, a population, by default. However, if it is desirable to set initial conditions for the optimization variable of the individuals of the population, this is also doable. Along the optimization process, the algorithm repeatedly modifies the population. At each iteration, the GA selects the best individuals from the current population, which approach an optimal solution, and uses them as parents to produce the children for the next generation. In order to create a new generation, GA scores each member of the current population by computing its objective function value. Members of the population that have the lowest value of the objective function are chosen over the others, since the goal is to minimize the objective function (see section 5.5). These members are called elite children. The characteristics of the other individuals (parents) that have lower values of the objective function, but are not the lowest values, are passed on to the subsequent generations (children), either by making random changes to a single parent (mutation) or by combining a pair of parents (crossover). Figure 6.1 illustrates these three cases. GA replaces the current population with the children to form the next generation. Over successive generations, the population converges towards an optimal solution and the algorithm stops when stopping criteria is met (MathWorks, 2018b). Stopping criteria is addressed the following paragraphs.

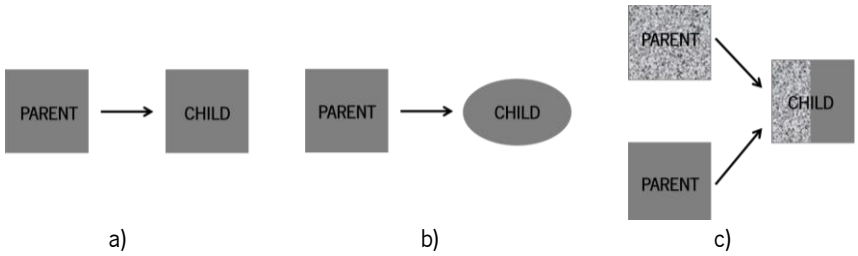


Figure 6.1 - Types of children formation in the genetic algorithm. a) Elite child. b) Mutation child. c) Crossover child (adapted from MathWorks (2018b)).

GA repeatedly runs a Simulink® simulation of the biomechanical model towards optimizing a determined cost function. It is possible to define some options for this algorithm, and the ones chosen in this problem were:

- `opts.MaxGenerations = 60`: number of iterations;
- `opts.PopulationSize = 200`: size of the population;
- `opts.InitialPopulationMatrix = repmat(p0,[20 1])`: this option enables to set the initial conditions, p_0 , of the population. p_0 was set to encompass 20 of the 200 bipeds used in the simulation. `repmat` repeats copies of p_0 matrix;
- `opts.PlotFcn = @gaplotbestf`: adds progress plot of objective function, as a function of the number of generations and the value of the cost function.

The maximum number of generations is the number of iterations the simulation will perform. Within each generation, 200 models (population size) are simulated. This means that, ultimately, a simulation with 60 generations and 200 iterations, would simulate 12000 models. These two options act as stopping criteria, that is, when the simulation performs 200 iterations with 60 models, the optimization stops.

In this optimization problem, it was chosen to set the parameters of some individuals of the initial population to a predetermined value, as seen in the option `opts.InitialPopulationMatrix`. This option creates a 20x1 matrix with each line containing the vector p_0 , which is a 1x23 vector containing all zeros. It has 23 columns since that is the number of optimization variables. This initial matrix sets 20 models to those initial conditions.

The optimization strategy is composed by two parts: one in which the model is rewarded and one in which the model is penalized. In the first part, the further the biomechanical model walks, within the finite simulation time, without falling, the more rewarded it gets. To implement this first part in the Simulink®, a To Workspace block was used to send to MATLAB®'s workspace the forward position travelled by the HAT, x_{HAT} , which would then be used in the created MATLAB® script for the optimization problem. Since x_{HAT} is a matrix containing all the positions of the HAT throughout the simulation time, time step by time step, in the MATLAB® script created only the last value of this matrix was chosen. This is the value that effectively indicates the maximum travelled position by the HAT.

The second part, uses the same strategy as Thatte & Geyer (2016), in which gaits with the minimum metabolic energy consumption are preferred over others in which energy consumption is higher. The optimization criterion is the metabolic cost of transport, which is generally expressed as the amount of energy spent to transport 1 kg of body mass over a distance of 1 meter (Cher, Stewart, et al., 2015; Lazzar, Taboga, et al., 2014). In this work, the calculation of the metabolic cost of transport is based on the work of Thatte & Geyer (2016), which can be evaluated as:

$$\text{Metabolic Cost of Transport} = \frac{W_m}{mgx} + \frac{1}{mgx} \int (c_1 \tau_{\text{cmd}}^2 + c_2 \tau_{\text{limit}}^2) dt \quad (6.2)$$

where, W_m accounts for the metabolic energy consumption of the biomechanical model muscles', τ_{cmd} is sum of the torques commanded by the neuromuscular swing control, τ_{limit} is the sum of torques produced by the model's mechanical hard stops, which prevent knee and ankle hyperextension, m is the mass of the model, g is the gravitational acceleration and x is the distance travelled over the simulation time. c_1 and c_2 ensure that the terms of the function have similar order of magnitude (Thatte & Geyer, 2016). W_m is the sum of the total rate of energy expenditure of each 14 MTUs, based on the work of Umberger, Gerritsen, et al. (2003). It is expressed in Watts per kilogram of muscle tissue (W/kg).

Assembling these two parts, the optimization objective function is as follows:

$$\text{Objective Function} = - \frac{x_{\text{HAT}}}{\text{Metabolic Cost of Transport}} \quad (6.3)$$

GA and the optimization strategies in general try to minimize the optimization objective function. However, it is desirable to maximize the implemented function, since it is required the higher distance travelled by the model, x_{HAT} , with the lower energy consumption, Metabolic Cost of Transport. Due to this fact, a minus sign appears in Eq. 6.3.

Besides the definition of the objective function and initial conditions in the MATLAB® script, in Simulink®, constraints were implemented to make the optimization problem converge quicker. These constraints serve as guides to the GA, making the simulation stop and acting as stopping criteria. By running into these constraints, GA is “informed” that that is not the way to go and changes the population, in the next generation, in order not to run into those constraints again. This helps the user guide the simulation to make it converge into a desired optimal solution. By placing these constraints, it is expected that the optimization algorithm converges into physiologically acceptable solutions. STOP blocks were used to model these constraints, meaning that if the model ran into at least one of these conditions, the simulation would immediately stop. These conditions were (it is important to refer that the xyz axis referred in these constraints follow the orientation of the world frame, Figure 5.5a):

- a) If the z position of the knee would fall below the z position of the ground;
- b) If the z position of the knee would be higher than the z position of the hip;
- c) If the model would walk for more than 100 meters in the x direction. This constraint was implemented in order to prevent additional computational cost;

- d) If the z position of the HAT's COM would be higher than the sum of the thickness of the foot, lengths of the shank and thigh and half the length of the HAT. If this condition would not be satisfied, this would mean that the model would be off the ground.
- e) If the z position of the HAT's centre of gravity would fall below the z position of the ground.

Figure 6.2 illustrates the constraints implemented.

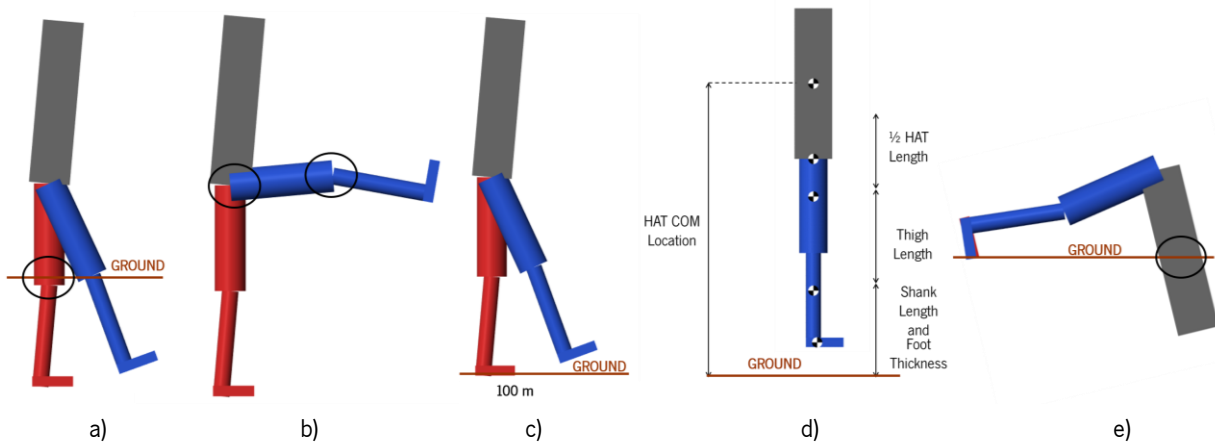


Figure 6.2 - Restrictions implemented in Simulink® to perform optimization. a), b), c) d) and e) refer to the bullet points above.

The simulation ran for 60 generations, with a population of 200 models, in flat ground and with a time step of 1 ms. This strategy was performed three times. In the first optimization problem, the initial set of optimization variables used were a 23x1 matrix containing all zeros, as already explained. After terminating the first simulation, the best set of optimization variables obtained was used as input to the second optimization simulation, that is, these variables were introduced in the initial population of the second optimization. This was performed in the third simulation as well. The fact of introducing the best set of optimization variables in the following optimization, guides the GA, giving to it clues about what it should follow to obtain the best values for the optimization variables, following the constraints and objective function determined. This strategy resulted in the final, best set of optimization parameters that were used as input to the healthy biomechanical model.

6.1.2. Solver Determination

The simulation of a dynamic system is done by computing its states at successive time steps (time intervals over which the computation occurs) over a specified time span. The size of these time steps is called the step size. The process of computing the states of a model in this manner is known as solving the model. Simulink® provides a set of programs, called solvers, each one embodying a particular

approach to solving the developed model. A solver applies a numerical method to solve the set of ordinary differential equations that represent the model. Solvers are classified considering the type of step size used in the computation as fixed step and variable step solvers. A fixed step solver does not alter its step size throughout simulation, being always constant. Depending on the simulation conditions (changing rate of the model's variables), a variable step solver might alter its step size in order to increase accuracy in quickly changing events (smaller step size) and to avoid taking too many steps if the model's variables are very stable (bigger step size) (MathWorks, 2017a).

To determine which solver to use, a choosing criterion was used: the faster the solver computes the biomechanical model simulation without losing accuracy in the produced results, the better. To determine this, four 20-second simulations were performed with four variable step solvers. Variable step solvers were chosen over the fixed step ones, since the biomechanical model, coming from Geyer website, was previously set with Ode15s, a variable-step solver, and because the model possesses parameters with variable changing rates throughout simulation.

These solvers have the particularity of dynamically adjusting their step size throughout simulation, that is, during the model's simulation, there might be events in which the model is very stable and does not vary much, and so the solver applies a bigger step size to avoid taking unnecessary steps. However, there might be other events in which a smaller step size must be applied, since the model varies a lot. This behaviour improves accuracy but, on one hand, it can sometimes lead to excessive simulation times, since computing the step size in a variable step solver adds to the computational overhead at each step. However, on the other hand, other times it can reduce the total number of time steps, and hence the simulation time (MathWorks, 2017a).

Besides the fact that Hartmut Geyer used Ode15s, other explanation for the use of this solver exists. The fact that the model possesses occurrences that might need a smaller step size (such as the contact between the foot and the ground where the ground contact model variables change rapidly) and others where a bigger step size is needed (such as when the leg is in swing and the same variables are very stable), this type of solver is useful in the model's simulation, since it might help reduce the simulation time by spending more time in events that need to be more accurately resolved, and less time in events in which the model is stable and varies very little. If a fixed step solver was used, the time required to resolve events where the model would vary very quickly and not would be the same, and therefore, one of the following would occur. Either the total simulation time would be too great due to the use of a fixed small step size not to lose accuracy in the events quickly varying, or the simulation time would be little,

due to the use of a bigger step size and, probably, result's accuracy would be lower. The use of a variable step solver enables to adjust the time step to be used, according to the events occurring during the simulation of the biomechanical model.

The obtained elapsed time of a 20-seconds simulation for the four variable step solvers tested is presented in Table 6.1. Even though the simulation time is set to 20 seconds, according to the type of solver used, the real time that the solver requires to perform that simulation is different due to the method used to compute the simulation.

Table 6.1 – Solver, respective elapsed time and method used by Simulink® to resolve the model's dynamics

Solver Name	Elapsed Time (s)	Method
Ode15s	552.202124	Numerical Differentiation Formulas
Ode23s	-	Second-order, modified Rosenbrock formula
Ode23t	562.655769	Trapezoidal rule
Ode23tb	637.602866	Trapezoidal rule plus backward differentiation formula

As seen in Table 6.1, the solver that performs the 20-seconds simulation faster is Ode15s. For the Ode23s, the elapsed time is not shown since the simulation was taking much longer than any of the other tested solvers and was stopped before it was terminated.

In order to determine if accuracy is lost over speed, the results of the three remaining solvers (Ode15s, Ode23t and Ode23s) were evaluated. To do so, the overall centre of mass motion of the biomechanical model in the sagittal plane was compared. The motion in analysis is the overall distance travelled by the model's centre of mass (COM) in the x, forward position, and y, vertical position, axes (similar to the motion presented in Figure 5.3) during the simulation time.

The COM is the point where the whole system's mass is assumed to be concentrated. As seen in Figure 6.3, if two objects with masses m_1 and m_2 are separated by distances x_1 and x_2 , the system's overall centre of mass, x_{cm} , can be evaluated as:

$$x_{cm} = \frac{m_1 x_1 + m_2 x_2}{m_1 + m_2} \quad (6.4)$$

If, instead of having only two objects, the system is composed by n objects, its overall centre of mass can be computed using the following equation:

$$x_{cm} = \frac{m_1 x_1 + m_2 x_2 + \dots + m_n x_n}{m_1 + m_2 + \dots + m_n} = \frac{\sum_{i=1}^n x_i m_i}{\sum_{i=1}^n m_i} \quad (6.5)$$

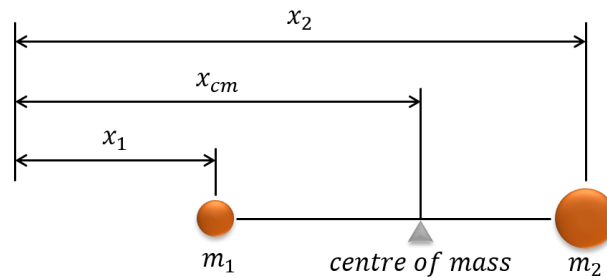


Figure 6.3 - Illustration of the COM between two objects with different masses, m_1 and m_2 , separated by distances x_1 and x_2 .

Equation 6.5 was used to calculate the overall COM of the biomechanical model, including the masses (see Table 5.1) and positions of the Head Arms and Trunk (HAT), both thighs, shanks and feet throughout the simulation. Figure 6.4 shows the plots of the overall forward and vertical COM position of the biomechanical model with the curves obtained for the three solvers superimposed.

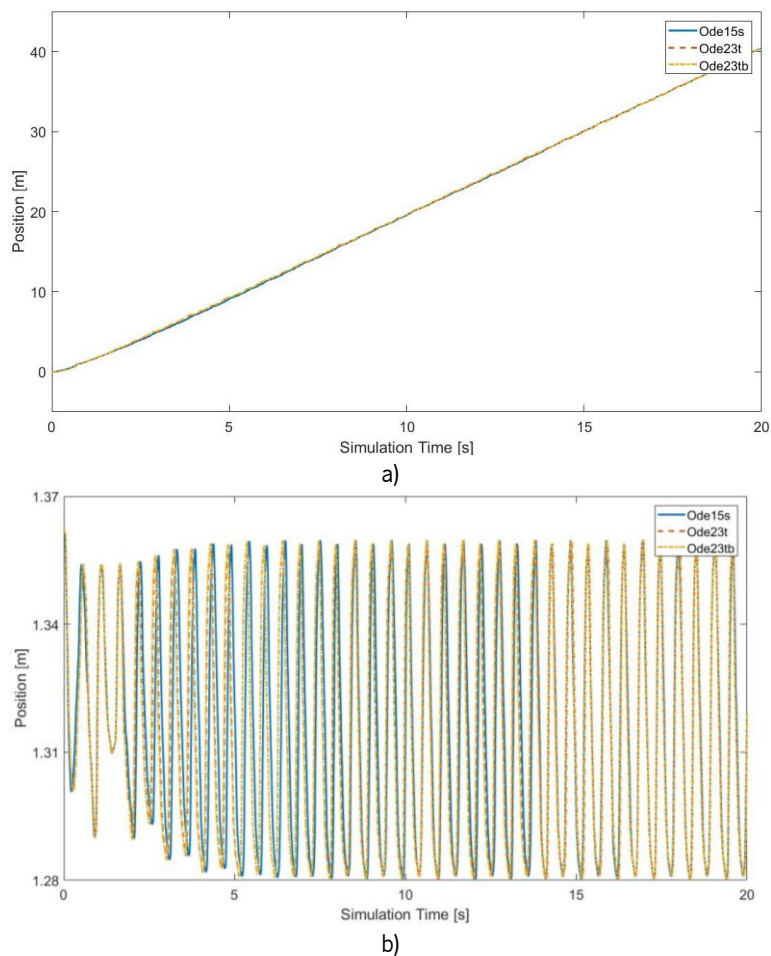


Figure 6.4 – Position of the overall centre of mass of the biomechanical model. Three tested solvers are displayed. a) Forward position and b) vertical position of the overall COM.

Observing Figure 6.4, no significant differences are encountered between the results given by all solvers. The overall shape of the graphs and the amplitude of the forward and vertical positions look very similar. This means that all together the models are walking throughout all the simulation time and producing a gait pattern similar considering each solver used.

In order to analytically determine whether there are significant differences between these three solvers, the error percentage between them was calculated as:

$$\% \text{ Error} = \left| \frac{\text{Experimental Value} - \text{Theoretical Value}}{\text{Theoretical Value}} \right| \times 100 \quad (6.6)$$

Ode15s was set to be the theoretical value, since it was previously predefined in the Simulink® code developed by Hartmut Geyer and because it is the faster solver (see Table 6.1). This way, Ode15s was compared to Ode23t and Ode23tb to determine whether the speed of the simulation would compromise or not the accuracy of the produced results. Table 6.2 comprises the percentage of error, which is the average error between the two solvers in comparison.

Table 6.2 - Error percentage between the assumed theoretical value, Ode15s, and the experimental values, Ode23t and Ode23tb, for forward and vertical COM position

Forward COM Position		Vertical COM Position	
Ode15s	0.1753 %	Ode15s	0.0508 %
Ode23t		Ode23t	
Ode15s	0.3788 %	Ode15s	0.0450 %
Ode23tb		Ode23tb	

Observing Table 6.2, it is clear that the errors between Ode15s and the other two solvers are very low, being much inferior than 5% (which is the error above which it was considered that accuracy would be compromised), both in the forward and vertical COM positions. Considering this statement, it is possible to use Ode15s in the biomechanical model's simulations. This way, a faster solver is used, without losing accuracy in the results produced by the simulation.

6.2. Healthy Model

After optimizing the model's walking gait and determining which solver to be used in the simulation, the biomechanical model's kinematic (joint angles) and kinetic (ground reaction forces and joint torques) data were obtained. This data is compared to outcomes present in literature. Until this point, no pathology

is applied, so the model is considered as a healthy one. After exposing the model's dynamics, a sensitivity analysis is performed, followed by a more detailed study of the influence of the ground contact model stiffness, k_v , in the vertical ground reaction force. The muscular activation patterns are also displayed.

6.2.1. Kinetic and Kinematic Outcomes

In this section the results obtained by the simulation of the biomechanical model are presented and differences between them and literature are stated. The discussion of the results and explanation of the cause of some disparities that might occur are presented throughout the chapter.

The kinetic and kinematic results were obtained from a 60-second simulation with a time step of 1ms, in which the model walked for 100 meters. As previously mentioned and as seen in Figure 5.8b, the model starts the walking gait with its left leg in stance and its right leg in swing, at an initial walking speed of $v_{x0}=1.3$ m/s. The results of the model's simulation pertain only to the left leg, being the right leg results' equal.

During gait, forces are applied under the surface of the foot every time a step is taken. The forces applied to the ground by the foot are called foot forces and, on the contrary, forces with the same magnitude but opposite direction are the ones applied to the foot by the ground, which are called ground reaction forces (GRF). There are three components of these forces: vertical, anterior-posterior and medial-lateral (Neumann, 2013). Since the biomechanical model used in this work performs movement only in the sagittal plane and considering the previously explained ground contact model (see chapter 5, section 5.4), only the vertical and anterior-posterior GRF exist. However, in this dissertation only the vertical component was analysed.

Since the magnitude of the GRF are highly dependent on body weight (BW), in order to make them comparable to other literature findings, the results presented in this dissertation are normalized to percentage of body weight (%BW). The obtained vertical ground reaction forces of both legs of the biomechanical model somewhat resembles the M-shape pattern characteristic for walking gaits (Figure 6.5), indicating some similarity of whole-body dynamics of model and humans for steady state walking.

The vertical GRF curve is typically split into two halves, with a maximum in each, as seen in Figure 6.5a. Figure 6.5b represents the GRF obtained by the model's simulation and it is observable that, before reaching the first maximum, another peak appears with a magnitude of 150% BW. It seems that the contact point located in the heel (which is the first touching the ground due to the occurrence of the heel strike in the beginning of the gait cycle) initially impacts the ground with a force of approximately 150%

BW, decreasing to around 50% BW and then increasing to 200% BW. These results were not expected, since, usually, the vertical GRF curve tends to go directly from zero to the first maximum (Figure 6.5a), and this is not observable in Figure 6.5b.

Besides this extra peak, the biomechanical model results' show some smaller oscillations at approximately 20% BW and 2% of gait cycle, before increasing to this extra peak. Observing Figure 6.5a, these were also not expected, since in normal walking, the foot effectively impacts the ground without occurring any oscillations like the ones presented in the biomechanical model's results.

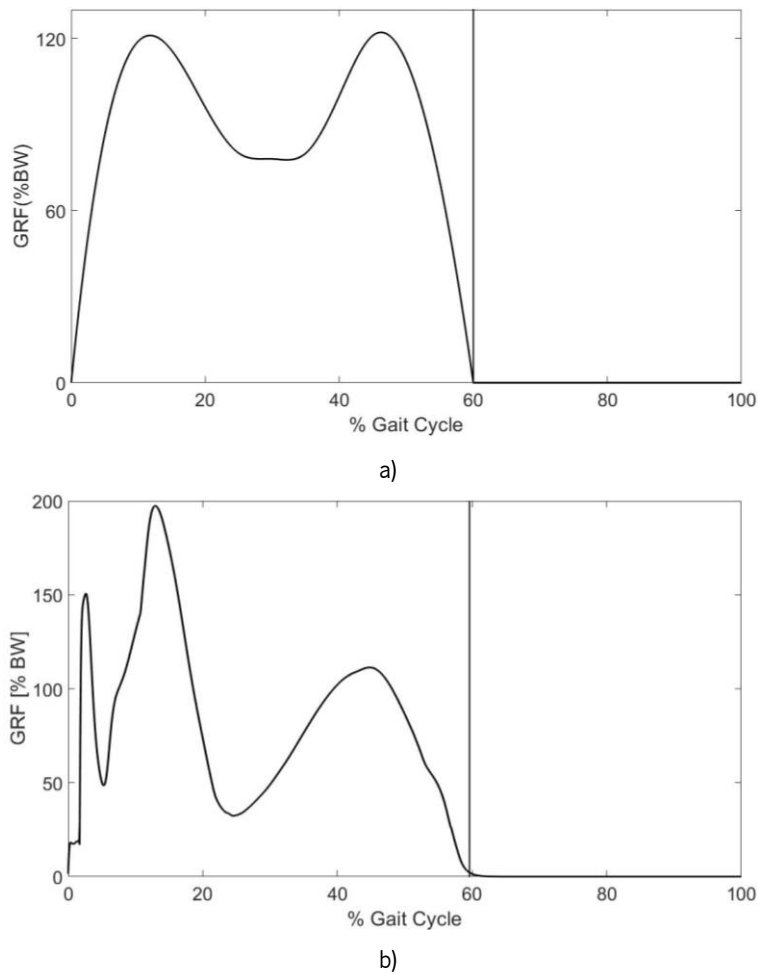


Figure 6.5 – Vertical Ground Reaction Force normalized to percentage of body weight for walking movement. These graphs are normalized to percentage of gait cycle. The black vertical line marks the occurrence of toe off. a) Literature results obtained from Neumann (2013). Toe off occurs at 60.0% of gait cycle. b) Biomechanical model's results (30Hz low-pass filtered). Toe off occurs at 59.6% of gait cycle. In this figure, it is displayed the mean \pm standard deviation.

In normal walking conditions, the first peak that occurs on the GRF curve determines the end of the loading response phase (characterized by the occurrence of heel strike) and initializes the midstance phase until a minimum on the GRF curve occurs, around 80% BW. The magnitude of this first maximum,

should be around 120% of body weight (Neumann, 2013) (Figure 6.5a). However, it is 200% BW in the model's results, which is higher than expected for human walking gait. Besides these discrepancies, the minimum that occurs between the two maximum peaks, should occur at approximately 30% of gait cycle with a magnitude of around 80% BW. However, the model's results differ from these standard values. The minimum occurs at approximately 25% of gait cycle, with a magnitude of about 45% BW.

When the midstance phase ends and the terminal stance phase begins, the model's GRF curve converges into another maximum around 110% BW (Figure 6.5b) and initializes the pre-swing phase, which ends with the occurrence of the toe off. This second peak occurs since there is contact between the toes and the ground. In the case of the biomechanical model, the contact point located in the front part of the foot, named ball CP, is in contact with the ground. The magnitude of this second maximum in the model is within the expected value for healthy human walking gait, which would be around 120% BW (Neumann, 2013) (Figure 6.5a). After this second maximum, at 60% of gait cycle, since toe off occurs and the foot is off the ground, there is no more contact between the foot and the ground, there is no vertical ground reaction force and, therefore, its value during the rest of gait cycle, which is the swing phase, is zero.

The two types of abnormal oscillations present in the biomechanical model's vertical GRF curve might arise due to some unappropriated detection of contact between the CP and the ground by the ground contact model. As previously explained in chapter 5, section 5.4, the detection of contact occurs when the CP position falls below a determined reference value, y_0 . What might be occurring in the first situation (oscillations at around 2% of gait cycle) is that the position of the CP located at the heel might be quickly oscillating in turn of this reference point before in fact impacting the ground. The second situation might be something similar, however contact is detected with a higher %BW between the occurrence of the two peaks (extra peak of 150% BW and first peak of 200% BW), with a decrease between these two occurrences. It seems that the contact point located in the heel (which is the first touching the ground due to the occurrence of the heel strike) initially impacts the ground with a force of approximately 150% BW, decreasing to around 50% BW and then increasing to 200% BW. These results were not expected, since, usually, the vertical GRF curve tends to go directly from zero to the first maximum (Figure 6.5a), and this is not observable in Figure 6.5b. These oscillations that occur until the curve reaches its maximum peak at 200% BW all together represent the impact of the foot on the ground, more specifically the occurrence of the heel strike gait event.

This initial part (until approximately 30% of gait cycle) of the model's GRF curve is somewhat far from what was expected for human walking gait. As above explained, this might be due to the type of ground contact model used to model the contact between the model's CP located on the foot and the ground. There are some options to try and make the model's GRF graph more similar to the literature one. One strategy would be to alter the contact model, including the alteration of the vertical ground reaction force laws (Eqs. 5.25 to 5.28) and/or the alteration of the way contact is detected to a more consistent manner. For instance, include a condition which states that if the CP's position falls below the reference value, it cannot be above that value for the rest of that current stance phase of gait. This would prevent the initial oscillations from occurring at 2% of gait cycle. Another strategy would be to include more contact points along the foot of the biomechanical model since the contact point throughout gait is not always the same in reality. However, in this biomechanical model, the existing contact points are fixed in the same position throughout simulation.

Kinematics is the branch of dynamics in which the motion of a system is studied independently of the external forces that produce it. A kinematic analysis involves the study of the position, velocity and acceleration of every element of the system (Tavares da Silva, 2003). In this chapter, the kinematic variables used to study the motion of the biomechanical model are its joints' position throughout gait, which, since they are designed as revolute joints, essentially are the joints' angles.

According to the Standardization and Terminology Committee (STC) of the International Society of Biomechanics (ISB), joint kinematics reporting is specific for different joints (Wu, Siegler, et al., 2002). For the hip joint, extension is negative, and flexion is considered positive (Neumann, 2013). For the knee joint, flexion is considered positive and extension, negative (Grood & Suntay, 1983). Finally, for the ankle joint, dorsi- and plantar flexion are defined as being positive and negative, respectively, (Wu, Siegler, et al., 2002). This convention was used to report the kinematic results of the biomechanical model utilized in this work.

In Figure 6.6 it is represented both the literature and the biomechanical model's hip joint angle, θ_H , normalized to percentage of gait cycle. In the beginning of the gait cycle there is an increased flexion in the model's results when comparing with results from Neumann (2013). Literature states a hip flexion angle of about 30 degrees at about 4% of gait cycle and the model's results show an approximately 40 degrees of flexion, occurring a little later in the gait cycle, at more or less 10%. The minimum of the hip angle curve, representing the extension phase, occurs a bit above 50% for the biomechanical model's results and at 50% in the literature, and its magnitude is around 10 degrees higher in the model's results.

Contrary to these findings, on the last part of gait cycle (from 80% of gait cycle on and comprising the last hip flexion) the biomechanical model tends to stabilize its hip angle at 30 degrees, however in literature at more or less 85% of gait cycle, the hip angle reaches another maximum of about 35 degrees and then decreases until 30 degrees, in the end of gait cycle.

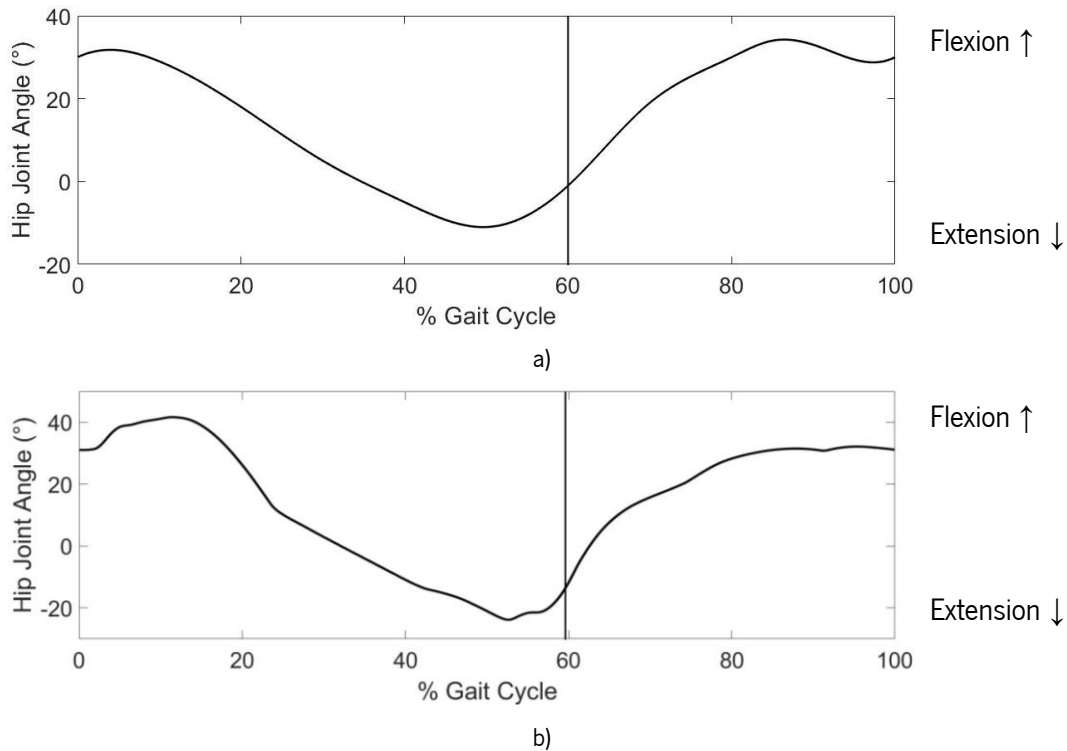


Figure 6.6 – Hip joint angle, θ_H , for walking movement. These graphs are normalized to percentage of gait cycle. The black vertical line marks the occurrence of toe off. a) Literature results obtained from Neumann (2013). Toe off occurs at 60.0% of gait cycle. b) Biomechanical model's results. Toe off occurs at 59.6% of gait cycle. In this figure, it is displayed the mean \pm standard deviation.

Figure 6.7 represents the knee angle, θ_K , throughout gait for literature (Figure 6.7a) and biomechanical model's results (Figure 6.7b). Concerning the knee angle of the biomechanical model, the flexion in the beginning of the gait cycle has a higher magnitude than expected when comparing these results with literature. The magnitude of this flexion peak in the biomechanical model's results and in literature findings is approximately 30 and 20 degrees, respectively. This implies that a higher initial knee flexion is occurring in the model's gait. After this initial phase, the knee begins its extension phase, which, according to literature, should end at about 40% of gait cycle, starting right away the following flexion phase. However, in the model's results the flexion phase ends at around 25% of gait cycle and then the magnitude of the angle stabilizes in the same value (around 2 degrees) until 40% of gait cycle, when there

is the beginning of the second flexion phase. Besides this discrepancy, the maximum extension angle's magnitude is similar in both findings (approximately 60 and 55 degrees for literature and the model).

As in the initial flexion phase, the magnitude of the peak representing the second flexion is different between literature and the model's results. In literature it is stated that in normal human walking, the second flexion phase should occur at around 75% of gait cycle, with a magnitude of 60 degrees. The biomechanical model produces a higher flexion than what was expected, with a magnitude of 55 degrees and at 54% of gait cycle, which is earlier than stated literature. For the rest of gait cycle, the results are similar, with the knee extending towards the following gait cycle, which starts with the heel strike.

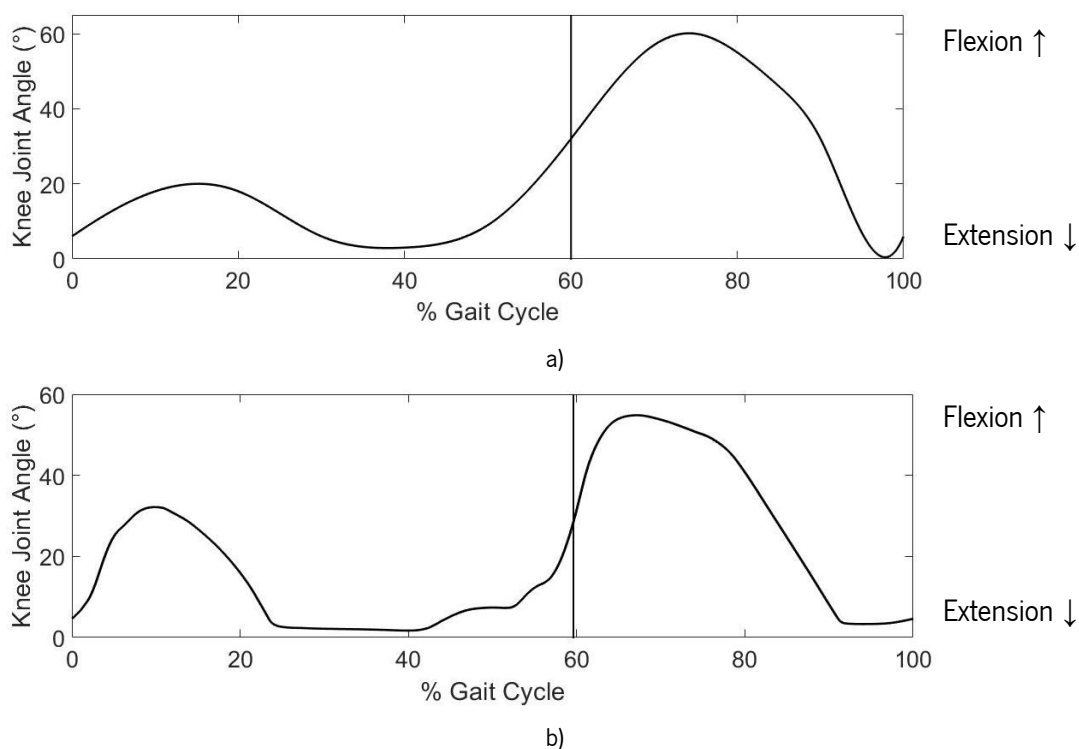


Figure 6.7 – Knee joint angle, θ_k , for walking movement. These graphs are normalized to percentage of gait cycle. The black vertical line marks the occurrence of toe off. a) Literature results obtained from Neumann (2013). Toe off occurs at 60.0% of gait cycle. b) Biomechanical model's results. Toe off occurs at 59.6% of gait cycle. In this figure, it is displayed the mean \pm standard deviation.

The last kinematic variable being analysed is the ankle angle, θ_a , presented in Figure 6.8. Once again, literature findings from Neumann (2013) (Figure 6.8a) are compared to those obtained from the biomechanical model's simulation (Figure 6.8b). Observing Figure 6.8b, it is clearly seen that the model's ankle angle throughout gait shows the two characteristic loading and unloading phases that occur in human walking gait (Figure 6.8a). These phases are represented by the two negative peaks seen in the graph, being the first and second peaks, the loading and unloading phases, respectively. In literature, the

loading phase is characterized by a magnitude of -10 degrees, occurring at approximately 5% of gait cycle. In the biomechanical model's results, this phase is increased and anticipated, occurring at 2% of gait cycle, with a magnitude of -17 degrees. This means that the biomechanical model starts its gait cycle with an increased plantarflexion, occurring earlier than expected, when compared to literature findings.

When the loading phase ends, there is the beginning of the dorsiflexion of the ankle joint. This phase occurs between 10% and 50% of gait cycle, approximately, being a very smooth transition. However, in the model's results this transition from plantar- to dorsiflexion, occurs from 2% to 45% of gait cycle, presenting some oscillations. These might arise due to the interaction between the foot and the ground. Since it is defined as a spring and a damper model, the damper properties of the ground might be influencing the foot's behaviour when in contact, leading to these oscillations in the ankle joint kinematics.

In normal walking gait, before the occurrence of toe off, the ankle joint begins to plantarflex again, corresponding to the unloading phase, until a minimum is reached. The minimum peak occurring in this phase generally presents a magnitude of approximately -20 degrees at 65% of gait cycle. The biomechanical model's results are a little different from these literature findings. This peak occurs at 60% of gait cycle, with a magnitude of -18 degrees. After the unloading phase, the ankle angle increases again, meaning that the joint is dorsiflexing, in order to prepare the foot for the next gait cycle, which begins with the heel strike.

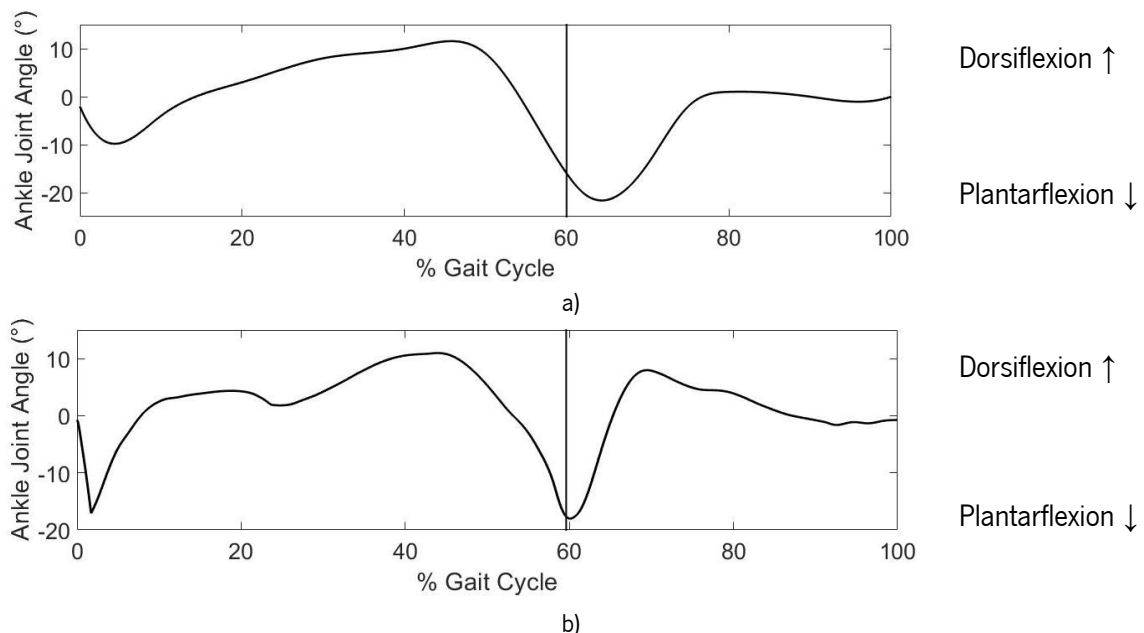


Figure 6.8 – Ankle joint angle, θ_A , for walking movement. These graphs are normalized to percentage of gait cycle. The black vertical line marks the occurrence of toe off. a) Literature results obtained from Neumann (2013). Toe off occurs at 60.0% of gait cycle. b) Biomechanical model's results. Toe off occurs at 59.6% of gait cycle. In this figure, it is displayed the mean \pm standard deviation.

Kinetics is the branch of mechanics dealing with the motion of a system, considering the forces that are acting on it. Throughout gait, the previously mentioned GRF that are applied to the foot by the ground, generate an external torque on the joints of the lower extremities, namely in the hip, knee and ankle joints. During early stance, the GRF produce external torques that lead to hip and knee flexion/extension and ankle plantar-/dorsiflexion. To prevent collapse of the lower limb, these external torques are resisted by internal torques created by the activation of the lower limb musculature (Neumann, 2013). In the following paragraphs, these internal joint torques produced by the joints of the lower limb are approached.

The convention used to report kinetic data in this work is the same as the one used by Neumann (2013). Hip and knee flexion torques are considered negative, whereas extension torque is positive. For the ankle joint, plantar- and dorsiflexion torques are considered positive and negative, respectively. Since Neumann (2013) had the internal joint torques normalized to body mass (Nm/kg), the biomechanical model's results were also normalized in this manner, in order to make the outcomes comparable.

Figure 6.9 illustrates the literature findings, as well as the biomechanical model's results for the hip joint internal torque. By the observing this figure, it is understandable that overall the internal hip joint torque stated in literature (Figure 6.9a) has a lower magnitude than the biomechanical model's results (Figure 6.9b). This conclusion is reached by looking at the y-axis of both graphs.

In literature, the maximum hip extension torque is about 1.2 Nm/kg, whilst the biomechanical model's results present a higher value, around 4.2 Nm/kg. This means that the model's hip joint produces a higher internal extension torque than what was expected for normal human walking gait. Besides these differences in magnitude, the state of gait in which these peaks occur differ. In the model's hip joint torque, the extension peak torque occurs at approximately 15% of gait cycle, which is a little latter than expected. Literature states that it should occur at 5%.

In literature, after generating this extension torque, the hip joint begins to produce a flexion torque. This is characterized by a minimum, observed in Figure 6.9a, at around 50% of gait cycle and with a magnitude of -0.5 Nm/kg. In the biomechanical model's results (Figure 6.9b) this minimum assumes a magnitude of -1.2 Nm/kg and occurs at approximately 43% of gait cycle. These results are a little different from one another.

However, from this point on, instead of directly producing the following extension torque (characterized by the increase in hip torque) as in literature, the biomechanical model's results oscillate. This occurs from the maximum hip flexion torque, at 43% of gait cycle, until a little after the heel strike, at approximately 61% of gait cycle. During this period, the hip torque increases a little, producing a small

extension torque, decreasing right after to produce a small flexion torque. Only after these oscillations, the hip joint torque increases to produce the final extension torque. In literature, this is characterized by a magnitude of 0.5 Nm/kg, occurring at 95% of gait cycle. Observing Figure 6.9b, the biomechanical model's results do not differ much from literature, with an extension torque of 0.7 Nm/kg, occurring at 93% of gait cycle.

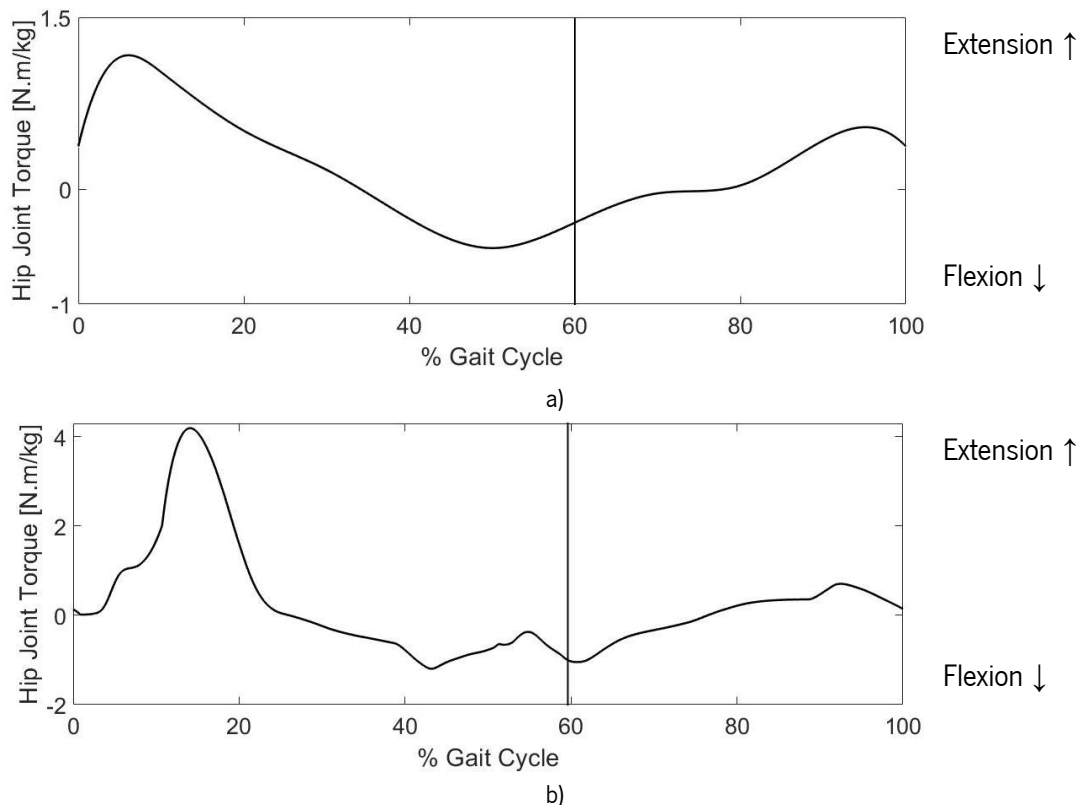


Figure 6.9 – Hip joint torque for walking movement. These graphs are normalized to percentage of gait cycle and to body mass. The black vertical line marks the occurrence of toe off. a) Literature results obtained from Neumann (2013). Toe off occurs at 60.0% of gait cycle. b) Biomechanical model's results. Toe off occurs at 59.6% of gait cycle. In this figure, it is displayed the mean \pm standard deviation.

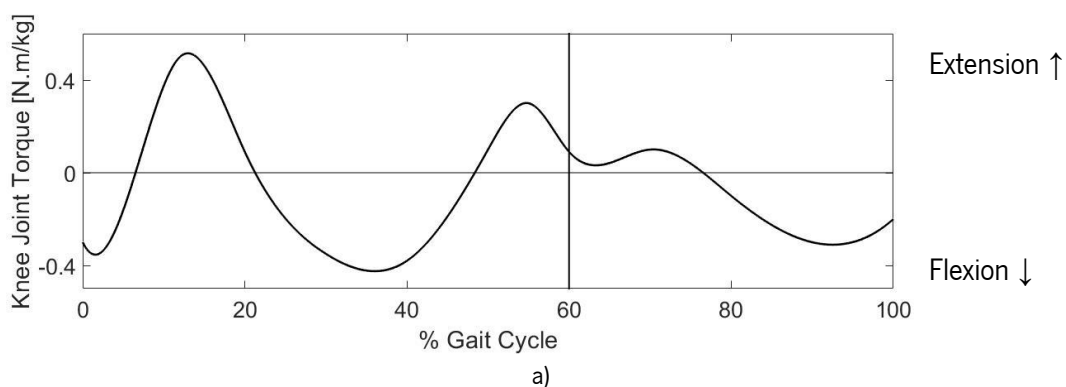
Figure 6.10 represents the internal knee joint torque normalized to body mass and to percentage of gait cycle. Overall, comparing literature results (Figure 6.10a) with the biomechanical model's results (Figure 6.10b), it is observable that they are very different, with the model's torque presenting much abrupt oscillations than the torque presented in literature, which exhibits a smoother variation. Besides this disparity, the maximum extension and flexion torque produced by the model are a little higher than what was expected, comparing to literature. This can be observed by the differences in the y-axis scale.

Comparing both graphs, it can be seen that the model's knee joint torque does not present the initial flexion torque, occurring between 0% and 2% of gait cycle in literature, with a magnitude of -0.5 Nm/kg.

Instead, it presents a slight extension torque occurring at 1% of gait cycle and with a magnitude of 0.2 Nm/kg. After this small extension torque, the model's results converge into a maximum extension torque, characteristic of the knee joint in this initial phase of stance. Literature states that this maximum torque should occur at 13% of gait cycle with a magnitude of 0.5 Nm/kg. Conversely, the biomechanical model's results present a maximum extension torque of 1.2 Nm/kg, occurring at 9% of gait cycle. The maximum knee extension torque occurs a little sooner than expected and with a higher magnitude.

The following knee flexion torque presents very different results when comparing the model with literature. Instead of presenting a smooth transition like the one occurring in literature between 13% and 35% of gait cycle, the model's results present a smooth decrease from 9% to approximately 16% of gait cycle with a magnitude of -0.70 Nm/kg, increasing to -0.2 Nm/kg at 23% of gait cycle, then abruptly decreasing its magnitude to a minimum of -1.1 Nm/kg. In literature, this flexion torque should present a magnitude of -0.42 Nm/kg, being unique on this period of gait cycle and not presenting oscillations.

The following occurrence in the knee torque should be a smooth transition to an extension torque of magnitude 0.3 Nm/kg, occurring at 55% of gait cycle. Once again the produced model's results differ from these findings. The model's peak knee extension torque occurs after toe off, which is later than expected. Besides this, the transition from the latter flexion torque to this extension one presents many oscillations when comparing to literature, and its magnitude is higher than expected, being 0.9 Nm/kg. After this peak, the model's results tend to decrease abruptly and stabilize around 0 Nm/kg, decreasing then to produce another flexion torque of -0.9 Nm/kg at 91% of gait cycle. Literature findings are different. After the extension torque occurring before toe off, the magnitude of this variable decreases a little, increasing again to 0.1 Nm/kg and then decreasing towards a flexion torque of magnitude -0.3 Nm/kg, occurring at 93% of gait cycle.



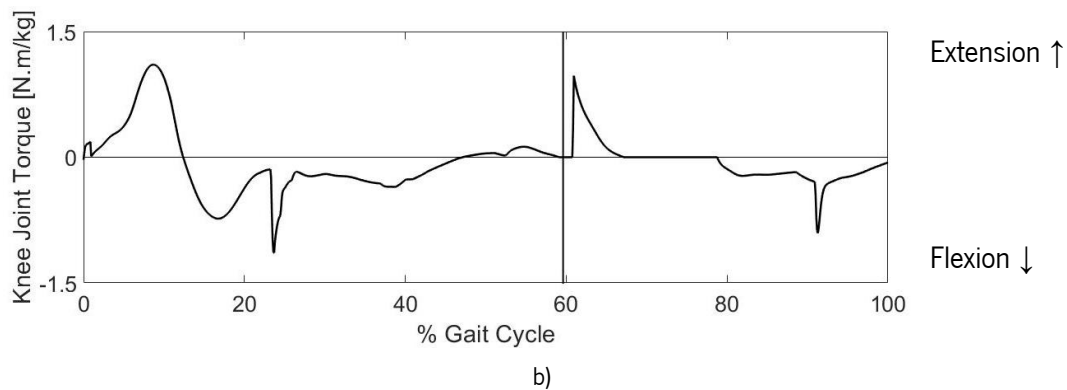
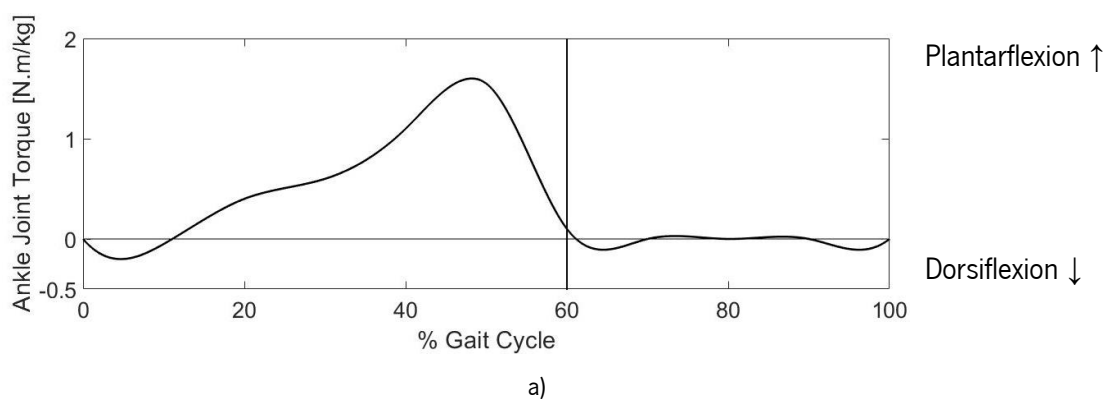


Figure 6.10 - Knee joint torque for walking movement. These graphs are normalized to percentage of gait cycle and to body mass. The black vertical line marks the occurrence of toe off. a) Literature results obtained from Neumann (2013). Toe off occurs at 60.0% of gait cycle. b) Biomechanical model's results. Toe off occurs at 59.6% of gait cycle. In this figure, it is displayed the mean \pm standard deviation.

Figure 6.11 presents the ankle joint internal torque normalized to body mass and to percentage of body weight of literature (Figure 6.11a) and of the biomechanical model (Figure 6.11b). Observing both graphs, it is clear that the biomechanical model's results obtained for the ankle joint are very similar to the ones found on literature, considering the overall shape of the graphs and their magnitude.

The gait cycle initializes with a small dorsiflexion torque of -0.20 Nm/kg at 5% of gait cycle, as stated in literature findings. The results presented by the biomechanical model are a little smaller than expected, with a magnitude of -0.06 Nm/kg at 1% of gait cycle. Even though this dorsiflexion torque is not very evident in the model's results, it still exists. From this point on, there is an increase in the ankle joint torque until it reaches a maximum, representing a plantarflexion torque. In literature it occurs at approximately 50% of gait cycle, with a magnitude of 1.60 Nm/kg. The biomechanical model's results are somewhat similar, occurring at 45% of gait cycle with a magnitude of 1.75 Nm/kg. After this plantarflexion torque, literature states that the internal ankle torque decreases smoothly, stabilizing around 0 Nm/kg. Similar results are encountered in the biomechanical model.



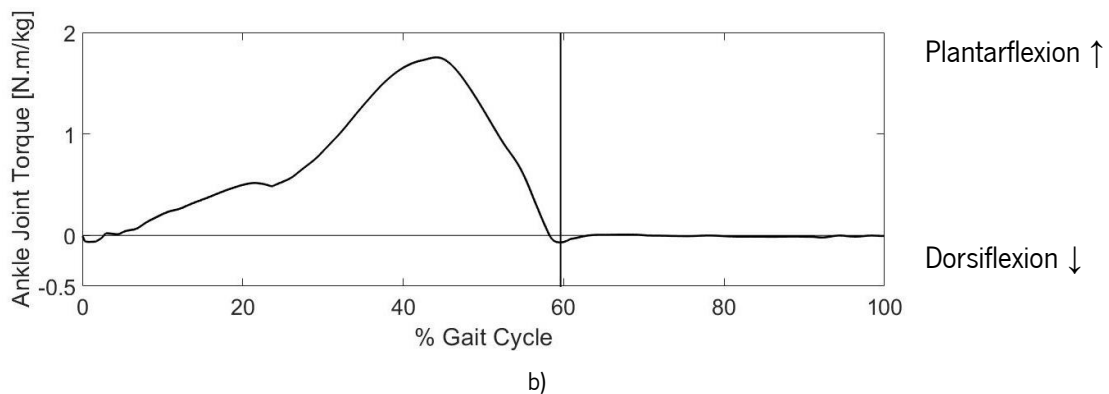


Figure 6.11 – Ankle joint torque for walking movement. These graphs are normalized to percentage of gait cycle and to body mass. The black vertical line marks the occurrence of toe off. a) Literature results obtained from Neumann (2013). Toe off occurs at 60.0% of gait cycle. b) Biomechanical model's results. Toe off occurs at 59.6% of gait cycle. In this figure, it is displayed the mean \pm standard deviation.

The biomechanical model's hip and knee torques are the ones that present more differences when comparing to literature. Besides the overall shape being different, the magnitude is also not similar, being higher than expected. This might be due to the modelling of the joint torques produced around these joints. Muscle and torque modelling is explained in detail in chapter 5, section 5.2. Altering the muscles that produce torque around these joints or altering their muscle models would be a strategy to try and make the internal hip and knee torque more similar to the ones found on literature. Another strategy would be to perform a sensitivity analysis to determine the parameters that influence the most the outputs of these torques and altering them according to the analysis results. Instead of performing a sensitivity analysis, altering the characteristic parameters of each muscle (see Table 5.2) based on other literature or on performed experimental proceedings, would be another option. Optimizing towards obtaining a more realistic hip and knee joint torque would be another option. The ankle joint internal torque is the one that more accurately mimics the human walking data.

6.2.2. Sensitivity Analysis – Vertical Ground Reaction Force

Since the biomechanical model's vertical ground reaction force was not very consistent and similar to results found on literature (Figure 6.5), a sensitivity analysis is performed in order to understand how the parameters involved in the construction of the ground contact model influence the overall shape and magnitude of the GRF curve. The parameters used are the ones included in Eqs. 5.25 to 5.30.

The parameters intervening in the calculation of the vertical ground reaction force comprises the vertical contact stiffness, k_v and the vertical maximum ground relaxation speed, \dot{y}_{max} . The horizontal ground reaction force is divided in two. The sliding force is influenced by the sliding friction coefficient, μ_{sl} , and

by the vertical GRF. The stiction force comprises the horizontal contact stiffness, k_x , and the horizontal maximum ground relaxation speed, \dot{x}_{max} . The interchange between these two horizontal GRF is influenced by the minimum speed from which stiction engages, \dot{x}_{lim} , and by the stiction coefficient, μ_{st} . Other parameter included in the sensitivity analysis is the initial velocity (forward propulsion) given to the model, v_{x0} . Table 6.3 comprises the reference values of these variables. The reference values are the ones used initially to produce the kinetic and kinematic results previously analysed.

Table 6.3 - Reference values for the parameters used in the sensitivity analysis

Vertical Ground Reaction Force		Horizontal Ground Reaction Force					Other
		Sliding	Transition		Stiction		
k_y (kN/m)	\dot{y}_{max} (m/s)	μ_{sl}	\dot{x}_{lim} (m/s)	μ_{st}	k_x (kN/m)	\dot{x}_{max} (m/s)	v_{x0} (m/s)
78.4	0.03	0.8	0.01	0.9	7.84	0.03	1.3

All these eight parameters were varied in a range of [-5 -3 -1 0 1 3 5] %. The biomechanical model's simulation ran for 60 seconds with a time step of 1ms, and the results were saved in each trial, being then superimposed to enable easier comparison. The following figures present the results obtained.

Figure 6.12 illustrates the influence of the vertical contact stiffness, k_v , on the vertical ground reaction force produced by the biomechanical model, normalized to percentage of gait cycle. Analysing the results, one can infer that k_v does not produce significant shape and/or magnitude alterations in the vertical GRF, and therefore it is not a sensitive parameter for the variable in study.

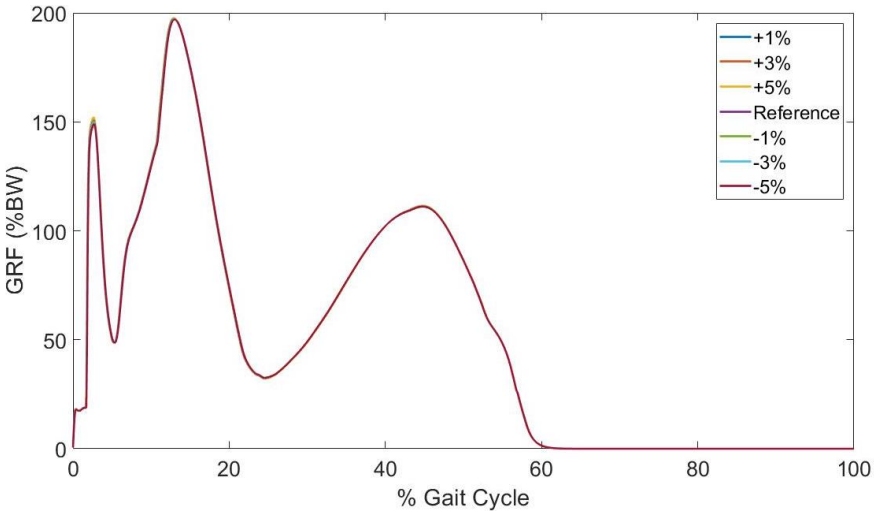


Figure 6.12 - Influence of the vertical contact stiffness, k_v , on the vertical ground reaction force. Results are normalized to % of body weight and to % of gait cycle.

In similarity to the ground contact stiffness, k_v , the vertical maximum ground relaxation speed, \dot{y}_{max} , does not produce significant alterations regarding the vertical ground reaction force's shape and/or magnitude. This is observable in Figure 6.13.

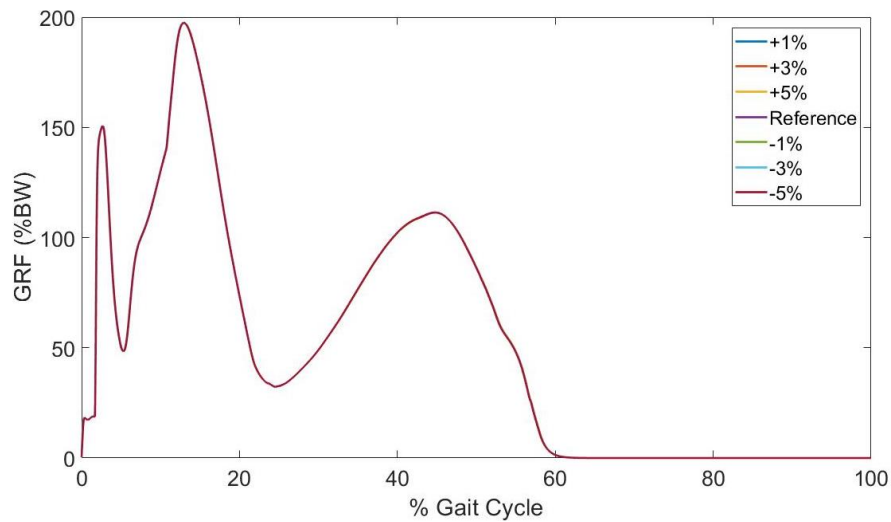


Figure 6.13 - Influence of the vertical ground relaxation speed, \dot{y}_{max} , on the vertical ground reaction force. Results are normalized to % of body weight and to % of gait cycle.

This strategy was applied to all parameters displayed in Table 6.3 and it was verified that the shape and/or magnitude of the vertical ground reaction force were not altered regarding alterations ranging from -5% to 5% in the referred contact model parameters and initial velocity. The graphs obtained for all the eight parameters were all similar to Figure 6.12 and Figure 6.13. Since this occurs, only figures regarding the sensitivity analysis of k_v and \dot{y}_{max} are displayed. Regarding these statements, it is possible to infer that the vertical ground reaction force of the biomechanical model is not sensitive to alterations of [-5 -3 -1 0 1 3 5] % in all eight parameters comprised in the ground contact model and the initial velocity.

6.2.3. Vertical Ground Reaction Force – Detailed Study

After performing the sensitivity analysis, a more detailed examination of the relation existing between the vertical ground reaction force and the vertical contact stiffness, k_v , was carried out. To this end, several increments of different magnitudes were applied to this ground contact model parameter in order to determine its influence on the magnitude and shape of the vertical GRF. This study was performed in order to try to minimize the occurrence of the extra peak (150% BW) verified in Figure 6.5b, as well as the magnitude of the of the second peak (200% BW), to make the biomechanical model's results more similar to results found in literature (Figure 6.5a).

The biomechanical model's simulation time was of 60 seconds with a time step of 1ms, and the results were saved in each trial, being then superimposed to enable easier comparison.

The initial value of k_v was 78.4kN/m and was reduced by approximately 0.5kN/m until it equalled 77kN/m in magnitude. However, as seen in Figure 6.14, there are no significant differences regarding the shape and magnitude of the vertical ground reaction force produced by these small alterations on k_v .

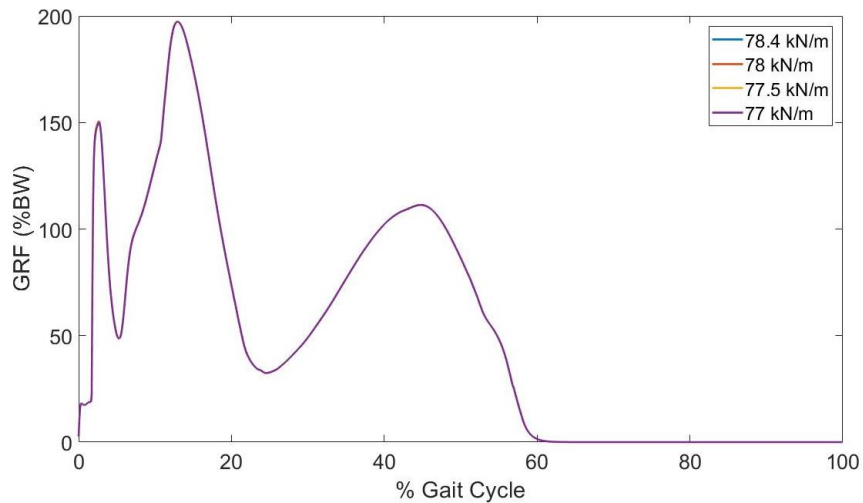


Figure 6.14 - Influence of 0.5 kN/m decreases of the vertical contact stiffness, k_v , on the vertical ground reaction force. Results are normalized to % of body weight (BW) and to % of gait cycle. Initial k_v value: 78.4kN/m.

Since no significant differences were observed, it was determined that a more prominent alteration should be performed. To this end, from $k_v = 70\text{kN/m}$, 10kN/m alterations were introduced to the vertical contact stiffness and the produced results on the vertical ground reaction force were observed. Figure 6.15 presents the obtained results. This reduction was performed until $k_v = 10\text{kN/m}$.

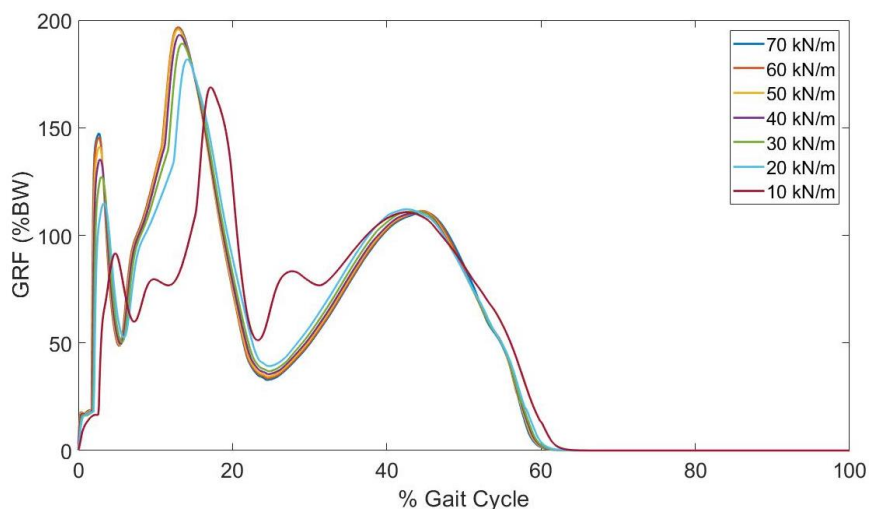


Figure 6.15 – Influence of 10 kN/m decreases of the vertical contact stiffness, k_v , on the vertical ground reaction force. Results are normalized to % of body weight (BW) and to % of gait cycle.

Observing the latter figure, it is noticeable that from within this range of magnitudes implemented to k_v , there is a significant decrease on the magnitude of the extra peak, passing from approximately 150% BW with $k_v=70\text{kN/m}$ to 92% BW with $k_v=10\text{kN/m}$. Besides this alteration, the magnitude of the first peak diminished from 200% BW with $k_v=70\text{kN/m}$ to 169% BW with $k_v=10\text{kN/m}$. These are positive changes, since the reduction in magnitude of these two peaks was desired in order to mimic the best way possible the vertical ground reaction force curve presented in literature (Figure 6.5b), which do not present the extra peak and the magnitude of the first peak is around 120% body weight (BW).

Considering the above-stated differences and regarding the vertical GRF curve with $k_v=10\text{kN/m}$, it is clear that the transition from the extra peak (92% BW) to the first peak (169% BW) is much less prominent than the transition occurring when $k_v=70\text{kN/m}$. With $k_v=70\text{kN/m}$ the vertical GRF curve ranges from 150% BW (extra peak) to 50% BW (from this point on, this event will be called depression) and then increases again to 200% BW (first peak). This gives a difference between extra peak and depression of 100% BW and between depression and first peak of 150% BW.

However, with $k_v=10\text{kN/m}$, the vertical GRF curve ranges from 92% BW (extra peak), to 60% BW (depression) and then increases again to 169% BW (first peak). This gives a difference between extra peak and depression of 32% BW and between depression and first peak of 109% BW. This leads to a thinking that using a vertical ground contact stiffness of 10kN/m is much more beneficial in a way that it promotes the reduction of the magnitude of the extra and first peaks and the difference in the transition magnitude between these events.

However, observing Figure 6.15 it is also evident that with $k_v=10\text{kN/m}$, there is the occurrence of oscillations between the extra peak and the depression and also between the first and second peaks. These extra oscillations were not present when $k_v=78.4\text{kN/m}$ (initial vertical contact stiffness) and they arose immediately after altering k_v from 20kN/m to 10kN/m . In order to determine which value for k_v to use in the following simulations, a more detailed analysis of the changes that occur between 20kN/m and 10kN/m is needed. To this end, the magnitude of the vertical contact stiffness was reduced by 5kN/m , achieving a value of 15kN/m . After this test, this parameter was progressively reduced by 1kN/m , until 11kN/m was reached. Figure 6.16 illustrates these results.

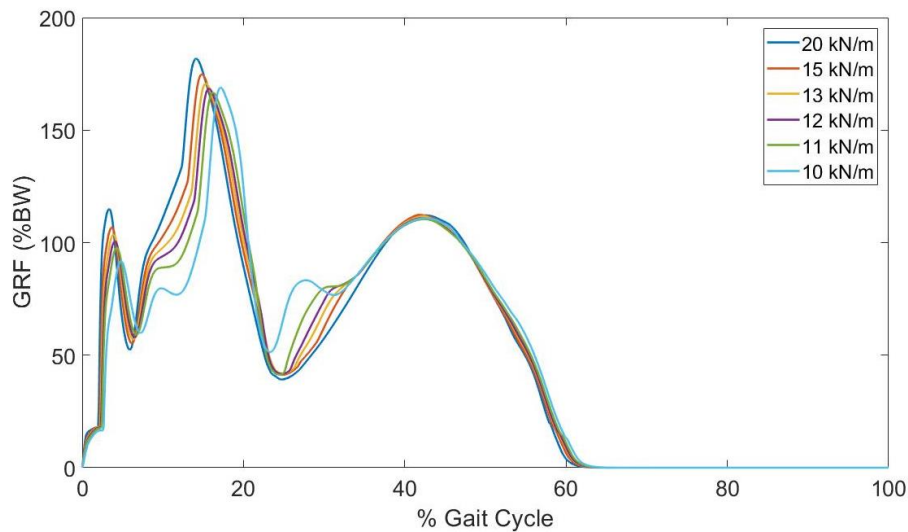


Figure 6.16 - Influence of decreases of the vertical contact stiffness, k_v , from 20kN/m to 10kN/m, on the vertical ground reaction force. Results are normalized to % of body weight (BW) and to % of gait cycle.

Observing Figure 6.16, one can determine that the previously referred oscillations are present in values of k_v equal to 10, 11, 12 and 13 kN/m. Oscillations between the extra peak and the initial peak and between the first and two peaks are more prominent in values of k_v equal to 10 and 11 kN/m, while values of k_v equal to 12 and 13 kN/m present fewer oscillations, but they cannot be ignored. Another important feature to be mentioned is the fact that when $k_v = 10$ kN/m is used, the magnitude of the first peak is higher than when values of 11 and 12 kN/m are used for the vertical contact stiffness. Considering this difference in amplitude of the first peak and the presented oscillations, $k_v = 10$ kN/m was not the chosen value. The values of 20 kN/m and 11 kN/m are also not eligible since there are values (12, 13 and 15 kN/m) with smaller oscillations and amplitudes regarding the extra and first peaks.

The choice lies between values of k_v of 12, 13 and 15 kN/m. The oscillations present in the vertical ground reaction force curve between the extra and first peaks, and between the first and second peaks regarding these three values for k_v are similar. However, concerning the magnitude of the extra and first peaks, 12 kN/m present a lower value than 15 or 13 kN/m. Considering these statements, and in order to choose the best value to be used for this ground contact model parameter in subsequent simulations using the biomechanical model, it was determined that the three values (12, 13 and 15 kN/m) should be plotted together with 78.4 kN/m (Figure 6.17) and comparisons made between curves.

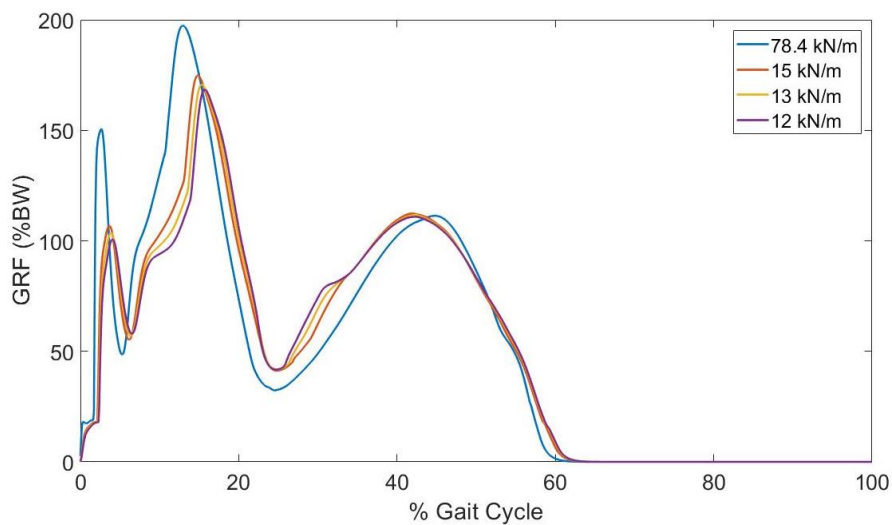
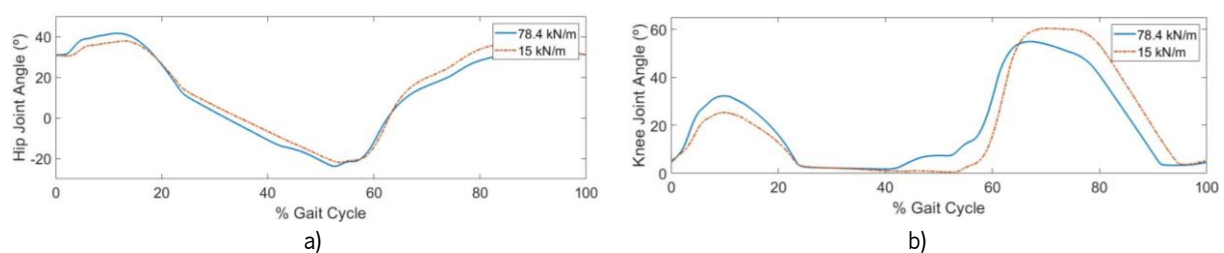


Figure 6.17 - Comparison of vertical ground reaction force curves generated by different values of vertical contact stiffness. Initial value of 78.4 kN/m and tested values of 15, 13 and 12 kN/m.

From the comparison figure above, it is observed that a vertical contact stiffness of 15kN/m is closer to the initial reference value of 78.4kN/m, in terms of overall shape. $k_v = 13\text{kN/m}$ and 12kN/m still present a sharp transition between the extra and first peak, as well as between the first and second peaks and due to this were not chosen. Considering this statement, the selected value for k_v is 15kN/m, which is going to be used in the subsequent simulations with the biomechanical model. The reduction from $k_v = 78.4\text{ kN/m}$ to $k_v = 15\text{kN/m}$ enabled a decrease in the magnitude of the extra and first peaks from approximately 150% BW and 200% BW to 107% BW and 175% BW, respectively, without compromising the overall shape of the vertical GRF curve. Overall, this was the aim of the present study.

Before implementing this new value for the vertical contact stiffness, it is important to analyse the curves pertaining to the joint angles and torques. This was the next analysis carried out. The curves are displayed in Figure 6.18. By observing it is possible to determine that regarding the hip and ankle joint angles (Figure 6.18a and c) and torques (Figure 6.18d and f), no significant differences were encountered. However, taking a closer look to the knee joint, some differences exist.



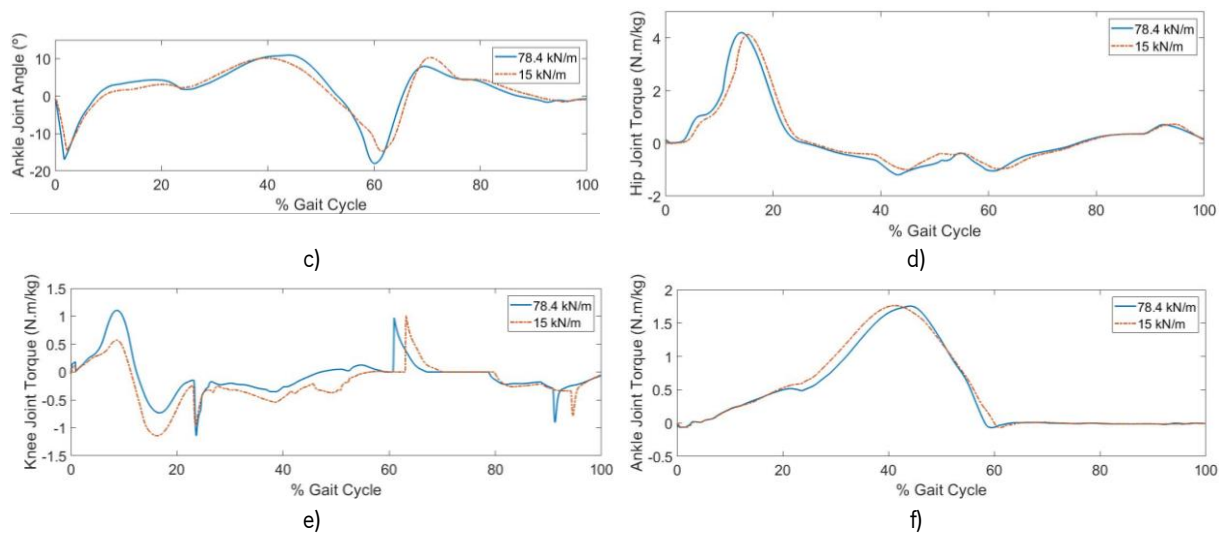


Figure 6.18 – Graphs showing the comparison between joint angles and torques with a vertical contact stiffness of 78.4 kN/m and 15 kN/m. Results are normalized to % of gait cycle. a) Hip joint angle. b) Knee joint angle. c) Ankle joint angle. d) Hip joint torque. e) Knee joint torque. f) Ankle joint torque.

Starting with the knee angle during gait, it is possible to see a lower knee flexion angle in the beginning of the gait cycle with $k_v = 15 \text{ kN/m}$ (25 degrees) rather than with $k_v = 78.4 \text{ kN/m}$ (32 degrees). Remembering that the model's results with $k_v = 78.4 \text{ kN/m}$ presented a higher initial knee flexion angle than expected by literature (20 degrees, Figure 6.7a), this decrease with $k_v = 15 \text{ kN/m}$ is a positive change in this parameter. The second knee flexion was previously ($k_v = 78.4 \text{ kN/m}$) lower than expected by literature, however, using $k_v = 15 \text{ kN/m}$, the peak flexion angle increased from 55 degrees to 60 degrees. This magnitude is the one predicted by literature (Figure 6.7a). These modifications enable the approximation of the model's angle to literature findings.

The initial knee extension torque with $k_v = 15 \text{ kN/m}$ is slightly lower than previous results with $k_v = 78.4 \text{ kN/m}$, which is also a positive occurrence, since the previous knee torque magnitude was too high relative to literature (Figure 6.10a). However, the immediately following knee flexion torque is higher with this new value for k_v . For the rest of the gait cycle, the curves are similar regarding shape and magnitude.

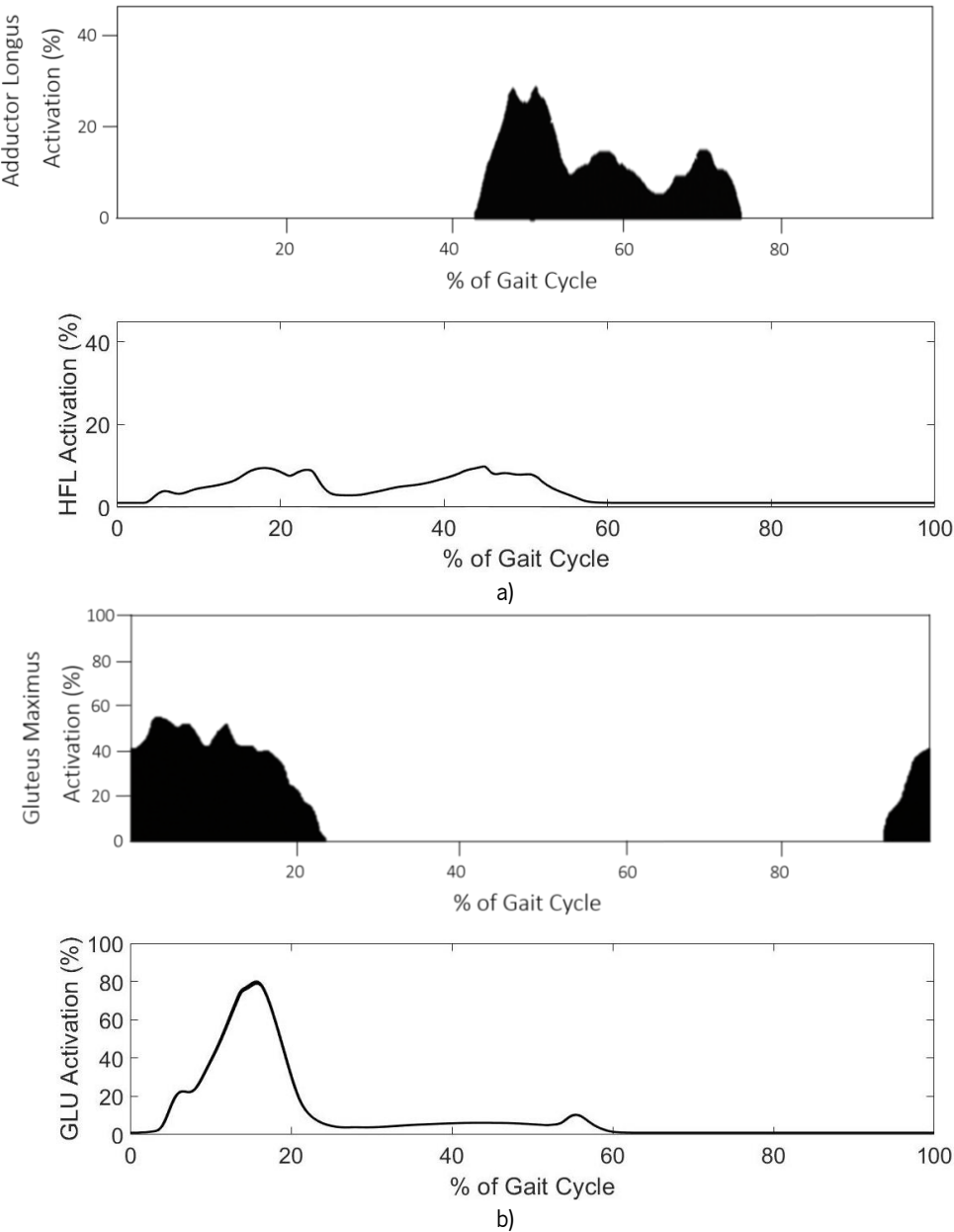
Since, overall, no more significant differences were encountered and considering the justifications provided above, $k_v = 15 \text{ kN/m}$ is possible to be utilized in subsequent simulations.

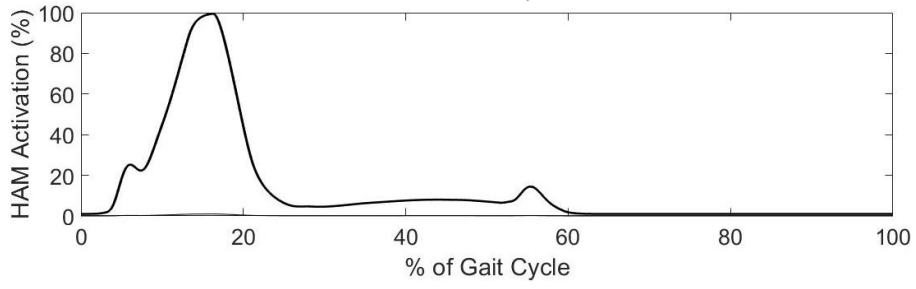
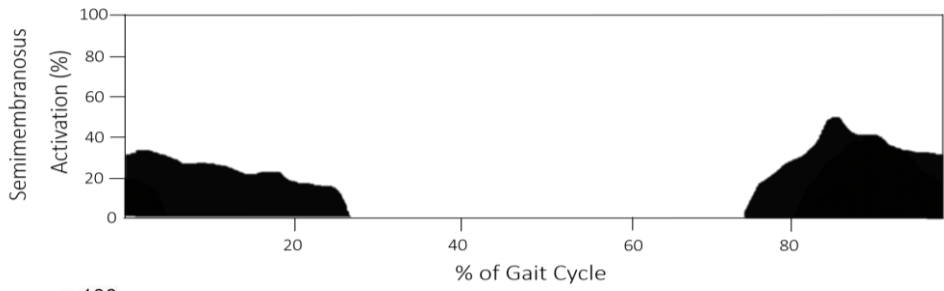
6.2.4. Muscular Activation Outcomes

Geyer & Herr (2010) compared the muscular activations of all the seven muscles (soleus, tibialis anterior, biarticular gastrocnemius, vasti lumped, biarticular hamstrings, hip flexor and gluteus muscle

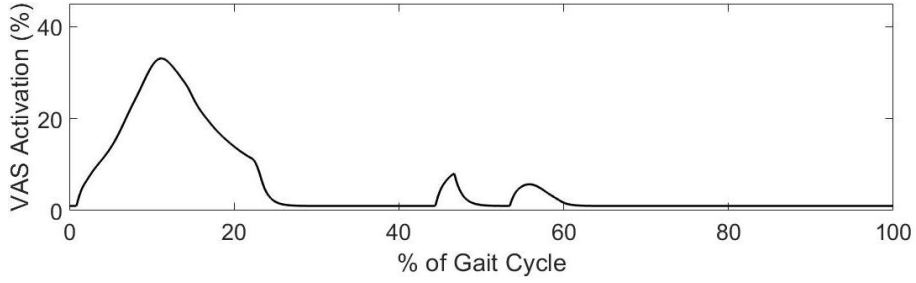
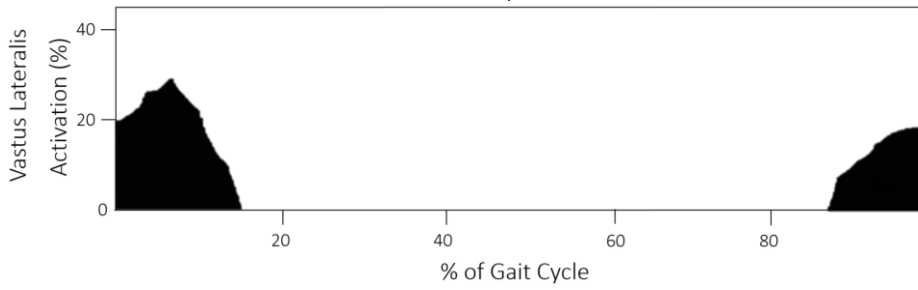
groups) included in the biomechanical model with literature findings from Jacquelin (1992). This strategy was also conducted in this dissertation to present and analyse the obtained results.

The muscular activations results were obtained from a 60-second simulation with a time step of 1ms, in which the model walked for 100 meters. The results of the model’s simulation pertain only to the left leg, being the right leg results’ equal. Figure 6.19 comprises the comparison of the outcomes of the biomechanical model and literature findings of Jacquelin (1992) regarding the seven muscles included in the model.

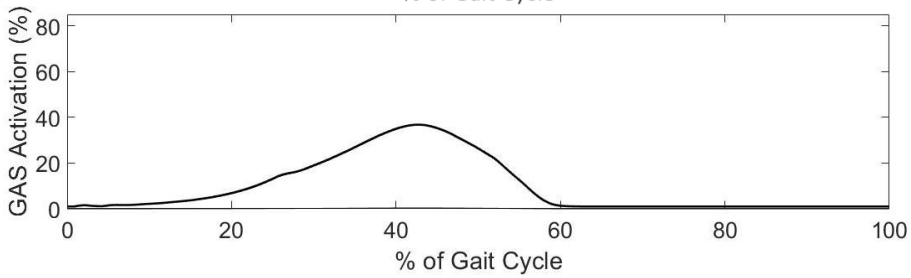
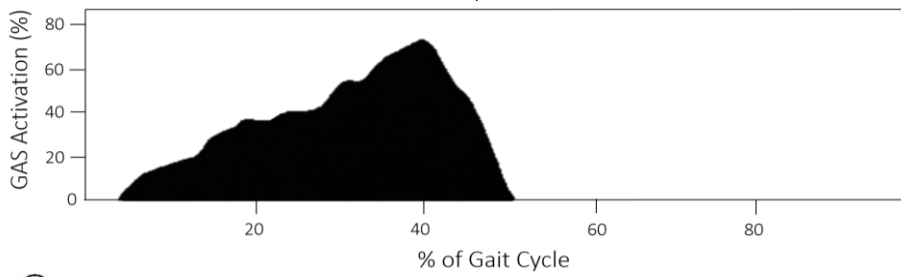




c)



d)



e)

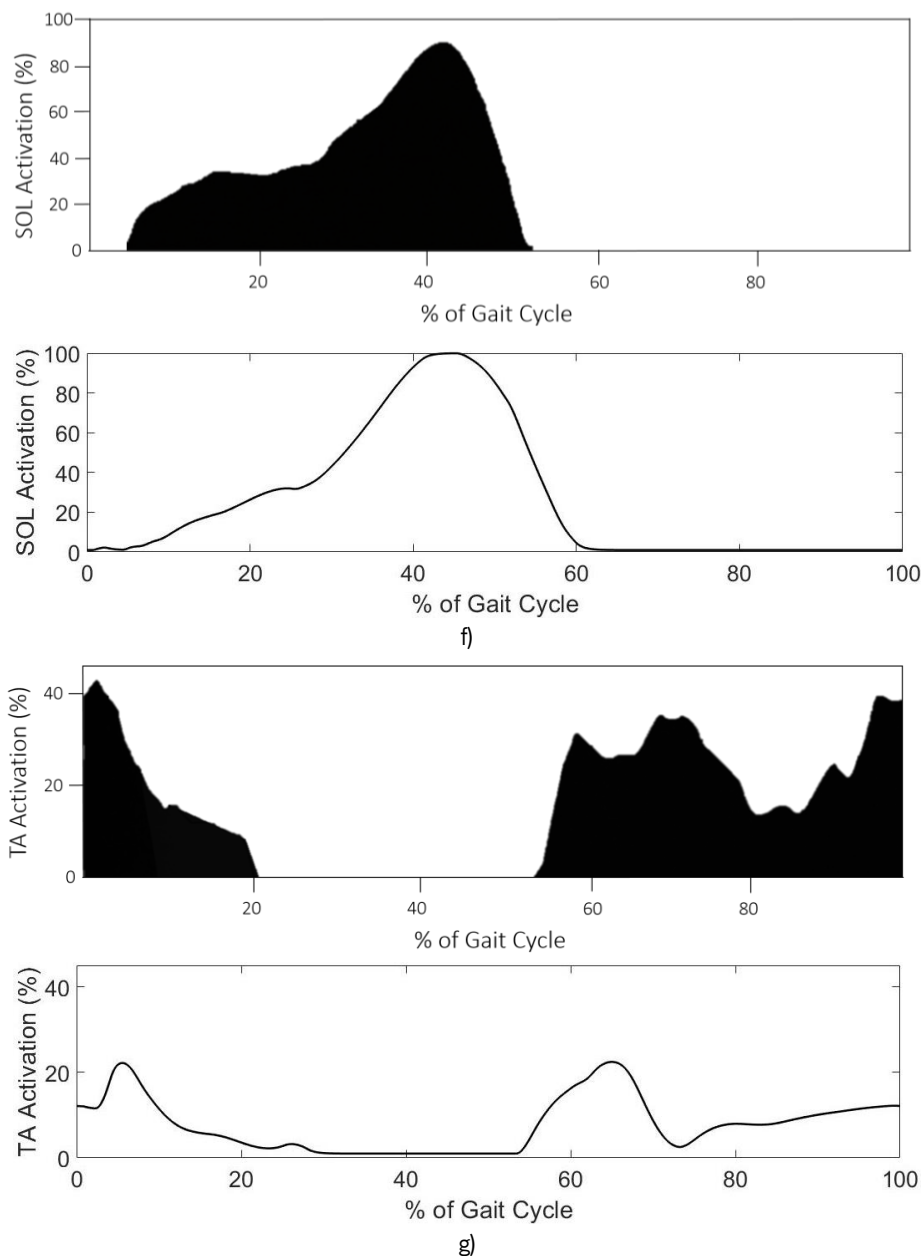


Figure 6.19 – Comparison between the muscular activations of the seven muscles included in the biomechanical model. On each bullet point, the first figure that appears regards to literature, whilst the second regards to the biomechanical model's result. Results are normalized to % of gait cycle. a) HFL - hip flexor muscle group is compared to the adductor longus muscle. b) GLU - gluteus muscle group is compared to the gluteus maximus muscle. c) HAM - biarticular hamstring muscle group is compared to the semimembranosus muscle. d) VAS - vasti lumped muscle group is compared to vastus lateralis muscle. e) GAS - biarticular gastrocnemius muscle. f) SOL - soleus muscle. g) TA - tibialis anterior muscle. See Chapter 2 for more information about the functions of these muscles.

Taking a general overview to Figure 6.19, it is possible to conclude that overall the muscular activations pertaining to the biomechanical model differ from literature findings from Jacquelin (1992). Starting by analysing Figure 6.19a, which comprises the muscular activation of the hip flexor muscle group (HFL) compared to a muscle that flexes the hip joint, named adductor longus. This was the chosen

muscle since, according to Jacquelin (1992), it is both the first and most persistent hip flexor, and since it was the one used to compare with the HFL activation by Geyer & Herr (2010). Observing both literature findings and the biomechanical model's results, it is possible to determine that discrepancies arise both in shape and magnitude, which is much lower regarding the model's results. Besides these differences, the model's HFL is activated much earlier in the gait cycle than it should, and no activation is present in the middle of the gait cycle, when it should be existent, according to literature.

The gluteus maximus muscle is used to compare muscular activation with gluteus muscle group (GLU) of the biomechanical model, since it is the muscle from the three existing gluteus muscle (maximus, medius and minimus), that produces hip extension (see Table 2.5) and because it was the one used by Geyer & Herr (2010). Similarly to HFL, GLU also presents magnitude and shape discrepancies when compared to literature (Figure 6.19b). Even though, in the biomechanical model, this muscle is activated in the beginning of the gait cycle as in literature, the magnitude of this activation is too high. An activation of about 50% was expected, rather than approximately 80%. From approximately 25% to 95% of gait cycle no activation is presented by this muscle in literature, however, the model's results differ. Some degree of activation is seen from 25% to 60% of gait cycle. While literature states the occurrence of an activation at the end of the gait cycle, the biomechanical model's results present no activation at all.

The hamstrings muscle group, as previously explained in Chapter 2, section 2.4, is composed by the semimembranosus, semitendinosus and biceps femoris muscles. The semimembranosus was chosen to compare its muscular activation with the biarticular hamstrings muscle group (HAM) from the biomechanical model since it was the one used by Geyer & Herr (2010). Observing Figure 6.19c, it is possible to see that, even though the biomechanical model's activation pattern is present in the beginning of the gait cycle as in the literature, the magnitude of the activation is much higher. A muscular activation of less than 40% should occur, instead of what occurs in the biomechanical model muscle, of 100%. After this initial activation, the muscle should remain silent (0% of muscular activation) until approximately 75% of gait cycle, increasing then the activation to a maximum of approximately 50%. This is not seen in HAM's activation graph, in which, after the initial peak, the activation decreases to about 10%, increasing then slightly at 58% of gait cycle and then decreasing to 0% for the rest of gait.

The vastus lateralis muscle was chosen to be compared with the vasti lumped muscle group (VAS) of the biomechanical model since it was the one used by Geyer & Herr (2010). Observing Figure 6.19d, it is possible to determine that the initial shape and magnitude of the VAS activation are similar to literature findings. However, from approximately 15% to 85% of gait cycle, no activation is present in the vastus

lateralis muscle. These literature findings are different from the biomechanical model's results, which present 0% of muscular activation from 25% to 45% of gait cycle, presenting some peaks and then for the rest of the gait cycle there is no muscular activation again. In literature findings, the vastus lateralis muscle presents some degree of activation (approximately 20%) from 85% to 100% of gait cycle. This is not observed in the model's results.

Figure 6.19e and f present the comparison between gastrocnemius (GAS) and soleus (SOL) muscles between literature and the biomechanical model's results, respectively. Overall the shape is very similar. However, the model's activation magnitude is lower (about 40%) for GAS and higher (100%) for SOL than literature findings, which are about 75% for GAS and 85% for SOL, respectively. No more significant differences are identified between results.

Figure 6.19g presents the muscular activation pattern of literature and biomechanical model results for the tibialis anterior (TA) muscle. In the beginning of the gait cycle, the model's TA presents a similar shape regarding activation, but a lower activation (approximately 22%), when compared to literature (approximately 40%). From 20% to approximately 55% of gait cycle, no muscular activation should exist regarding literature findings. However, in the model's results, no activation is present from 30% to 55% of gait cycle, meaning that TA from the model stays activated for a longer period than it should during gait. From 60% of gait cycle, the model's results increase in magnitude, but it is still lower (approximately 22%) than literature findings (approximately 30%). In the last part of the gait cycle, the overall shape is not very similar, with the model's TA presenting lower activation.

Considering the discussion presented above, it is clear that the muscular activation patterns of the biomechanical model are somewhat far from what is predicted by literature, even though the joint angles and the ankle torque are very similar to what is stated in literature (see section 6.2.1). In order to try and approximate the biomechanical model's results to literature findings, it should be considered another approach. For instance, instead of calculating the muscular activations analytically (see Figure 5.15) by means of implementing the Laplace transform of Eq. 5.21, the electromyographic (EMG) activity of the muscles analysed in this section could be used and inputted directly into the biomechanical model.

6.3. Pathological Model

After obtaining the desired healthy walking gait of the biomechanical model and subsequent to the improvements performed at vertical ground reaction force level, a knee joint pathology is applied. Primarily, the selected knee condition, which is the anterior cruciate ligament (ACL) injury, as well as the

treatment techniques and strength outcomes in the injured and uninjured limbs, are approached and explained. After this, the computational implementation of the pathology in the biomechanical model is described. Lastly, in a similar manner to what was performed for the healthy biomechanical model, in this section, the pathological model's kinematic (joint angles) and kinetic (ground reaction forces and joint torques) data are presented and compared to literature findings.

6.3.1. Anterior Cruciate Ligament: Injury and Treatment Strategies

The location of the knee between the long bones of the lower extremity, combined with its weight-bearing and locomotion functions, makes it susceptible to injury. Knee pathologies are very common and can occur in people of all ages, interfering with activities of the daily life. Knee joint pathologies primarily consist of bursitis, meniscal lesions or tears, ligament injuries and osteoarthritis. This work focuses only on the anterior cruciate ligament tear and outcomes after its surgical repair.

The anterior cruciate ligament is an intraarticular structure located in the centre of the knee joint between the femur and the tibia. Its primary function is to act as the main stabilizer of this articulation, preventing anteroposterior displacement, designated subluxation, of the tibia relative to the femur (Fältström, 2016; Prodromos, 2017).

In sports, anterior cruciate ligament tears are one of the most knee common injuries. They can be classified as noncontact or contact injuries. The former are the most common (approximately 70%) way of injuring this knee structure and they occur when the foot is planted on the ground and a cutting or twisting effort is made (Meisterling, Schoderbek, et al., 2009). Activities, such as basketball, involving sudden changes in direction combined with acceleration/deceleration of the body produce large rotational moments and forces at the knee, particularly when they are inadequately planned. These actions can cause anterior cruciate ligament (ACL) injuries, sometimes leading to its rupture (Figure 6.20).

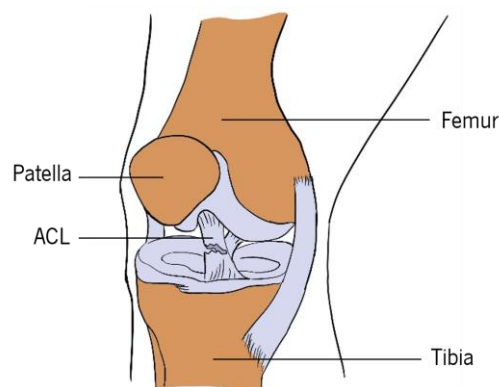


Figure 6.20 – Anterior cruciate ligament (ACL) tear.

The rupture of the anterior cruciate ligament occurs when there is excessive anterior tibial subluxation, meaning there is an excess anterior translation of the tibia relative to the femur (Hall, 2012; Neumann, 2013; Standring, 2008). Contact ACL injuries are often an outcome of a direct anterior or lateral blow of the knee joint (Meisterling, Schoderbek, et al., 2009).

Several risk factors are associated with anterior cruciate ligament tear and they can be classified as intrinsic or extrinsic and as modifiable or non-modifiable. For instance, intrinsic non-modifiable risk factors include female sex and the occurrence of previous ACL injury. In the category of intrinsic modifiable, there is, for instance, the high body mass index (BMI) and muscle fatigue. Extrinsic factors, such as the weather conditions (hot or dry climate), are classified as non-modifiable, whilst cutting and pivoting sports are included in the modifiable risk factor category.

The rupture of the ACL results in local instability of the knee, a change in the location of the centre of rotation of the joint, a change in the area of tibiofemoral contact during gait, and altered joint kinetics, with subsequent onset of osteoarthritis. The proposed treatment for an anterior cruciate ligament tear or injury may require surgery (ACL reconstruction surgery with subsequent rehabilitation) or not, with this latter relying on rehabilitation strategies only. Surgical repair of the ACL rupture involves the reconstruction of the ligament using either the middle third of the patellar tendon, the semitendinosus muscle, or both the semitendinosus and gracilis muscles (chapter 2). In both of these treatments, the main goal is the same: to obtain the best functionality of the knee joint without increasing the risk of subsequent injuries or degenerative changes in the joint (Fältström, 2016; Hall, 2012; Neumann, 2013; Standring, 2008).

Rehabilitation strategies are an important part of the treatment after an ACL injury and they usually last for up to four months after the occurrence of the injury or until the knee function is restored. Surgical treatment is considered if the patient still exhibits knee pain symptoms, functional instability and a low level of activity or quality of life, during or after rehabilitation. This treatment for an ACL injury is often recommended to younger and more active patients (Fältström, 2016). After the reconstructive ACL surgery, patients undergo postoperative rehabilitation protocols in order to restore the knee joint functionality. These rehabilitation programs usually last about six to twelve months after surgery, and after this time patients are usually allowed to return to their daily life activities. The clinical decision for patients to return to their previous activities lies in the fact that the injured and uninjured limb differences regarding quadriceps muscle group strength must be equal to or less than 10%. Deficits that exceed this target value are associated with decreased knee joint function and performance (Lepley, 2015).

According to Hiemstra, Webber, et al. (2007), the functional outcome of the knee joint after an anterior cruciate ligament reconstructive surgery has a positive correlation with knee flexor and extensor strength (N.m/kg) measurements. Lower extremity muscle weakness, particularly in the quadriceps (extensor activity) and hamstrings (flexor activity) muscle groups, is common after ACL injury and reconstructive surgery, often persisting well beyond the postoperative rehabilitation period. Quadriceps strength deficits in the injured limb reported range from 5% to 40% and have been noted for as long as 7 years after surgery. Hamstrings strength deficits in the injured limb have been reported to range from 9% to 27% and have been reported 3 years after surgery. Similarly, quadriceps and hamstrings strength deficits in the uninjured limbs of patients who have had ACL reconstruction have been reported to be 21% and 14%, respectively, 3 years after surgical repair (Thomas, Villwock, et al., 2013). Table 6.4 presents the deficits experienced by patients after an anterior cruciate ligament reconstruction and rehabilitation procedures organized by injured and uninjured limb.

Table 6.4 - Quadriceps and Hamstrings muscle group strength (N.m/kg) deficits in the injured and uninjured leg after anterior cruciate ligament reconstruction and rehabilitation procedures (Thomas, Villwock, et al., 2013)

	Injured Limb	Uninjured Limb
Quadriceps	5% - 40%	21%
Hamstrings	9% - 27%	14%

The uninjured limb strength deficits reported by Thomas, Villwock, et al. (2013) and presented in Table 6.4 may arise from inhibition of motor activation of the analysed muscles, de-conditioning or inadequate reconditioning of the knee joint (Hiemstra, Webber, et al., 2007). According to Shelbourne, Biggs, et al. (2007), deconditioned is defined as an impairment causing physical fitness loss and therefore a deconditioned knee joint results in functional loss of knee extension, decrease strength and function. The injured limb quadriceps strength deficits reported in Table 6.4 are a consequence of muscle inhibition and is assumed to be a natural compensation mechanism that arises in order to prevent anterior subluxation that may result in painful and damaging movement of the knee joint (Kim, Lee, et al., 2016).

Loss of quadriceps muscle strength may contribute to reduced knee joint stability, fatigue, and a diminished ability to adequately dampen impact forces and evenly distribute load on the joint surface during different weightbearing activities. These implications may prevent individuals from participating at their desired level of sports and leisure activities in the short term, and in the long term, play a role in future development of knee osteoarthritis (OA) (Eitzen, Grindem, et al., 2016).

6.3.2. Computational Implementation of the Knee Joint Pathology

In this dissertation, the main outcomes regarding muscle strength deficits of a knee joint pathology, ACL tear, after reconstructive surgery are applied to the developed healthy biomechanical model (see section 6.2). This strategy is done in order to, in future developments, apply the biomechanical model to the study of more efficient rehabilitation strategies. These strategies may include the analysis of the addition of a computer aided design (CAD) medical device with a control strategy to the model.

As it was earlier referred, lower extremity muscle weakness, particularly in the quadriceps and hamstrings, is common after ACL injury and reconstruction (Table 6.4). Since strength is displayed in torque units (N.m/kg) in Thomas, Villwock, et al. (2013), this was the parameter altered in the biomechanical model in order to mimic this knee pathology. A reduction in muscle torque of the vasti lumped muscle group (VAS), in the biomechanical model representing the quadriceps muscle group (see chapter 2, section 2.4), and of the biarticular hamstrings muscle group (HAM) (see Figure 5.10), was performed according to values claimed by Thomas, Villwock, et al. (2013).

Some tests were performed in order to determine the maximum percentage of muscle strength deficit the biomechanical model could bear without falling. The strategy used was to progressively increase the strength deficit of the quadriceps and hamstrings muscle groups, both individually (tests 1 and 2) and as a group (test 3) and analyse if model's walking gait did not cause it to fall. It is not desirable that the biomechanical model's falls, since, if that occurred, it would not be possible to analyse its walking gait kinetic and kinematic data.

The results shown in Table 6.5 represent the percentage of deficit the model can stand without falling. In tests 1 and 2, several increments of one unit were applied individually to the hamstrings and vasti (quadriceps) muscle groups, respectively, until a maximum deficit the model could bear without falling. For the hamstrings and the quadriceps, the maximum deficit the model could bear without falling was 18% and 40%, respectively.

In test 3, the same strategy was used, but this time both muscle groups were affected by the deficit at the same time and with the same increments in percentage. The maximum strength deficit the biomechanical model was able to bear without falling was of 18% in both muscle groups. Percentages higher than the ones stated in the below table are not within the range of feasible deficits the model bears.

Table 6.5 - Quadriceps and hamstrings muscle groups test deficits results

	Quadriceps Deficit	Hamstrings Deficit
Test 1	0%	18%
Test 2	40%	0%
Test 3	18%	18%

These results state that the model can still walk with a higher deficit in the quadriceps muscle group (test 2), than a higher deficit in hamstrings muscle group (test 1). Test 2 determined that the higher quadriceps deficit the model could bear without falling, meaning it produced a fairly natural gait, was of 40%. However, from test 1 it was determined that the model is able to walk with a lower deficit in the hamstrings, of 18%, when compared to the deficit of the quadriceps in test 2. From these results, one can state that the hamstrings muscle force is more significant to produce a walking gait, than the hamstrings muscle force.

Considering the results from the table above, the case in which both muscles are reduced in 18% (test 3) was evaluated. All the results obtained from the pathological model are superimposed to the ones obtained previously for the healthy model.

6.3.3. Kinetic and Kinematic Outcomes

The kinematics and dynamics of the pathological biomechanical model were obtained, in a similar manner as the healthy biomechanical model, from a 60-second simulation with a time step of 1ms, in which the model walked for 100m. The model started the walking gait in the same position as the healthy model and at the same initial speed, $v_{x0}=1.3$ m/s. The pathology was applied to the right leg (injured limb) and no deficit in strength (Nm/kg) was applied on the left leg (uninjured limb).

The kinematic and kinetic data obtained from both the healthy and pathological biomechanical model's simulations is compared, in relative terms, to each other based on results from Noehren, Wilson, et al. (2013). The authors performed an instrumented gait analysis on 40 females (20 ACL-reconstructed, 20 healthy controls). All participants included in the ACL-reconstructed group must have had a unilateral ACL reconstruction, completed rehabilitation, and returned to playing sports. In their study, only females were included, since, as explained in section 6.3.1, the female sex possesses a higher tendency of occurring ACL injuries. The ACL-reconstructed group must have been involved in the practice of sports at the time of injury. The healthy control group had to be free of any injury for at least six months.

Their purpose was to define the alterations in impact forces and the accompanying sagittal plane kinematic and kinetic mechanics between the ACL-reconstructed group and a healthy control group. Their findings indicate: greater initial vertical impact force, smaller knee extensor moments, smaller hip angle (flexion), larger hip extensor moment and no differences in knee angles.

According to Noehren, Wilson, et al. (2013), their study found higher initial vertical impact forces during walking in patients possessing an ACL-reconstructed joint when compared to their healthy control subjects. In dissertation, the same strategy is performed: the results of the healthy biomechanical model are compared to results from the model with pathology implemented. The presented results regard to the right leg of the biomechanical model.

Figure 6.21 represents the vertical ground reaction force of the healthy and pathological biomechanical model. Observing it, it is possible to conclude that the model's results are in accordance with Noehren, Wilson, et al. (2013), since the first peak (initial vertical impact force) of the pathological model, presents a higher magnitude (183% BW) than the healthy one (175% BW).

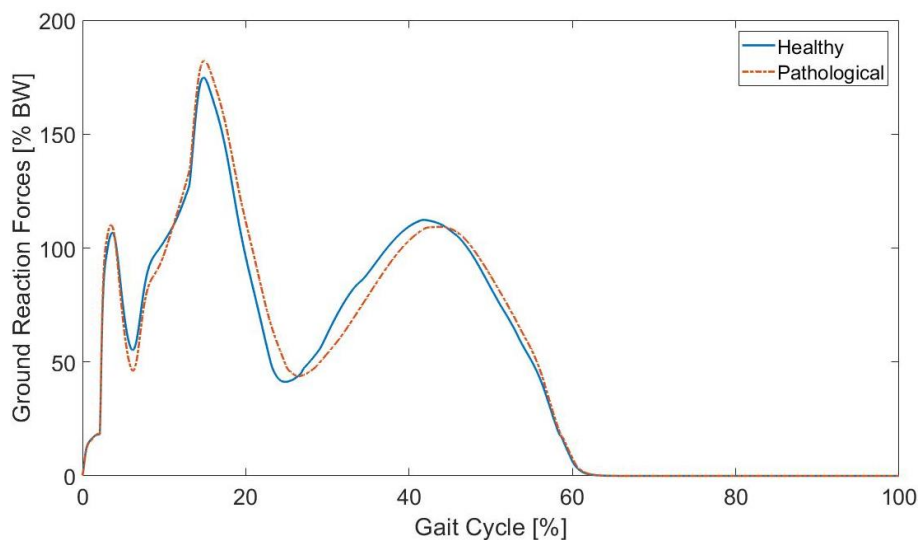


Figure 6.21 - Biomechanical model vertical ground reaction force normalized to % of body weight and to % of gait cycle (30Hz low-pass filtered).

Regarding the kinematic results of Noehren, Wilson, et al. (2013), they state that at the time of initial vertical impact (initial peak on vertical ground reaction force graph) during the gait of patients possessing ACL-reconstructed joints, there was the observation of smaller hip flexion angle, as well as no significant differences in the knee joint angle. No statements are done regarding the ankle angle.

Observing the biomechanical model's results, there is a higher hip flexion angle (Figure 6.22a), contrary to results from literature. However, the model's results regarding the knee angle (Figure 6.22b) are similar to literature, since no significant differences are encountered between healthy and pathological models. The same is applicable to the ankle joint angle (Figure 6.22c).

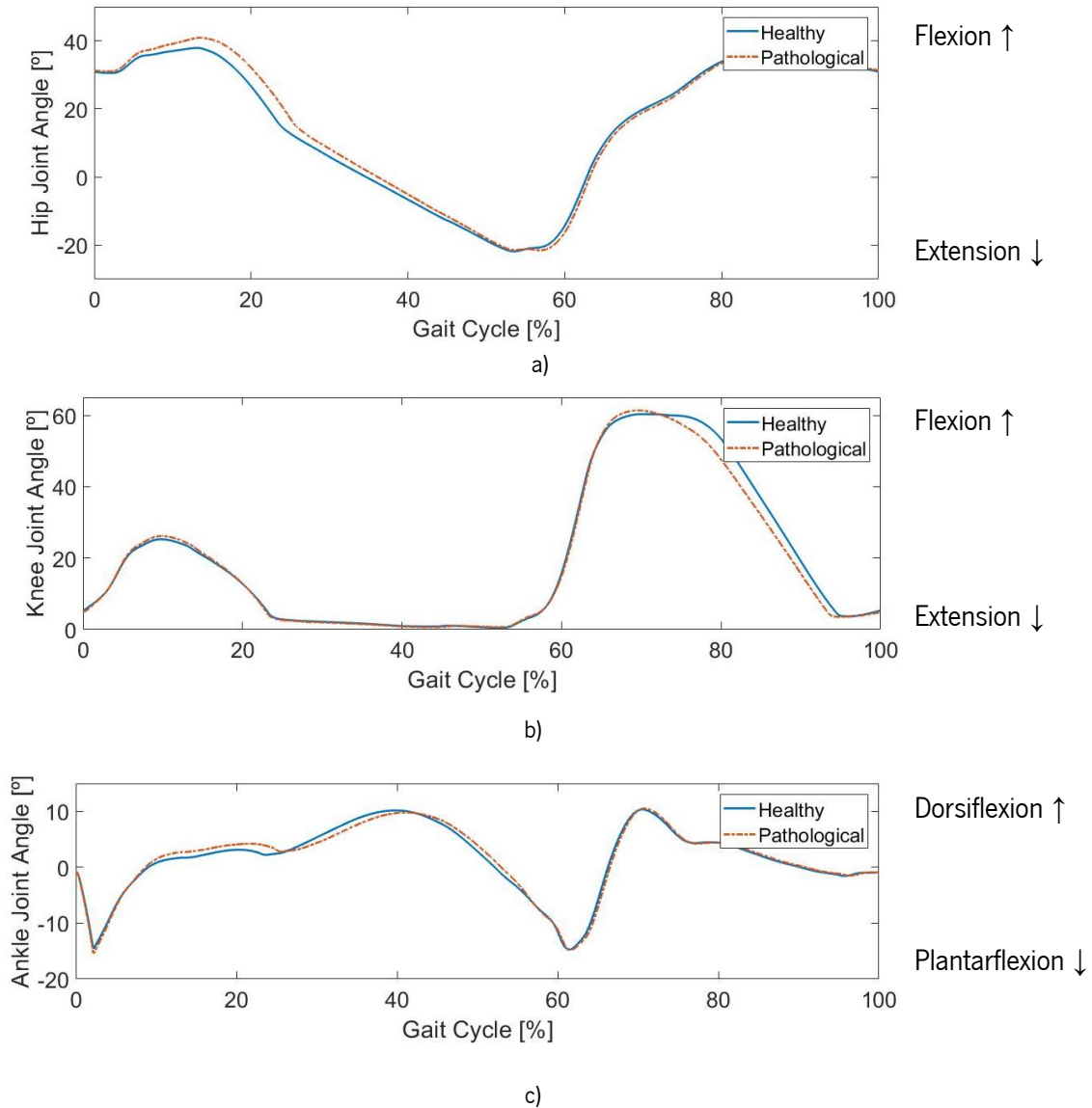


Figure 6.22 – Healthy and pathological (ACL-reconstructed) kinematic results of the biomechanical model. These graphs are normalized to % of gait cycle. a) Hip joint angle. b) Knee joint angle. c) Ankle joint angle.

The literature results for the kinetic data states that there is the occurrence of a smaller knee extensor torque and a greater hip extensor torque at the time of initial impact peak (initial peak on vertical ground reaction force graph). Similarly to the kinematic data, no statements are done regarding the ankle angle. Observing Figure 6.23, it is possible to infer that no significant differences are encountered regarding the

hip torque (Figure 6.23a), which is not what was predicted by literature findings of Noehren, Wilson, et al. (2013). The knee extensor torque (Figure 6.23b) at the time of initial impact peak is higher for the model including pathology rather than the healthy one. These results are also not in accordance to statements of literature. The ankle joint torque presents no significant differences between groups.

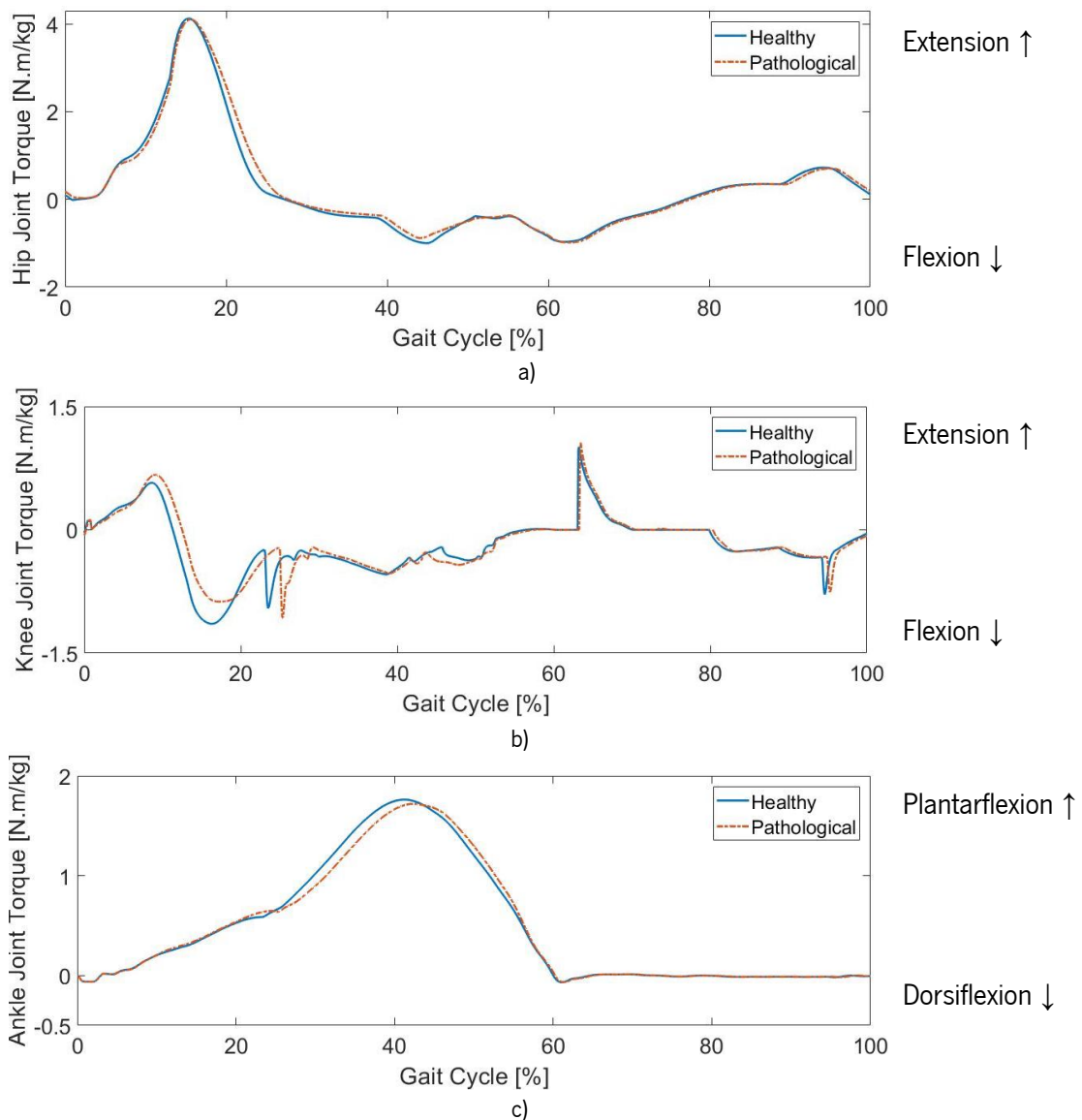


Figure 6.23 – Healthy and pathological (ACL-reconstructed) kinetic results of the biomechanical model. These graphs are normalized to % of gait cycle. a) Hip joint torque. b) Knee joint torque. c) Ankle joint torque.

The biomechanical model's obtained results for both the kinematic and kinetic data show disparities when comparing them to literature findings. The only variables which present good agreement to findings from Noehren, Wilson, et al. (2013) are the vertical ground reaction force (GRF) and knee angle. Aside

from these variables, kinetic and kinematic data did not reproduce their findings. Considering these discrepancies, it should be noted that the strategy used to computationally model the chosen pathology (reducing the torque produced by the quadriceps and hamstrings muscle groups by the amount of deficit stated in Thomas, Villwock, et al. (2013)) might not be the more anatomically correct way of implementing this knee joint pathology. To this end, in the following paragraphs it is proposed another approach.

A different approach to the one presented and implemented in this dissertation should be carried out by means of experimental procedures. It should be recruited two groups of subjects: one comprising only healthy subjects, that is, with no previous clinical history of lower limb pathologies or injuries, and other comprising subjects with an anterior cruciate ligament injury, which was latter surgically reconstructed and subject to rehabilitation processes. All participants should complete an instrumented walking gait analysis with reflective markers placed in anatomically important locations. Besides the reflective markers to measure the kinetic data of subjects during their walking gait, ground reaction forces should also be measured using force plates. Lastly, electromyographic (EMG) data of the seven muscles included in the biomechanical model (soleus, tibialis anterior, biarticular gastrocnemius, vasti lumped, biarticular hamstrings, hip flexor and gluteus muscle groups) should as well be recorded throughout the experiment for both groups of subjects.

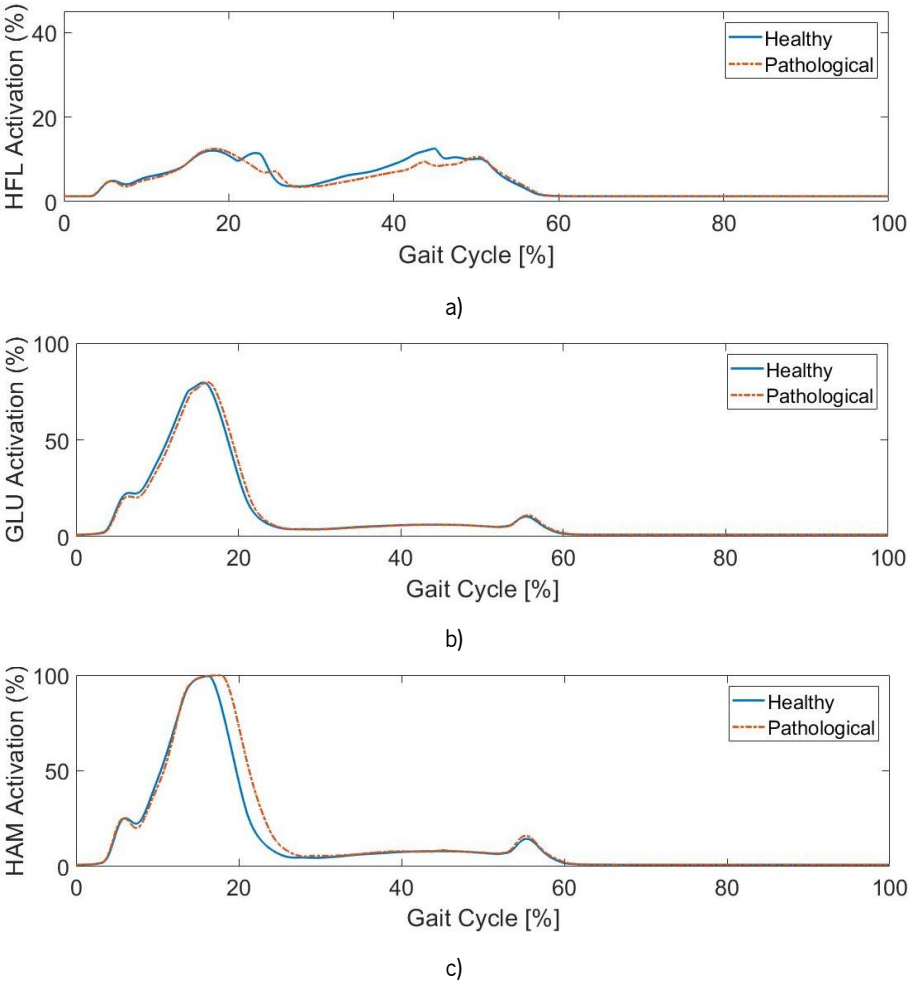
In the biomechanical model used, the muscular activations are calculated in the Muscle Actuation layer or module by means of implementing the Laplace transform of Eq. 5.21 (see Excitation Contraction Coupling of Figure 5.15). Since the optimization strategy implemented (see section 6.1.1) was designed so that the model would produce a fairly natural walking gait with characteristics of a human being with no pathology, the calculation of the muscular activations in the pathological model might not be the most anatomically correct way to calculate them in this ACL study. Instead of only altering the strength of the muscles affected by the knee condition, ignoring the analytical calculation of the muscular activation (see Eq. 5.21 and Figure 5.15) and inputting into the biomechanical model as well the history of muscular activations during the gait of an ACL-reconstructed subject, might be a good strategy to computationally implement this condition. This should also be done to the healthy biomechanical model.

Along with this alteration, muscle and attachment parameters (see Table 5.2), such as θ_{max} and F_{max} , should also be altered to match the characteristics of patients in ACL-reconstructed conditions. In the present study of this dissertation, only the torque of the vasti lumped and biarticular hamstrings muscle groups were reduced by the amounts stated in Thomas, Villwock, et al. (2013). The rest of the muscular parameters were held equal to the healthy biomechanical model (section 6.2 and Table 5.2). This might

be an influencing factor of the produced kinetic and kinematic results. If no literature is found regarding the parameters encountered in Table 5.2 for the analysed knee joint pathology, additional experimental procedures should be performed in order to determine them. If the adequate values for those parameters regarding the anterior cruciate ligament reconstruction were used, the results could be closer to literature findings.

6.3.4. Muscular Activation Outcomes

From the above-mentioned simulation with the pathological biomechanical model, and besides obtaining only the kinematic and kinetic data, the muscular activation patterns were also obtained. The figure below provides a comparison between the healthy and pathological muscular activation patterns of the seven muscle-tendon units comprising the both biomechanical models. The presented results are normalized to percentage (%) of gait cycle.



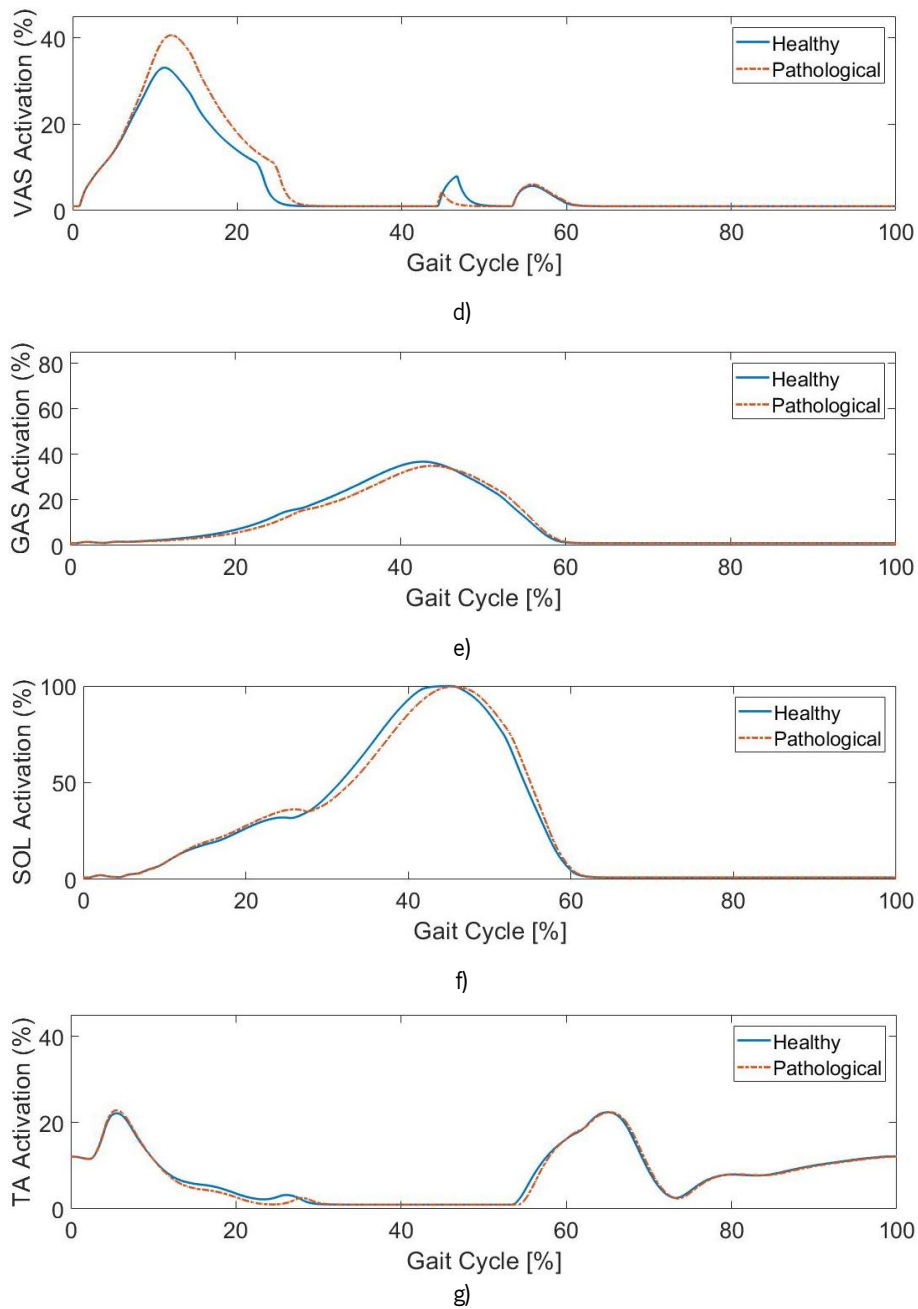


Figure 6.24 – Comparison between healthy and pathological muscle activation patterns throughout one gait cycle. Results are normalized to % of gait cycle. a) HFL - hip flexor muscle group. b) GLU - gluteus muscle group. c) HAM - biarticular hamstring muscle group. d) VAS - vasti lumped muscle group. e) GAS - biarticular gastrocnemius muscle. f) SOL - soleus muscle. g) TA - tibialis anterior muscle. See Chapter 2 for more information about the functions of these muscles.

Observing Figure 6.24, it is possible to determine that overall no significant differences regarding the muscular activation patterns arise when implementing the knee joint pathology in the utilized biomechanical model. The two major differences lie in the HAM and VAS graphs. At around 20% of gait cycle, the HAM's muscular activation shows a later presence in the gait cycle, however with the same magnitude of 100%. This means that HAM stays activated longer when pathology is implemented. For

the rest of the gait cycle, the curves under analysis present no more significant differences. The VAS pattern presents a higher activation at approximately 15% of gait cycle when the pathology implemented rather than when the biomechanical model is mimicking a healthy individual. However, at approximately 45% of gait cycle, the pathological pattern presents a decreased activation when compared to the healthy one. Since no literature was found comparing the healthy and ACL-deficient muscular patterns of the investigated muscles, no significant conclusions can be drawn. However, it is proposed in the future to experimentally measure the EMG activity of these muscles in order to perform a more detailed study.

6.4. Summary and Discussion

The present chapter presents a detailed overview of the procedures performed in order to make the biomechanical model produce both a natural healthy and a pathological walking gait. The chapter initiates with a description of the preparation procedures performed in order to make the model walk as natural as a healthy human being. On one hand, this process resolved an optimization problem using the Genetic Algorithm from MATLAB. The optimization function's main goal was that the biomechanical model travelled the most distance possible without falling, while spending the minimum metabolic energy in doing such a task. After several optimization iterations, the optimization problem implemented converged into the best solution, outputting the best set of optimization parameters that best correspond to the optimization objective function employed.

After being able to make the biomechanical model produce a fairly natural walking gait without falling, the determination of which solver of Simulink to use was performed. The overall centre of mass of the biomechanical model was calculated and 60-second simulations were ran in order to determine the amount of time they took to be complete. The error between the tested solvers was calculated and a decision was made: the ode15s solver might be used, since it is the fastest of the solvers tested and result's accuracy is not lost over speed.

After the preparation of the biomechanical model, kinetic (joint torques and ground reaction forces), kinematic (joint angles) and muscular activation data was obtained for the healthy biomechanical model. This data was compared with literature results and conclusions were drawn. The next step was to implement pathology, the anterior ligament tear, on the healthy biomechanical model. This was achieved by reducing the torque produced by the muscles affected by this knee joint condition. The same data (kinetic and kinematic) was analysed and also compared to literature findings.

7. CONCLUDING REMARKS

In the present chapter, the overall conclusions regarding the development of this dissertation are drawn. Future developments to further improve and analyse the biomechanical model and the pathology implemented are proposed.

7.1. Conclusions

In the present dissertation, a three-dimensional biomechanical model previously developed by Geyer & Herr (2010) was utilized to study the walking dynamics of both healthy and pathological (anterior cruciate ligament injured knee joint) scenarios of human performance. This implementation relied on the use of four interrelated layers in MATLAB Simulink, namely the Body Mechanics, the Muscle Actuation, the Neural Control and the Optimization layers.

The preparation procedures performed in order to make the biomechanical model walk as natural as a healthy human being relied on resolving an optimization problem using the Genetic Algorithm from MATLAB. The optimization function's main goal was that the biomechanical model would travel the further distance possible without falling, while spending the minimum metabolic energy in doing such a task. After several iterations, the optimization problem implemented converged into the best solution, outputting the best set of optimization parameters that best correspond to the optimization objective function employed.

The determination of which solver of Simulink to use was performed after this optimization problem development. The error between the tested solvers was calculated and a decision was made: the ode15s solver might be used, since it is the fastest of the solvers tested and result's accuracy is not compromised. After the preparation of the biomechanical model, kinetic (joint torques and ground reaction forces), kinematic (joint angles) and muscular activation data was obtained for the healthy biomechanical model. This data was compared with literature results. The results present a higher correlation with literature findings regarding the kinematic data for all three analysed joints. However, considering the hip and knee's joint torques, significant differences are encountered when comparing them to literature. In order to try to put the biomechanical model's results closer to literature findings, it would be important to further optimize the model utilizing different approaches, for instance, a different optimization algorithm or even a different optimization function or parameters.

The next step was to implement pathology, namely the anterior ligament characteristics after surgical procedure and rehabilitation strategies, on the healthy biomechanical model. This was achieved by reducing the torque produced by the muscles affected by the knee joint condition. Kinetic and kinematic data was analysed. The only variables that positively correlated with literature findings were the vertical ground reaction force and knee joint angle. Regarding the vertical GRF, the first peak was higher for the ACL-deficient model, rather than for the healthy biomechanical model. The hip joint angle and torque and

knee joint torque were, in general, different than expected. No conclusions are stated in literature regarding the ankle joint torque and angle during walking.

7.2. Future Developments

There is much to improve to achieve the goals proposed for the biomechanical model used in this dissertation. One limitation of this model is the fact that, even though it is three-dimensional, it only performs movement in one plane, the sagittal one. However, other perspective regarding this fact might arise, and that is that the main movement humans perform when walking is in this plane, with little movement being present on the other planes, the frontal and transverse ones. However, a suggestion is given here in order to improve the number of movements the biomechanical model is able to perform and to more physiologically mimic the human being. To make the model walk in 3D, it is proposed, in the Body Mechanics layer, the inclusion of a planar joint at hip joint level to permit movements of adduction and abduction. These movements are not permitted by the rotational joint that is currently modelled in this joint. In addition to this change, it would be important to, in the Muscle Actuation layer, model the muscles that represent the movements of the hip joint in the frontal plane, that is, the adductor and abductors (see Table 2.5).

Regarding the healthy biomechanical model, one suggestion made is that it must be further optimized in order to produce kinematics and kinetics even closer to human walking gait. In particular, in the vertical ground reaction force curve, the first peak should be lowered to approximately 120% of body weight in order to match the second maximum on the curve. The extra peak should be eliminated. To this end, another suggestion is that in future developments of this theme, the spring-damper formulation of the ground contact model is altered, as well as its parameters (see Table 6.3). Besides the formulation of the ground contact model, another limitation that the biomechanical model presents is the fact that it only possesses two contact points at its feet (in the heel and in the toes), meaning that contact is only limited to those two CPs. This is not what occurs in reality, in which there is a surface of contact between the foot and the ground when a person walks. Considering this statement, it is proposed the alteration of the points or area of contact between the foot and the ground of the model.

Besides the alteration of the ground contact model and the contact points, the healthy biomechanical model's hip and knee joint torques should be enhanced due to the amount of oscillations the graphs of these torques present. Since the joint torque is equal to the product of the muscle force and the muscle's lever arm (see Eq. 5.3), in order to achieve a better similarity between the model's results and literature,

the alteration of either the formulation of the muscle force or the muscle's lever arm is proposed for future developments. If no such alterations are desired to be made, the alteration of the number of muscles that produce muscle torque about the hip and knee joints must be exploited in detail.

The pathological biomechanical model also needs much improvement since it is only able to walk for 100 meters without falling with a deficit in the quadriceps and hamstrings muscles group torque of 18%. This percentage is a little far from the quadriceps deficits that patients experience after anterior cruciate ligament reconstruction, as seen in Table 6.4. So, in order to model this pathology in a more realistic way, it is proposed to optimize the pathological model with higher muscle force deficits in order to make it walk without falling. This way, the biomechanical model would be able to walk and to reproduce the walking kinematics and dynamics of patients with deficits characteristics of this knee joint pathology.

For both the healthy and pathological biomechanical models, it is important to note that the parameters used regarding anthropometric characteristics (Table 5.1), the muscle and attachment parameters (Table 5.2) and the muscle's pre-stimulation (Table 5.3) are estimations arising from different authors, obtained from different experimental conditions and procedures. According to De Groot, Van Campen, et al. (2010), there is a wide variation regarding parameters reported in literature and are often compiled from different sources. Considering these statements and the fact that muscle properties are known to vary with gender, age and level of activity a person possesses, these parameters are therefore not subject-specific, which might influence the biomechanical model's dynamics. Performing a detailed study of these parameters (for instance, a sensitivity analysis) and analyse the response of the biomechanical model to the alteration, would be interesting to be done in future developments of this theme.

Other parameters that need to be tested are the incorporation of slopes on the ground, the scaling of the model in order for it to be adjustable to different patients, the performance of different activities, such as stairs up and down, and the inclusion of a computer-aided design model for future rehabilitation studies using this biomechanical model. These parameters may be required to be tested in this biomechanical model, since they were included in the customer requirements (see Table 4.1) analysed in chapter 4.

BIBLIOGRAPHIC REFERENCES

- Affatato, S. (2012). *Wear of Orthopaedic Implants and Artificial Joints*. Woodhead Pub.
- Akao, Y. (2004). *Quality Function Deployment : Integrating Customer Requirements into Product Design* (First Ed.). New York: Taylor & Francis.
- Anderson, C. (2007). *Equations for Modeling the Forces Generated by Muscles and Tendons - BioE215 Physics-based Simulation of Biological Structures*, Stanford University, internal publication, California.
- Aubert, X. (1956). *Le couplage énergétique de la contraction musculaire*. Thèse d'agregation, Université Catholique de Louvain. Brussels: Edition Arscia.
- Biewener, A. A. (2016). Locomotion as an emergent property of muscle contractile dynamics. *Journal of Experimental Biology*, 219(2), 285–294.
- Blewis, M. (2008). *Bioengineering synovial fluid with theoretical and experimental models of the synovial joint*. A dissertation for the degree Doctor of Philosophy in Bioengineering, UC San Diego.
- Boyd, S., & Vandenberghe, L. (2004). *Convex Optimization*. Cambridge: Cambridge University Press.
- Buhrmann, T., & Di Paolo, E. A. (2014). Spinal circuits can accommodate interaction torques during multijoint limb movements. *Frontiers in Computational Neuroscience*, 8, 144.
- Caillé, J., Ildefonse, M., & Rougier, O. (1985). Excitation-contraction coupling in skeletal muscle. *Progress in Biophysics and Molecular Biology*, 46(3), 185–239.
- Callaghan, J. J., Rosenberg, A. G., Rubash, H. E., Simonian, P. T., & Wickiewicz, T. L. (2003). *The Adult Knee*. (J. J. Callaghan, Ed.) (First Ed.). Lippincott Williams & Wilkins, 2003.
- Cher, P. H., Stewart, I. B., & Worringham, C. J. (2015). Minimum cost of transport in human running is not ubiquitous. *Medicine and Science in Sports and Exercise*, 47(2), 307–314.
- Cohen, L. (1995). *Quality Function Deployment - How to Make QFD Work for You* (Sixth Ed.). Addison-Wesley.
- Desai, R. (2018). (5) Sarcomere length-tension relationship (video) | Khan Academy. Retrieved August 11, 2018, from <https://www.khanacademy.org/science/health-and-medicine/circulatory-system/preload-and-afterload/v/sarcomere-length-tension-relationship>
- Dutton, M. (2016). *Dutton's Orthopaedic examination, evaluation, and intervention*. (M. Weitz & B. Kearns, Eds.) (4th ed.). McGraw-Hill Education.
- Dzeladini, F., van den Kieboom, J., & Ijspeert, A. (2014). The contribution of a central pattern generator

- in a reflex-based neuromuscular model. *Frontiers in Human Neuroscience*, 8, 371.
- Eitzen, I., Grindem, H., Nilstad, A., Moksnes, H., & Risberg, M. A. (2016). Quantifying Quadriceps Muscle Strength in Patients With ACL Injury, Focal Cartilage Lesions, and Degenerative Meniscus Tears. *Orthopaedic Journal of Sports Medicine*, 4(10), 232596711666771.
- Engel, K., Herpers, R., & Hartmann, U. (2011). Biomechanical Computer Models. *Theoretical Biomechanics*, 93–112.
- Fältström, A. (2016). One Anterior Cruciate Ligament injury is enough! Linköping University Electronic Press.
- Flores, P. (2006). *Biomecânica das Articulações Humanas*, Universidade do Minho, Escola de Engenharia, publicação interna, Guimarães.
- Fukunaga, T., Kawakami, Y., Kubo, K., & Kanehisa, H. (2002). Muscle and tendon interaction during human movements. *Exercise and Sport Sciences Reviews*, 30(3), 106–110.
- Fulkerson, J. P., & Shea, K. P. (2004). *Disorders of the Patello-femoral Joint* (Fourth Ed.). Philadelphia: Lippincott Williams & Wilkins.
- Gardinier, E. S., Manal, K., Buchanan, T. S., & Snyder-Mackler, L. (2012). Gait and neuromuscular asymmetries after acute anterior cruciate ligament rupture. *Medicine and Science in Sports and Exercise*, 44(8), 1490–1496.
- Geyer, H., & Herr, H. (2010). A Muscle-reflex model that encodes principles of legged mechanics produces human walking dynamics and muscle activities. *IEEE Transactions on Neural Systems and Rehabilitation Engineering*, 18(3), 263–273.
- Geyer, H., Seyfarth, A., & Blickhan, R. (2003). Positive force feedback in bouncing gaits? *Proceedings of the Royal Society B: Biological Sciences*, 270(1529), 2173–2183.
- Gray, H. (1918). *Anatomy of the Human Body*. Lea & Febiger.
- Good, E. S., & Suntay, W. J. (1983). A Joint Coordinate System for the Clinical Description of Three-Dimensional Motions: Application to the Knee. *Journal of Biomechanical Engineering*, 105(2), 136–144.
- Günther, M., & Ruder, H. (2003). Synthesis of two-dimensional human walking: A test of the λ -model. *Biological Cybernetics*, 89(2), 89–106.
- Halbleib, L., Wormington, P., Cieslak, W., & Street, H. (1993). Application of Quality Function Deployment to the Design of a Lithium Battery. *IEEE Transactions on Components, Hybrids, and Manufacturing Technology*, 16(8), 802–807.

- Hall, S. J. (2012). *Basic biomechanics* (Sixth Ed.). New York: McGraw-Hill Education.
- Harris, D., & Harris, S. (2012). *Digital Design and Computer Architecture* (Second Ed.). Morgan Kaufmann.
- Hiemstra, L. A., Webber, S., MacDonald, P. B., & Kriellaars, D. J. (2007). Contralateral limb strength deficits after anterior cruciate ligament reconstruction using a hamstring tendon graft. *Clinical Biomechanics*, 22(5), 543–550.
- Hill, A. V. (1938). The Heat of Shortening and the Dynamic Constants of Muscle. *Proceedings of the Royal Society B: Biological Sciences*, 126(843), 136–195.
- Jacquelin, P. (1992). *Gait analysis : normal and pathological function*. SLACK Incorporated, Thorofare, New Jersey.
- Jacques, G. E., Ryan, S., Naumann, S., Milner, M., & Cleghorn, W. L. (1994). Application of Quality Function Deployment in Rehabilitation Engineering. *IEEE Transactions on Rehabilitation Engineering*, 2(3), 158–164.
- Kim, H. J., Lee, J. H., Ahn, S. E., Park, M. J., & Lee, D. H. (2016). Influence of anterior cruciate ligament tear on thigh muscle strength and hamstring-to-quadriceps ratio: A meta-analysis. *PLoS ONE*, 11(1), e0146234.
- Knudson, D. (2007). *Fundamentals of Biomechanics* (Second Ed.). Boston, MA: Springer Science & Business Media.
- Lazzer, S., Taboga, P., Salvadego, D., Rejc, E., Simunic, B., Narici, M. V, ... di Prampero, P. E. (2014). Factors affecting metabolic cost of transport during a multi-stage running race. *Journal of Experimental Biology*, 217(5), 787–795.
- Lepley, L. K. (2015). Deficits in Quadriceps Strength and Patient-Oriented Outcomes at Return to Activity After ACL Reconstruction: A Review of the Current Literature. *Sports Health*, 7(3), 231–238.
- Li, Z.-M. (2006). Functional degrees of freedom. *Motor Control*, 10(4), 301–310.
- Li, Z.-M., & Tang, J. (2007). Coordination of thumb joints during opposition. *Journal of Biomechanics*, 40(3), 502–510.
- Liu, G. R., & Quek, S. S. (2014). Computational Modeling. In *The Finite Element Method* (pp. 1–11). Elsevier.
- Logan, G. D., & Radcliffe, D. F. (1997). Potential for use of a House of Quality matrix technique in rehabilitation engineering. *IEEE Transactions on Rehabilitation Engineering*, 5(1), 106–115.
- Maganaris, C. N. (2001). Force-length characteristics of in vivo human skeletal muscle. *Acta Physiologica*

- Scandinavica, 172(4), 279–285.
- Maganaris, C. N. (2003). Force-length characteristics of the in vivo human gastrocnemius muscle. *Clinical Anatomy: The Official Journal of the American Association of Clinical Anatomists and the British Association of Clinical Anatomists*, 16(3), 215–223.
- Margo, B. J., Radnay, C. S., Scuderi, G. R., Margo, B. J., Radnay, C. S., & Scuderi, G. R. (2010). Chapter 1 - Anatomy of the Knee. In *The Knee -A Comprehensive Review*. World Scientific Publishing Co. Pte. Ltd.
- MathWorks. (2017a). About Solvers - MATLAB Simulink Documentation (r2017b). Retrieved March 11, 2018, from <https://www.mathworks.com/help/simulink/ug/choosing-a-solver.html>
- MathWorks. (2017b). Genetic Algorithm - MATLAB Simulink - Global Optimization Toolbox (r2017b). Retrieved March 11, 2018, from <https://www.mathworks.com/discovery/genetic-algorithm.html>
- MathWorks. (2018a). Genetic Algorithm Terminology - MATLAB Simulink Documentation (r2018a). Retrieved June 26, 2018, from <https://www.mathworks.com/help/gads/some-genetic-algorithm-terminology.html>
- MathWorks. (2018b). How the Genetic Algorithm Works - MATLAB Simulink Documentation (r2018a). Retrieved June 26, 2018, from <https://www.mathworks.com/help/gads/how-the-genetic-algorithm-works.html>
- MathWorks. (2018c). Inertial Reference Frame - MATLAB Simulink Documentation (r2018a). Retrieved June 26, 2018, from <https://www.mathworks.com/help/physmod/sm/ref/worldframe.html>
- MathWorks. (2018d). Joint with one revolute and two prismatic primitives - MATLAB Simulink Documentation (r2018a).
- McMahon, T. A. (1984). *Muscles, reflexes, and locomotion*. Princeton University Press.
- Meisterling, S. W., Schoderbek, R. J., & Andrews, J. R. (2009). Anterior Cruciate Ligament Reconstruction. *Operative Techniques in Sports Medicine*, 17(1), 2–10.
- Muraoka, T., Kawakami, Y., Tachi, M., & Fukunaga, T. (2001). Muscle fiber and tendon length changes in the human vastus lateralis during slow pedaling. *Journal of Applied Physiology*, 91(5), 2035–2040.
- Nair, B. S. (2002). *Digital electronics and logic design*. PHI Learning Pvt. Ltd.
- Neumann, D. A. (2013). *Kinesiology of the Musculoskeletal System: Foundations for Rehabilitation (Second Ed.)*. Mosby - Elsevier.
- Noehren, B., Wilson, H., Miller, C., & Lattermann, C. (2013). Long-term gait deviations in anterior cruciate

- ligament-reconstructed females. *Medicine and Science in Sports and Exercise*, 45(7), 1340–1347.
- Oatis, C. A. (2009). *Kinesiology : The Mechanics and Pathomechanics of Human Movement* (Second Ed.). Philadelphia: Lippincott Williams & Wilkins.
- Oda, T., Kanehisa, H., Chino, K., Kurihara, T., Nagayoshi, T., Kato, E., ... Kawakami, Y. (2005). In Vivo Length-Force Relationships on Muscle Fiber and Muscle Tendon Complex in the Tibialis Anterior Muscle. *International Journal of Sport and Health Science*, 3(Special_Issue_2), 245–252.
- Openstax College. (2013). *Anatomy and Physiology*. Houston, TX: OpenStax CNX. Retrieved from
- Palastanga, N., & Soames, R. (2012). *Anatomy and human movement : structure and function* (Sixth Ed.). Elsevier Health Sciences.
- Prodromos, C. C. (2017). *The anterior cruciate ligament : reconstruction and basic science* (Second Ed.). Elsevier Health Sciences.
- Reid, C. R., Bush, P. M., Cummings, N. H., McMullin, D. L., & Durrani, S. K. (2010). A Review of Occupational Knee Disorders. *Journal of Occupational Rehabilitation*, 20(4), 489–501.
- Ridola, C. G., Cappello, F., Marcianò, V., Francavilla, C., Montalbano, A., Farina-Lipari, E., & Palma, A. (2007). The synovial joints of the human foot. *Italian Journal of Anatomy and Embryology*, 112(2), 61–80.
- Roberts, P. (2007). Section 6 - Quality Function Deployment. In Warwick Manufacturing Group, University of Warwick.
- Rodriguez-Merchan, C., & Oussedik, S. (2015). *Total Knee Arthroplasty: A Comprehensive Guide*. Springer International Publishing.
- Roth, C. H. (2004). *Fundamentals of logic design*. Nelson Education.
- Sandow, A. (1952). Excitation-contraction coupling in muscular response. *The Yale Journal of Biology and Medicine*, 25(3), 176–201.
- Schuenke, M., Schulte, E., & Schumacher, U. (2009). *THIEME Atlas of Anatomy, Vol. 1: General Anatomy and Musculoskeletal System (Latin Nomenclature Edition)*. (A. M. Gilroy, B. R. MacPherson, & L. M. Ross, Eds.) (2nd ed.). New York: Thieme Medical Publishers, Inc.
- Scott, S. H., & Winter, D. A. (1993). Biomechanical model of the human foot: Kinematics and kinetics during the stance phase of walking. *Journal of Biomechanics*, 26(9), 1091–1104.
- Shelbourne, K. D., Biggs, A., & Gray, T. (2007). Deconditioned Knee: The Effectiveness of a Rehabilitation Program that Restores Normal Knee Motion to Improve Symptoms and Function. *North American Journal of Sports Physical Therapy : NAJSPT*, 2(2), 81–89.

- Spaulding, S. J. (2005). *Meaningful motion : biomechanics for occupational therapists*. Elsevier Health Sciences.
- Sperelakis, N. (2012). *Cell Physiology Source Book: Essentials of Membrane Biophysics*. Elsevier/Academic Press.
- Squire, J. M. (2016). Muscle contraction: Sliding filament history, sarcomere dynamics and the two Huxleys. *Global Cardiology Science & Practice*, 2016(2), e201611.
- Standring, B. S. (2008). *Gray's Anatomy: the Anatomical Basis of Clinical Practice*. (40th Ed.). Elsevier Health Sciences UK.
- Stoll, H. . (1999). *Product design methods and practices*. CRC Press.
- Tavares da Silva, M. P. (2003). *Human Motion Analysis using Multibody Dynamics and optimization tools*. Universidade Técnica de Lisboa, Instituto Superior Técnico.
- Thatte, N., & Geyer, H. (2016). Toward Balance Recovery With Leg Prostheses Using Neuromuscular Model Control. In *IEEE Transactions on Biomedical Engineering* (Vol. 63, pp. 904–913).
- Thomas, A. C., Villwock, M., Wojtys, E. M., & Palmieri-Smith, R. M. (2013). Lower extremity muscle strength after anterior cruciate ligament injury and reconstruction. *Journal of Athletic Training*, 48(5), 610–620.
- Umberger, B. R., Gerritsen, K. G. M., & Martin, P. E. (2003). A model of human muscle energy expenditure. *Computer Methods in Biomechanics and Biomedical Engineering*, 6(2), 99–111.
- van Ingen Schenau, G. J. (1984). An alternative view of the concept of utilisation of elastic energy in human movement. *Human Movement Science*, 3(4), 301–336. [https://doi.org/10.1016/0167-9457\(84\)90013-7](https://doi.org/10.1016/0167-9457(84)90013-7)
- Walter Shelton. (2010). *The Knee*. In *AANA Advanced Arthroscopic Surgical Techniques* (pp. 178–182). Saunders/Elsevier.
- Winter, D. A. (2009). *Biomechanics and Motor Control of Human Movement*. John Wiley & Sons.
- Wu, G., Siegler, S., Allard, P., Kirtley, C., Leardini, A., Rosenbaum, D., ... Stokes, I. (2002). ISB recommendation on definitions of joint coordinate system of various joints for the reporting of human joint motion—part I: ankle, hip, and spine. *Journal of Biomechanics*, 35(4), 543–548.
- Yamaguchi, G. T., Sawa, A. G.-U., Moran, D. W., Fessler, M. J., & Winters, M., J. (1990). A survey of human musculotendon actuator parameters in Multiple Muscle Systems: Biomechanics and Movement Organization. In J. Winters & S.-Y. Woo (Eds.) (pp. 717–778). Springer-Verlag, New York.
- Zatsiorsky, V. M., & Prilutsky, B. I. (2012). *Biomechanics of skeletal muscles*. Human Kinetics.

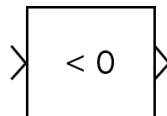
Zienkiewicz, O. C., Taylor, R. L., & Zhu, J. Z. (2013). The Standard Discrete System and Origins of the Finite Element Method. In *The Finite Element Method: its Basis and Fundamentals* (pp. 1–20). Elsevier.

APPENDIX I – LANGUAGE UTILIZED IN THE SIMULINK® ENVIRONMENT

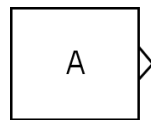
As stated in MathWorks®'s website (<https://www.mathworks.com/help/simulink/>), Simulink® is “a block diagram environment” to be used, amongst other applications, in simulation. To this end, it provides “a graphical editor, customizable block libraries, and solvers for modelling and simulating dynamic systems”. Since it is incorporated in MATLAB®, the user is able to include MATLAB algorithms into Simulink® models and export the results of the simulation to MATLAB®'s workspace.

This appendix presents a description of the language used in this dissertation when referring to modelling with Simulink®. Each block mentioned in this dissertation is presented in the following bullet points, accompanied with its representative diagram. The information was taken from Simulink® Documentation (<https://www.mathworks.com/help/simulink/blocklist.html>).

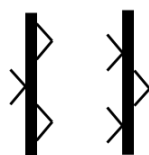
- Compare to Zero Block: this block determines how an input signal compares to zero with the operator parameter, which can be == (input equal to zero), ~= (input different from zero), < (input less than zero), <= (input less or equal than zero), > (input greater than zero) or >= (input greater or equal than zero). The output of the Compare to Zero block is either a 0, if the comparison is false, or a 1, if the comparison is true. The below diagram is displayed with < operator parameter.



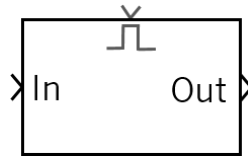
- Constant Block: generates a real or complex constant value, A, which can be a vector, matrix or scalar.



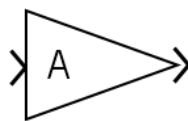
- Demux/Mux: the demux (left diagram) block extracts and outputs separately the elements of an input vector. Conversely, the mux (right diagram) block combines several same data type input signals into a vector.



- Enabled Subsystem: an enabled subsystem is a subsystem whose execution is enabled or disabled by the activation or deactivation of an external input (coloured in grey in the below diagram).



- Gain Block: this block multiplies the input signal by a constant, A. Both the input signal and the gain can be a scalar, vector or matrix.



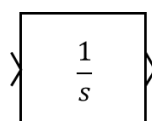
- Goto/From Blocks: Goto blocks (left diagram) pass its input to their corresponding From blocks (right diagram), acting then as its output. The use of these two blocks allows the user to pass a signal from one block to another without connecting them. This is useful when the Simulink® code is already too full, which might compromise readability. The input and output of the Goto and From blocks, respectively, can be a real or complex vector. While a Goto block is able to transfer its input signal to more than one From block, the other way around is not possible, that is a From block can accept a signal from only one Goto block. These two blocks are connected by the use of Goto tags, [A], univocally identifying them.



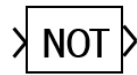
- Inport/Output Blocks: inports/outputs are blocks used to create input/outputs for a system, enabling signal entry/exit into/out of the system.



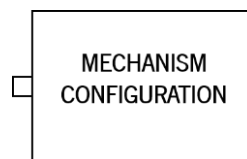
- Integrator Block: this block integrates the input signal and outputs the value of the integral of the input signal with respect to time. It is possible to define the block's initial condition.



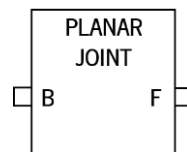
- Logical Operator Block: this block performs a specified logical operation on its inputs signal, namely AND, OR, NAND, NOR, XOR, NXOR or NOT. The diagram is applied to the logical operator NOT.



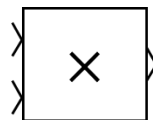
- Mechanisms Configuration Block: this block enables the user to set determined mechanical and simulation parameters to the system under development, for instance, the gravity vector. This is an optional parameter, and if omitted the gravity vector is set to zero.



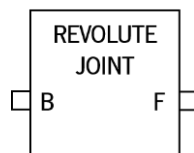
- Planar Joint Block: this block comprises a planar joint, providing one rotational and two translational degrees of freedom, due to the inclusion of one revolute and two prismatic primitives. It is possible to define state targets, such as initial velocity and position.



- Product Block: this blocks outputs the results of a multiplication or division of its inputs, which can either be scalars or matrices.

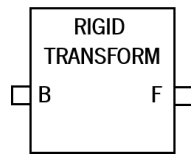


- Revolute Joint Block: this block implements a joint with one degree of freedom, permitting only rotation. It is possible to define state targets, such as initial velocity and position.

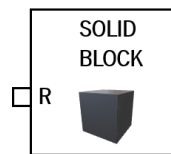


- Rigid Transform Block: this Simulink® block applies a transformation between two frames, the base (B) and the follower (F). It rotates and/or translates the follower frame with respect to the

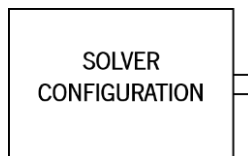
base frame. Both frames remain fixed with respect to each other during the entire time simulation of the system.



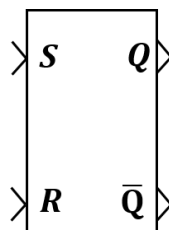
- Solid Block: this block creates a solid element with a certain geometry, inertia and colour.



- Solver Configuration Block: this block enables the user to specify the parameters regarding the solver used, such as the type of solver.



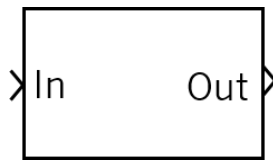
- SR Flip-Flop Block: this block implements the truth table of an SR Flip-Flop. This circuit is constructed using NOR gates and possesses two inputs (S and R) and two outputs (Q and \bar{Q}).



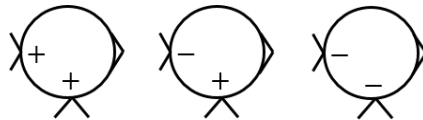
- STOP Block: this block enables the simulation to be stopped whenever the variables connected to its input are different from the logic 0.



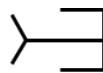
- Subsystem: a subsystem is a Simulink® block that contains a subset of grouped blocks inside it, in order to create block hierarchy.



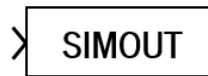
- Sum Block: this block permits to add or subtract inputs, which can be scalar, vectors or matrices.



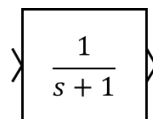
- Terminator: this block terminates an unconnected output port. If a simulation is running with blocks having unconnected output ports, Simulink® exits warning messages. By using terminator blocks this is prevented.



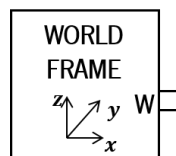
- To Workspace Block: this block writes the input signal to MATLAB®'s workspace. The data is only accessed when the simulation stops or pauses.



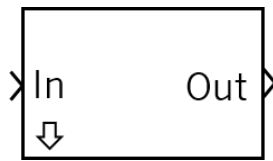
- Transfer Fnc Block: this block models a linear system by the implementation of the Laplace-domain variable s .



- World Frame Block: represents the global reference frame of the system under development in Simulink®. As explained in chapter 5, section 5.1, the world frame obeys to the right-hand rule, and directly or indirectly all the other frames comprising the system are defined in respect to it.



In this work, it is also mentioned the use of mask blocks. Essentially, and as stated in Simulink® Documentation website, a mask is “a custom user interface for a block”. When applying a mask to a block or to a set of blocks, it is possible to encapsulate it and attribute to it its own parameters.



In this work, the MTUs are modelled using masks. Essentially a general subsystem is created with the components present in Figure 5.15. This subsystem is then encapsulated, creating a mask, in which specific parameters are defined, such as the MTU's maximum isometric force, optimal length, maximum contraction velocity and slack length. On one hand, if the user clicks on the arrow it enters the subsystem, viewing the referred components of Figure 5.15. On the other hand, if the user double-clicks on subsystem, a dialog box opens with boxes to input those four parameters. Even though the entire construction of each MTU is the same, these four parameters vary according to the MTU, distinguishing them.

Throughout the dissertation is also mentioned the existence of sensors, for instance, in the optimization constraint implemented in Simulink® to determine the distance travelled by HAT's COM in order to stop the simulation if this distance exceeded 100m. These sensors are not a predefined blocks existing in Simulink®'s libraries. They are built by the user using several blocks inside a subsystem, as seen in Figure I.1.

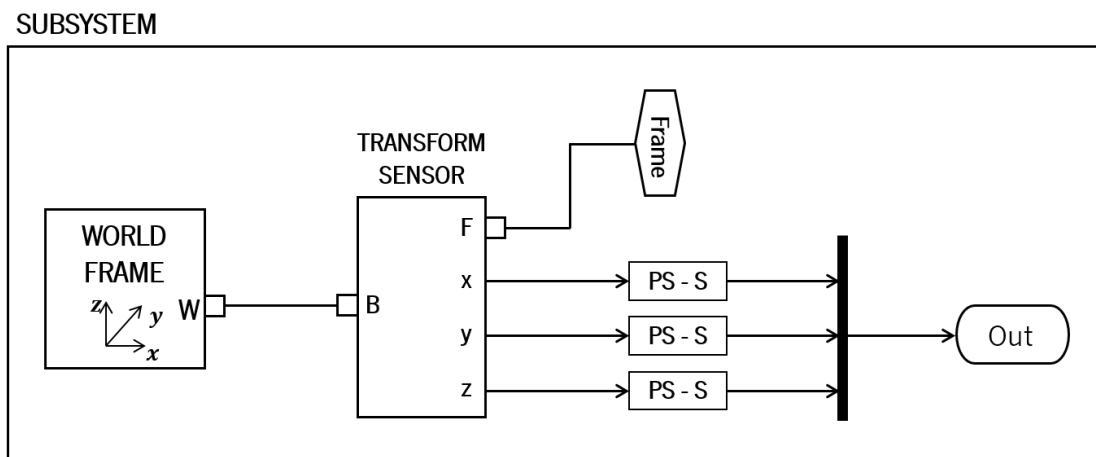


Figure I.1 - Implementation of a sensor to measure the translation of Frame in the x, y and z axes in relation to the World Frame.

The implementation of this figure enables the measurement of the x, y and z coordinates of Frame in relation to the World Frame. In the example of measuring the distance travelled HAT's COM, only the x coordinate is used and Frame of the above presented figure is the frame placed in the centre

of mass of the HAT segment. The use of the World Frame is done in order to measure the HAT's position in relation to the global frame of the system. The Transform Sensor block senses the 3D transformation that occurs between these two frames (B and F). It is capable of measuring the rotation, angular velocity, angular acceleration, translation, velocity and acceleration of the follower frame relative to the base frame. In this case, the x, y and z translations are being measured.

The blocks in front of the Transform Sensor are called PS-Simulink Converter Blocks and enable the transformation of the input physical signal (PS) into a unitless Simulink output signal (S). These blocks are used since the outputs of the Transform Sensor block represent a physical quantity with units which are not read by Simulink® blocks, reading only Simulink® signals. Since in this case, there are three signals, a mux is used, which is connected to an output.